9988
NACA TN 2476
TECH LIBRARY KAFB, NM
0065553

# NATIONAL ADVISORY COMMITTEE FOR AERONAUTICS

## TECHNICAL NOTE 2476

# AN EMPIRICAL METHOD PERMITTING RAPID DETERMINATION OF THE AREA, RATE, AND DISTRIBUTION OF WATER-DROP IMPINGEMENT ON AN AIRFOIL OF ARBITRARY SECTION AT SUBSONIC SPEEDS

By Norman R. Bergrun

Ames Aeronautical Laboratory
Moffett Field, Calif.

Washington

September 1951

AFMDC
TECHNICAL LIBRARY
AFL 2811

TECH LIBRARY KAFB, NM
0065553



NATIONAL ADVISORY COMMITTEE FOR AERONAUTICS

TECHNICAL NOTE 2476

# AN EMPIRICAL METHOD PERMITTING RAPID DETERMINATION OF THE AREA, RATE, AND DISTRIBUTION OF WATER-DROP IMPINGEMENT ON AN AIRFOIL OF ARBITRARY SECTION AT SUBSONIC SPEEDS

By Norman R. Bergrun

## SUMMARY

An empirical method for the determination of the area, rate, and distribution of water-drop impingement on airfoils of arbitrary section is presented. The procedure represents an initial step toward the development of a method which is generally applicable in the design of thermal ice-prevention equipment for airplane wing and tail surfaces. Results given by the proposed empirical method are expected to be sufficiently accurate for the purpose of heated-wing design, and can be obtained from a few numerical computations once the velocity distribution over the airfoil has been determined.

The empirical method presented for incompressible flow is based on results of extensive water-drop trajectory computations for five airfoil cases which consisted of 15-percent-thick airfoils encompassing a moderate lift-coefficient range. The differential equations pertaining to the paths of the drops were solved by a differential analyzer.

The method developed for incompressible flow is extended to the calculation of area and rate of impingement on straight wings in subsonic compressible flow to indicate the probable effects of compressibility for airfoils at low subsonic Mach numbers.

## INTRODUCTION

The design of thermal ice-prevention equipment for airplane wing and tail surfaces has progressed to the point where the amount and distribution of heat flow can be calculated for specified flight and icing conditions (reference 1). This design procedure requires information as to the area, rate, and distribution of water-drop impingement on the leading edge of the airfoil section being analyzed. At the present time, an approximation of area and rate of water-drop impingement is achieved by using a method involving the substitution of a circular cylinder for the airfoil leading edge, as suggested in

references 1 and 2. This substitution method is adequate for design purposes for some combinations of cylinder diameter and drop size, but it can produce sizable errors for other combinations (references 1, 3, and 4).

A second means of estimating the area and rate of water-drop impingement on airfoils is provided by reference 3. This method is more accurate than the cylinder substitution method, but the calculation procedure is somewhat laborious and, as a result, its use is not too practicable in a complete design study where a large number of trajectories are usually required.

To establish a procedure which would eliminate the laborious computations of water-drop trajectories in the design of wing thermal ice-prevention equipment, it became apparent that a large number of water-drop trajectories would be required for study. Experience with calculating trajectories by the method of reference 3 had shown that the pattern of water-drop impingement for drop sizes usually encountered in flight can be related most directly to velocity distribution over the surface of the airfoil. Airfoil shape itself appeared to have an effect on the pattern of impingement, but to a lesser degree than velocity distribution. Five airfoil cases were chosen as being the minimum which could be expected to provide sufficient data to include the effects of these two factors. Water-drop trajectories were computed for these five cases.

This report presents the results of the water-drop-trajectory computations. From a generalization of these data, a method is derived that permits a relatively rapid determination of the area, rate, and distribution of water-drop impingement for a fairly large number of airfoil surfaces of arbitrary profile. The derivation and limitations of this method and the procedure for its use are presented herein. The water-drop trajectories for the five airfoil cases were computed on the differential analyzer at the University of California, Los Angeles, under contract with the NACA; and appreciation is extended to the staff of the University for its aid and cooperation during the conduct of the program.

## SYMBOLS

The following nomenclature is used throughout this report:

$a$ airfoil mean-line designation, fraction of chord from leading edge over which design load is uniform

$a_d$ instantaneous drop-acceleration ratio, dimensionless

$A_o$ area normal to flow direction outlined by several trajectories at free-stream conditions, square feet

$A_s$ area of impingement outlined on an airfoil surface by trajectories starting at free-stream conditions from an initial area of $A_o$, square feet

$c$ chord length of airfoil, feet

$C$ concentration factor $\left(\frac{dA_o}{dA_s}\right)$, dimensionless

$C_d$ drag coefficient of drop, dimensionless

$c_l$ section lift coefficient, dimensionless

$C_P$ pressure coefficient $\left[1-\left(\frac{U_a}{V}\right)^2\right]$, dimensionless

$C_{P_M}$ pressure coefficient at Mach number $M$, dimensionless

$E$ collection efficiency of airfoil, percent

$G$ rate of change of velocity along the stagnation streamline at the stagnation point $\left[\left.\frac{d(U_a/V)}{dS}\right|_{\Psi=0}\right]$, dimensionless

$h$ frontal height of airfoil, fraction of chord

$k$ slope of airfoil contour at a particular chordwise position, dimensionless

$L$ length of span, feet

$m$ liquid-water content of icing cloud, pounds of water per cubic foot of air

$M$ Mach number, dimensionless

$M_a$ weight rate of water-drop impingement per unit of surface area, pounds per hour, square foot

$M_s$ weight rate of impingement of water drops on a body, per unit span, pound per hour, foot

$P$ ratio of the vector difference between the local air and drop velocities to free-stream velocity $\left(\frac{\overline{U}_a-\overline{U}_d}{V}\right)$, dimensionless

$r$ radius of drop, feet

$R$ Reynolds number for drop at relative velocity $PV$ $\left(\frac{2PVr}{\nu}\right)$

$R_V$ Reynolds number for drop at free-stream velocity $V$ $\left(\frac{2Vr}{\nu}\right)$

$s$ distance along airfoil surface from leading edge, positive on upper surface and negative on lower surface, feet

$S$ distance along water-drop trajectory, fraction of chord

$t$ time, seconds

$t_e$ equivalent ellipse thickness ratio for a low-drag airfoil $\left(\frac{2\rho}{t_{max}}\right)$, fraction of chord

$t_{max}$ maximum thickness of airfoil, fraction of chord

$u$ component of local velocity parallel to chord line, feet per second

$U$ local velocity of air or drop, feet per second

$v$ component of local velocity perpendicular to chord line, feet per second

$V$ free-stream air velocity, feet per second

$x,y$ rectangular coordinates for a system of axes having the origin at the airfoil leading edge and the $x$ axis, positive toward the trailing edge, lying along the airfoil chord, fraction or percent of chord

$x',y'$ rectangular coordinates for a system of axes having the origin at the airfoil leading edge and the $x'$ axis, positive in the free-stream direction, lying parallel to free-stream direction, fraction or percent of chord

$\Delta y$ total airfoil-ordinate intercept established by two impinging trajectories starting from infinity at a distance $\Delta y_o$ apart, fraction of chord

$\Delta y_o$ distance between two trajectories at infinity, fraction of chord

$\Delta y_{o_t}$ distance between two trajectories which start at infinity and impinge tangentially on the airfoil, fraction of chord

$\alpha$ angle of attack, degrees

$\beta$ Prandtl-Glauert factor, equal to $(1-M^2)^{1/2}$, dimensionless

$\gamma$ specific weight, pounds per cubic foot

$\theta$ angular displacement between local velocity and $x$ axis, degrees

$\nu$ kinematic viscosity of air, square feet per second

$\rho$ airfoil leading-edge radius, fraction of airfoil chord

$\tau$ time scale $\left(\frac{tV}{c}\right)$, dimensionless

$\psi$ scale modulus $\left(9\,\frac{\gamma_a}{\gamma_d} \times \frac{c}{r}\right)$, dimensionless

$\Psi$ stream function, dimensionless

## Subscripts

a air

av average

cr critical

d drop

e effective

$l$ lower surface

M conditions at a particular Mach number

max maximum

o initial condition

s condition at airfoil surface

t tangential

u upper surface

## DERIVATION OF THE METHOD

The method, derived herein, for calculating area, rate, and distribution of drop impingement assumes that airfoil velocity distribution can be considered as the primary factor influencing the paths of water drops which approach an airfoil. Hence, it was desired to find a relatively simple relation between the airfoil velocity distribution (which in itself is a function of airfoil contour) and the area, rate, and distribution of impingement. Accordingly, trajectories around airfoils of known surface velocity distribution were obtained for analysis, and, from this information, generalizations were made as to the behavior of drops in the presence of the different airfoil velocity fields.

### Description of Procedure Used to Obtain Water-Drop Trajectories

The five airfoil cases selected for the water-drop-trajectory investigation are listed in the following table:

| Case | Airfoil | Angle of attack (deg) | $c_l$ | Leading-edge radius (percent chord) |
|---|---|---|---|---|
| 1 | 15-percent-thick symmetrical Joukowski | 0 | 0 | 2.67 |
| 2 | Do | 2 | .22 | 2.67 |
| 3 | Do | 4 | .44 | 2.67 |
| 4 | 15-percent-thick cambered Joukowski | 0 | .44 | 2.67 |
| 5 | NACA $65_2$-015 (symmetrical) | 4 | .44 | 1.505 |

This table shows the systematic changes in the variables which affect velocity distribution. Cases 1, 2, and 3 were intended to reveal the effects of systemmatically altering airfoil velocity distribution by changing angle of attack; case 4, compared to cases 1

and 3, the effects of altering velocity distribution by the addition of a basic load distribution obtained by cambering the mean line; and cases 3 and 5, the effects of changing general airfoil shape for a given angle of attack and lift coefficient. The upper- and lower-surface velocity distributions over the forward region of each of the five airfoils are shown in figure 1. Velocity distributions for Joukowski airfoils are used where possible because the required velocity components in the field of flow are more readily obtained than for most other airfoils. It is noted in figure 1 that the variables selected did not result in a wide variety of velocity distributions, but it is believed that these distributions are of sufficient scope to allow a generalization of the trajectory data, at least for cases in which there are no marked nose-pressure peaks.

The water-drop-trajectory computations were made to encompass a speed range of 100 to 350 miles per hour (assuming incompressible flow), a drop-diameter range of 20 to 100 microns, and a variation in altitude from sea level to 20,000 feet. Airfoil chord length was varied from 3 inches to 30 feet. These variables were combined into the dimensionless parameters, $\psi$ and $R_V$, which then were used as the independent variables throughout the trajectory computations. The range in values of $\psi$ and $R_V$ resulting from a combination of each minimum value and a combination of each maximum value of the three constituent variables is about 150 to 20,000 for $\psi$ and about 35 to 1000 for $R_V$. These ranges in $\psi$ and $R_V$ encompass most other possible combinations of the selected values of speed, drop size, altitude, and chord length, but the data calculated for these ranges in $\psi$ and $R_V$ are not necessarily limited to the particular values of the constituent variables used to establish the ranges in $\psi$ and $R_V$.

The problem of obtaining area, rate, and distribution of water-drop impingement on an airfoil is one of determining the solution to a set of simultaneous differential equations yielding the trajectory or path which a water drop will follow. These equations, a derivation of which may be found in reference 5, are essentially those which result from imposing conditions of dynamic equilibrium on a drop moving in an air stream. In dimensionless form, the equations are

$$\frac{d(u_d/V)}{d\tau} = \frac{\psi}{R_V}\left(\frac{C_d R}{24}\right)\left(\frac{u_a}{V} - \frac{u_d}{V}\right) \tag{1}$$

$$\frac{d(v_d/V)}{d\tau} = \frac{\psi}{R_V}\left(\frac{C_d R}{24}\right)\left(\frac{v_a}{V} - \frac{v_d}{V}\right) \tag{2}$$

$$\left(\frac{R}{R_V}\right)^2 = \left(\frac{u_a}{V} - \frac{u_d}{V}\right)^2 + \left(\frac{v_a}{V} - \frac{v_d}{V}\right)^2 \tag{3}$$

Basically, equations (1) and (2) define the acceleration of a drop at any instant in orthogonal (x and y) directions. Consequently, a double integration of these equations, starting from a selected initial point $(x_o, y_o)$, yields x and y values necessary to plot a drop trajectory. Equation (3) is required to proceed with the solutions of equations (1) and (2). In performing the integrations, knowledge of the quantity $C_dR/24$ (the ratio of the actual drag coefficient given by Stokes law of resistance) is required; also required are magnitudes of the air-velocity components $u_a/V$ and $v_a/V$ as a function of drop location relative to the body. (See reference 5.) Variation of the term $C_dR/24$ with local Reynolds number R was taken from reference 6, while the variation of the air-velocity components $u_a/V$ and $v_a/V$ throughout the flow field was obtained analytically for the Joukowski airfoils. In the case of the NACA $65_2$-015 airfoil, however, the velocity distribution throughout the flow field was obtained by an electrolytic analogy method.[1]

In carrying out the differential analyzer computations for the five airfoil cases, the general procedure was to assign values to the terms $\psi$ and $R_V$ in equations (1), (2), and (3), to establish initial conditions, and then to obtain the water-drop-trajectory traces from the analyzer. For each combination of $\psi$ and $R_V$ selected, several trajectories were traced until the two trajectories were found, one for the upper surface and one for the lower surface, which were tangent to the airfoil surface at the point of drop impact. The importance of these two tangential trajectories lies in the fact that all drops between the tangential trajectories hit the airfoil and all drops outside will miss. In some cases, after the tangential trajectories were

[1]The electrolytic analogy method was based on the fact that the streamlines in an inviscid incompressible fluid and the equipotential lines in an electrical field are governed by the same equations. By means of this analogy and suitably constructed apparatus, velocities at any point in the flow field around a body could be measured directly. Accuracy of the electrolytic analogy method of obtaining velocities was assessed by comparing measured velocities with theoretically calculated values for two bodies. Comparisons were made for a small cylinder, with and without circulation, and for a 15-percent-thick Joukowski airfoil (of various chord lengths) with and without circulation. For optimum test conditions, the accuracy in velocities was about ±5 percent out to approximately one-half chord forward of the airfoil. Between one-half and one chord length forward of the airfoil, velocities could be obtained with an estimated accuracy of ±10 percent.

established, the distance between them was divided into six approximately equal spaces, and trajectories started at the boundary of each space were traced. These intermediate trajectories were used to obtain an indication of the distribution of water-drop impingement over the airfoil surface.

## Water-Drop-Trajectory Data

All the tangential trajectories, and the trajectories traced for distribution of impingement, are presented for the five airfoil cases in figures 2 through 6. The drop trajectories, which were calculated for assigned values of the independent variables $\psi$ and $R_V$ directly yield values of trajectory starting ordinates and surface positions of drop impingement. These variables, which, by the method of analysis shown in reference 1, can be used to determine the values of the dependent variables, area, rate, and distribution of impingement, are tabulated in tables I through V for each of the airfoil cases. Also included in the tables are the velocity components of the drops at the point of impingement.

## Manner in Which Water-Drop-Trajectory Data Were Generalized

The objective in generalizing the water-drop-trajectory data obtained from the differential analyzer is to establish a relatively simple method for determining the impingement pattern of water drops on an arbitrarily selected airfoil at a given attitude for specified values of $\psi$ and $R_V$. It is desirable that application of such a method should require only information which is usually available for the airfoil profile, or which is easily procured, such as the pressure distribution. Therefore, the first part of this section will present the reasoning associated with deriving such a method for incompressible flow from the results of the trajectory data; the latter part is devoted to an extension of the basic method to subsonic compressible flow.

Generalization in regard to area of water-drop impingement.- In order to determine the area of water-drop impingement on the leading edge of an airfoil for specified meteorological and flight conditions, the values of $s/c$ for the trajectories which impinge tangentially on the upper and lower surfaces must be obtained. In computational methods like those of references 3, 5, and 6, the procedure essentially has been to select values of $\psi$ and $R_V$ and then to determine the trajectory. Various trajectories are computed until the tangential trajectory for the upper and lower surfaces is found. The two

tangential trajectories located determine the farthest positions of drop impingement on the airfoil surface for the selected values of $\psi$ and $R_V$ and permit calculating area of impingement from the equation

$$A_s = \left[\left(\frac{s}{c}\right)_{u_t} - \left(\frac{s}{c}\right)_{l_t}\right] Lc$$

In the derivation of the empirical method, herein presented, the reverse procedure was employed; that is, a point on the airfoil was selected $(s/c)$ and the corresponding $\psi$ and $R_V$ values which are associated with the tangential trajectories at that point were determined. The nature of the relationship between $s/c$ and the parameters $\psi$ and $R_V$ is shown in figure 7. Data for the figure are those of table IV for the cambered airfoil at zero angle of attack and a lift coefficient of 0.44. From figure 7, it can be seen that any specified value of $s/c$ in the figure can correspond to an infinite number of combinations of $R_V$ and $\psi$. Consequently it becomes necessary to select values of one variable and to solve for the other. In the derivation of the method of this report, values of $R_V$ are assumed and corresponding values of $\psi$ are computed.

If the data of figure 7 could be made available for all airfoils of interest, the problem of determining $s/c$ for various values of $\psi$ and $R_V$ would, of course, be simple. Because obtaining such data for all airfoils is impractical, the problem in the general case arises in determining the relation between $R_V$, $\psi$, and $s/c$. To determine this relationship, equations (1), (2), and (3) are utilized to derive an expression for the scale modulus $\psi$, which is

$$\psi = \frac{a_d R_V}{\left(\frac{C_d R}{24}\right)\left(\frac{R}{R_V}\right)} \tag{4}$$

where

$$a_d = \sqrt{\left[\frac{d(u_d/V)}{d\tau}\right]^2 + \left[\frac{d(v_d/V)}{d\tau}\right]^2}$$

Equation (4) expresses generally the relation between $\psi$ and $R_V$ at all points in a trajectory, and, therefore, it is applicable at the airfoil surface for an arbitrarily selected value of $s/c$ which corresponds to some particular tangential trajectory. It remains to

establish the values of $C_dR/24$, $R/R_V$, and $a_d$ for the selected value of $s/c$. Actually, since $C_dR/24$ is a known function of $R$, the problem reduces to approximating $R/R_V$ and $a_d$ at the airfoil surface.

Evaluation of $R/R_V$ at airfoil surface: To determine $R/R_V$ the method of this report is based on a graphical solution utilizing the hodograph plane. It is in this connection that the trajectory data from the differential analyzer are plotted in the hodograph plane in figure 8 for each of the five airfoil cases. To show the general relation of drop velocities to air velocities, the hodograph of air at the airfoil surface is also shown for each case. It is interesting to note in figure 8 that the velocity components for all drops, regardless of the combination of $\psi$ and $R_V$, can be represented by one faired curve.[2] Of particular interest, however, is the fact that the hodograph for the drops, for both upper and lower airfoil surfaces, always passes through the point $u_d/V = \cos \alpha$, $v_d/V = \sin \alpha$. Thus, in the simplest case of an airfoil at zero angle of attack, the hodograph of the drops always passes through an abscissa value of unity because this point corresponds physically to the point of maximum airfoil thickness where straight-line tangential trajectories always impinge upon the airfoil with free-stream air velocity. The coordinates at the origin of the air and drop hodographs correspond physically, of course, to the airfoil stagnation point.

To show the connection between the results of the trajectory data for the five airfoil cases and the case of an arbitrary airfoil, figure 9 is presented. Figure 9(a) depicts several water-drop trajectories in the physical plane impinging tangentially at the same point $s/c$ on an airfoil which is at an angle of attack $\alpha$. These trajectories, for purposes of explanation, may be assumed to correspond to various points on a line of constant $s/c$ in figure 7. Accordingly, there is an infinite number of particular combinations

[2]An inspection of figure 8(e) will show that, for the upper surface of the NACA $65_2$-015 airfoil, the curve was not faired through all the data points. The reason is that the velocity components for some of the data points were in error. This can be shown by noting that every data point will not fall on a line connecting the origin and a point on the air hodograph having the same $s/c$ value as the data point. Each data point must lie on such a line because the slope of a trajectory tangential to the airfoil at some $s/c$ position and the slope of the airfoil at the same $s/c$ position are equal. The data points in figure 8(e) considered to be inconsistent with this criterion are designated with tag marks and are not heavily relied upon for establishing the drop hodograph.

of $\psi$ and $R_V$ which are affine to any particular position of tangential drop impingement $(s/c)_t$. In figure 9(a), a single vector representing the drop velocity for all the trajectories is drawn tangentially to the airfoil at the point of drop impingement. Only one vector is shown because the tangential trajectory hodographs presented in figure 8 indicate that all drops impinging tangentially at a common point may be considered to have the same velocity. Also shown in figure 9(a) is a vector representing the air velocity at the point of impingement for the trajectories. The angle between the drop- and air-velocity vectors and the $x$ axis is designated by the angle $\theta$. In figure 9(b), a typical air and drop hodograph is shown and the same vectors as shown in the physical plane are indicated. It should be noted that the difference in length of air and drop vectors at a particular $s/c$ position is numerically equal to the value of $R/R_V$ given by equation (3).

As can be seen from figure 8, all five airfoils exhibit the same characteristic in regard to the single-valued nature of the term $R/R_V$ with chordwise position, and it will be assumed that all other airfoils will display the same characteristic. However, in order to calculate values of $R/R_V$ for an arbitrary airfoil, both hodographs of the air and of the tangential trajectories are required. The hodograph of the air velocity at the airfoil surface is easily obtained from the velocity distribution over the airfoil, but the shape of the hodograph for the tangential trajectories is more difficult to obtain. This is because the data of figure 8 yield only the information that the tangential-trajectory hodograph always will pass through the point $u_d/V = 0$, $v_d/V = 0$ and the point $u_d/V = \cos\alpha$, $v_d/V = \sin\alpha$.

With two points on the trajectory hodograph always known, it was concluded that, if one more point could be established, preferably where the vertical-velocity component reaches the maximum value, the general shape of the trajectory hodograph would be reasonably ascertainable. It was noted from the hodographs in figure 8 that peak values of $v_a/V$ and $v_d/V$ were at nearly the same location on the airfoil surface. That is, values of $v_{a_{max}}/V$ and $v_{d_{max}}/V$ nearly always fall on a straight line through the origin, and it remains to determine just where on the line the value of $v_{d_{max}}/V$ will fall. In this connection, it was decided to compare, for the five airfoil cases, values of the vertical component of relative velocity between drop and air attained at the position of maximum vertical air velocity. Accordingly, values of $(v_{a_{max}}/V) - (v_{d_{max}}/V)$ and $v_{a_{max}}/V$ were obtained from figure 8 and these are plotted in figure 10. An inspection of the data in figure 10 shows that the four Joukowski airfoil cases provide data sufficient to establish a relation between $(v_{a_{max}}/V) - (v_{d_{max}}/V)$ and $v_{a_{max}}/V$; but too little

information is available for the NACA 65-series sections to firmly establish a relation between $(v_{a_{max}}/V) - (v_{d_{max}}/V)$ and $v_{a_{max}}/V$. The point plotted in figure 10 for the NACA $65_2$-015 airfoil upper surface does not lie on the curve established by the Joukowski airfoil data, and a question arises as to whether this difference is real or due to a possible improper fairing in figure 8(e) of the upper-surface drop hodograph. While this question cannot be resolved until further data are available, qualitatively it would seem that the drop velocities should tend to approach more nearly the air velocities in the case of low-drag airfoils because these shapes are not so conducive to abruptly altering the paths of water drops.

To show how figure 10 can be used as an aid in the construction of the drop hodograph for an airfoil of arbitrary profile and attitude, figure 11 is presented. The procedure is first to draw the air hodograph and establish $v_{a_{max}}/V$. Then, the maximum vertical velocity of the tangential-trajectory hodograph is determined as being less than $v_{a_{max}}/V$ by the amount $(v_{a_{max}}/V) - (v_{d_{max}}/V)$ in accordance with the curve in figure 10. The value of $v_{d_{max}}/V$ so determined is assumed to lie on a straight line connecting the origin and $v_{a_{max}}/V$. The position of $v_{d_{max}}/V$ along the radial line determines the value of $(R/R_V)_{v_{a_{max}}}$ at that particular position. Values of $R/R_V$ for other $s/c$ positions are taken, as a first approximation, as being in the same ratio to the air velocity at the particular $s/c$ position as the value of $R/R_V$ at $v_{a_{max}}/V$ is to $U_a/V$ at $v_{a_{max}}/V$ (curve A in figure 11). Values of $R/R_V$ calculated in this manner usually are too large near the point $u_d/V = \cos\alpha$, $v_d/V = \sin\alpha$ (point X, figure 11), so that a drop hodograph so constructed would probably not pass through this point as it should. To overcome this discrepancy in the drop hodograph as computed by a proportion based on the peak point of the air hodograph, a curve without reflex is faired tangentially into the proportional drop hodograph from the point $u_d/V = \cos\alpha$, $v_d/V = \sin\alpha$. The combination of the proportional curve and the faired curve comprises the drop hodograph, which is labeled curve B in figure 11. For the five airfoil cases, maximum deviations of the drop hodographs obtained by the foregoing method from the drop hodographs in figure 8 were of the order of 15 percent.

Two other methods were considered for establishing drop hodographs. One method assumed $R/R_V$ to maintain a constant value equal to the value prevailing at the point $u_d/V = \cos\alpha$, $v_d/V = \sin\alpha$.

The other method assumed the ratio $\frac{R/R_V}{U_a/V}$ to maintain a constant value determined by the value of $R/R_V$ and $U_a/V$ at the point $u_d/V = \cos\alpha$, $v_d/V = \sin\alpha$. The drop hodographs given by each of these two methods also are shown for the example in figure 11. The curves are labeled C and D, respectively. These two methods have the advantage of not requiring the use of the hodograph and figure 10; however, they are considerably more inaccurate (maximum deviations from the drop hodographs for the five airfoil cases being in the order of 30 percent) due to the neglect of factors of apparent influence on the drop trajectories. Use of either one of these latter two methods is suggested for particular airfoil cases which might happen to fall beyond the scope of the data presented in figure 10.

After the tangential-trajectory hodograph has been established in relation to the hodograph for air, values of $R/R_V$ are available for various chordwise positions on the airfoil. These values are used in equation (4) for arbitrarily selected values of $R_V$ and $s/c$. Since values of $R_V$ are arbitrarily selected, values of $R$ are ascertainable. Furthermore, values of the term $C_dR/24$ can be calculated because $C_dR/24$ is a function of $R$ in accordance with table VI. Thus, to solve equation (4), the only other term to be evaluated is $a_d$.

Evaluation of the drop-acceleration term $a_d$: The remaining term to be evaluated in equation (4) is the acceleration of the drop at the airfoil surface $a_d$. To determine the variation of this term with chordwise position, values of $a_d$ were calculated from the trajectory data by equation (4) for each of the airfoil cases presented in tables I through V. The procedure used in making the calculations was to compute the value of $R/R_V$ by utilizing values of the orthogonal drop-velocity components from tables I through V for corresponding values of $\psi$ and $R_V$. The term was calculable through knowledge of $R/R_V$ and $R_V$. The terms $R/R_V$, $C_dR/24$, $R_V$, and $\psi$ were then substituted into equation (4) and solved for $a_d$. The results of this procedure are presented in figure 12 for each of the five airfoil cases.

An inspection of figure 12 shows that drop acceleration at the surface of the airfoil, like the hodograph of drop velocities for tangentially impinging trajectories, can be considered a single relation regardless of the combinations of $\psi$ and $R_V$. How the singular nature of the acceleration values arises can be shown by rewriting equation (4) as follows:

$$a_d = \psi\left(\frac{C_d}{24}\right)\left(\frac{R}{R_V}\right)_t^2 \tag{5}$$

However, since the term $(R/R_V)_t$ is taken to be constant for a given position on the surface, equation (5) may be written

$$a_d = (\text{const})\ \psi C_d \tag{6}$$

where the constant depends on the chordwise position and the value of $(R/R_V)_t$ at that position. Thus, according to equation (6), it is apparent that, if the product of $\psi$ and $C_d$ remains constant for various values of $R_V$ at a given chordwise position, then the value of $a_d$ also will remain constant. Hence, to show the constancy of $a_d$ at various chordwise positions for various $R_V$ values, products of $\psi$ and $C_d$ were calculated for every combination of $\psi$ and $R_V$ presented in tables I through V for the five airfoils. The procedure used was to select a value of $R_V$ and to derive $C_d$ by using the value of $(R/R_V)_t$ noted on the hodograph for the $s/c$ position corresponding to the particular $R_V$ value chosen. The products of $\psi C_d$ were compared with other $\psi C_d$ products corresponding to the same physical point on the airfoil; but these latter products were calculated by using values of $\psi$ obtained from a plot of the tabulated values of $\psi$ and $s/c$ for various values of $R_V$. This procedure was adopted in order to obtain products corresponding to farthest positions of impingement not given directly in tables I through V. Comparisons of the products are made in tables VII through XI. These comparisons show that, for a given $s/c$ position, the product of $\psi$ and $C_d$ generally is of the same order of magnitude for a wide range of $\psi$ and $R_V$ values, particularly at the lower values of $s/c$. Therefore, the assumption that $a_d$ is constant for a particular chordwise position seems fairly well justified.

The problem of evaluating drop acceleration now has been reduced to finding, for a number of $s/c$ positions on the airfoil, a value of $a_d$ which corresponds to each $s/c$ value chosen.

In approximating the drop acceleration at a point where the drop trajectory is tangent to the airfoil surface, several procedures are possible, as was the case with the term $R/R_V$. Of the various procedures investigated, the one which will be presented herein is considered most acceptable because the resultant accuracy is commensurate with that produced by the most accurate procedure presented for obtaining $R/R_V$. In addition, the procedure is simple in application. For this procedure, the approximation is made that the tangential acceleration of a drop at a given point on the surface

is the same as the acceleration of the air along the airfoil surface at the same point.[3] The equation used to express the drop acceleration in terms of air velocity at the airfoil surface is:

$$a_d = \frac{U_a}{V} \times \frac{d(U_a/V)}{d(s/c)} \tag{7}$$

The velocity gradient term in equation (7) can be evaluated simply by plotting $U_a/V$ against $s/c$, and obtaining the slope of the resulting curve at the desired $s/c$ positions.

Results obtained by using equation (7) to approximate values of $a_d$ for the five airfoil cases are shown in figure 12 where the calculated point values are denoted by square symbols. It will be noted that equation (7) appears to provide good results for the symmetrical Joukowski airfoil case (fig. 12(a)), and over most of the lower surface of each of the other four airfoil cases (figs. 12(b), 12(c), 12(d), and 12(e)). For these latter four airfoil cases, equation (7) provides upper-surface drop-acceleration values toward the leading edge of the airfoil which appear in good agreement with the trajectory data; but farther aft, the ability of equation (7) to predict appropriate values diminishes appreciably, particularly for the Joukowski and NACA $65_2$-015 airfoils at $4^\circ$ angle of attack (figs. 12(c) and 12(e)). In these instances, the inability of equation (7) to yield drop acceleration values fairly far aft on the airfoil surface apparently is because the drops impinging in this region have sufficiently large inertia so as not to respond to the very rapid changes in surface-air velocities prevailing near the position of maximum air velocity. Except quite near the leading edge, the trajectories are fairly straight, indicating that the impinging drops do not respond appreciably to the vertical components of air velocity. Thus, it seemed that a suitable representation of drop acceleration for the case of an airfoil with a velocity peak located near the leading edge might be obtained by assuming that the

[3] Only the tangential component of drop acceleration needs to be approximated since the normal component of drop acceleration can be shown to be equal to zero at the point of drop impingement for tangential trajectories. That the normal acceleration of the drop is zero at the point of impingement can be shown by writing the equations expressing dynamic equilibrium of a drop. The terms involving the drop and air velocities are resolved normally and tangentially. A substitution of the boundary conditions at the point of impingement shows that the normal acceleration must equal zero at this point.

drop acceleration was influenced mostly by the $x$ components of air velocity. In equation (7), then $U_a/V$ would be replaced by $u_a/V$ so that

$$a_d = \frac{u_a}{V} \times \frac{d(u_a/V)}{d(s/c)} \tag{8}$$

Equation (8) was used to calculate additional drop-acceleration values for the upper surfaces of the airfoils presented in figure 12 and the results obtained are compared in these figures with drop acceleration values given by the trajectory data. The points calculated by equation (8) are shown as triangles in figure 12, and represent a good approximation of the upper surface $a_d$ values fairly far aft on these surfaces.

The question arises as to whether it would be possible in the general case, when the differential analyzer data points shown in figure 12 were not present, to detect the inadequacy of equation (7) to represent the correct values of $a_d$. In this connection it should be noted that the point on the curve for $a_d = 0$ can always be selected because this point corresponds to the chordwise position of the tangentially impinging straight-line trajectory having the maximum $s/c$ intercept. This particular trajectory can always be established by constructing a line tangent to the upper surface of the airfoil and parallel to the free-stream velocity. With this point located it would be quite evident that the square data points (equation (7)) in figure 12(e), for instance, could not represent the correct curve, and that equation (8) should be used to obtain additional points to provide a reasonable guide. The technique of fairing a curve, through calculated drop-acceleration values, to a value of zero acceleration at the extreme position of drop impingement can be used also for the lower surface of airfoils; but the technique can be applied only in those instances where the airfoil angle of attack is sufficiently low to permit a straight-line trajectory to impinge tangentially at some point on the airfoil surface.

Summary of calculation of scale modulus $\psi$ : The two preceding subsections have shown how the terms in equation (4) can be evaluated to obtain values of $\psi$ for selected $R_V$ values at chosen positions on the airfoil surface. However, a special procedure for evaluating $\psi$ at the stagnation point is necessary, since equation (4) cannot be used to evaluate the scale modulus at or very near the stagnation point. This procedure is more suitably discussed in connection with the section on rate of impingement which follows.

For a further verification of the calculation of scale modulus, appendix A includes a comparison of results of empirical calculations of farthest position of impingement with results obtained from formal solutions of the trajectory equations for five airfoils.

Generalization in regard to rate of impingement.- Another quantity of interest to the designer of an aircraft thermal-ice-prevention system is rate of drop impingement on an airfoil. An expression for weight rate of drop impingement per unit length of span, according to reference 7, is given by

$$M_s = 3600Vm\Delta y_{o_t}' \tag{9}$$

In order to evaluate the rate of impingement $M_s$, the term $\Delta y_{o_t}'$ must be known. When methods like those of references 3, 5, and 6 are employed, $\Delta y_{o_t}'$ can be determined directly from the calculated trajectories which impinge tangentially upon the airfoil. For an empirical procedure where no trajectories are available, however, determination of $\Delta y_{o_t}'$ must be based upon quantities which are known. Preceding sections have shown that $(s/c)_{u_t}$ and $(s/c)_{l_t}$ can be established as a function of $\psi$ for various values of $R_V$; hence, the airfoil ordinates corresponding to the farthest position of drop impingement on the upper and lower surfaces $y_{u_t}$ and $y_{l_t}$ also can be ascertained as a function of $\psi$ for various values of $R_V$. Because values of $y_{u_t}$ and $y_{l_t}$ can be obtained readily for a wide range of $\psi$ and $R_V$ values, the data were examined for a relationship involving $\Delta y_{o_t}$ (for small angles of attack, $\Delta y_{o_t}$ is approximately equal to $\Delta y_{o_t}'$) and the quantity $y_{u_t}-y_{l_t}$ which will be called $\Delta y_t$. In this regard, $\Delta y_{o_t}$ was compared to $\Delta y_t$ over the range of $\psi$ and $R_V$ values presented in tables I through V for the five airfoil cases. The results are shown in figure 13.

An inspection of figure 13 shows that, for each airfoil, the ratio of $\Delta y_{o_t}$ to $\Delta y_t$ can be considered linear with respect to the log of the scale modulus $\psi$ for various $R_V$ values. The linearity exists for values of $(\Delta y_o/\Delta y)_t \leq 0.8$ for the Joukowski airfoils, and a value of $(\Delta y_o/\Delta y)_t \leq 0.9$ for the NACA $65_2$-015 airfoil; but this linearity appears to be characteristic only of airfoils as cylinder data from reference 6, when plotted in the same manner, do not show this property. In figures 13(c) and (e), the ratio noticeably exceeds unity, the reason being that the projected frontal height h (equal to $\Delta y_{o_t}'$ for the limiting case of straight-line trajectories) exceeds the airfoil maximum thickness when the airfoil

angle of attack is other than zero. Of special interest in figure 13, however, is the fact that the ratio $(\Delta y_o/\Delta y)_t$ must become zero at some particular value of $\psi$ for a given value of $R_V$. This "critical" value of $\psi$ can be calculated from an aerodynamic property of the airfoil. According to reference 6, for symmetrical bodies at zero angle of attack, the critical value of $\psi$ (i.e., values greater than that for which no drops impinge on the body) is given by

$$\psi_{cr} = 4R_V \left.\frac{\partial(u_a/V)}{\partial x}\right|_{\Psi=0} \tag{10}$$

For symmetrical bodies at an attitude other than 0°, or for unsymmetrical bodies at an arbitrary attitude, the same form of equation (10) applies, but with the notation slightly altered, thus

$$\psi_{cr} = 4R_V \left.\frac{\partial(U_a/V)}{\partial S}\right|_{\Psi=0} \tag{11}$$

This change is made because the small drop which just impinges at the stagnation point of the airfoil closely follows the stagnation streamline which, in the general case, is not a straight line. For simplicity, though, equation (11) shall be written

$$\psi_{cr} = 4R_V G \tag{12}$$

In order to use equation (12), the problem presents itself of assigning a value of G for the case of an aribtrary airfoil. Fortunately, the problem is relieved by the fact that the answers sought, s/c and E, are effected only in a minor way by variations in G.[4] Thus, it was believed that for determining G the airfoil could be replaced by a shape more amenable to calculation. It was assumed that a symmetrical Joukowski airfoil would be representative of that type section having maximum thickness fairly well forward, and an ellipse representative of that type section having maximum thickness well aft (low-drag airfoils). Since the major factors influencing the value of G are thickness and angle of attack,

[4]Calculations have shown that negligible changes in s/c and E are incurred for a change in G as large as 10 percent.

calculations of G were made for a symmetrical Joukowski airfoil and an ellipse of different thickness and lift coefficients.[5] The results of these calculations are presented in figure 14. The data in 14(a) are intended for use with airfoils resembling Joukowski airfoils, and may be used directly. The data in figure 14(b) are intended for use with low-drag profiles; however, it is first necessary to establish an "equivalent ellipse" thickness ratio for the low-drag section being used. An equivalent ellipse is defined for the purposes of figure 14(b) as an ellipse having its leading-edge radius equal to the leading-edge radius of the airfoil, and a thickness equal to the airfoil maximum thickness. The major axis of the ellipse is thus established, and the ellipse thickness ratio can be computed. An equation expressing the thickness ratio of the equivalent ellipse in terms of the airfoil leading-edge radius and thickness ratio is:

$$t_e = \frac{2\rho}{t_{max}} \tag{13}$$

With the aid of figure 14, the value of $\psi_{cr}$ for a large number of airfoils can be estimated for any $R_V$ value in accordance with equation (12). Not only does this value correspond to the condition of zero rate of impingement, but it corresponds to the condition of zero area of impingement. Hence, the critical value of $\psi$ can be used for obtaining an additional point for area of impingement computations, and this value will correspond to the s/c value at the stagnation point.

While the condition of no drops impinging on the airfoil surface yields one point on the curves, $(\Delta y_o/\Delta y)_t$ versus log $\psi$, at least one more point is required for each value of $R_V$ in order to establish the linear relationships observed in figure 13. To locate a second point on an isopleth of $R_V$, it is desirable to determine a value of $\psi$ corresponding to a chosen value of $(\Delta y_o/\Delta y)_t$ somewhat less than unity. The reason for this specification is to procure a spread in the values of $(\Delta y_o/\Delta y)_t$ used to establish the linear relationships between $(\Delta y_o/\Delta y)_t$ and log $\psi$, for isopleths of $R_V$ which were noted in figure 13.

[5]No account is taken of the effect of a cambered profile on the velocity gradient G. The reason for this is that tests with an electrolytic tank have shown that the effects of camber are very small in comparison with the effects of thickness, and calculations have shown that only large variations in G are important in affecting the values of s/c and E.

In developing a procedure for determining what value of $\psi$ is associated with a specified value of $(\Delta y_o/\Delta y)_t$ on an isopleth of $R_V$, the data from the five airfoil cases were examined for values of some parameter, related to $(s/c)_{u_t}$ and $(s/c)_{l_t}$, which could be used to fix the value of $\psi$. The parameter used to supply the necessary values was the efficiency of drop impingement E. The relationship between E and $(\Delta y_o/\Delta y)_t$ is given by

$$E = \left(\frac{\Delta y_o}{\Delta y}\right)_t \left(\frac{\Delta y_t}{t_{max}}\right) \tag{14}$$

Equation (14) can be derived by starting from the definition of E in terms of the initial drop trajectory ordinates

$$E = \frac{\left(y_{o_u}' - y_{o_l}'\right)_t}{h} = \frac{\Delta y_{o_t}'}{h} \tag{15}$$

At the small angles of attack associated with most flight conditions, h in equation (15) can be replaced by $t_{max}$ and $\Delta y_{o_t}'$ by $\Delta y_{o_t}$ so that

$$\Delta y_{o_t} = E t_{max} \tag{16}$$

Then, if both sides of equation (16) are divided by $\Delta y_t$ and the terms rearranged, equation (14) is obtained.

The trajectory data for the five airfoil cases provided, for different values of $R_V$, relatively constant values of E corresponding to a value of[6] $(\Delta y_o/\Delta y)_t = 0.8$. These efficiency values were

[6]The procedure utilized was to determine from curves of $(\Delta y_o/\Delta y)_t$, as a function of $\psi$ (fig. 13), the value of $\psi$ at which $(\Delta y_o/\Delta y)_t = 0.8$ for different values of $R_V$. Then, data from tables I through V were used to establish curves of E as a function of $\psi$ for the same values of $R_V$. On the efficiency curves, the value of E corresponding to $(\Delta y_o/\Delta y)_t = 0.8$ for a particular value of $R_V$ could be determined by locating, for the same $R_V$ value, the value of $\psi$ which was established from curves of figure 13 to correspond to $(\Delta y_o/\Delta y)_t = 0.8$.

used to obtain an average efficiency value for each airfoil case. Then, by using equation (14), an average value of $\Delta y_t/t_{max}$ could be computed for each airfoil case by using the average efficiency values and a value of $(\Delta y_o/\Delta y)_t = 0.8$. The results are presented in the following table:

| Case number | Efficiency of impingement, E (percent) | | | | | | | | | $\frac{\Delta y_t}{t_{max}}$ |
|---|---|---|---|---|---|---|---|---|---|---|
| | $R_V$ | | | | | | | | Average value for each case | |
| | 16 | 32 | 64 | 128 | 256 | 512 | 1024 | 2048 | | |
| I | -- | 77.5 | -- | 77.0 | -- | 75.5 | -- | 78.0 | 77.0 | 0.963 |
| II | 76.0 | -- | 74.5 | -- | 75.5 | -- | 77.5 | -- | 75.8 | .948 |
| III | 72.0 | -- | 73.0 | -- | 72.0 | -- | 70.5 | -- | 71.8 | .898 |
| IV | 77.0 | -- | 82.0 | -- | 86.0 | -- | 82.0 | -- | 81.7 | 1.022 |
| V | 55.0 | -- | 59.0 | -- | 56.5 | -- | 55.0 | -- | 56.4 | .705 |

The values of $\Delta y_t/t_{max}$ tabulated in the preceding table exhibit some variation between airfoil cases, and figure 15 is presented to show this variation when $\Delta y_t/t_{max}$ is assumed to be a function only of angle of attack. In figure 15, a curve is presented for the Joukowski airfoils, but not for the NACA $65_2$-015 airfoil because the trajectory data provides only one point. Until additional information is available on the variation of $\Delta y_t/t_{max}$ with angle of attack, it is recommended that the variation shown in figure 15 be used. It is possible, then, to determine, for a given value of $R_V$, an approximate value of $\psi$ at which $(\Delta y_o/\Delta y)_t = 0.8$. The procedure which may be used for determining this value of $\psi$ is shown graphically in figure 16. From curves of $(s/c)_{u_t}$ and $(s/c)_{l_t}$ as a function of log $\psi$ for a specified value of $R_V$ (fig. 16(a)), curves of $y_{u_t}$ and $y_{l_t}$ as a function of log $\psi$ are established for the same value of $R_V$ (fig. 16(b)). For the relation shown by figure 16(b), there is a value of $\Delta y_t/t_{max}$ which is the same as the one chosen from the relation in figure 15 corresponding to the airfoil angle of attack. This particular value of $\Delta y_t/t_{max}$ corresponds to the $\psi$ value at which $(\Delta y_o/\Delta y)_t = 0.8$ for the particular $R_V$ value chosen (fig. 16(c)), and the second point on an isopleth of $R_V$ for $(\Delta y_o/\Delta y)_t$ as a function of log $\psi$ is thereby determined.

The previous discussion has shown how values of $\Delta y_{o_t}$ may be obtained for various $\psi$ and $R_V$ values. However, in the design of a thermal ice-protection system, by the method discussed in reference 1, it is sometimes more convenient to determine the rate of water-drop impingement by using the airfoil collection efficiency E rather than by using the term $\Delta y_{o_t}'$. In such circumstances, equation (9) becomes

$$M_s = 3600\ V_m\ E\ t_{max}$$

wherein E is given by equation (14). When equation (14) is used and the angle of attack is other than zero, the limit efficiency value corresponding to straight-line trajectories will be greater than unity because h usually is somewhat greater than $t_{max}$.

Appendix A includes a comparison of results of calculations of efficiency of impingement by the empirical method of this report with results obtained from formal solutions of the trajectory equations for the five airfoil cases.

Generalization in regard to distribution of impingement.- Of secondary importance in the design of heated wings is the distribution of water-drop impingement over the length of interception along the airfoil surface. However, knowledge of distribution of water drops over an airfoil is sometimes quite useful and, therefore, a discussion of the subject is believed worthwhile.

An examination of the trajectory data did not reveal any direct way to obtain an empirical functional relation between impingement distribution, scale modulus, and free-stream-drop Reynolds number. Therefore, a graphical construction was resorted to in order to approximate the distribution of drop impingement over an airfoil surface. That a graphical procedure could be used in this manner was found by examining plots of the concentration factor[7] C as a function of s/c for various combinations of $\psi$ and $R_V$. Typical variations of these factors are presented in figure 17 calculated from data for the five airfoil cases. For each of the airfoil cases presented in figure 17, two curves represented by solid lines are shown. One curve is typical for combinations of $\psi$ and $R_V$ corresponding to curved trajectories, and the other curve is typical for the combination of $\psi$ and $R_V$ corresponding to straight-line trajectories ($\psi$=0, value of $R_V$ arbitrary). The curve for $\psi$=0 is obtained by drawing a number of straight-line trajectories to the airfoil to obtain values of the concentration factor, $C = dA_o/dA_s$, and represents the locus of maximum possible values of C. This curve, which will be referred to as a limit curve, can always be obtained for a given airfoil because

[7]The use of the concentration factor C in the computation of heat requirement due to drop impingement is discussed in reference 1.

straight-line trajectories can always be reproduced, but the curves for values of C less than maximum cannot be obtained because the shapes of the curved trajectories corresponding to these values cannot be determined. Because of the shape of the C distribution curves noted for the five airfoil cases in figure 17, a triangular distribution has been found useful to represent approximately the distribution curves for curved trajectories. If a triangular distribution is assumed, as shown by a dashed line for each of the airfoil cases in figure 17, the following equation may be written for the maximum value of C on the triangular distribution:

$$\int_{s_{l_t}}^{s_{u_t}} C ds = \frac{1}{2} C_{max} \left(s_{u_t} + s_{l_t}\right)$$

from which

$$C_{max} = \frac{\int_{s_{l_t}}^{s_{u_t}} C ds}{\left(s_{av}\right)_t} \tag{17}$$

The denominator of equation (17) can be evaluated from the curves of farthest positions of tangential drop impingement. The numerator may be evaluated from the equation

$$\int_{s_{l_t}}^{s_{u_t}} C ds = Eh \tag{18}$$

so that

$$C_{max} = \frac{Eh}{\left(s_{av}\right)_t} \tag{19}$$

That the relation expressed in equation (18) exists can be shown by recalling from equations (9) and (15) that the total weight rate of drop impingement on an airfoil may be written as

$$M_s = 3600 \, Vm \, Eh \tag{20}$$

Equation (20) may also be written as the summation, between the farthest positions of impingement, of the local weight rates of impingement per unit surface area, thus

$$M_s = \int_{s_{l_t}}^{s_{u_t}} M_a ds \tag{21}$$

According to reference 1, $M_a$ in equation (21) can be expressed by

$$M_a = 3600\ VmC \tag{22}$$

where

$$C = dA_o/dA_s \tag{23}$$

By substitution of the value of $M_a$ from equation (22) into equation (21), the result is obtained that

$$M_s = 3600\ Vm \int_{s_{l_t}}^{s_{u_t}} Cds \tag{24}$$

Then, by comparing equations (20) and (24), equation (18) can be obtained.

Use of equation (19) permits the calculation of $C_{max}$ for a triangular distribution because all the terms of the right-hand member are known. The value of $C_{max}$ is taken to be on a line connecting the points $C=1.0$, $s/c=0$, and $C=0$, and $s/c$ for the stagnation point. The reason for this assumption is that the very large drops are very little deviated from their paths, and the very small drops tend to follow the stagnation streamline.

The value of $C_{max}$ obtained from equation (19) always will be low. However, if the triangular approximation is altered to correspond more nearly to the shape of the limit curve for the $C$ values, while retaining the enclosed area the same as the triangular area, more accurate concentration-factor values can be obtained. The altering of the curve is an attempt to establish the locus of concentration-factor values as it would be given by data obtained for calculated trajectories.

Generalization in regard to calculating area and efficiency of impingement at high subsonic speeds.– With the advent of airplanes in the 500 to 600 miles per hour speed range, considerable interest has been shown in the effects which compressibility may have on area and rate of drop impingement.

The differential analyzer computations for the five airfoil cases of this study were made to encompass airspeeds up to about 350 miles per hour on the basis that any effects of compressibility could be neglected. Consequently, no corrections to the velocity field were introduced for any of the airfoils to account for compressibility. However, for higher speeds, the effects of compressibility would be expected to become more pronounced and some method of taking compressibility into account should be considered.

The effects of compressibility: In compressible flow below the critical Mach number, streamlines at a large distance forward of the airfoil have nearly the same shape as for incompressible flow. Nearer the airfoil, deviations of the compressible flow streamlines from the incompressible flow streamlines are greater (reference 8). Thus, in compressible flow, drops may be considered to start at infinity at the same initial conditions as they would for incompressible flow, but terminate on the airfoil surface at velocities governed by the local compressible-flow surface-air velocities. These velocities are, in general, higher than corresponding incompressible-flow velocities; therefore, compressibility may have some effect on farthest position and efficiency of drop impingement.

If it is presumed that drops in compressible flow react to a change in surface-air velocities (due to changes in flow field arising from compressibility) in much the same manner as drops react to changes in flow field caused by a change in airfoil basic thickness, load distribution, or angle of attack, the same general procedure used to calculate farthest position and rate of impingement for incompressible flow can be applied to the calculations for compressible flow.

To obtain the air hodograph for compressible flow when experimental data are not available, the equation

$$\left(\frac{U_a}{V}\right)_M = \left[1 + \frac{1-(1 + 0.7025M^2C_{P_M})^{0.2883}}{0.2025M^2}\right]^{1/2} \tag{25}$$

(taken from reference 9) may be used to evaluate the magnitude of the velocity vectors. The pressure coefficient, $C_{P_M}$, in equation (25) can be calculated using the Prandtl-Glauert equation

$$C_{P_M} = \frac{1}{\beta} \times C_p$$

where

$$\beta = \sqrt{1-M^2}$$

and $C_p$ is the pressure coefficient at a point on the airfoil surface when the flow is incompressible. The pressure coefficient $C_p$ is related to the surface-air velocity at the same point on the surface by the equation

$$C_p = 1-\left(\frac{U_a}{V}\right)^2 \tag{26}$$

Values of $U_a/V$ used in equation (26) to calculate various values of $C_p$ are the same as those used to establish the air hodograph for incompressible flow.

Effect of compressibility on the farthest position and efficiency of drop impingement: Because of incompressible-flow hodograph is altered to another shape for compressible flow, the drop hodograph also will be modified, utilizing the procedure developed for the incompressible case. The changes in the drop and air hodographs in turn alter the values of $a_d$ and $(R/R_V)_t$ at points along the airfoil surface. According to equation (4), if changes in $a_d$ and the product $(R/R_V)_t$ $(C_dR/24)$ are not proportionate, the scale modulus will be altered for given $(s/c)_t$ and $R_V$ values. To show the effect of compressibility on the scale modulus, some calculations of farthest position and efficiency of drop impingement were made for the 15-percent-thick Joukowski airfoil at zero lift and $M=0.6$ (which is near the critical value). A value of $R_V=225$ was chosen for the calculations (430 mph, 15,000 ft, 0° F, and drop diameter of 25 microns). The results of these computations are compared in figure 18 with empirical results for incompressible flow. Figure 18(a), which presents the farthest position of drop impingement as a function of scale modulus, shows that the scale modulus has been increased slightly over most of the range in $(s/c)_t$ for the isopleth of $R_V$ chosen. This result is equivalent to the farthest position of impingement being increased from the value of $(s/c)_t$ corresponding to the same $\psi$ and $R_V$ value in incompressible flow. For the conditions chosen, the increase in farthest position of impingement is small and, for most practical purposes, may be neglected. Figure 18(b) shows that compressibility also slightly increases impingement efficiency. This result can be explained by equation (14) which indicates that increases in E are effected by increases in either the value of $(\Delta y_o/\Delta y)_t$ or $\Delta y_t$, or both. Increases in the values of both of these terms, for given $\psi$ and $R_V$ values, occur

for increased values of farthest position of impingement, and hence impingement efficiency is increased. The increase in efficiency due to compressibility for the same airfoil also is small and, like the increases in farthest position of drop impingement, may be neglected for most practical purposes. It should be noted, though, that the computations for farthest position and efficiency of impingement were made for a relatively low Mach number (0.6), and that somewhat larger changes in both parameters for given $\psi$ and $R_V$ values may be possible for airfoils having appreciably higher critical Mach numbers. However, it is suggested that the empirical method as applied to compressible flow not be used for airfoil sections having high critical Mach numbers (0.9) in view of the fact that no data exist for giving validity to the extrapolation of the method of this report to compressible flow.

## PROCEDURE FOR USING THE METHOD TO CALCULATE AREA, RATE, AND DISTRIBUTION OF WATER-DROP IMPINGEMENT ON AN ARBITRARY AIRFOIL

Previous sections have shown how the empirical method of this report may be applied to determine area, rate, and distribution of impingement for an arbitrary airfoil in either incompressible or compressible flow. The procedure to be followed in using the method will now be explained by means of an example of the computations in the case of an NACA 23015 airfoil, in incompressible flow, at $c_l=0.5$. The detailed computation procedure in this example is arranged in a form believed to be most readily usable; and the various phases of the computations are presented in a step-wise manner, each phase consisting of several operations for ease in following the procedure. The procedure for compressible flow is nearly the same as for incompressible flow, hence, only the procedure for incompressible flow is illustrated. However, where differences in procedure would occur for the case of compressible flow, these are noted.

### Area of Impingement

The procedure for calculating area of impingement consists primarily in determining values of $(s/c)_{u_t}$ and $(s/c)_{l_t}$. The following steps explain how the empirical relations derived from the trajectory data are used to determine these values, and figure 19 incorporates necessary accompanying graphical relationships.

Step 1: The following curves are needed for use during the computation procedure:

(a) A large-scale plot of the airfoil (fig. 19(a))

(b) A plot of $s/c$ versus $x$ for both upper and lower surfaces (fig. 19(b))

(c) A plot of $k$ for various $x$ positions (fig. 19(c))

(d) Chordwise distribution of incompressible-flow air velocities over the airfoil surface (fig. 19(d))

Step 2: Construction of the air hodograph:

(a) On a coordinate system using vertical air-velocity components as ordinates and horizontal velocity components as abscissas, measure values of air velocity as vectors emanating from the origin. (These values are obtained from the velocity distribution (fig. 19(d)) established in step 1(d)). The slope of the velocity vectors with respect to the horizontal axis is determined by the shape-factor curve established in step 1(c). Figure 19(e) illustrates this step for the NACA 23015 airfoil.

(b) Connect the end points of all vectors noting that the envelope curve (the hodograph) passes through the origin for the physical coordinates corresponding to the stagnation point. Refer to figure 19(e) for illustration.

(c) For compressible flow over a straight wing below the critical Mach number, compute the velocities for the air hodograph from

$$\left(\frac{U}{V}\right)_M = \left[1 + \frac{1-\left(1+0.7025M^2C_{P_M}\right)^{0.2883}}{0.2025M^2}\right]^{1/2}$$

Step 3: Construction of drop hodograph:

(a) From the hodograph established in step 2(b) (incompressible flow) or step 2(c) (compressible flow), note the maximum value of vertical air-velocity component $v_{a_{max}}/V$ for both upper and lower surfaces. For the NACA 23015 airfoil, the air hodograph shows that $v_{a_{max}}/V$ for

the upper surface is 0.915 and for the lower surface, 0.39.

(b) Using figure 10, determine the value of $(v_{a_{max}}/V) - (v_{d_{max}}/V)$ for both surfaces. A subtraction of $(v_{a_{max}}/V) - (v_{d_{max}}/V)$ from $v_{a_{max}}/V$ will yield the vertical location of $v_{d_{max}}/V$. Project $v_{d_{max}}/V$ horizontally for each surface until it intersects the ray connecting the origin and $v_{a_{max}}/V$. In this manner, the value of $(R/R_V)_t$ corresponding to $v_{a_{max}}/V$ is determined graphically. In the case of the NACA 23015 airfoil, $(v_{a_{max}}/V) - (v_{d_{max}}/V)$ for the upper surface is 0.245 and for the lower surface, 0.068. These values are measured from the air hodograph (fig. 19(f)) to provide values of $(R/R_V)_t$ corresponding to upper and lower surface values of $v_{a_{max}}/V$.

(c) Establish the vector passing through the origin and inclined with the horizontal axis at an angle equal to the airfoil angle of attack. The length of this vector is made equal to unity (fig. 19(f)).

(d) For both airfoil surfaces, establish an approximate tangential-trajectory hodograph which follows the equation

$$\frac{U_d}{V} = \left(\frac{U_d}{V}\right)_{v_{a_{max}}} \times \frac{U_a/V}{(U_a/V)_{v_{a_{max}}}} \tag{27}$$

The hodograph determined by equation (27) for the upper surface of the NACA 23015 airfoil is designated as curve A in figure 19(g) and as curve B for the lower surface. When equation (27) provides, for either the upper or lower surface, a drop hodograph which fails to pass through the point $u_d/V = \cos\alpha$, $v_d/V = \sin\alpha$ (point X in fig. 19(g)), a curve should be faired from point X to connect tangentially with the approximate drop hodograph as determined by equation (27). In the example case, neither the upper nor lower surface drop hodographs passes through point X, and therefore curves are faired from this point to the approximate drop hodographs. The faired curves are labeled C and D in figure 19(g) for the upper and lower surfaces, respectively. For the upper surface, the approximate drop hodograph almost passes through point X, so little difficulty is experienced in fairing a connecting curve. However, for the lower surface, the approximate drop hodograph deviates considerably from point X leaving a larger latitude for fairing a curve from this point than was the

case for the upper surface. In this instance, the contour of the air hodograph was followed as a guide in fairing a curve from point X to the approximate drop hodograph. The combination of curves A and C for the upper surface, and curves B and D for the lower surface, comprise the resultant tangential-trajectory hodograph for each surface.

(e) Convert the $x$ values used in the air hodograph of figure 19(e) to $s/c$ values by utilizing the relationship in figure 19(b) between $x$ and $s/c$. This step is shown also in figure 19(g).

(f) Measure the values of $(R/R_V)_t$ as determined by the drop and air hodographs in figure 19(g) and plot these values against their corresponding $s/c$ positions. This step is performed in figure 19(h) for the upper and lower surfaces of the NACA 23015 airfoil.

Step 4: Calculation of drop-acceleration values at the airfoil surface.

(a) Use the air-velocity distribution over the airfoil surface (fig. 19(d)) and the relation between $x$ and $s/c$ (fig. 19(b)) to establish the relation required between $U_a/V$ and $s/c$ for both upper and lower surfaces. Equation (7) then can be used to calculate values for $a_d$. Values obtained for $a_d$ by equation (7) are plotted against their respective surface positions $s/c$, and this is done in figure 19(i) for the upper and lower surfaces of the NACA 23015 airfoil.

(b) Include in the plot of $a_d$ versus $s/c$ (fig. 19(i)) the value of $s/c$ at which $a_d$ is zero on each surface. The value of $s/c$ at which $a_d$ is zero corresponds to the extreme position of tangential drop impingement on the airfoil surface. For each surface, the extreme position of drop impingement can be obtained by drawing two straight-line trajectories in the free-stream direction, one tangent to the airfoil upper surface and the other tangent to the lower surface. The point of tangency for each straight-line trajectory defines the $s/c$ value corresponding to an $a_d$ value of zero. For the NACA 23015 airfoil at a lift coefficient of 0.5, the extreme position of impingement on the upper surface is at $s/c=23.0$ and on the lower surface, at $s/c=53.0$.

(c) For each surface, fair a curve through the calculated values of $a_d$ to the value of $s/c$ found in step 4(b) corresponding to $a_d$ of zero. This step is also performed in figure 19(i). On the upper surface, values of $a_d$ given by equation (7) were considered in error over a small range of $s/c$ near the peak in the velocity distribution curve (fig. 19(d)), and consequently little weight was given the points in this region when extending the faired curve to $a_d=0$ at the extreme position of drop impingement. A few additional points can be calculated by equation (8) to aid in the fairing of the drop-acceleration curve, but since in this example the extreme position of impingement is fairly far forward $(s/c = 23.0)$ and equation (7) will yield positive $a_d$ values for $s/c$ values as far aft as 11 percent, use of equation (8) was deemed unnecessary.

Step 5: Computation of scale moduli corresponding to arbitrarily selected values of farthest position of impingement.

(a) Using drop-acceleration values obtained from figure 19(i) of step 4 and $(R/R_V)_t$ values from figure 19(h) of step 3, calculate values of scale modulus $\psi$ from equation (4). The computations are made for arbitrarily selected values of $R_V$ and $s/c$. Values of $C_dR/24$ required for solving equation (4) can be obtained from interpolation of the data presented in table VI, or preferably from a semi-logarithmic plot of the data. A small range of tabulated $C_dR/24$ values, including the values involved in the computation of $\psi$ for the NACA 23015 airfoil is shown graphically in figure 19(j). The computations of $\psi$ for the NACA 23015 airfoil are shown in the following table:

CALCULATION OF SCALE MODULI FOR CHOSEN AREAS OF IMPINGEMENT AND DIFFERENT $R_V$ VALUES

| s/c | $a_d$ | $a_d R_V$ | $(R/R_V)_t$ | R | $\frac{C_d R}{24}$ | $\left(\frac{R}{R_V}\right)_t \times \frac{C_d R}{24}$ | $\psi$ |
|---|---|---|---|---|---|---|---|
| $R_V=10$ | | | | | | | |
| UPPER SURFACE | | | | | | | |
| 5 | 8.6 | 86 | 0.365 | 3.65 | 1.42 | .518 | 166 |
| 10 | 2.8 | 28 | .405 | 4.05 | 1.45 | .586 | 48 |
| 15 | 1.0 | 10 | .412 | 4.12 | 1.46 | .600 | 17 |
| 20 | .2 | 2 | .405 | 4.05 | 1.45 | .586 | 4 |
| LOWER SURFACE | | | | | | | |
| 5 | 2.7 | 27 | 0.10 | 1.0 | 1.17 | 0.117 | 231 |
| 10 | 1.0 | 10 | .12 | 1.2 | 1.20 | .144 | 70 |
| 20 | .6 | 6 | .10 | 1.0 | 1.17 | .117 | 51 |
| 30 | .35 | 3.5 | .085 | .85 | 1.14 | .097 | 36 |
| 40 | .17 | 1.7 | .072 | .72 | 1.13 | .081 | 21 |
| 45 | .10 | 1.0 | .070 | .70 | 1.12 | .078 | 13 |
| $R_V=100$ | | | | | | | |
| UPPER SURFACE | | | | | | | |
| 5 | 8.6 | 860 | 0.365 | 36.5 | 2.88 | 1.05 | 819 |
| 10 | 2.8 | 280 | .405 | 40.5 | 3.00 | 1.21 | 230 |
| 15 | 1.0 | 100 | .412 | 41.2 | 3.02 | 1.24 | 80 |
| 20 | .2 | 20 | .405 | 40.5 | 3.00 | 1.21 | 16 |
| LOWER SURFACE | | | | | | | |
| 5 | 2.7 | 270 | 0.10 | 10 | 1.80 | 0.180 | 1500 |
| 10 | 1.0 | 100 | .12 | 12 | 1.90 | .228 | 439 |
| 20 | .6 | 60 | .10 | 10 | 1.80 | .180 | 333 |
| 30 | .35 | 35 | .085 | 8.5 | 1.72 | .146 | 240 |
| 40 | .17 | 17 | .072 | 7.2 | 1.64 | .118 | 144 |
| 45 | .10 | 10 | .070 | 7.0 | 1.63 | .114 | 88 |

Step 6: Establishing the curves of farthest position of impingement.

(a) Plot the values of $\psi$ calculated in step 5 against the corresponding values of s/c as ordinates for isopleths

of $R_V$. Use a semilogarithmic scale, plotting the ordinates arithmetically. This is done for the NACA 23015 airfoil in figure 19(k).

(b) On the plots of $s/c$ begun in step 6(a), denote by lines drawn at constant $s/c$ values the value of extreme position of drop impingement on each upper and lower surface. For the NACA 23015 airfoil, at a lift coefficient of 0.5, the extreme positions of impingement have been found in step 4(b) as being at $s/c=23.0$ on the upper surface, at $s/c=53.0$ on the lower surface.

(c) Calculate from equation (12) the critical-scale modulus value for each isopleth of $R_V$. The value of $G$ required to evaluate equation (12) for either incompressible or compressible flow can be obtained from figure 14. The value of $\psi_{cr}$ calculated for a given value of $R_V$ corresponds to $s/c$ at the stagnation point. Values of $\psi_{cr}$ calculated from equation (12) for different values of $R_V$ also should be plotted on the graph of farthest position of impingement (fig. 19(k)) begun in step 6(a). Since the NACA 23015 airfoil can be considered to have the same type of profile as Joukowski airfoils, figure 14(a) is used to obtain a value of $G$ for evaluating equation (12). For a value of $c_l=0.5$ and a thickness ratio of 0.15, figure 14(a) shows the value of $G$ to be 37.5. When this value of $G$ is used in equation (12), $\psi_{cr}$ has the following values:

| $R_V$ | $\psi_{cr}$ |
|---|---|
| 10 | 1500 |
| 100 | 15000 |

(d) For each isopleth of $R$, fair a curve through the values of $s/c$ plotted in steps 6(a) and 6(c) (fig.19(k)). These curves should approach asymptotically, as a limiting value, the farthest position of drop impingement for the upper and lower airfoil surfaces. Figure 19(k) then may be used for design purposes by determining the values of $(s/c)_u$ and $(s/c)_l$ for particular values of $\psi$ and $R_V$.

## Rate of Impingement

The procedure for the determination of the total rate of impingement, as has been explained in reference 1, consists of summing the rate of water-drop impingement for each of the drop sizes in an assumed

drop-size distribution. This is possible for each size of drop by use of the equation:

$$M_s = 3600\ EV\ my_{max}$$

The values of $V$, $m$, and $y_{max}$ are directly obtainable from a knowledge of the nature of the icing conditions and the airfoil shape. The procedure for calculating efficiency of impingement consists essentially of evaluating equation (14). The following steps explain how the empirical relationships derived from the trajectory data are used to solve equation (14), and figure 20 is presented to show the necessary accompanying graphical relationships.

Step 1.- The following relationship should be established for use during the computational procedure: $s/c$ as a function of $y/c$ for both upper and lower surfaces. This relationship is shown for the NACA 23015 airfoil in figure 20(a).

Step 2.-Establishing $(\Delta y_o/\Delta y)_t$ as a function of $\psi$ for isopleths of $R_V$.

(a) Using the farthest position of impingement curves (fig. 19(k)), establish the airfoil ordinates at points of tangential drop impingement as a function of $\log \psi$ for isopleths of $R_V$. This is done in figure 20(b) for the NACA 23015 airfoil for $R_V$ values of 10 and 100.

(b) On the curves established in figure 20(b), establish the values of $\psi$ at which $(\Delta y_o/\Delta y)_t=0.8$. This can be done by using figure 15 which provides, for different angles of attack, values of $\Delta y_t/t_{max}$ corresponding to the value of $(\Delta y_o/\Delta y)_t=0.8$. For the NACA 23015 airfoil (assuming the NACA 23015 airfoil to be similar in profile to the Joukowski airfoils), figure 15 gives $\Delta y_t/t_{max}=0.9$ at $\alpha=3.6^{\circ}$. This value can be used in figure 20(b) to determine the values of $\psi$ corresponding to $(\Delta y_o/\Delta y)_t=0.8$ by locating the $\psi$ values at which $\Delta y_t=0.9t_{max}$. For the NACA 23015 airfoil, these $\psi$ values in figure 20(b) are taken to be:

| $R_V$ | $\psi$ |
|---|---|
| 10 | 28 |
| 100 | 130 |

(c) Construct a semilogarithmic plot, assigning values of scale moduli as abscissas (logarithmic scale) and values of $(\Delta y_o/\Delta y)_t$ as ordinates (arithmetic scale). Then, for each particular chosen value of $R_V$, plot the values of $\psi_{cr}$ corresponding to a value of $(\Delta y_o/\Delta y)_t=0$ and also the values of $\psi$ corresponding to a value of $(\Delta y_o/\Delta y)_t=0.8$. This is done in figure 20(c) for the NACA 23015 airfoil. In figure 20(c), the values of $\psi_{cr}$ are denoted by circles and the values of $\psi$ at $(\Delta y_o/\Delta y)_t=0.8$ are denoted by squares.

(d) Using the points plotted in step 2(c), connect with a straight line each pair of points having the same $R_V$ value. This procedure establishes $(\Delta y_o/\Delta y)_t$ as a function of $\psi$ for isopleths of $R_V$ and is illustrated in figure 20(c) for the NACA 23015 airfoil. The curves in figure 20(c) have been extrapolated to approach a limit value of $(\Delta y_o/\Delta y)_t=1.13$ which corresponds to $h/t_{max}=1.09$ for straight-line tangential trajectories.

Step 3.-Calculation of impingement efficiency:

(a) Equation (14) now is used to calculate impingement efficiency for various $\psi$ and $R_V$ values. To evaluate equation (14) for a selected value of $R_V$, record values of $(\Delta y_o/\Delta y)_t$ for arbitrary values of $\psi$ from the relationship (fig. 20(c)) established in step 2(c). For the same $\psi$ values, obtain corresponding $\Delta y_t$ values directly from the curves established (fig. 20(b)) in step 2(c).

(b) Plot the values of E obtained in (a) above against the corresponding values of scale modulus in isopleths of $R_V$. A semilogarithmic scale is recommended, with values of E being plotted as ordinates on the arithmetic scale (fig. 20(d)). Figure 20(d) then may be used for design purposes by determining values of E for particular values of $\psi$ and $R_V$.

## Distribution of Impingement

Distribution of impingement is considered defined, as explained in reference 1, when values of the concentration factor C are determined over the region of drop impingement. The empirical procedure consists first of evaluating distribution of impingement for straight-line trajectories. By establishing the distribution of impingement for straight-line trajectories, a limit curve (the locus of maximum values of C) is obtained which can be used as a guide modifying an approximate distribution for the particular trajectories of interest. Figure 21 is presented to illustrate the steps involved for the NACA 23015 airfoil. These steps are subsequently described.

Step 1.–Impingement distribution on an airfoil caused by straight–line trajectories (the limit curve).

(a) To determine the impingement distribution on an airfoil for straight–line trajectories, the procedure is to plot the airfoil contour and draw several straight–line trajectories, in a streamwise direction, so that they impinge upon the airfoil. The two tangential trajectories should be included. This procedure is illustrated in figure 21(a) for the NACA 23015 airfoil.

(b) For each trajectory appearing in the plot made in (a), note the trajectory starting ordinates and the corresponding positions of impingement, $s/c$. Plot these values, using position of impingement $s/c$ as abscissas, and fair a curve through the points (fig. 21(b)).

(c) Establish concentration factor values for arbitrarily selected values of position of impingement by obtaining the slope, at various points, of the curve plotted in (b). A plot of these concentration factor values against position of impingement values yields the limit curve corresponding to straight–line trajectories. Note that the maximum value is always unity at the airfoil leading edge, and the minimum values are zero at the extreme position of tangential drop impingement.

Step 2.–Determining impingement distribution for an arbitrary value of scale modulus and free–stream Reynolds number.

(a) Calculate a maximum value of concentration factor from equation (19). Values of $s/c$ and $E$ needed to evaluate this equation for a selected value of $R_V$ and various values of $\psi$ may be obtained from efficiency and farthest position of impingement curves already established. For the NACA 23015 airfoil, the value of $C_{max}$ becomes

$$C_{max} = \frac{Eh}{(s_{av})_t} = \frac{(0.75)(0.164)}{1/2(0.135+0.45)} = 0.42$$

for a value of $\psi=100$ and a value of $R_V=100$.

(b) Plot the value of $C_{max}$ obtained in (a) against position of impingement, $s/c$. Assume that $C_{max}$ lies on a straight line connecting the points $C=1.0$, $s/c=0$, and $C=0$ for $s/c$ at the stagnation point. See figure 21(c).

(c) Using the value of $C_{max}$ obtained in step (b), form a triangular distribution of drop impingement by drawing straight lines from the point $C_{max}$ to the points $(s/c)_{u_t}$, C=0 and $(s/c)_{l_t}$, C=0. This step is also illustrated in figure 21(c).

(d) Modify the triangular distribution established in (c) to conform to the general shape of the distribution curve established in step 1(c) for straight-line trajectories. In performing this modification, the value of $C_{max}$ is usually increased such that the new curve contains the same area as did the triangular distribution. The modified curve is shown in figure 21(c) for a particular combination of $\psi$ and $R_V$. For other combinations of $\psi$ and $R_V$ that may be needed for design purposes, other figures similar to figure 21(c) would have to be constructed.

## EVALUATION OF THE EMPIRICAL METHOD DEVELOPED IN THIS REPORT

The degree to which the final values of farthest position and efficiency of drop impingement as calculated herein depend upon the accuracy of determination of the intermediate quantities $(R/R_V)_t$, $a_d$, and G was investigated by determining the effect of arbitrarily altering these three quantities a given percentage. With this procedure, the effect on farthest position and efficiency of impingement can be appraised for the selected changes in the three variables; also, some concept can be gained of the approximate error in the empirical method itself. When computations were made for the 15-percent-thick symmetrical Joukowski airfoil at $\alpha = 4^{\circ}$, and the values of $(R/R_V)_t$, $a_d$, and G were altered by ±10 percent in all possible combinations, it was found for farthest position of impingement that in no case was changing G significant. The combination of positive and negative changes providing the largest change in $\psi$ resulted in a change in s/c of about 2-percent chord over most of the range in values of $\psi$. The empirical method contributed an additional change of only about 1/2-percent chord. For efficiency of impingement, the effect of a change in the term G alone was to make a change in efficiency of about 0.5 percent; the combination of positive and negative changes in $(R/R_V)_t$ and $a_d$ providing maximum change in $\psi$ made a change in efficiency of about 3 percent over most of the range in $\psi$ values. As compared with these changes, the approximations of the empirical method led to efficiency of impingement values which differed from the differential analyzer values by about −15 percent.

While the foregoing values will not be necessarily representative for all other airfoils, they nevertheless seem to indicate the order of magnitude of error in area and efficiency of impingement to be expected when the error in the terms $(R/R_V)_t$, $a_d$, and G can be kept within ±10 percent. Whether this sort of accuracy always can be realized by using the procedures suggested in this report can be ascertained only as more water-drop trajectory data become available.

## CONCLUDING REMARKS

Results of water-drop trajectory data obtained from a differential analyzer have provided a basis for the initial development of a general method for empirically determining area, rate, and distribution of water-drop impingement on airfoil sections of arbitrary profile. The method, as applied to the incompressible-flow regime, is more firmly established for airfoils resembling the Joukowski airfoils investigated than for low-drag airfoils, since the basic data were obtained for four Joukowski airfoil cases and only one low-drag section. Because the differential analyzer data were obtained only for cases involving incompressible flow, the method as applied to compressible flow will not provide area and rate-of-impingement data having as much validity as the data for incompressible flow. There is no doubt that further water-drop trajectory data are needed, particularly for thin airfoils (order of 5-percent thick) at high speeds, and airfoils at high angle of attack (in the neighborhood of 12°). Whether these new data would revise the procedure presented herein, replace it, or substantiate it remains to be seen. Until such data are available, however, the method of this report should provide more complete and accurate information on the rate, area, and distribution of water-drop impingement on an arbitrary airfoil than any other known empirical means.

Ames Aeronautical Laboratory,
National Advisory Committee for Aeronautics,
Moffett Field, Calif., May 8, 1951.

# APPENDIX A

## COMPARISON OF RESULTS OF EMPIRICAL CALCULATIONS OF FARTHEST POSITION AND EFFICIENCY OF IMPINGEMENT WITH RESULTS OBTAINED FROM FORMAL SOLUTIONS OF TRAJECTORY EQUATIONS FOR SIX AIRFOILS

After a new design method has been developed based on a limited amount of data, it is desirable, but not always possible, to evaluate the accuracy of the method by applying it to cases where checks on the method exist. Unfortunately, in this investigation no experimental data exist and very little calculated data are available on water-drop trajectories beyond that reported herein. However, there is some justification for checking the results of this method against the more accurate calculations for the five airfoil cases since these data (except for distribution of impingement) were used only to establish a procedure which, when applied, would not necessarily yield the same values for area and percent impingement as the data. Consequently, the empirical relationships just established were applied to the five airfoil cases, and values of farthest position and efficiency of impingement were then obtained and compared with the results of the differential analyzer study. These comparisons for farthest position and efficiency of impingement are shown in figures 22 and 23, respectively. In addition, a comparison is made in figures 24 and 25 for a 12-percent-thick Joukowski airfoil computed by the method of reference 3, and also by the method of this report.

In examining figures 22 and 24, which compare farthest position of impingement values, it can be seen that the calculated points compare fairly well with curves obtained as a result of formal solutions of the trajectory equations. A favorable comparison also appears to exist in the case of efficiency of impingement, as is shown by the curves in figures 23 and 25. Discrepancies exist, but these may be expected in view of the empirical relations used as a basis for the computations. It will be noticed that values of farthest position of impingement were not obtained for values approaching the limit position of drop impingement on upper and lower surfaces. This omission is due to the fact that the values of drop acceleration approach zero as the farthest position of impingement approaches the limit values on both upper and lower surfaces. As a result, scale moduli corresponding to these positions of impingement are difficult to obtain accurately because a small error in drop acceleration makes a large error in scale modulus. For all practical purposes, though, inability to calculate points near the limit values makes little difference because the conditions in this range are seldom realized in flight.

Since the empirically calculated values for both farthest position and efficiency of impingement are in reasonable agreement with the theoretical values, it appears to be justifiable to presume that calculations can be made with reasonable accuracy for other airfoils, at least in the same angle-of-attack range. Extension to other airfoils of the method using the hodograph technique tacitly includes the assumption that the vertical components of the tangential drop velocities bear the same relation to the maximum vertical velocities of the air as established in figure 10 for the five airfoils of this study.

## REFERENCES

1. Neel, Carr B., Bergrun, Norman R., Jukoff, David, and Schlaff, Bernard A.: The Calculation of the Heat Required for Wing Thermal Ice Prevention in Specified Icing Conditions. NACA TN 1472, 1947.

2. Patterson, D. M.: A Simplified Procedure for the Determination of Heat Requirements for Ice Protection of Fixed Areas of Aircraft. Central Air Documents Office, Technical Data Digest, vol. 14, no. 4, 15 February 1949, pp. 15-23.

3. Bergrun, Norman R.: A Method for Numerically Calculating the Area and Distribution of Water Impingement on the Leading Edge of an Airfoil in a Cloud. NACA TN 1397, 1947.

4. Neel, Carr B., Jr.: Calculation of Heat Required for Wing Thermal Ice Prevention in Specified Icing Conditions. S.A.E. Quarterly Transactions, vol. 2, no. 3, July 1948, pp. 369-378.

5. Guibert, A. G., Janssen, E., and Robbins, W. M.: Determination of Rate, Area, and Distribution of Impingement of Waterdrops on Various Airfoils from Trajectories Obtained on the Differential Analyzer. NACA RM 9A05, 1949.

6. Langmuir, Irving, and Blodgett, Katherine B.: A Mathematical Investigation of Water Droplet Trajectories. General Electric Co. Rep., 1945. (Also available as Army Air Forces Tech. Rep. No. 5418, Feb. 1946, and as Dept. of Commerce Pub. P. B. No. 27565.)

7. Glauert, Muriel: A Method of Constructing the Paths of Raindrops of Different Diameters Moving in the Neighborhood of (1) a Circular Cylinder, (2) an Aerofoil, Placed in a Uniform Stream of Air; and a Determination of the Rate of Deposit of the Drops on the Surface and the Percentage of Drops Caught. R.&M. No. 2025, British A.R.C., 1940.

8. Stack, John: Compressible Flows in Aeronautics. Jour. Aero. Sci., vol. 12, no. 2, April 1945, pp. 127-148.

9. Allen, H. Julian, and Nitzberg, Gerald E.: The Effect of Compressibility on the Growth of the Laminar Boundary Layer on Low-Drag Wings and Bodies. NACA TN 1255, 1947.

TABLE I.– RESULTS FROM DIFFERENTIAL ANALYZER STUDIES OF WATER-DROP IMPINGEMENT ON A 15-PERCENT-THICK SYMMETRICAL JOUKOWSKI AIRFOIL

[$c_l$=0; $\alpha$=0°]

| Figure number | $\psi$ | $R_V$ | $y_o$ | Surface | s/c | $u_d/V$ | $v_d/V$ |
|---|---|---|---|---|---|---|---|
| 1(a) | 2 | 128 | 0.074 | Upper[1] | 0.265 | 1.0 | 0 |
| 1(a) | 2 | 128 | –.074 | Lower[1] | –.265 | 1.0 | 0 |
| 1(b) | 8 | 512 | .074 | Upper[1] | .273 | .997 | .004 |
| 1(b) | 8 | 512 | –.074 | Lower[1] | –.273 | .997 | –.004 |
| 1(c) | 32 | 2048 | .072 | Upper[1] | .262 | .997 | .013 |
| 1(c) | 32 | 2048 | –.072 | Lower[1] | –.262 | .997 | –.013 |
| 1(d) | 4 | 32 | .073 | Upper[1] | .273 | 1.0 | .012 |
| 1(d) | 4 | 32 | –.073 | Lower[1] | –.273 | 1.0 | –.012 |
| 1(e) | 16 | 128 | .070 | Upper[1] | .244 | 1.005 | .023 |
| 1(e) | 16 | 128 | .045 | Upper | .068 | .99 | .013 |
| 1(e) | 16 | 128 | .020 | Upper | .021 | .982 | .009 |
| 1(e) | 16 | 128 | –.020 | Lower | –.021 | .982 | –.009 |
| 1(e) | 16 | 128 | –.045 | Lower | –.068 | .99 | –.013 |
| 1(e) | 16 | 128 | –.070 | Lower[1] | –.244 | 1.005 | –.023 |
| 1(f) | 64 | 512 | .0655 | Upper[1] | .225 | 1.004 | .043 |
| 1(f) | 64 | 512 | –.0655 | Lower[1] | –.225 | 1.004 | –.043 |
| 1(g) | 256 | 2048 | .058 | Upper[1] | .188 | 1.007 | .092 |
| 1(g) | 256 | 2048 | .040 | Upper | .058 | .949 | .069 |
| 1(g) | 256 | 2048 | .020 | Upper | .023 | .931 | .029 |
| 1(g) | 256 | 2048 | –.020 | Lower | –.023 | .931 | –.029 |
| 1(g) | 256 | 2048 | –.040 | Lower | –.058 | .949 | –.069 |
| 1(g) | 256 | 2048 | –.058 | Lower[1] | –.188 | 1.007 | –.092 |
| 1(h) | 8 | 8 | .059 | Upper[1] | .197 | .994 | .078 |
| 1(h) | 8 | 8 | –.059 | Lower[1] | –.197 | .994 | –.078 |
| 1(i) | 32 | 32 | .056 | Upper[1] | .185 | .992 | .089 |
| 1(i) | 32 | 32 | –.056 | Lower[1] | –.185 | .992 | –.089 |
| 1(j) | 128 | 128 | .0485 | Upper[1] | .150 | .989 | .149 |
| 1(j) | 128 | 128 | –.0485 | Lower[1] | –.150 | .989 | –.149 |
| 1(k) | 512 | 512 | .038 | Upper[1] | .108 | .941 | .225 |
| 1(k) | 512 | 512 | –.038 | Lower[1] | –.108 | .941 | –.225 |
| 1(l) | 2048 | 2048 | .025 | Upper[1] | .072 | .856 | .349 |
| 1(l) | 2048 | 2048 | –.025 | Lower[1] | –.072 | .856 | –.349 |
| 1(m) | 64 | 8 | .0255 | Upper[1] | .078 | .870 | .321 |
| 1(m) | 64 | 8 | .018 | Upper | .031 | .693 | .192 |
| 1(m) | 64 | 8 | .008 | Upper | .010 | .698 | .061 |
| 1(m) | 64 | 8 | –.008 | Lower | –.010 | .698 | –.061 |
| 1(m) | 64 | 8 | –.018 | Lower | –.031 | .693 | –.192 |

[1]Denotes tangential trajectories.

TABLE I.– CONCLUDED

| Figure number | $\psi$ | $R_V$ | $y_o$ | Surface | s/c | $u_d/V$ | $v_d/V$ |
|---|---|---|---|---|---|---|---|
| 1(m) | 64 | 8 | –0.0255 | Lower[1] | –0.078 | 0.870 | –0.321 |
| 1(n) | 256 | 32 | .021 | Upper[1] | .073 | .828 | .359 |
| 1(n) | 256 | 32 | –.021 | Lower[1] | –.073 | .828 | –.359 |
| 1(o) | 1024 | 128 | .015 | Upper[1] | .052 | .741 | .451 |
| 1(o) | 1024 | 128 | .010 | Upper | .020 | .572 | .198 |
| 1(o) | 1024 | 128 | .005 | Upper | .009 | .563 | .109 |
| 1(o) | 1024 | 128 | –.005 | Lower | –.009 | .563 | –.109 |
| 1(o) | 1024 | 128 | –.010 | Lower | –.020 | .572 | –.198 |
| 1(o) | 1024 | 128 | –.015 | Lower[1] | –.052 | .741 | –.451 |
| 1(p) | 4096 | 512 | .0110 | Upper[1] | .038 | .584 | .452 |
| 1(p) | 4096 | 512 | –.0110 | Lower[1] | –.038 | .584 | –.452 |
| 1(q) | 16384 | 2048 | .004 | Upper[1] | .022 | .329 | .469 |
| 1(q) | 16384 | 2048 | –.004 | Lower[1] | –.022 | .329 | –.469 |
| 1(r) | 512 | 8 | .0035 | Upper[1] | .023 | .355 | .514 |
| 1(r) | 512 | 8 | –.0035 | Lower[1] | –.023 | .355 | –.514 |
| 1(s) | 8192 | 128 | .0020 | Upper[1] | .015 | .251 | .401 |
| 1(s) | 8192 | 128 | –.0020 | Lower[1] | –.015 | .251 | –.401 |
| 1(t) | 32768 | 512 | .0005 | Upper[1] | .016 | .187 | .459 |
| 1(t) | 32768 | 512 | –.0005 | Lower[1] | –.016 | .187 | –.459 |

[1]Denotes tangential trajectories.

TABLE II.– RESULTS FROM DIFFERENTIAL ANALYZER STUDIES OF WATER-DROP IMPINGEMENT ON A 15-PERCENT-THICK SYMMETRICAL JOUKOWSKI AIRFOIL

[$c_l$=0.22, $\alpha$=2°]

| Figure number | $\psi$ | $R_V$ | $y_o$ | Surface | s/c | $u_d/V$ | $v_d/V$ |
|---|---|---|---|---|---|---|---|
| 2(a) | 4 | 256 | –0.0046 | Upper[1] | 0.236 | 1.001 | 0.041 |
| 2(a) | 4 | 256 | –.1548 | Lower[1] | –.316 | .998 | .035 |
| 2(b) | 16 | 1024 | –.0055 | Upper[1] | .223 | 1.003 | .044 |
| 2(b) | 16 | 1024 | –.1539 | Lower[1] | –.310 | .998 | .030 |
| 2(c) | 2 | 16 | –.0081 | Upper[1] | .226 | 1.009 | .053 |
| 2(c) | 2 | 16 | –.1533 | Lower[1] | –.311 | .997 | .027 |
| 2(d) | 8 | 64 | –.0095 | Upper[1] | .212 | 1.011 | .062 |
| 2(d) | 8 | 64 | –.0381 | Upper | .045 | .983 | .054 |
| 2(d) | 8 | 64 | –.0667 | Upper | .005 | .984 | .044 |
| 2(d) | 8 | 64 | –.0956 | Lower | –.026 | .974 | .039 |
| 2(d) | 8 | 64 | –.1243 | Lower | –.082 | .972 | .033 |
| 2(d) | 8 | 64 | –.1532 | Lower[1] | –.308 | .997 | .022 |
| 2(e) | 32 | 256 | –.0140 | Upper[1] | .196 | 1.015 | .083 |
| 2(e) | 32 | 256 | –.0410 | Upper | .041 | .980 | .066 |
| 2(e) | 32 | 256 | –.0683 | Upper | .003 | .969 | .052 |
| 2(e) | 32 | 256 | –.0958 | Lower | –.026 | .970 | .038 |
| 2(e) | 32 | 256 | –.1232 | Lower | –.078 | .975 | .024 |
| 2(e) | 32 | 256 | –.1508 | Lower[1] | –.295 | .995 | .013 |
| 2(f) | 128 | 1024 | –.0214 | Upper[1] | .168 | 1.021 | .126 |
| 2(f) | 128 | 1024 | –.0464 | Upper | .034 | .958 | .100 |
| 2(f) | 128 | 1024 | –.0721 | Upper | .002 | .941 | .063 |
| 2(f) | 128 | 1024 | –.0977 | Lower | –.027 | .939 | .032 |
| 2(f) | 128 | 1024 | –.1231 | Lower | –.079 | .955 | .004 |
| 2(f) | 128 | 1024 | –.1488 | Lower[1] | –.265 | .992 | –.008 |
| 2(g) | 16 | 16 | –.0435 | Upper[1] | .149 | 1.010 | .160 |
| 2(g) | 16 | 16 | –.1598 | Lower[1] | –.245 | .984 | –.023 |
| 2(h) | 64 | 64 | –.0493 | Upper[1] | .128 | 1.012 | .202 |
| 2(h) | 64 | 64 | –.0705 | Upper | .027 | .908 | .140 |
| 2(h) | 64 | 64 | –.0902 | Lower | –.001 | .881 | .083 |
| 2(h) | 64 | 64 | –.1130 | Lower | –.027 | .881 | .033 |
| 2(h) | 64 | 64 | –.1345 | Lower | –.071 | .921 | –.013 |
| 2(h) | 64 | 64 | –.1558 | Lower[1] | –.225 | .983 | –.052 |
| 2(i) | 256 | 256 | –.0587 | Upper[1] | .100 | .999 | .283 |
| 2(i) | 256 | 256 | –.0763 | Upper | .022 | .852 | .189 |
| 2(i) | 256 | 256 | –.0940 | Lower | –.002 | .827 | .103 |
| 2(i) | 256 | 256 | –.1118 | Lower | –.023 | .815 | .015 |

[1]Denotes tangential trajectories.

TABLE II.– CONCLUDED

| Figure number | $\psi$ | $R_V$ | $y_o$ | Surface | s/c | $u_d/V$ | $v_d/V$ |
|---|---|---|---|---|---|---|---|
| 2(i) | 256 | 256 | -0.1298 | Lower | -0.058 | 0.863 | -0.050 |
| 2(l) | 256 | 256 | -.1475 | Lower[1] | -.177 | .963 | -.105 |
| 2(j) | 1024 | 1024 | -.0743 | Upper[1] | .063 | .914 | .424 |
| 2(j) | 1024 | 1024 | -.1360 | Lower[1] | -.118 | .902 | -.195 |
| 2(k) | 128 | 16 | -.0955 | Upper[1] | .055 | .881 | .472 |
| 2(k) | 128 | 16 | -.1065 | Upper | .009 | .640 | .235 |
| 2(k) | 128 | 16 | -.1160 | Lower | -.004 | .637 | .113 |
| 2(k) | 128 | 16 | -.1250 | Lower | -.017 | .642 | -.006 |
| 2(k) | 128 | 16 | -.1335 | Lower | -.036 | .685 | -.109 |
| 2(k) | 128 | 16 | -.1430 | Lower[1] | -.098 | .854 | -.246 |
| 2(l) | 512 | 64 | -.1005 | Upper[1] | .038 | .767 | .528 |
| 2(l) | 512 | 64 | -.1080 | Upper | .009 | .560 | .270 |
| 2(l) | 512 | 64 | -.1155 | Lower | -.004 | .542 | .132 |
| 2(l) | 512 | 64 | -.1230 | Lower | -.016 | .535 | -.011 |
| 2(l) | 512 | 64 | -.1310 | Lower | -.03 | .611 | -.140 |
| 2(l) | 512 | 64 | -.1382 | Lower[1] | -.079 | .813 | -.300 |
| 2(m) | 2048 | 256 | -.1085 | Upper[1] | .028 | .562 | .611 |
| 2(m) | 2048 | 256 | -.1130 | Upper | .004 | .394 | .255 |
| 2(m) | 2048 | 256 | -.1182 | Lower | -.005 | .379 | .118 |
| 2(m) | 2048 | 256 | -.1228 | Lower | -.014 | .377 | -.050 |
| 2(m) | 2048 | 256 | -.1275 | Lower | -.029 | .500 | -.235 |
| 2(m) | 2048 | 256 | -.1325 | Lower[1] | -.055 | .688 | -.356 |
| 2(n) | 8192 | 1024 | -.1165 | Upper[1] | .015 | .210 | .514 |
| 2(n) | 8192 | 1024 | -.1190 | --- | 0 | .270 | .230 |
| 2(n) | 8192 | 1024 | -.1218 | Lower | -.004 | .260 | .085 |
| 2(n) | 8192 | 1024 | -.1250 | Lower | -.012 | .273 | -.110 |
| 2(n) | 8192 | 1024 | -.1275 | Lower[1] | -.031 | .520 | -.390 |
| 2(o) | 1024 | 16 | -.1232 | Upper[1] | .008 | .186 | .610 |
| 2(o) | 1024 | 16 | -.1262 | Lower[1] | -.015 | .100 | -.243 |
| 2(p) | 4096 | 64 | -.1243 | Upper[1] | .003 | .090 | .434 |
| 2(p) | 4096 | 64 | -.1278 | Lower[1] | -.015 | .246 | -.235 |
| 2(q) | 16384 | 256 | -.1254 | Upper[1] | .002 | .103 | .506 |
| 2(q) | 16384 | 256 | -.1275 | Lower[1] | -.014 | .175 | .295 |

[1]Denotes tangential trajectories.

TABLE III.– RESULTS FROM DIFFERENTIAL ANALYZER STUDIES OF WATER-DROP IMPINGEMENT ON A 15-PERCENT-THICK SYMMETRICAL JOUKOWSKI AIRFOIL

[$c_l$=0.44; $\alpha$=4°]

| Figure number | $\psi$ | $R_V$ | $y_o$ | Surface | s/c | $u_d/V$ | $v_d/V$ |
|---|---|---|---|---|---|---|---|
| 3(a) | 4 | 256 | -0.1682 | Upper[1] | 0.204 | 0.9996 | 0.0785 |
| 3(a) | 4 | 256 | -.3215 | Lower[1] | -.408 | .9946 | .0705 |
| 3(b) | 16 | 1024 | -.1692 | Upper[1] | .194 | 1.0086 | .1005 |
| 3(b) | 16 | 1024 | -.3223 | Lower[1] | -.400 | .9976 | .0705 |
| 3(c) | 2 | 16 | -.1818 | Upper[1] | .192 | 1.0034 | .0962 |
| 3(c) | 2 | 16 | -.3330 | Lower[1] | -.409 | .9891 | .0688 |
| 3(d) | 8 | 64 | -.1837 | Upper[1] | .170 | 1.0055 | .1032 |
| 3(d) | 8 | 64 | -.3073 | Lower | -.135 | .9802 | .0728 |
| 3(d) | 8 | 64 | -.2824 | Lower | -.064 | .9782 | .0789 |
| 3(d) | 8 | 64 | -.2577 | Lower | -.024 | .9663 | .1120 |
| 3(d) | 8 | 64 | -.2330 | Upper | .004 | .9793 | .0940 |
| 3(d) | 8 | 64 | -.2083 | Upper | .037 | .9854 | .1011 |
| 3(d) | 8 | 64 | -.3320 | Lower[1] | -.400 | .9930 | .0638 |
| 3(e) | 32 | 256 | -.1881 | Upper[1] | .148 | 1.0174 | .1381 |
| 3(e) | 32 | 256 | -.2121 | Upper | .034 | .9764 | .1221 |
| 3(e) | 32 | 256 | -.2358 | Upper | .002 | .9653 | .1050 |
| 3(e) | 32 | 256 | -.2594 | Lower | -.024 | --- | --- |
| 3(e) | 32 | 256 | -.2832 | Lower | -.062 | --- | --- |
| 3(e) | 32 | 256 | -.3068 | Lower | -.124 | .9652 | .0628 |
| 3(e) | 32 | 256 | -.3316 | Lower[1] | -.379 | .9831 | .0618 |
| 3(f) | 128 | 1024 | -.1994 | Upper[1] | .127 | 1.0294 | .2031 |
| 3(f) | 128 | 1024 | -.2074 | Upper | .062 | .9804 | .0931 |
| 3(f) | 128 | 1024 | -.2205 | Upper | .028 | .9514 | .1670 |
| 3(f) | 128 | 1024 | -.2386 | Upper | .004 | .9304 | .1410 |
| 3(f) | 128 | 1024 | -.2748 | Lower | -.041 | .9273 | .0869 |
| 3(f) | 128 | 1024 | -.3077 | Lower | -.125 | .9433 | .0519 |
| 3(f) | 128 | 1024 | -.3316 | Lower[1] | -.350 | 1.0200 | .0468 |
| 3(g) | 16 | 16 | -.2403 | Upper[1] | .121 | 1.0116 | .2241 |
| 3(g) | 16 | 16 | -.3665 | Lower[1] | -.336 | .9628 | .0415 |
| 3(h) | 64 | 64 | -.2472 | Upper[1] | .100 | 1.0133 | .2881 |
| 3(h) | 64 | 64 | -.3422 | Lower | -.113 | .8940 | .0448 |
| 3(h) | 64 | 64 | -.3231 | Lower | -.060 | .8712 | .0731 |
| 3(h) | 64 | 64 | -.3043 | Lower | -.028 | .8694 | .1147 |
| 3(h) | 64 | 64 | -.2853 | Lower | -.004 | .8638 | .1675 |
| 3(h) | 64 | 64 | -.2665 | Upper | .018 | .8990 | .2148 |
| 3(h) | 64 | 64 | -.3606 | Lower[1] | -.286 | .9578 | .0135 |
| 3(i) | 256 | 256 | -.2622 | Upper[1] | .068 | 1.0121 | .4088 |
| 3(i) | 256 | 256 | -.2775 | Upper | .012 | .8138 | .2746 |
| 3(i) | 256 | 256 | -.2925 | Lower | -.008 | .7827 | .1843 |

[1]Denotes tangential trajectories.

TABLE III.– CONCLUDED

| Figure number | $\psi$ | $R_V$ | $y_o$ | Surface | s/c | $u_d/V$ | $v_d/V$ |
|---|---|---|---|---|---|---|---|
| 3(i) | 256 | 256 | −0.3078 | Lower | −0.028 | 0.7864 | 0.1092 |
| 3(i) | 256 | 256 | −.3353 | Lower | −.084 | .8281 | .0149 |
| 3(i) | 256 | 256 | −.3444 | Lower | −.125 | .8660 | .0142 |
| 3(i) | 256 | 256 | −.3537 | Lower[1] | −.247 | .9558 | −.0313 |
| 3(j) | 1024 | 1024 | −.2782 | Upper[1] | .043 | .8758 | .5817 |
| 3(j) | 1024 | 1024 | −.3440 | Lower[1] | −.155 | .8780 | −.1212 |
| 3(k) | 128 | 16 | −.3126 | Upper[1] | .042 | .8255 | .5550 |
| 3(k) | 128 | 16 | −.3598 | Lower | −.067 | .7143 | .0364 |
| 3(k) | 128 | 16 | −.3500 | Lower | −.040 | .6586 | .0228 |
| 3(k) | 128 | 16 | −.3406 | Lower | −.022 | .6048 | .1031 |
| 3(k) | 128 | 16 | −.3313 | Lower | −.006 | .615 | .2444 |
| 3(k) | 128 | 16 | −.3220 | Upper | −.006 | .6562 | .3437 |
| 3(k) | 128 | 16 | −.3688 | Lower[1] | −.145 | .8632 | −.1358 |
| 3(l) | 512 | 64 | −.3216 | Upper[1] | .026 | .6392 | .7017 |
| 3(l) | 512 | 64 | −.3303 | Lower | −.004 | .5021 | .3024 |
| 3(l) | 512 | 64 | −.3383 | Lower | −.015 | .4678 | .1513 |
| 3(l) | 512 | 64 | −.3441 | Lower | −.027 | .5197 | .0390 |
| 3(l) | 512 | 64 | −.3500 | Lower | −.042 | .5566 | −.0782 |
| 3(l) | 512 | 64 | −.3558 | Lower | −.062 | .6465 | −.1363 |
| 3(l) | 512 | 64 | −.3605 | Lower[1] | −.112 | .8133 | −.2045 |
| 3(m) | 2048 | 256 | −.3293 | Upper[1] | .015 | .4240 | .7513 |
| 3(m) | 2048 | 256 | −.3324 | Upper | .002 | .3300 | .4553 |
| 3(m) | 2048 | 256 | −.3373 | Lower | −.008 | .2858 | .2442 |
| 3(m) | 2048 | 256 | −.3432 | Lower | −.022 | .3548 | .0060 |
| 3(m) | 2048 | 256 | −.3471 | Lower | −.032 | .4137 | −.1191 |
| 3(m) | 2048 | 256 | −.3501 | Lower | −.045 | .4956 | −.1923 |
| 3(m) | 2048 | 256 | −.3529 | Lower[1] | −.072 | .6575 | −.2912 |
| 3(n) | 8192 | 1024 | −.3382 | Upper[1] | .004 | .0918 | .7521 |
| 3(n) | 8192 | 1024 | −.3405 | Lower | −.005 | .1918 | .4371 |
| 3(n) | 8192 | 1024 | −.3441 | Lower | −.012 | .1787 | .1520 |
| 3(n) | 8192 | 1024 | −.3458 | Lower | −.020 | .2767 | .0669 |
| 3(n) | 8192 | 1024 | −.3474 | Lower | −.031 | .2867 | −.2011 |
| 3(n) | 8192 | 1024 | −.3480 | Lower[1] | −.041 | .4186 | −.2832 |
| 3(o) | 1024 | 16 | −.3495 | Upper[1] | .004 | .1147 | .6545 |
| 3(o) | 1024 | 16 | −.3544 | Lower[1] | −.035 | .3496 | −.2808 |
| 3(p) | 4096 | 64 | −.3495 | Upper[1] | .002 | .1047 | .6945 |
| 3(p) | 4096 | 64 | −.3530 | Lower[1] | −.026 | .2146 | −.2157 |
| 3(q) | 16384 | 256 | −.3504 | Upper[1] | .002 | .1597 | .8494 |
| 3(q) | 16384 | 256 | −.3535 | Lower[1] | −.025 | .2746 | −.2256 |

[1]Denotes tangential trajectories.

TABLE IV.– RESULTS FROM DIFFERENTIAL ANALYZER STUDIES OF WATER-DROP IMPINGEMENT ON A 15-PERCENT-THICK CAMBERED JOUKOWSKI AIRFOIL

[a=1.0 MEAN LINE; $c_l$=0.44; $\alpha$=0°]

| Figure number | $\psi$ | $R_V$ | $y_o$ | Surface | s/c | $u_d/V$ | $v_d/V$ |
|---|---|---|---|---|---|---|---|
| 4(a) | 4 | 256 | 0.0935 | Upper[1] | 0.317 | 1.003 | 0.007 |
| 4(a) | 4 | 256 | –.0565 | Lower[1] | –.216 | .998 | –.002 |
| 4(b) | 16 | 1024 | .0915 | Upper[1] | .310 | 1.008 | .013 |
| 4(b) | 16 | 1024 | –.0565 | Lower[1] | –.213 | .999 | –.006 |
| 4(c) | 2 | 16 | .0855 | Upper[1] | .305 | 1.009 | .022 |
| 4(c) | 2 | 16 | –.0600 | Lower[1] | –.215 | .994 | –.001 |
| 4(d) | 8 | 64 | .0818 | Upper[1] | .294 | 1.012 | .031 |
| 4(d) | 8 | 64 | .0536 | Upper | .096 | .992 | .022 |
| 4(d) | 8 | 64 | .0253 | Upper | .038 | .988 | .020 |
| 4(d) | 8 | 64 | –.0038 | Upper | .002 | .985 | .011 |
| 4(d) | 8 | 64 | –.0318 | Lower | –.033 | .984 | .003 |
| 4(d) | 8 | 64 | –.0610 | Lower[1] | –.212 | .999 | –.008 |
| 4(e) | 32 | 256 | .0775 | Upper[1] | .275 | 1.022 | .050 |
| 4(e) | 32 | 256 | .0503 | Upper | .092 | .989 | .042 |
| 4(e) | 32 | 256 | .0225 | Upper | .034 | .976 | .030 |
| 4(e) | 32 | 256 | –.0045 | Upper | .001 | .972 | .017 |
| 4(e) | 32 | 256 | –.0325 | Lower | –.033 | .973 | .002 |
| 4(e) | 32 | 256 | –.0600 | Lower[1] | –.199 | .990 | –.016 |
| 4(f) | 128 | 1024 | .0660 | Upper[1] | .243 | 1.033 | .090 |
| 4(f) | 128 | 1024 | .0420 | Upper | .077 | .976 | .075 |
| 4(f) | 128 | 1024 | .0160 | Upper | .030 | .954 | .054 |
| 4(f) | 128 | 1024 | –.0085 | – – – | 0 | .943 | .024 |
| 4(f) | 128 | 1024 | –.0335 | Lower | –.032 | .946 | –.006 |
| 4(f) | 128 | 1024 | –.0585 | Lower[1] | –.183 | .984 | –.036 |
| 4(g) | 16 | 16 | .0377 | Upper[1] | .211 | 1.028 | .128 |
| 4(g) | 16 | 16 | –.0770 | Lower[1] | –.180 | .978 | –.042 |
| 4(h) | 64 | 64 | .0312 | Upper[1] | .192 | 1.038 | .168 |
| 4(h) | 64 | 64 | .0100 | Upper | .061 | .936 | .131 |
| 4(h) | 64 | 64 | –.0110 | Upper | .022 | .898 | .095 |
| 4(h) | 64 | 64 | –.0315 | Lower | –.003 | .884 | .048 |
| 4(h) | 64 | 64 | –.0525 | Lower | –.031 | .891 | –.007 |
| 4(h) | 64 | 64 | –.0731 | Lower[1] | –.157 | .971 | –.073 |
| 4(i) | 256 | 256 | .0180 | Upper[1] | .158 | 1.038 | .238 |
| 4(i) | 256 | 256 | .0010 | Upper | .050 | .893 | .188 |
| 4(i) | 256 | 256 | –.0165 | Upper | .018 | .839 | .127 |
| 4(i) | 256 | 256 | –.0340 | Lower | –.004 | .820 | .054 |
| 4(i) | 256 | 256 | –.0510 | Lower | –.028 | .838 | –.017 |
| 4(i) | 256 | 256 | –.0680 | Lower | –.120 | .940 | –.129 |

[1]Denotes tangential trajectories.

TABLE IV.– CONCLUDED

| Figure number | $\psi$ | $R_V$ | $y_o$ | Surface | $s/c$ | $u_d/V$ | $v_d/V$ |
|---|---|---|---|---|---|---|---|
| 4(j) | 1024 | 1024 | 0 | Upper[1] | 0.109 | 1.000 | 0.357 |
| 4(j) | 1024 | 1024 | –.0620 | Lower[1] | –.085 | .883 | –.220 |
| 4(k) | 128 | 16 | –.028 | Upper[1] | .092 | .958 | .405 |
| 4(k) | 128 | 16 | –.0382 | Upper | .032 | .727 | .288 |
| 4(k) | 128 | 16 | –.0480 | Upper | .012 | .638 | .189 |
| 4(k) | 128 | 16 | –.0575 | Lower | –.004 | .649 | .060 |
| 4(k) | 128 | 16 | –.0670 | Lower | –.019 | .644 | –.046 |
| 4(k) | 128 | 16 | –.0772 | Lower[1] | –.068 | .838 | –.264 |
| 4(l) | 512 | 64 | –.0347 | Upper[1] | .072 | .911 | .487 |
| 4(l) | 512 | 64 | –.0425 | Upper | .025 | .634 | .350 |
| 4(l) | 512 | 64 | –.050 | Upper | .010 | .535 | .208 |
| 4(l) | 512 | 64 | –.0582 | Lower | –.005 | .485 | .031 |
| 4(l) | 512 | 64 | –.066 | Lower | –.018 | .544 | –.124 |
| 4(l) | 512 | 64 | –.0725 | Lower[1] | –.053 | .754 | –.319 |
| 4(m) | 2048 | 256 | –.0440 | Upper[1] | .046 | .686 | .576 |
| 4(m) | 2048 | 256 | –.050 | Upper | .015 | .448 | .360 |
| 4(m) | 2048 | 256 | –.0548 | Upper | .005 | .381 | .192 |
| 4(m) | 2048 | 256 | –.0594 | Lower | –.004 | .368 | .048 |
| 4(m) | 2048 | 256 | –.0638 | Lower | –.013 | .407 | –.103 |
| 4(m) | 2048 | 256 | –.0685 | Lower[1] | –.038 | .604 | –.384 |
| 4(n) | 8192 | 1024 | –.0548 | Upper[1] | .025 | .471 | .650 |
| 4(n) | 8192 | 1024 | –.0569 | Upper | .007 | .258 | .308 |
| 4(n) | 8192 | 1024 | –.0590 | Lower | –.001 | .178 | .082 |
| 4(n) | 8192 | 1024 | –.0610 | Lower | –.008 | .184 | –.079 |
| 4(n) | 8192 | 1024 | –.0630 | Lower | –.012 | .211 | –.168 |
| 4(n) | 8192 | 1024 | –.0650 | Lower[1] | –.025 | .464 | –.428 |
| 4(o) | 1024 | 16 | –.0604 | Upper[1] | .022 | .346 | .561 |
| 4(o) | 1024 | 16 | –.0700 | Lower[1] | –.018 | .317 | –.368 |
| 4(p) | 4096 | 64 | –.0650 | Upper[1] | .015 | .285 | .527 |
| 4(p) | 4096 | 64 | –.0675 | Lower[1] | –.012 | .143 | –.253 |
| 4(q) | 16384 | 256 | –.0655 | Upper[1] | .006 | .113 | .391 |
| 4(q) | 16384 | 256 | –.0670 | Lower[1] | –.008 | .046 | –.118 |

[1]Denotes tangential trajectories.

TABLE V.– RESULTS FROM DIFFERENTIAL ANALYZER STUDIES OF WATER-DROP IMPINGEMENT ON AN NACA $65_2$-015 AIRFOIL

[$c_l$=0.44; $\alpha$=4°]

| Figure number | $\psi$ | $R_V$ | $y_o$ | Surface | s/c | $u_d/V$ | $v_d/V$ |
|---|---|---|---|---|---|---|---|
| 5(a) | 4 | 256 | -0.1281 | Upper[1] | 0.281 | 1.0023 | 0.0814 |
| 5(a) | 4 | 256 | -.2817 | Lower[1] | -.523 | .9973 | .0704 |
| 5(b) | 16 | 1024 | -.1298 | Upper[1] | .267 | 1.0073 | .0864 |
| 5(b) | 16 | 1024 | -.2818 | Lower[1] | -.514 | .9973 | .0704 |
| 5(c) | 2 | 16 | -.1395 | Upper[1] | .259 | 1.0047 | .0945 |
| 5(c) | 2 | 16 | -.1646 | Upper | .031 | .9881 | .0875 |
| 5(c) | 2 | 16 | -.2026 | Lower | -.022 | .9847 | .0825 |
| 5(c) | 2 | 16 | -.2246 | Lower | -.074 | .9867 | .0793 |
| 5(c) | 2 | 16 | -.2467 | Lower | -.150 | .9857 | .0753 |
| 5(c) | 2 | 16 | -.2687 | Lower | -.256 | .9847 | .0742 |
| 5(c) | 2 | 16 | -.2909 | Lower[1] | -.514 | .9927 | .0711 |
| 5(d) | 8 | 64 | -.1424 | Upper[1] | .240 | 1.0107 | .1065 |
| 5(d) | 8 | 64 | -.1719 | Upper | .016 | .9847 | .0935 |
| 5(d) | 8 | 64 | -.2163 | Lower | -.050 | .9757 | .0824 |
| 5(d) | 8 | 64 | -.2409 | Lower | -.125 | .9807 | .0743 |
| 5(d) | 8 | 64 | -.2655 | Lower | -.236 | .9797 | .0712 |
| 5(d) | 8 | 64 | -.2899 | Lower[1] | -.512 | .9907 | .0641 |
| 5(e) | 32 | 256 | -.1493 | Upper[1] | .209 | 1.0187 | .1326 |
| 5(e) | 32 | 256 | -.1702 | Upper | .023 | .9761 | .1155 |
| 5(e) | 32 | 256 | -.2193 | Lower | -.052 | .9617 | .0874 |
| 5(e) | 32 | 256 | -.2437 | Lower | -.131 | .9647 | .0743 |
| 5(e) | 32 | 256 | -.2685 | Lower | -.249 | .9717 | .0632 |
| 5(e) | 32 | 256 | -.2894 | Lower[1] | -.506 | 1.0057 | .0531 |
| 5(f) | 128 | 1024 | -.1603 | Upper[1] | .150 | 1.0207 | .1805 |
| 5(f) | 128 | 1024 | -.1826 | Upper | .008 | .9517 | .1375 |
| 5(f) | 128 | 1024 | -.2282 | Lower | -.068 | .9427 | .0853 |
| 5(f) | 128 | 1024 | -.2505 | Lower | -.145 | .9407 | .0642 |
| 5(f) | 128 | 1024 | -.2726 | Lower | -.267 | .9557 | .0462 |
| 5(f) | 128 | 1024 | -.2878 | Lower[1] | -.485 | .9837 | .0382 |
| 5(g) | 16 | 16 | -.1951 | Upper[1] | .128 | 1.0015 | .2008 |
| 5(g) | 16 | 16 | -.3202 | Lower[1] | -.481 | .9776 | .0383 |
| 5(h) | 64 | 64 | -.2030 | Upper[1] | .092 | .9956 | .2597 |
| 5(h) | 64 | 64 | -.2136 | Upper | .012 | .9155 | .2055 |
| 5(h) | 64 | 64 | -.2535 | Lower | -.048 | .8795 | .1092 |
| 5(h) | 64 | 64 | -.2787 | Lower | -.127 | .8975 | .0609 |
| 5(h) | 64 | 64 | -.3013 | Lower | -.247 | .9255 | .0227 |
| 5(h) | 64 | 64 | -.3111 | Lower[1] | -.417 | .9756 | .0074 |
| 5(i) | 256 | 256 | -.2143 | Upper[1] | .047 | .9416 | .3416 |
| 5(i) | 256 | 256 | -.2343 | Lower | -.007 | .8256 | .1964 |

[1]Denotes tangential trajectories.

TABLE V.– CONTINUED

| Figure number | $\psi$ | $R_V$ | $y_o$ | Surface | s/c | $u_d/V$ | $v_d/V$ |
|---|---|---|---|---|---|---|---|
| 5(i) | 256 | 256 | –0.2543 | Lower | –0.040 | 0.8086 | 0.1102 |
| 5(i) | 256 | 256 | –.2717 | Lower | –.093 | .8316 | .0410 |
| 5(i) | 256 | 256 | –.2892 | Lower | –.184 | – – – | – – – |
| 5(i) | 256 | 256 | –.2983 | Lower[1] | –.355 | .9686 | –.0443 |
| 5(j) | 1024 | 1024 | –.2267 | Upper[1] | .026 | .8575 | .4614 |
| 5(j) | 1024 | 1024 | –.2313 | Upper | .010 | .7726 | .3935 |
| 5(j) | 1024 | 1024 | –.2492 | Lower | –.015 | .6715 | .1972 |
| 5(j) | 1024 | 1024 | –.2692 | Lower | –.060 | .6295 | .0300 |
| 5(j) | 1024 | 1024 | –.2782 | Lower | –.104 | .7875 | –.0251 |
| 5(j) | 1024 | 1024 | –.2853 | Lower | –.166 | .7495 | –.0692 |
| 5(j) | 1024 | 1024 | –.2883 | Lower[1] | –.245 | .9175 | .0942 |
| 5(k) | 128 | 16 | –.2633 | Upper[1] | .021 | .7926 | .4950 |
| 5(k) | 128 | 16 | –.2798 | Lower | –.012 | .6436 | .2336 |
| 5(k) | 128 | 16 | –.2945 | Lower | –.042 | .6395 | .1003 |
| 5(k) | 128 | 16 | –.3028 | Lower | –.080 | .7194 | –.0500 |
| 5(k) | 128 | 16 | –.3059 | Lower | –.104 | .7634 | –.0860 |
| 5(k) | 128 | 16 | –.3091 | Lower[1] | –.185 | .8804 | –.1302 |
| 5(l) | 512 | 64 | –.2676 | Upper[1] | .018 | .7536 | .5779 |
| 5(l) | 512 | 64 | –.2719 | Upper | .005 | .6496 | .4378 |
| 5(l) | 512 | 64 | –.2857 | Lower | –.020 | .4935 | .1605 |
| 5(l) | 512 | 64 | –.2926 | Lower | –.034 | .5504 | .0403 |
| 5(l) | 512 | 64 | –.3015 | Lower | –.079 | .6954 | –.0989 |
| 5(l) | 512 | 64 | –.3035 | Lower[1] | –.145 | .8284 | –.1540 |
| 5(m) | 2048 | 256 | –.2737 | Upper[1] | .014 | .6606 | .6718 |
| 5(m) | 2048 | 256 | –.2748 | Upper | .007 | .5986 | .5868 |
| 5(m) | 2048 | 256 | –.2781 | – – – | 0 | .5216 | .4106 |
| 5(m) | 2048 | 256 | –.2861 | Lower | –.012 | .4085 | .2245 |
| 5(m) | 2048 | 256 | –.2906 | Lower | –.022 | .3905 | .0604 |
| 5(m) | 2048 | 256 | –.2965 | Lower | –.048 | .5485 | –.0967 |
| 5(m) | 2048 | 256 | –.2989 | Lower[1] | –.100 | .7584 | –.1768 |
| 5(n) | 8192 | 1024 | –.2798 | Upper[1] | .010 | .5976 | .7847 |
| 5(n) | 8192 | 1024 | –.2801 | Upper | .005 | – – – | – – – |
| 5(n) | 8192 | 1024 | –.2850 | Lower | –.004 | – – – | – – – |
| 5(n) | 8192 | 1024 | –.2886 | Lower | –.010 | .3035 | .2454 |
| 5(n) | 8192 | 1024 | –.2932 | Lower | –.022 | .2124 | .0033 |
| 5(n) | 8192 | 1024 | –.2945 | Lower | –.030 | .3423 | –.0863 |
| 5(n) | 8192 | 1024 | –.2958 | Lower | –.033 | .3983 | –.1068 |
| 5(n) | 8192 | 1024 | –.2971 | Lower[1] | –.065 | .6765 | –.1867 |
| 5(o) | 1024 | 16 | –.2933 | Upper[1] | .008 | .4372 | .8238 |
| 5(o) | 1024 | 16 | –.3037 | Lower[1] | –.040 | .4891 | –.1997 |

[1]Denotes tangential trajectories.

TABLE V.– CONCLUDED

| Figure number | $\psi$ | $R_V$ | $y_o$ | Surface | s/c | $u_d/V$ | $v_d/V$ |
|---|---|---|---|---|---|---|---|
| 5(p) | 4096 | 64 | –0.2947 | Upper[1] | 0.008 | 0.5712 | 0.8627 |
| 5(p) | 4096 | 64 | –.3026 | Lower[1] | –.024 | .2221 | –.1126 |
| 5(q) | 16384 | 256 | –.2952 | Upper[1] | .008 | .5730 | .9007 |
| 5(q) | 16384 | 256 | –.3028 | Lower[1] | –.019 | .1099 | –.0525 |

[1]Denotes tangential trajectories.

TABLE VI.– VALUES OF $C_dR/24$ AS A FUNCTION OF R

| R | $C_dR/24$ | R | $C_dR/24$ |
|---|---|---|---|
| 0.00 | 1.000 | 500 | 11.46 |
| .05 | 1.009 | 600 | 12.97 |
| .1 | 1.018 | 800 | 15.81 |
| .2 | 1.037 | 1,000 | 18.62 |
| .4 | 1.073 | 1,200 | 21.3 |
| .6 | 1.108 | 1,400 | 24.0 |
| .8 | 1.142 | 1,600 | 26.9 |
| 1.0 | 1.176 | 1,800 | 29.8 |
| 1.2 | 1.201 | 2,000 | 32.7 |
| 1.4 | 1.225 | 2,500 | 40.4 |
| 1.6 | 1.248 | 3,000 | 47.8 |
| 1.8 | 1.267 | 3,500 | 55.6 |
| 2.0 | 1.285 | 4,000 | 63.7 |
| 2.5 | 1.332 | 5,000 | 80.0 |
| 3.0 | 1.374 | 6,000 | 96.8 |
| 3.5 | 1.412 | 8,000 | 130.6 |
| 4.0 | 1.447 | 10,000 | 166.3 |
| 5.0 | 1.513 | 12,000 | 204 |
| 6.0 | 1.572 | 14,000 | 243 |
| 8.0 | 1.678 | 16,000 | 285 |
| 10.0 | 1.782 | 18,000 | 325 |
| 12 | 1.901 | 20,000 | 365 |
| 14 | 2.008 | 25,000 | 470 |
| 16 | 2.109 | 30,000 | 574 |
| 18 | 2.198 | 35,000 | 674 |
| 20 | 2.291 | 40,000 | 778 |
| 25 | 2.489 | 50,000 | 980 |
| 30 | 2.673 | 60,000 | 1175 |
| 35 | 2.851 | 80,000 | 1552 |
| 40 | 3.013 | 100,000 | 1905 |
| 50 | 3.327 | $1.2\times10^5$ | 2234 |
| 60 | 3.60 | $1.4\times10^5$ | 2549 |
| 80 | 4.11 | $1.6\times10^5$ | 2851 |
| 100 | 4.59 | | |
| 120 | 5.01 | | |
| 140 | 5.40 | | |
| 160 | 5.76 | | |
| 180 | 6.16 | | |
| 200 | 6.52 | | |
| 250 | 7.38 | | |
| 300 | 8.26 | | |
| 350 | 9.00 | | |
| 400 | 9.82 | | |

TABLE VII.– COMPARISON OF PRODUCTS OF SCALE MODULUS AND DROP DRAG COEFFICIENT FOR THE UPPER AND LOWER SURFACES OF A 15-PERCENT-THICK SYMMETRICAL JOUKOWSKI AIRFOIL

[$\alpha=0^{\circ}$; $c_l=0$]

| s/c | $R_{V_1}$ | $\psi_1$ | $R_{V_2}$ | $\psi_2$ | $R_{V_3}$ | $\psi_3$ | $R_{V_4}$ | $\psi_4$ | $R_{V_5}$ | $\psi_5$ | $C_{d_1}\psi_1$ | $C_{d_2}\psi_2$ | $C_{d_3}\psi_3$ | $C_{d_4}\psi_4$ | $C_{d_5}\psi_5$ |
|---|---|---|---|---|---|---|---|---|---|---|---|---|---|---|---|
| 0.197 | 8 | 8.0 | 32 | 24.5 | 128 | 52.0 | 512 | 105.0 | 2048 | 210.0 | 122.3 | 122.2 | 106.0 | 101.4 | 113.6 |
| .078 | 8 | 64.0 | 32 | 220.0 | 128 | 500.0 | 512 | 1000.0 | 2048 | 1810.0 | 831.9 | 953.9 | 914.6 | 874.0 | 921.7 |
| .023 | 8 | 512.0 | 32 | 1700.0 | 128 | 4250.0 | 512 | 9700.0 | 2048 | 13500.0 | 7650.5 | 8302.2 | 8535.7 | 9705.8 | 7253.0 |
| .273 | 8 | – – – | 32 | 4.0 | 128 | 5.0 | 512 | 8.8 | 2048 | 15.6 | – – – | 24.1 | 11.8 | 9.6 | 9.1 |
| .185 | 8 | 9.8 | 32 | 32.0 | 128 | 65.5 | 512 | 132.0 | 2048 | 260.0 | 146.5 | 157.1 | 132.0 | 125.9 | 139.8 |
| .073 | 8 | 73.5 | 32 | 256.0 | 128 | 560.0 | 512 | 1100.0 | 2048 | 2030.0 | 977.8 | 1133.3 | 1041.2 | 978.5 | 1044.2 |
| .265 | 8 | – – – | 32 | 4.3 | 128 | 2.0 | 512 | 14.7 | 2048 | 27.5 | – – – | 27.7 | 29.4 | 16.5 | 164.2 |
| .244 | 8 | 3.1 | 32 | 8.3 | 128 | 16.0 | 512 | 42.2 | 2048 | 64.0 | 57.2 | 49.0 | 37.3 | 45.6 | 37.3 |
| .150 | 8 | 17.3 | 32 | 58.5 | 128 | 128.0 | 512 | 250.0 | 2048 | 460.0 | 239.6 | 267.6 | 244.6 | 229.4 | 240.5 |
| .052 | 8 | 140.0 | 32 | 475.0 | 128 | 1024.0 | 512 | 2250.0 | 2048 | 3860.0 | 1944.9 | 2180.9 | 1962.7 | 2079.6 | 2017.2 |
| .015 | 8 | 1130.0 | 32 | 3400.0 | 128 | 8192.0 | 512 | 27000.0 | 2048 | 37000.0 | 16884.8 | 16604.4 | 16452.8 | 27016.2 | 19878.6 |
| .273 | 8 | – – – | 32 | 2.9 | 128 | 5.0 | 512 | 8.0 | 2048 | 15.6 | – – – | 18.3 | 12.2 | 10.0 | 9.3 |
| .225 | 8 | 4.7 | 32 | 13.4 | 128 | 27.3 | 512 | 64.0 | 2048 | 112.0 | 77.7 | 72.3 | 59.3 | 64.7 | 62.5 |
| .108 | 8 | 35.5 | 32 | 122.0 | 128 | 260.0 | 512 | 512.0 | 2048 | 940.0 | 470.9 | 538.0 | 482.6 | 415.0 | 483.0 |
| .038 | 8 | 220.0 | 32 | 730.0 | 128 | 1720.0 | 512 | 4096.0 | 2048 | 6000.0 | 3096.5 | 3385.0 | 3319.8 | 3760.8 | 3147.6 |
| .016 | 8 | 1085.0 | 32 | 3300.0 | 128 | 8250.0 | 512 | 32768.0 | 2048 | 26500.0 | 13930.5 | 14157.2 | 14931.5 | 28546.2 | 13440.0 |
| .262 | 8 | 2.0 | 32 | 4.9 | 128 | 9.0 | 512 | 17.0 | 2048 | 32.0 | 37.6 | 29.4 | 21.3 | 18.5 | 18.7 |
| .188 | 8 | 9.2 | 32 | 29.0 | 128 | 60.0 | 512 | 124.0 | 2048 | 256.0 | 137.8 | 141.9 | 120.8 | 118.0 | 137.6 |
| .072 | 8 | 76.0 | 32 | 265.0 | 128 | 575.0 | 512 | 1170.0 | 2048 | 2048.0 | 1002.1 | 660.3 | 1063.1 | 945.6 | 1048.5 |
| .022 | 8 | 580.0 | 32 | 1860.0 | 128 | 4900.0 | 512 | 11200.0 | 2048 | 16348.0 | 8683.2 | 9113.1 | 9872.0 | 10682.5 | 8814.1 |

TABLE VIII.– COMPARISON OF PRODUCTS OF SCALE MODULUS AND DROP DRAG COEFFICIENT FOR A 15-PERCENT-THICK JOUKOWSKI AIRFOIL

[$\alpha=2^{\circ}$; $c_l=0.22$]

(a) Upper Surface

| s/c | $Rv_1$ | $\psi_1$ | $Rv_2$ | $\psi_2$ | $Rv_3$ | $\psi_3$ | $Rv_4$ | $\psi_4$ | $Cd_1\psi_1$ | $Cd_2\psi_2$ | $Cd_3\psi_3$ | $Cd_4\psi_4$ |
|---|---|---|---|---|---|---|---|---|---|---|---|---|
| 0.226 | 16 | 2.0 | 64 | 4.2 | 256 | 9.6 | 1024 | 17.0 | 14.2 | 11.1 | 11.6 | 10.8 |
| .149 | 16 | 16.0 | 64 | 40.0 | 256 | 95.0 | 1024 | 185.0 | 106.8 | 102.3 | 110.8 | 113.1 |
| .055 | 16 | 128.0 | 64 | 325.0 | 256 | 700.0 | 1024 | 1310.0 | 826.0 | 808.1 | 796.8 | 788.5 |
| .008 | 16 | 1024.0 | 64 | 2380.0 | 256 | 6200.0 | 1024 | 9700.0 | 9450.0 | 7893.9 | 10258.8 | 7026.6 |
| .212 | 16 | 3.7 | 64 | 8.0 | 256 | 18.4 | 1024 | 35.0 | 26.1 | 21.4 | 22.3 | 22.1 |
| .128 | 16 | 24.5 | 64 | 64.0 | 256 | 140.0 | 1024 | 276.0 | 161.1 | 162.2 | 161.7 | 168.1 |
| .038 | 16 | 220.0 | 64 | 512.0 | 256 | 1155.0 | 1024 | 2150.0 | 1449.0 | 1300.0 | 1334.3 | 1310.4 |
| .003 | 16 | 1700.0 | 64 | 4096.0 | 256 | 12500.0 | 1024 | --- | 13430.6 | 11462.5 | 16280.6 | --- |
| .236 | 16 | --- | 64 | --- | 256 | 4.0 | 1024 | 8.0 | ---- | ---- | 4.9 | 5.1 |
| .196 | 16 | 5.8 | 64 | 12.9 | 256 | 32.0 | 1024 | 61.0 | 40.2 | 34.1 | 38.2 | 38.1 |
| .100 | 16 | 45.0 | 64 | 115.0 | 256 | 256.0 | 1024 | 475.0 | 286.5 | 284.3 | 290.1 | 284.2 |
| .024 | 16 | 372.0 | 64 | 930.0 | 256 | 2048.0 | 1024 | 3700.0 | 2534.9 | 2919.6 | 2424.0 | 2289.5 |
| .002 | 16 | 2300.0 | 64 | 5300.0 | 256 | 16384.0 | 1024 | --- | 26270.1 | 20785.4 | 27433.4 | --- |
| .223 | 16 | 2.4 | 64 | 4.7 | 256 | 11.0 | 1024 | 16.0 | 16.9 | 12.6 | 13.4 | 10.2 |
| .168 | 16 | 10.7 | 64 | 25.6 | 256 | 62.0 | 1024 | 128.0 | 71.8 | 63.6 | 72.8 | 78.8 |
| .063 | 16 | 106.0 | 64 | 263.0 | 256 | 560.0 | 1024 | 1024.0 | 670.2 | 648.5 | 630.8 | 630.3 |
| .010 | 16 | 850.0 | 64 | 2100.0 | 256 | 5400.0 | 1024 | 8192.0 | 6679.1 | 6121.9 | 7023.0 | 5454.7 |

TABLE VIII.– CONCLUDED

(b) Lower Surface

| s/c | $R_{V_1}$ | $\psi_1$ | $R_{V_2}$ | $\psi_2$ | $R_{V_3}$ | $\psi_3$ | $R_{V_4}$ | $\psi_4$ | $C_{d_1}\psi_1$ | $C_{d_2}\psi_2$ | $C_{d_3}\psi_3$ | $C_{d_4}\psi_4$ |
|---|---|---|---|---|---|---|---|---|---|---|---|---|
| -0.311 | 16 | 2.0 | 64 | 6.0 | 256 | 10.0 | 1024 | 17.2 | 25.2 | 25.7 | 18.1 | 14.9 |
| -.245 | 16 | 16.0 | 64 | 45.5 | 256 | 89.0 | 1024 | 170.0 | 195.0 | 187.0 | 155.9 | 143.9 |
| -.098 | 16 | 128.0 | 64 | 370.0 | 256 | 780.0 | 1024 | 1440.0 | 1372.0 | 1385.1 | 1253.7 | 1131.4 |
| -.015 | 16 | 1024.0 | 64 | 4000.0 | 256 | 13000.0 | 1024 | 21200.0 | 19660.0 | 24463.4 | 31159.7 | 23460.3 |
| -.308 | 16 | 2.5 | 64 | 8.0 | 256 | 12.4 | 1024 | 21.6 | 31.8 | 34.0 | 22.3 | 18.7 |
| -.225 | 16 | 22.1 | 64 | 64.0 | 256 | 121.0 | 1024 | 237.0 | 257.2 | 249.3 | 205.0 | 194.6 |
| -.079 | 16 | 163.0 | 64 | 512.0 | 256 | 1130.0 | 1024 | 2100.0 | 1748.2 | 1843.4 | 1815.8 | 1652.5 |
| -.015 | 16 | 1000.0 | 64 | 4096.0 | 256 | 13200.0 | 1024 | 21100.0 | 14382.4 | 19346.4 | 25814.3 | 19672.2 |
| -.316 | 16 | - - - | 64 | - - - | 256 | 4.0 | 1024 | - - - - | - - - - | - - - - | 7.1 | - - - - |
| -.295 | 16 | 5.2 | 64 | 14.3 | 256 | 32.0 | 1024 | 52.5 | 64.9 | 60.1 | 57.2 | 45.3 |
| -.177 | 16 | 43.0 | 64 | 121.0 | 256 | 256.0 | 1024 | 490.0 | 482.2 | 454.7 | 422.7 | 554.5 |
| -.055 | 16 | 265.0 | 64 | 850.0 | 256 | 2048.0 | 1024 | 3750.0 | 2804.8 | 3024.9 | 3263.0 | 2923.7 |
| -.014 | 16 | 1100.0 | 64 | 4250.0 | 256 | 16384.0 | 1024 | - - - | 19103.7 | 23730.3 | 35962.1 | - - - |
| -.310 | 16 | 2.0 | 64 | 6.2 | 256 | 11.0 | 1024 | 16.0 | 25.5 | 26.4 | 19.8 | 13.9 |
| -.265 | 16 | 11.1 | 64 | 31.3 | 256 | 62.5 | 1024 | 128.0 | 137.0 | 129.0 | 110.2 | 108.6 |
| -.118 | 16 | 91.0 | 64 | 272.0 | 256 | 560.0 | 1024 | 1024.0 | 993.8 | 996.3 | 909.4 | 811.4 |
| -.031 | 16 | 480.0 | 64 | 1600.0 | 256 | 3900.0 | 1024 | 8192.0 | 6575.0 | 7249.8 | 7381.0 | 7400.0 |

TABLE IX.– COMPARISON OF PRODUCTS OF SCALE MODULUS AND DROP DRAG COEFFICIENT FOR A 15-PERCENT-THICK SYMMETRICAL JOUKOWSKI AIRFOIL

[$\alpha=4^{\circ}$; $c_l=0.44$]

(a) Upper Surface

| s/c | $R_{V_1}$ | $\psi_1$ | $R_{V_2}$ | $\psi_2$ | $R_{V_3}$ | $\psi_3$ | $R_{V_4}$ | $\psi_4$ | $C_{d_1}\psi_1$ | $C_{d_2}\psi_2$ | $C_{d_3}\psi_3$ | $C_{d_4}\psi_4$ |
|---|---|---|---|---|---|---|---|---|---|---|---|---|
| 0.192 | 16 | 2.0 | 64 | 3.6 | 256 | 7.6 | 1024 | 16.5 | 11.3 | 8.1 | 7.9 | 9.4 |
| .121 | 16 | 16.0 | 64 | 34.3 | 256 | 64.5 | 1024 | 137.0 | 87.2 | 74.3 | 65.5 | 76.2 |
| .042 | 16 | 128.0 | 64 | 335.0 | 256 | 520.0 | 1024 | 1000.0 | 635.0 | 680.2 | 2274.9 | 540.7 |
| .004 | 16 | 1024.0 | 64 | 3000.0 | 256 | 7400.0 | 1024 | --- | 8740.0 | 9352.9 | 10161.2 | --- |
| .170 | 16 | 4.4 | 64 | 8.0 | 256 | 17.0 | 1024 | 36.0 | 24.8 | 18.0 | 17.8 | 20.7 |
| .100 | 16 | 27.5 | 64 | 64.0 | 256 | 112.0 | 1024 | 230.0 | 147.4 | 138.3 | 114.3 | 116.9 |
| .026 | 16 | 230.0 | 64 | 512.0 | 256 | 970.0 | 1024 | 1680.0 | 1117.3 | 1023.0 | 919.8 | 896.5 |
| .002 | 16 | --- | 64 | 4096.0 | 256 | 13000.0 | 1024 | --- | --- | 13065.4 | 18246.3 | --- |
| .204 | 16 | --- | 64 | --- | 256 | 4.0 | 1024 | 9.0 | --- | --- | 4.1 | 5.1 |
| .148 | 16 | 8.0 | 64 | 15.5 | 256 | 32.0 | 1024 | 68.0 | 44.5 | 34.5 | 33.1 | 38.4 |
| .068 | 16 | 63.0 | 64 | 150.0 | 256 | 256.0 | 1024 | 490.0 | 328.7 | 317.2 | 255.1 | 270.4 |
| .015 | 16 | 370.0 | 64 | 990.0 | 256 | 2048.0 | 1024 | 2850.0 | 2203.4 | 2320.8 | 2225.7 | 1661.6 |
| .002 | 16 | --- | 64 | --- | 256 | 16384.0 | 1024 | --- | --- | --- | 22147.7 | --- |
| .194 | 16 | --- | 64 | 3.3 | 256 | 6.8 | 1024 | 16.0 | --- | 7.4 | 7.1 | 9.1 |
| .127 | 16 | 13.6 | 64 | 29.0 | 256 | 55.0 | 1024 | 128.0 | 74.9 | 64.0 | 56.6 | 72.2 |
| .043 | 16 | 130.0 | 64 | 320.0 | 256 | 500.0 | 1024 | 1024.0 | 542.1 | 544.0 | 477.9 | 552.7 |
| .004 | 16 | --- | 64 | 2900.0 | 256 | 7400.0 | 1024 | 8192.0 | --- | 10190.8 | 11236.8 | 6156.6 |

TABLE IX.– CONCLUDED

(b) Lower Surface

| s/c | $Rv_1$ | $\psi_1$ | $Rv_2$ | $\psi_2$ | $Rv_3$ | $\psi_3$ | $Rv_4$ | $\psi_4$ | $C_{d_1}\psi_1$ | $C_{d_2}\psi_2$ | $C_{d_3}\psi_3$ | $C_{d_4}\psi_4$ |
|---|---|---|---|---|---|---|---|---|---|---|---|---|
| -0.409 | 16 | 2.0 | 64 | 2.0 | 256 | – – | 1024 | 7.0 | 39.8 | 10.6 | – – – | 8.7 |
| -.336 | 16 | 16.0 | 64 | 35.0 | 256 | 84.0 | 1024 | 152.0 | 254.6 | 150.4 | 201.2 | 168.6 |
| -.145 | 16 | 128.0 | 64 | 330.0 | 256 | 740.0 | 1024 | 1150.0 | 1220.6 | 1372.5 | 1297.1 | 971.9 |
| -.035 | 16 | 1024.0 | 64 | 2400.0 | 256 | 6600.0 | 1024 | 11500.0 | 10233.0 | 10232.0 | 11898.0 | 999.1 |
| -.400 | 16 | 3.7 | 64 | 8.0 | 256 | 9.5 | 1024 | 20.0 | 72.9 | 41.5 | 26.7 | 24.5 |
| -.286 | 16 | 20.8 | 64 | 64.0 | 256 | 170.0 | 1024 | 280.0 | 285.2 | 239.8 | 369.8 | 288.6 |
| -.112 | 16 | 187.0 | 64 | 512.0 | 256 | 1100.0 | 1024 | 1700.0 | 1847.1 | 2161.5 | 1968.5 | 1460.9 |
| -.026 | 16 | 1670.0 | 64 | 4096.0 | 256 | 12000.0 | 1024 | 27000.0 | 20155.0 | 13461.0 | 24002.1 | 25598.0 |
| -.408 | 16 | 2.3 | 64 | 2.5 | 256 | 4.0 | 1024 | 7.0 | 45.2 | 13.1 | 10.9 | 8.6 |
| -.379 | 16 | 7.4 | 64 | 16.0 | 256 | 32.0 | 1024 | 60.0 | 133.8 | 77.5 | 86.6 | 70.6 |
| -.247 | 16 | 42.5 | 64 | 102.0 | 256 | 256.0 | 1024 | 420.0 | 520.5 | 344.6 | 519.6 | 405.3 |
| -.072 | 16 | 350.0 | 64 | 900.0 | 256 | 2048.0 | 1024 | 3400.0 | 3890.6 | 2792.0 | 3948.3 | 3119.2 |
| -.025 | 16 | 1700.0 | 64 | 4500.0 | 256 | 16384.0 | 1024 | 28000.0 | 20822.0 | 15201.0 | 33260.0 | 27025.0 |
| -.400 | 16 | 3.8 | 64 | 6.2 | 256 | 9.5 | 1024 | 16.0 | 72.9 | 32.1 | 26.7 | 19.6 |
| -.350 | 16 | 12.5 | 64 | 28.0 | 256 | 65.0 | 1024 | 128.0 | 204.8 | 123.7 | 158.8 | 143.6 |
| -.155 | 16 | 114.0 | 64 | 295.0 | 256 | 6500.0 | 1024 | 1024.0 | 1087.1 | 1227.0 | 1139.4 | 865.4 |
| -.041 | 16 | 760.0 | 64 | 1950.0 | 256 | 4700.0 | 1024 | 8192.0 | 7987.6 | 5727.3 | 8729.8 | 7280.3 |

TABLE X.– COMPARISON OF PRODUCTS OF SCALE MODULUS AND DROP DRAG COEFFICIENT FOR A 15-PERCENT-THICK CAMBERED JOUKOWSKI AIRFOIL

[$\alpha=0^{\circ}$; $c_l=0.44$; a=1.0 MEAN LINE]

(a) Upper Surface

| s/c | $Rv_1$ | $\psi_1$ | $Rv_2$ | $\psi_2$ | $Rv_3$ | $\psi_3$ | $Rv_4$ | $\psi_4$ | $Cd_1\psi_1$ | $Cd_2\psi_2$ | $Cd_3\psi_3$ | $Cd_4\psi_4$ |
|---|---|---|---|---|---|---|---|---|---|---|---|---|
| 0.305 | 16 | 2.0 | 64 | 5.0 | 256 | 10.7 | 1024 | 21.5 | 15.0 | 13.9 | 13.5 | 13.9 |
| .211 | 16 | 16.0 | 64 | 47.0 | 256 | 112.5 | 1024 | 222.0 | 122.9 | 134.0 | 143.9 | 146.5 |
| .092 | 16 | 128.0 | 64 | 338.0 | 256 | 730.0 | 1024 | 1380.0 | 1116.0 | 1074.3 | 1017.2 | 971.6 |
| .022 | 16 | 1024.0 | 64 | 2550.0 | 256 | 5100.0 | 1024 | 9300.0 | 14170.0 | 11670.1 | 9747.6 | 8457.7 |
| .294 | 16 | 3.1 | 64 | 8.0 | 256 | 17.5 | 1024 | 34.2 | 22.9 | 22.4 | 22.0 | 22.2 |
| .192 | 16 | 22.0 | 64 | 64.0 | 256 | 152.0 | 1024 | 292.0 | 172.4 | 185.9 | 197.0 | 194.5 |
| .072 | 16 | 203.0 | 64 | 512.0 | 256 | 1070.0 | 1024 | 2050.0 | 1900.4 | 1697.8 | 1563.6 | 1496.0 |
| .015 | 16 | 1510.0 | 64 | 4096.0 | 256 | 7400.0 | 1024 | 13000.0 | 20354.5 | 18122.2 | 13735.2 | 11553.5 |
| .317 | 16 | – – – | 64 | – – – | 256 | 4.0 | 1024 | 8.4 | – – – – | – – – – | 5.1 | 5.5 |
| .275 | 16 | 5.1 | 64 | 13.5 | 256 | 32.0 | 1024 | 63.0 | 37.4 | 37.2 | 39.3 | 40.5 |
| .158 | 16 | 38.5 | 64 | 107.0 | 256 | 256.0 | 1024 | 475.0 | 304.2 | 313.9 | 333.6 | 317.7 |
| .046 | 16 | 305.0 | 64 | 1000.0 | 256 | 2048.0 | 1024 | 3850.0 | 3619.9 | 4035.1 | 3533.4 | 3208.3 |
| .006 | 16 | 3500.0 | 64 | 9600.0 | 256 | 16384.0 | 1024 | 29000.0 | 41119.9 | 38413.8 | 27985.0 | 24083.6 |
| .310 | 16 | – – – | 64 | 3.4 | 256 | 7.9 | 1024 | 16.0 | – – – – | 9.6 | 10.1 | 10.6 |
| .243 | 16 | 9.4 | 64 | 26.2 | 256 | 64.7 | 1024 | 128.0 | 70.3 | 73.6 | 81.4 | 83.2 |
| .109 | 16 | 92.0 | 64 | 245.0 | 256 | 540.0 | 1024 | 1024.0 | 771.4 | 753.3 | 730.9 | 706.2 |
| .025 | 16 | 870.0 | 64 | 2120.0 | 256 | 4300.0 | 1024 | 8192.0 | 12211.0 | 9806.6 | 8287.0 | 7515.4 |

TABLE X.– CONCLUDED

(b) Lower Surface

| s/c | $R_{V_1}$ | $\psi_1$ | $R_{V_2}$ | $\psi_2$ | $R_{V_3}$ | $\psi_3$ | $R_{V_4}$ | $\psi_4$ | $C_{d_1}\psi_1$ | $C_{d_2}\psi_2$ | $C_{d_3}\psi_3$ | $C_{d_4}\psi_4$ |
|---|---|---|---|---|---|---|---|---|---|---|---|---|
| -0.215 | 16 | 2.0 | 64 | 6.6 | 256 | 8.0 | 1024 | 12.0 | 22.6 | 25.6 | 13.3 | 9.7 |
| -.180 | 16 | 16.0 | 64 | 36.5 | 256 | 67.8 | 1024 | 140.0 | 162.0 | 130.3 | 104.6 | 106.3 |
| -.068 | 16 | 128.0 | 64 | 345.0 | 256 | 740.0 | 1024 | 1520.0 | 988.0 | 993.3 | 952.5 | 1005.8 |
| -.018 | 16 | 1024.0 | 64 | 225.0 | 256 | 6300.0 | 1024 | 12500.0 | 9680.0 | 7605.0 | 9266.1 | 9154.0 |
| -.212 | 16 | 3.2 | 64 | 8.0 | 256 | 10.0 | 1024 | 19.0 | 36.1 | 31.0 | 16.6 | 15.4 |
| -.157 | 16 | 26.5 | 64 | 64.0 | 256 | 122.0 | 1024 | 250.0 | 257.1 | 221.2 | 182.6 | 186.3 |
| -.053 | 16 | 183.0 | 64 | 512.0 | 256 | 1430.0 | 1024 | 2400.0 | 1410.4 | 1469.8 | 1449.5 | 1580.8 |
| -.012 | 16 | 1700.0 | 64 | 4096.0 | 256 | 11000.0 | 1024 | 22000.0 | 15049.1 | 13150.4 | 15489.9 | 15616.7 |
| -.216 | 16 | - - - | 64 | - - - | 256 | 4.0 | 1024 | 10.0 | - - - - | - - - - | 9.5 | 8.1 |
| -.199 | 16 | 8.3 | 64 | 19.0 | 256 | 32.0 | 1024 | 58.0 | 89.4 | 71.0 | 53.6 | 45.5 |
| -.120 | 16 | 49.0 | 64 | 129.0 | 256 | 256.0 | 1024 | 508.0 | 435.3 | 414.9 | 361.5 | 360.1 |
| -.038 | 16 | 320.0 | 64 | 840.0 | 256 | 2048.0 | 1024 | 4200.0 | 2643.6 | 2554.3 | 2748.6 | 2882.8 |
| -.008 | 16 | 2500.0 | 64 | 6400.0 | 256 | 16384.0 | 1024 | 28500.0 | 18407.6 | 17738.0 | 20373.0 | 18450.6 |
| -.213 | 16 | 2.6 | 64 | 5.6 | 256 | 6.0 | 1024 | 16.0 | 29.8 | 22.1 | 10.1 | 13.0 |
| -.183 | 16 | 14.3 | 64 | 33.0 | 256 | 62.0 | 1024 | 128.0 | 147.9 | 119.8 | 96.9 | 98.5 |
| -.085 | 16 | 89.0 | 64 | 245.0 | 256 | 508.0 | 1024 | 1024.0 | 714.4 | 725.7 | 668.6 | 692.2 |
| -.025 | 16 | 610.0 | 64 | 1500.0 | 256 | 4000.0 | 1024 | 8192.0 | 5854.3 | 5121.0 | 5952.4 | 6055.4 |

TABLE XI.– COMPARISON OF PRODUCTS OF SCALE MODULUS AND DROP DRAG COEFFICIENT FOR AN NACA $65_2$-015 AIRFOIL

[$\alpha=0^\circ$; $c_l=0.44$]

(a) Upper Surface

| s/c | $R_{V_1}$ | $\psi_1$ | $R_{V_2}$ | $\psi_2$ | $R_{V_3}$ | $\psi_3$ | $R_{V_4}$ | $\psi_4$ | $C_{d_1}\psi_1$ | $C_{d_2}\psi_2$ | $C_{d_3}\psi_3$ | $C_{d_4}\psi_4$ |
|---|---|---|---|---|---|---|---|---|---|---|---|---|
| 0.259 | 16 | 2.0 | 64 | 5.0 | 256 | 10.0 | 1024 | 20.5 | 13.3 | 12.8 | 11.6 | 12.5 |
| .128 | 16 | 16.0 | 64 | 41.0 | 256 | 92.0 | 1024 | 161.0 | 106.8 | 104.9 | 107.3 | 98.7 |
| .021 | 16 | 128.0 | 64 | 390.0 | 256 | 760.0 | 1024 | 1400.0 | 859.0 | 1004.2 | 892.1 | 861.6 |
| .008 | 16 | 1024.0 | 64 | 3000.0 | 256 | 9000.0 | 1024 | --- | 9973.3 | 10410.1 | 13503.7 | --- |
| .240 | 16 | 3.5 | 64 | 8.0 | 256 | 17.1 | 1024 | 33.7 | 23.4 | 20.6 | 19.9 | 20.7 |
| .092 | 16 | 25.0 | 64 | 64.0 | 256 | 137.0 | 1024 | 248.0 | 165.9 | 163.7 | 159.3 | 151.6 |
| .018 | 16 | 160.0 | 64 | 512.0 | 256 | 1050.0 | 1024 | 1800.0 | 1102.3 | 1349.7 | 1249.6 | 1121.6 |
| .008 | 16 | --- | 64 | 4096.0 | 256 | --- | 1024 | --- | --- | 12800.0 | --- | --- |
| .281 | 16 | --- | 64 | --- | 256 | 4.0 | 1024 | 7.6 | --- | --- | 4.7 | 4.6 |
| .209 | 16 | 5.9 | 64 | 14.4 | 256 | 32.0 | 1024 | 59.0 | 39.3 | 36.9 | 37.2 | 36.1 |
| .047 | 16 | 52.0 | 64 | 128.0 | 256 | 256.0 | 1024 | 500.0 | 342.0 | 324.3 | 295.6 | 303.9 |
| .014 | 16 | 260.0 | 64 | 890.0 | 256 | 2048.0 | 1024 | 3500.0 | 1980.5 | 2534.9 | 2612.2 | 2304.7 |
| .008 | 16 | --- | 64 | --- | 256 | 16384.0 | 1024 | --- | --- | --- | 25005.3 | --- |
| .267 | 16 | --- | 64 | 3.7 | 256 | 7.6 | 1024 | 16.0 | --- | 9.4 | 8.8 | 9.8 |
| .150 | 16 | 12.2 | 64 | 32.0 | 256 | 71.0 | 1024 | 128.0 | 81.7 | 82.4 | 82.8 | 78.6 |
| .026 | 16 | 97.0 | 64 | 270.0 | 256 | 530.0 | 1024 | 1024.0 | 641.1 | 687.5 | 614.6 | 624.5 |
| .010 | 16 | 540.0 | 64 | 2100.0 | 256 | 5000.0 | 1024 | 8192.0 | 4657.4 | 6593.7 | 6910.3 | 5729.5 |

TABLE XI.– CONCLUDED

(b) Lower Surface

| s/c | $R_{V_1}$ | $\psi_1$ | $R_{V_2}$ | $\psi_2$ | $R_{V_3}$ | $\psi_3$ | $R_{V_4}$ | $\psi_4$ | $C_{d_1}\psi_1$ | $C_{d_2}\psi_2$ | $C_{d_3}\psi_3$ | $C_{d_4}\psi_4$ |
|---|---|---|---|---|---|---|---|---|---|---|---|---|
| -0.514 | 16 | 2.0 | 64 | 5.0 | 256 | 10.0 | 1024 | 16.0 | 27.2 | 21.9 | 18.4 | 13.2 |
| -.481 | 16 | 16.0 | 64 | 31.0 | 256 | 74.0 | 1024 | 135.0 | 213.0 | 137.2 | 132.4 | 119.9 |
| -.185 | 16 | 128.0 | 64 | 345.0 | 256 | 900.0 | 1024 | 1620.0 | 2330.0 | 2013.4 | 2079.1 | 1732.5 |
| -.040 | 16 | 1024.0 | 64 | 2400.0 | 256 | 5800.0 | 1024 | 15800.0 | 17910.0 | 13499.9 | 12989.4 | 15734.6 |
| -.512 | 16 | 2.7 | 64 | 8.0 | 256 | 13.5 | 1024 | 21.0 | 36.5 | 34.9 | 24.8 | 18.5 |
| -.417 | 16 | 28.0 | 64 | 64.0 | 256 | 160.0 | 1024 | 275.0 | 396.1 | 289.8 | 303.3 | 226.5 |
| -.145 | 16 | 172.0 | 64 | 512.0 | 256 | 1250.0 | 1024 | 2360.0 | 3275.0 | 3107.2 | 2975.1 | 2587.9 |
| -.024 | 16 | 1200.0 | 64 | 4096.0 | 256 | 10800.0 | 1024 | --- | 20475.7 | 18420.0 | 18749.1 | --- |
| -.523 | 16 | --- | 64 | --- | 256 | 4.0 | 1024 | --- | ---- | ---- | 7.4 | --- |
| -.506 | 16 | 6.0 | 64 | 12.3 | 256 | 32.0 | 1024 | 52.0 | 82.9 | 54.6 | 59.7 | 46.3 |
| -.355 | 16 | 42.0 | 64 | 98.0 | 256 | 256.0 | 1024 | 448.0 | 623.7 | 476.3 | 512.2 | 396.7 |
| -.100 | 16 | 282.0 | 64 | 780.0 | 256 | 2048.0 | 1024 | 4000.0 | 5617.2 | 4927.4 | 5051.8 | 4516.0 |
| -.019 | 16 | --- | 64 | --- | 256 | 16384.0 | 1024 | --- | --- | --- | 19462.9 | --- |
| -.514 | 16 | 2.0 | 64 | 5.0 | 256 | 10.0 | 1024 | 16.0 | 27.4 | 22.0 | 18.5 | 14.2 |
| -.485 | 16 | 14.8 | 64 | 29.5 | 256 | 70.0 | 1024 | 128.0 | 205.8 | 131.7 | 130.9 | 114.5 |
| -.245 | 16 | 83.5 | 64 | 215.0 | 256 | 570.0 | 1024 | 1024.0 | 1316.1 | 1101.6 | 1188.3 | 952.1 |
| -.065 | 16 | 500.0 | 64 | 1330.0 | 256 | 3280.0 | 1024 | 8192.0 | 9869.7 | 8340.7 | 8014.6 | 9250.3 |

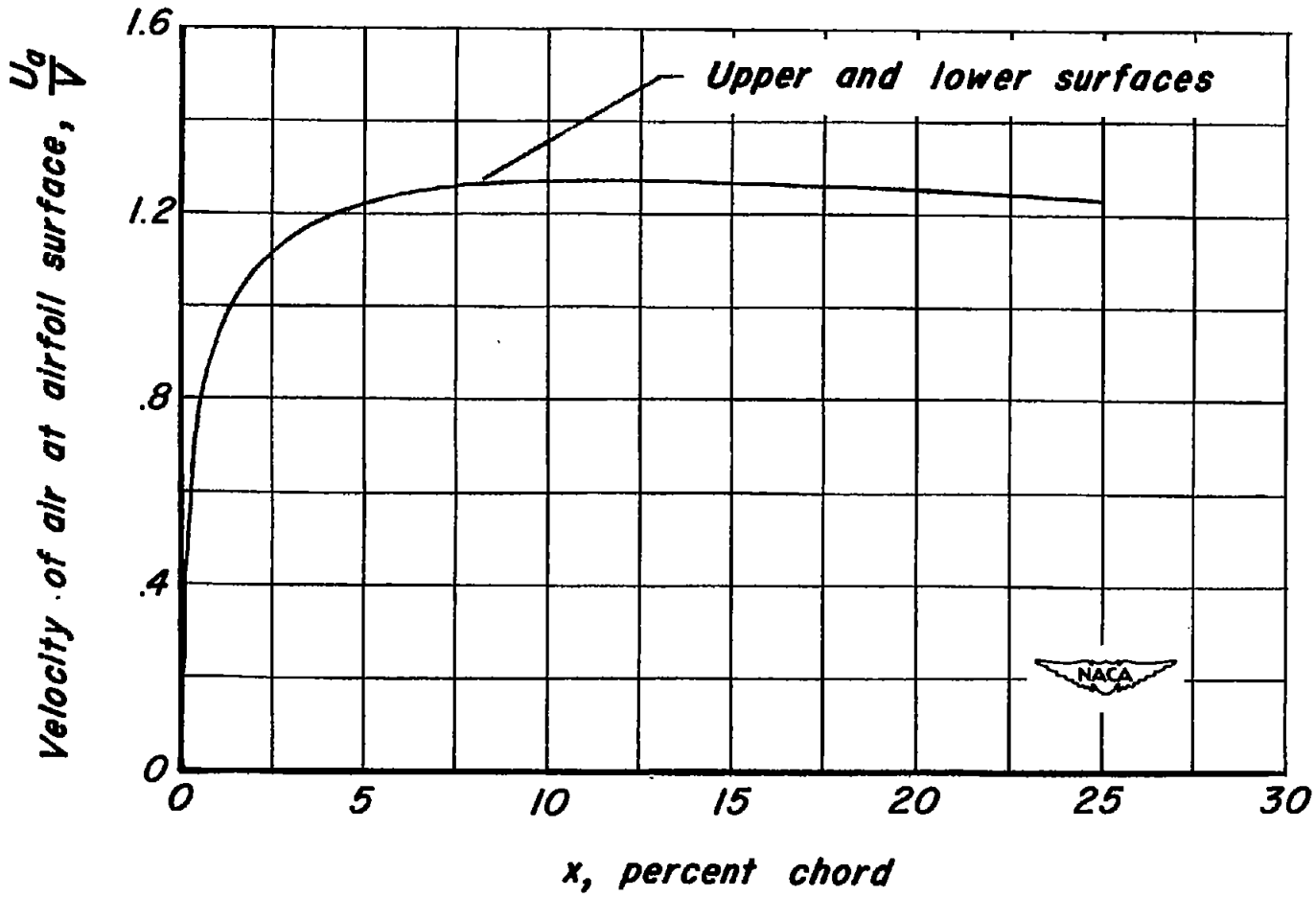


(a) 15-percent-thick symmetrical Joukowski; $\alpha = 0°$.

Figure 1.- Airfoil velocity distributions for the five airfoil cases comprising the differential analyzer study.

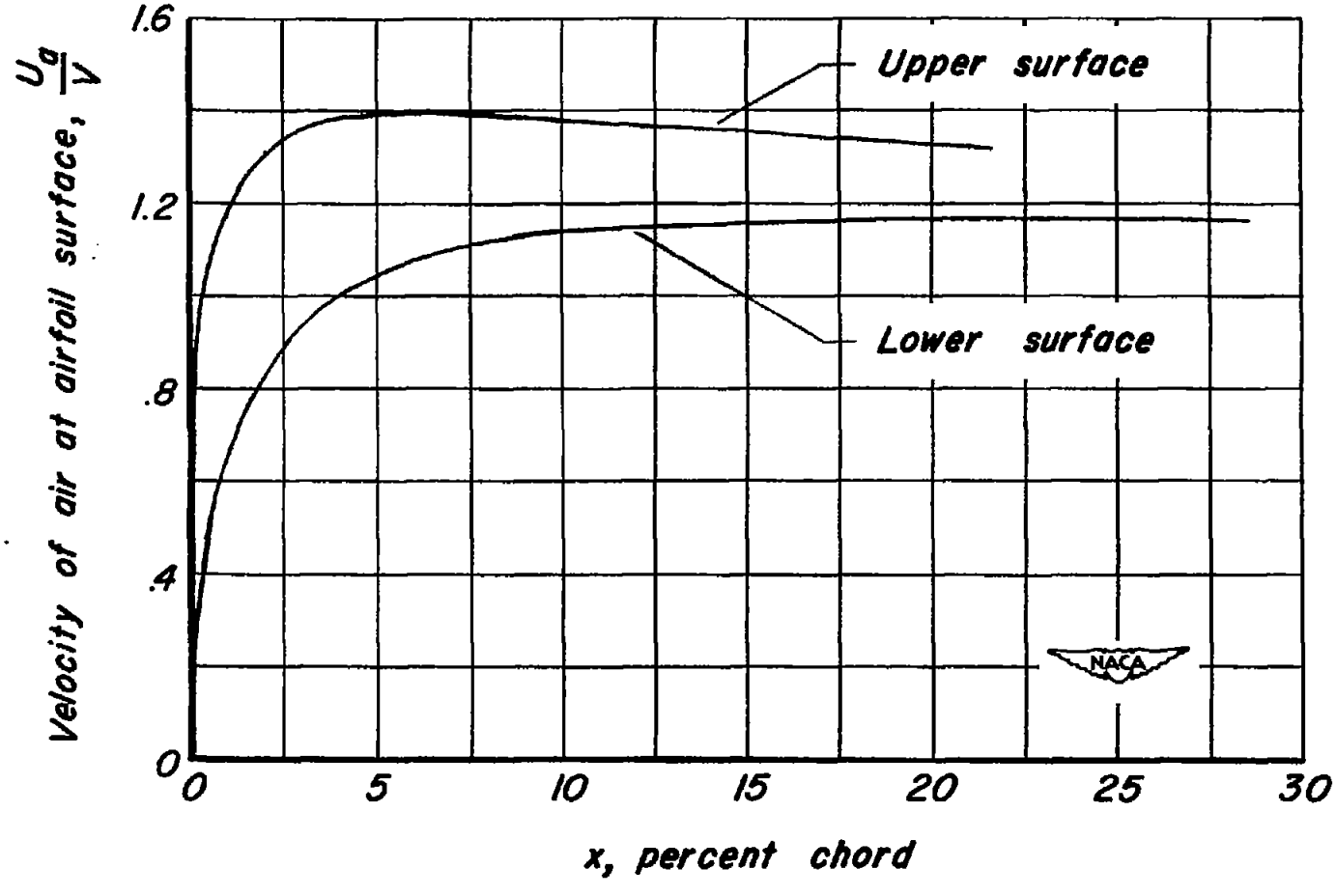


(b) 15-percent-thick symmetrical Joukowski; $\alpha = 2°$.

Figure 1.- Continued.

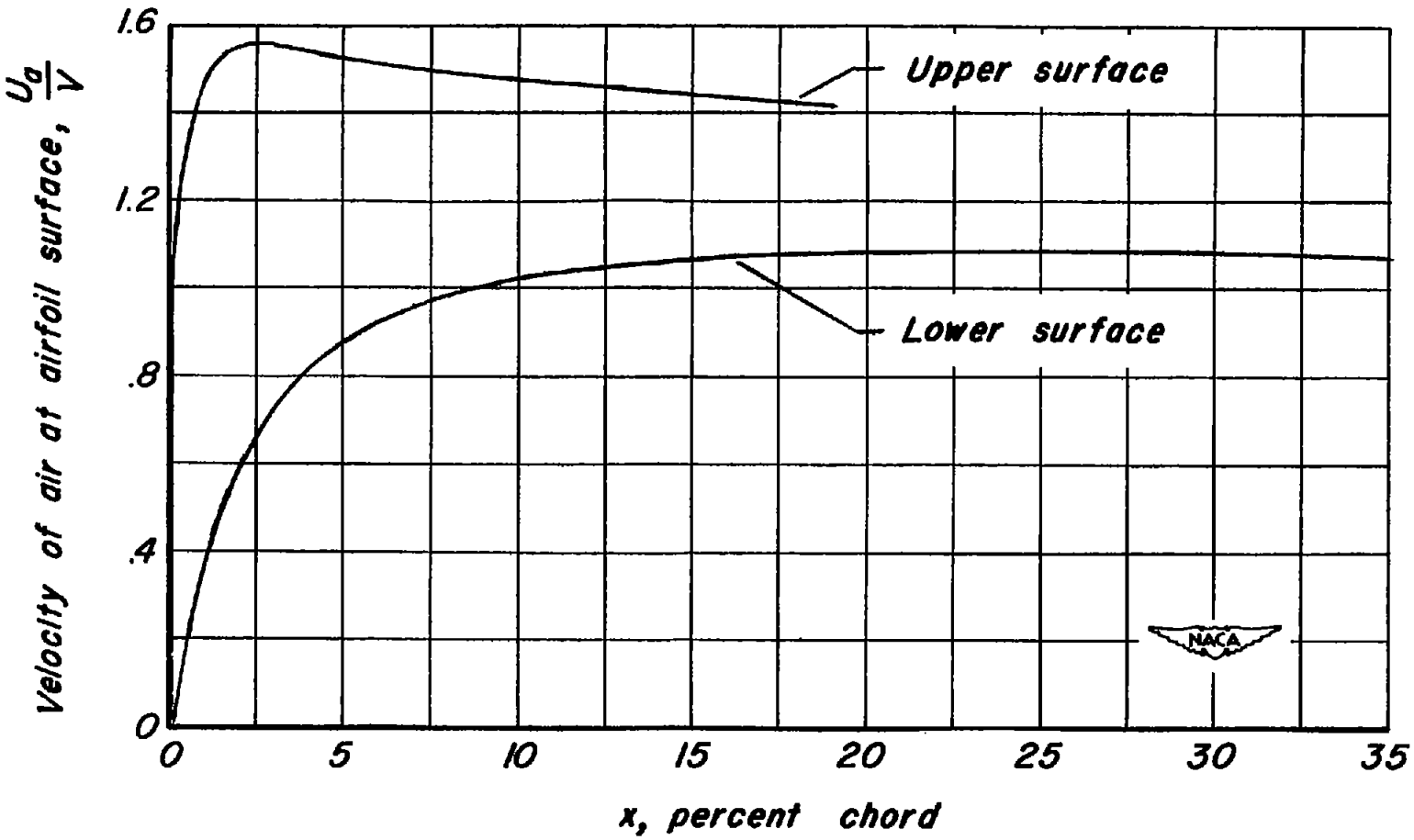


(c) 15-percent-thick symmetrical Joukowski; $\alpha = 4°$.

Figure 1.- Continued.

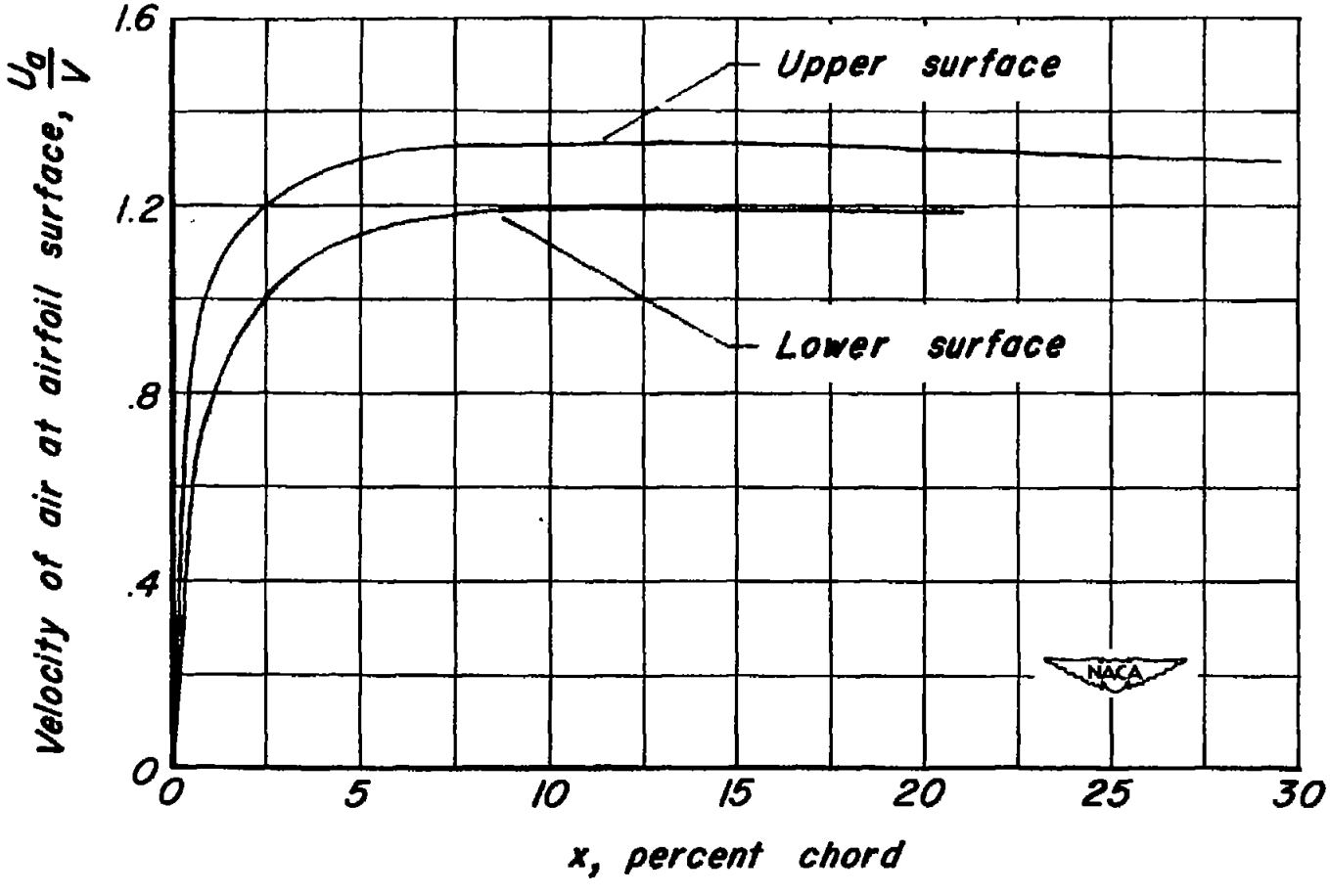


(d) 15-percent-thick cambered Joukowski; $c_l = 0.44$; $\alpha = 0°$; $a = 1.0$ mean line.

Figure 1.- Continued.

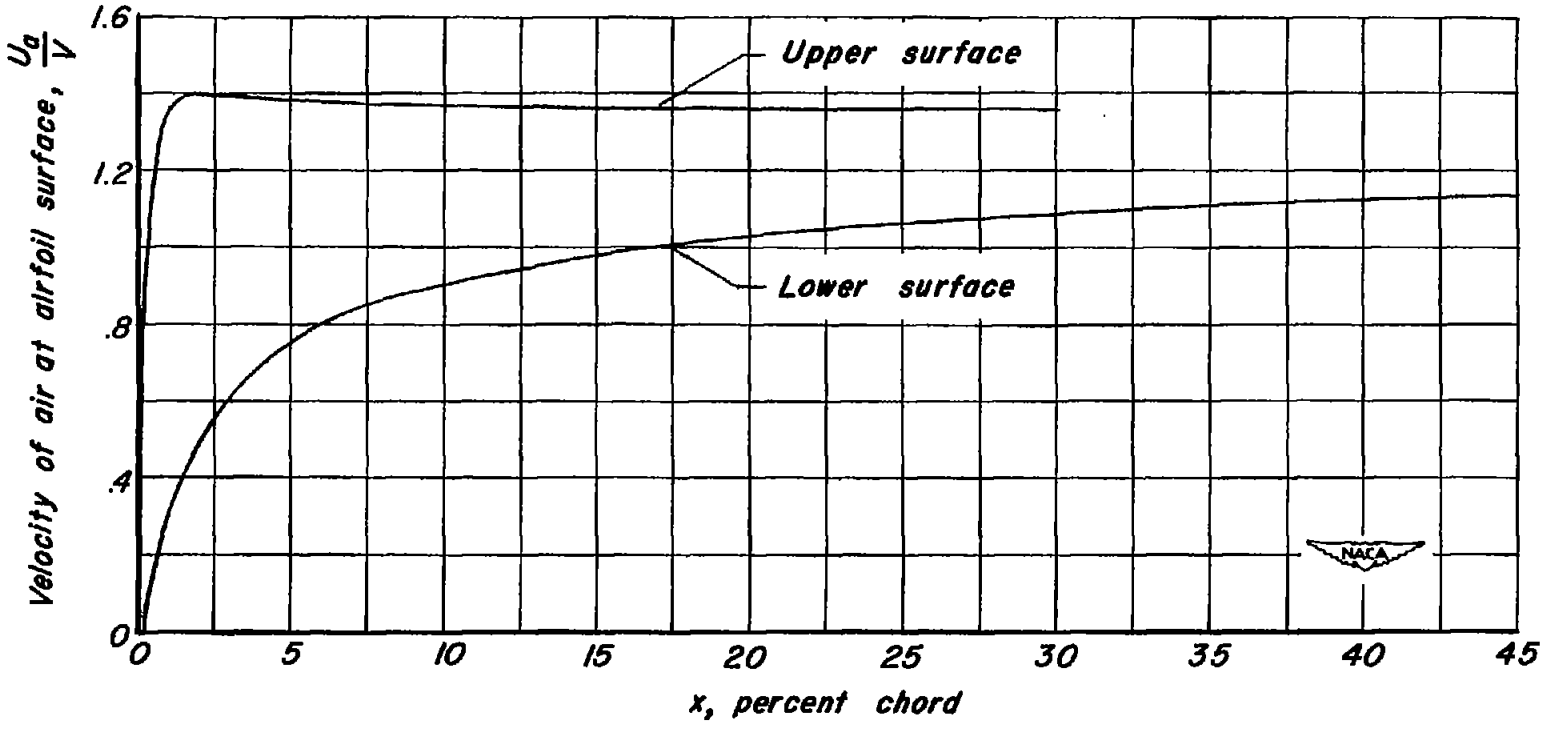


(e) NACA $65_2$-015 airfoil; $\alpha = 4°$.

*Figure 1.- Concluded.*

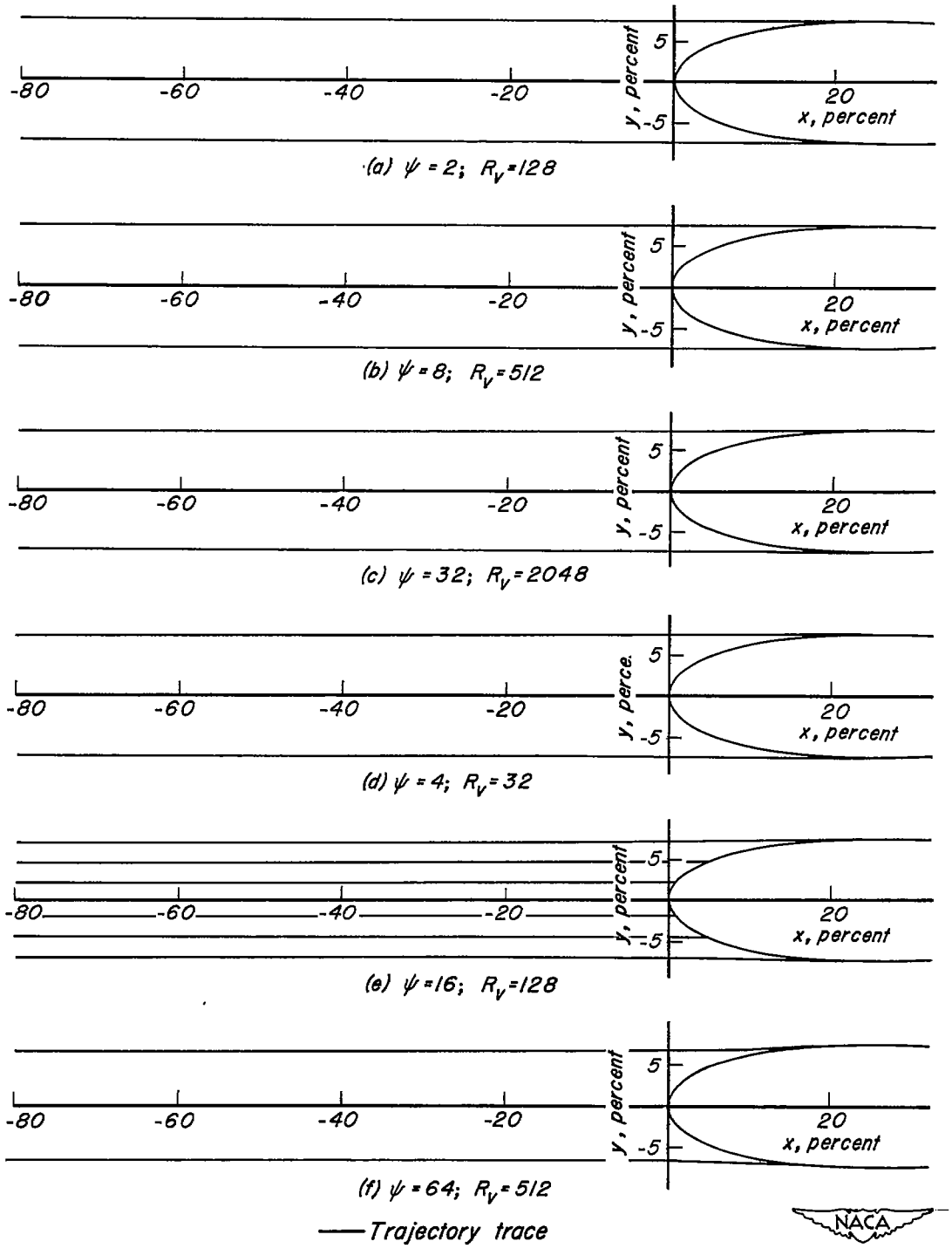


*Figure 2.- Water-drop trajectory traces from a differential analyzer for a 15-percent-thick symmetrical Joukowski airfoil; $c_l = 0$; $\alpha = 0°$.*

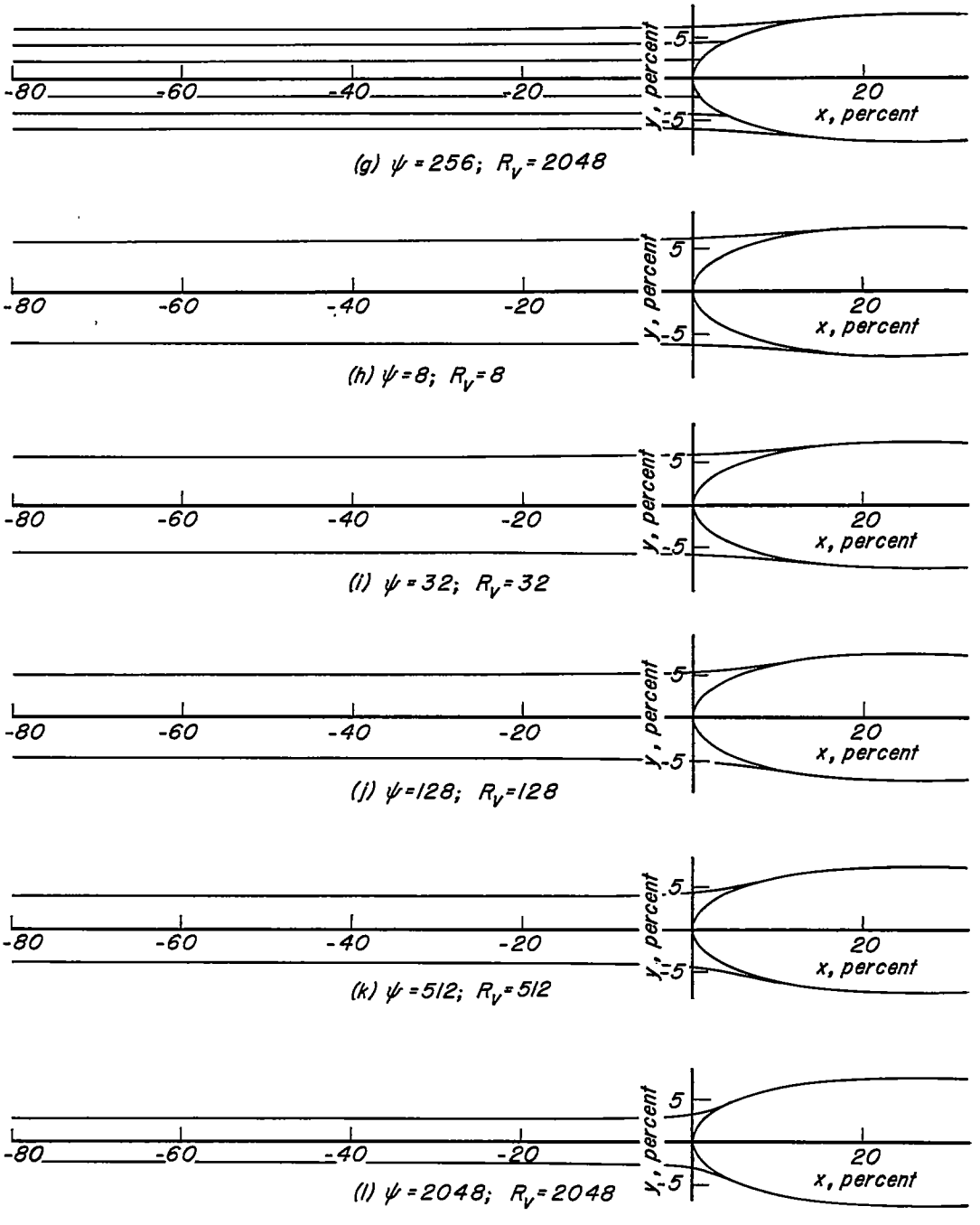


Figure 2.- Continued.

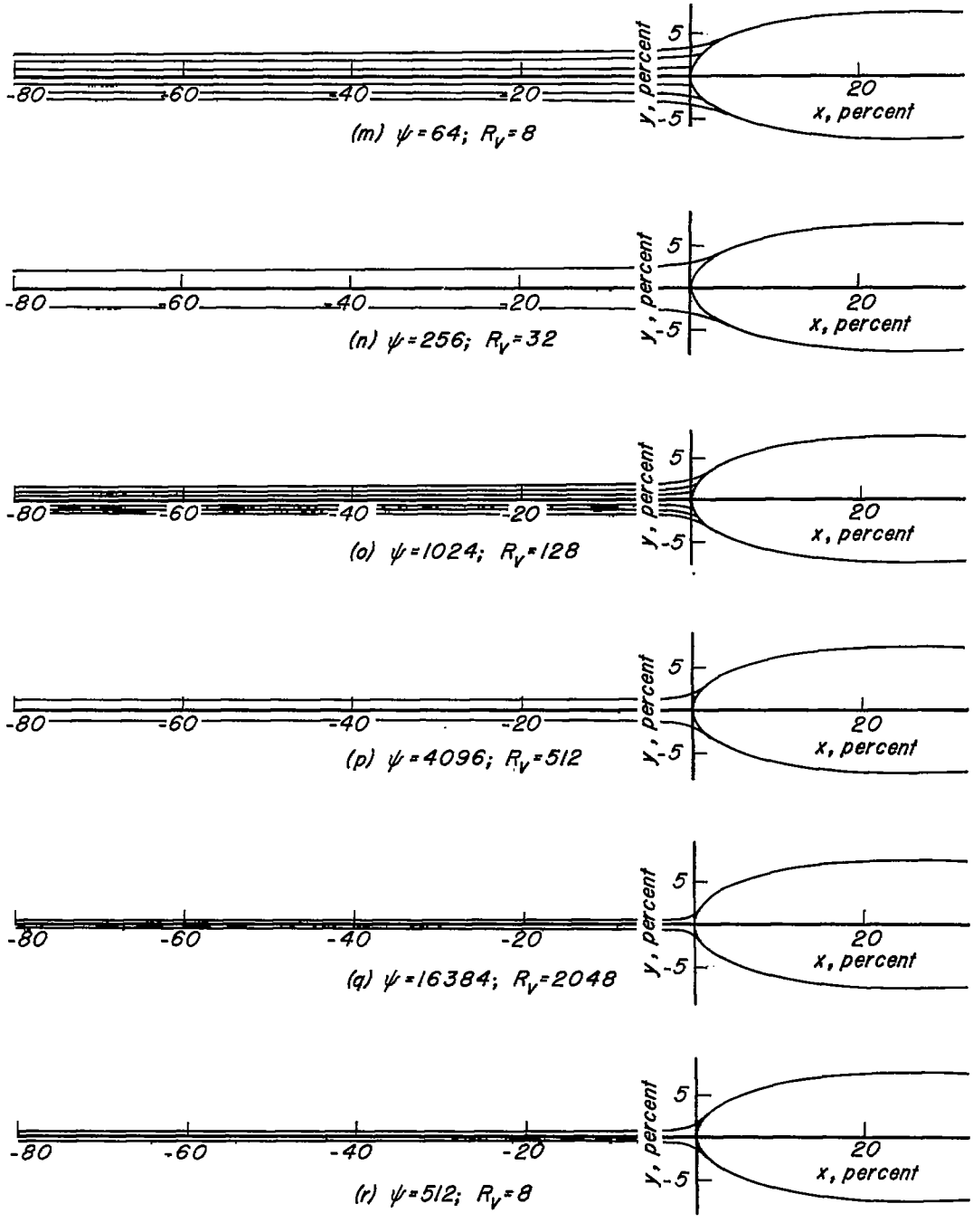


Figure 2.- Continued.

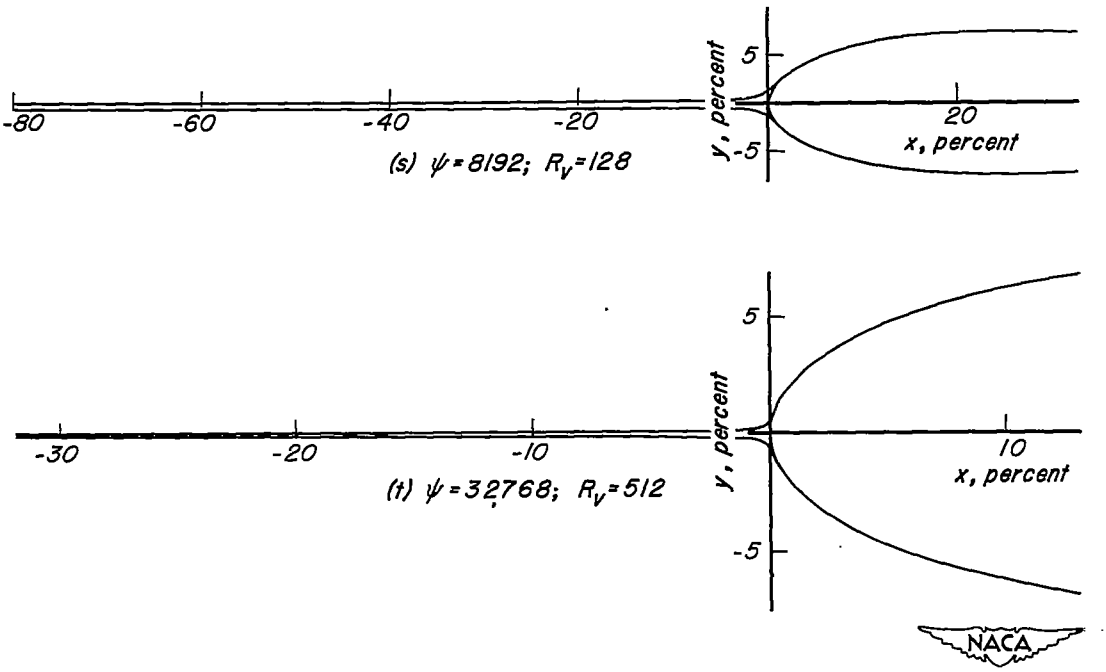


*Figure 2.- Concluded.*

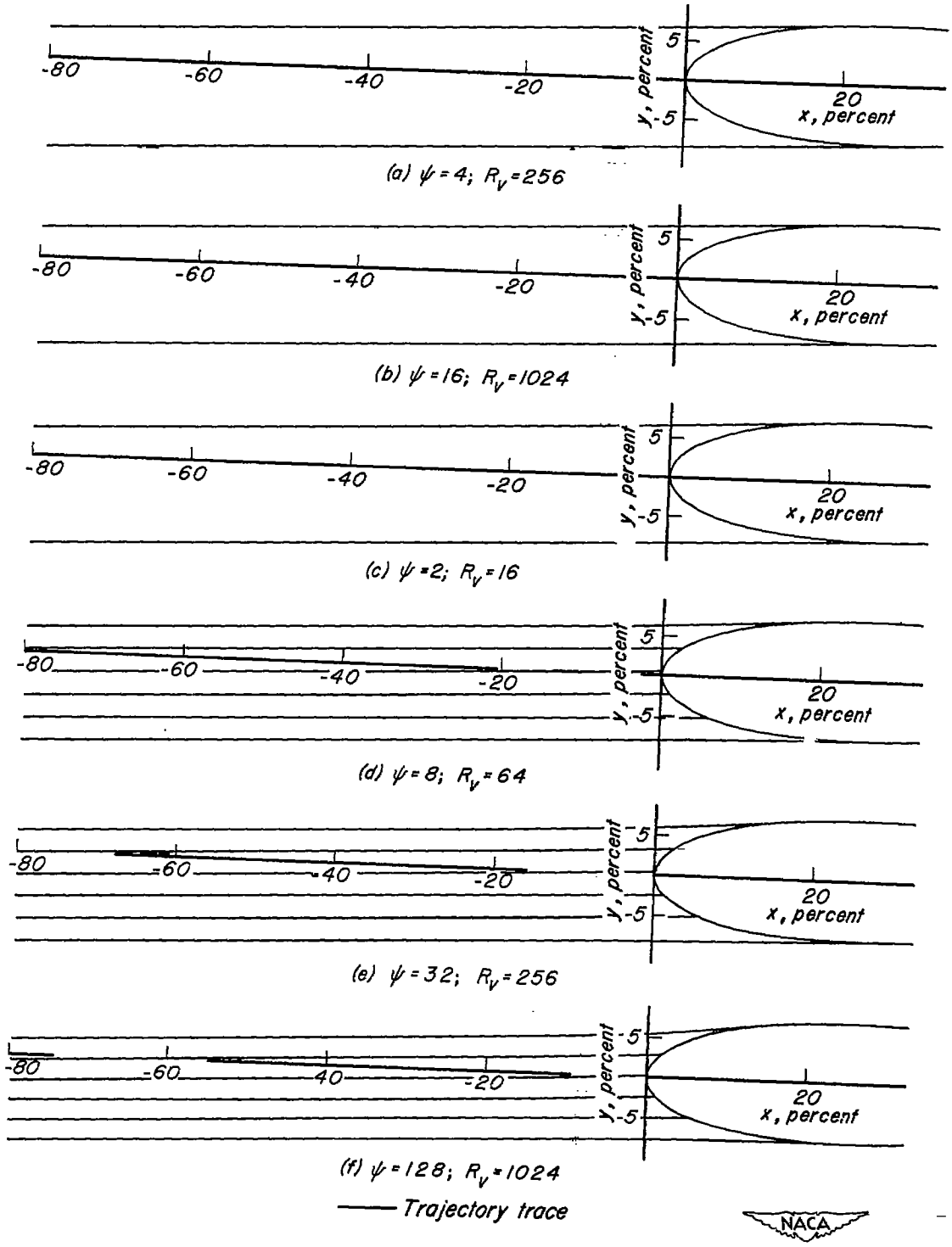


*Figure 3.- Water-drop trajectory traces from a differential analyzer for a 15-percent-thick symmetrical Joukowski airfoil; $c_l = 0.22$; $\alpha = 2°$.*

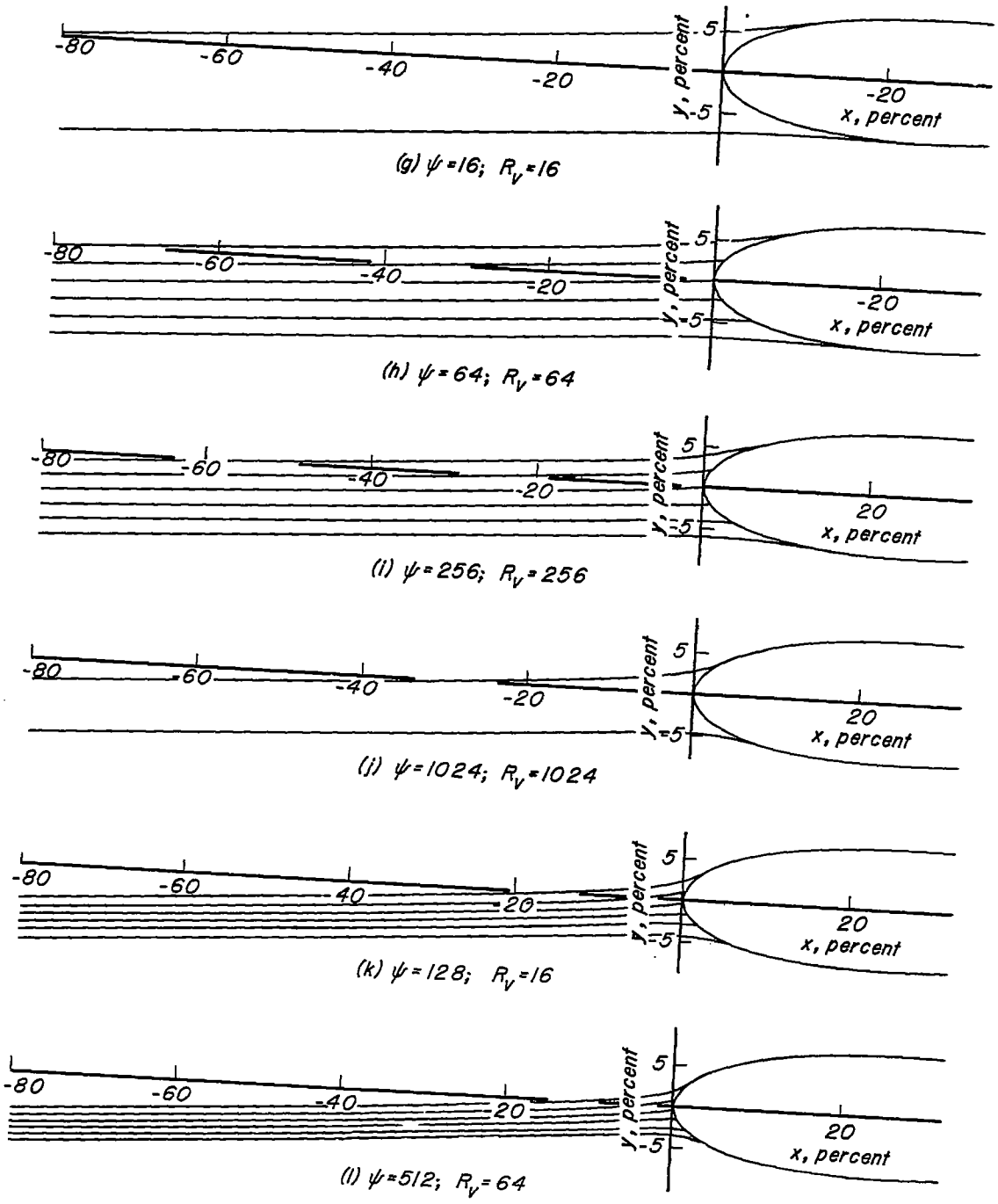


Figure 3.-Continued.

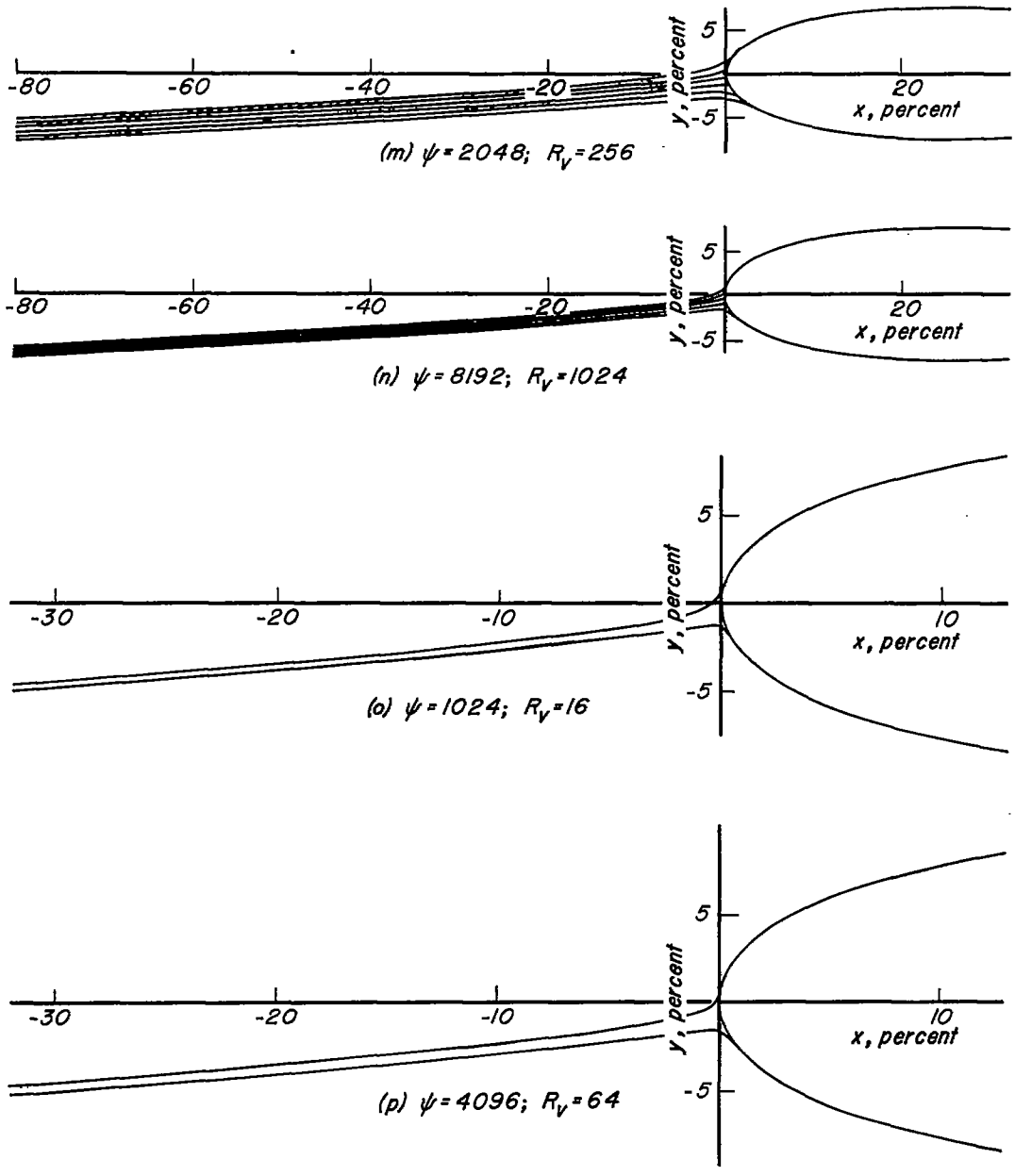


*Figure 3.- Continued.*

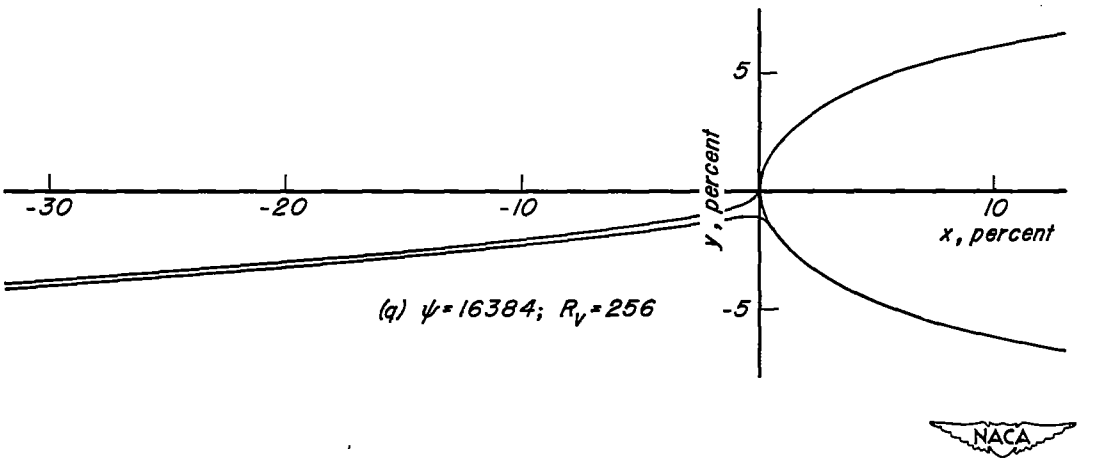


*Figure 3.-Concluded.*

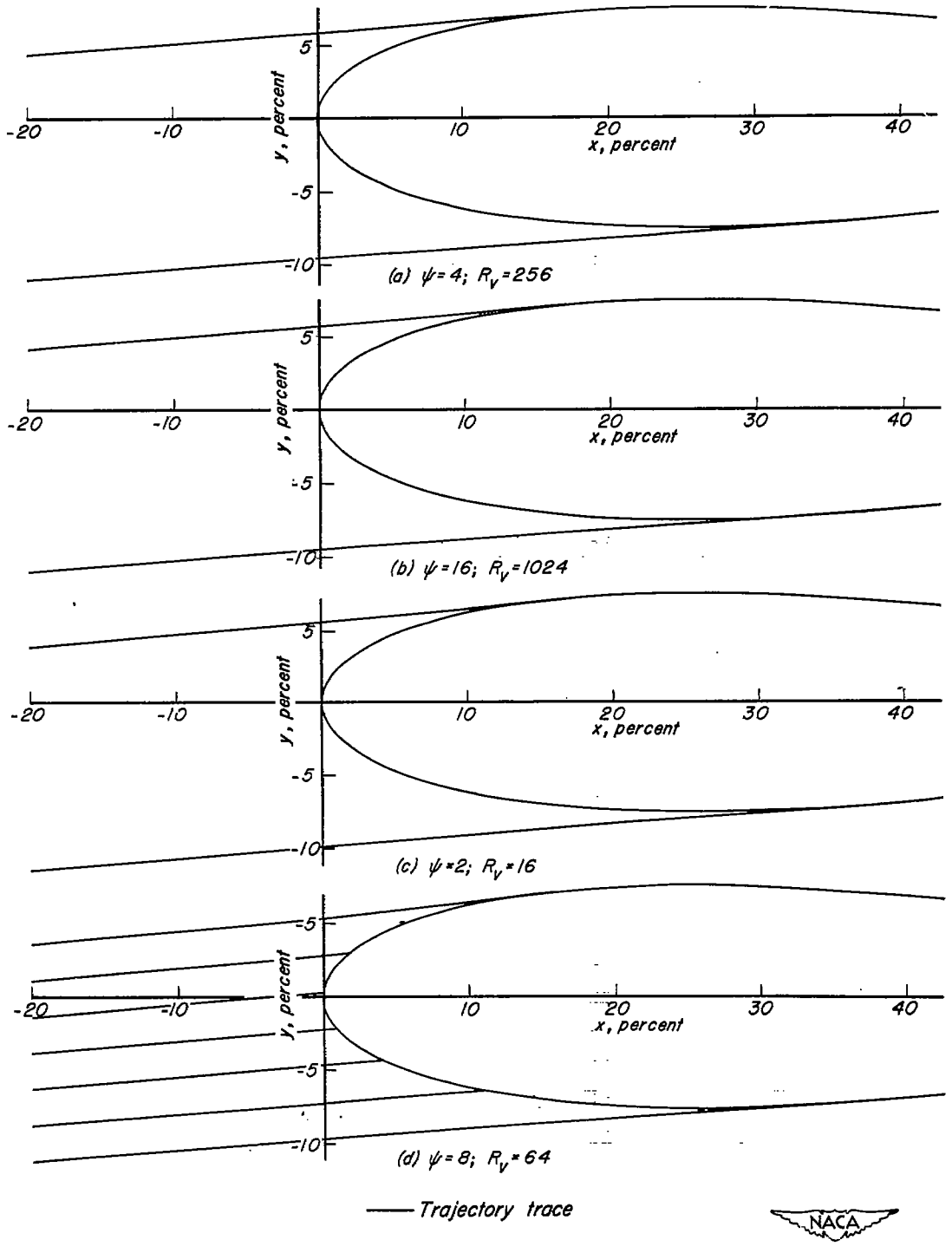


*Figure 4.-Water-drop trajectory traces from a differential analyzer for a 15-percent-thick symmetrical Joukowski airfoil; $c_l = 0.44$; $\alpha = 4°$.*

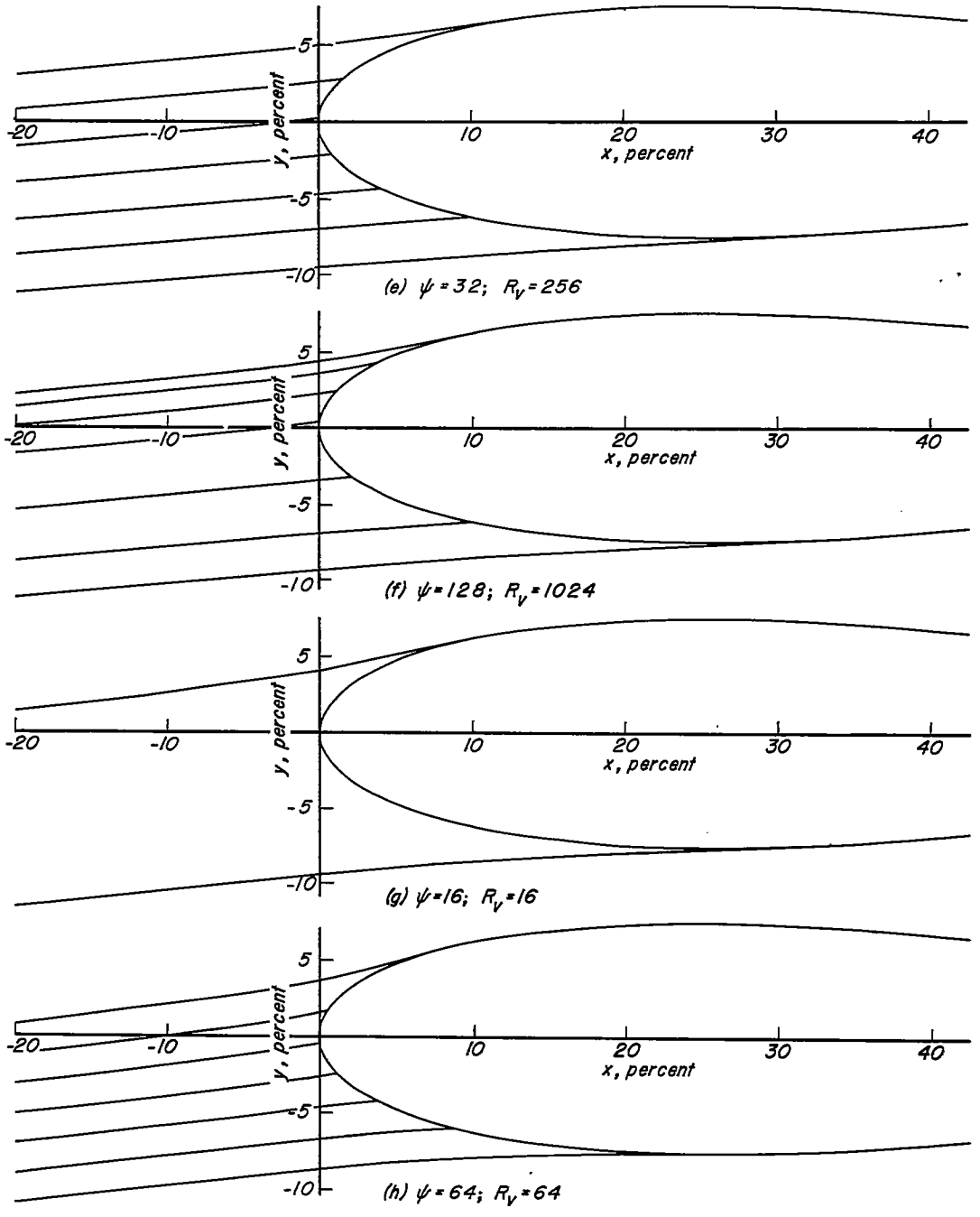


Figure 4.-Continued.

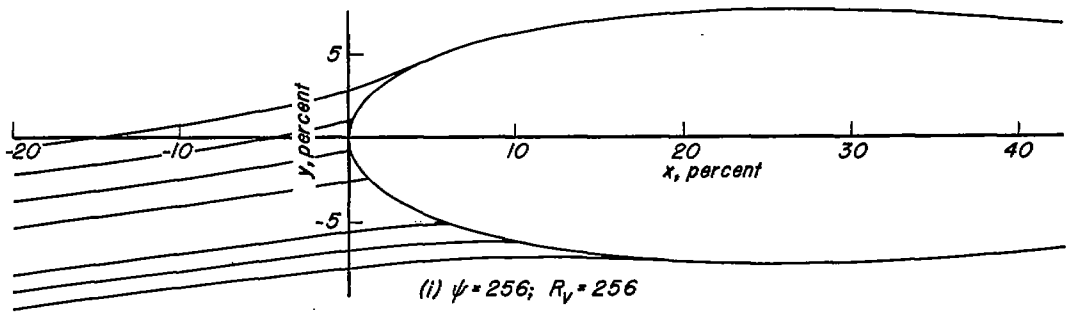


(i) $\psi = 256$; $R_V = 256$

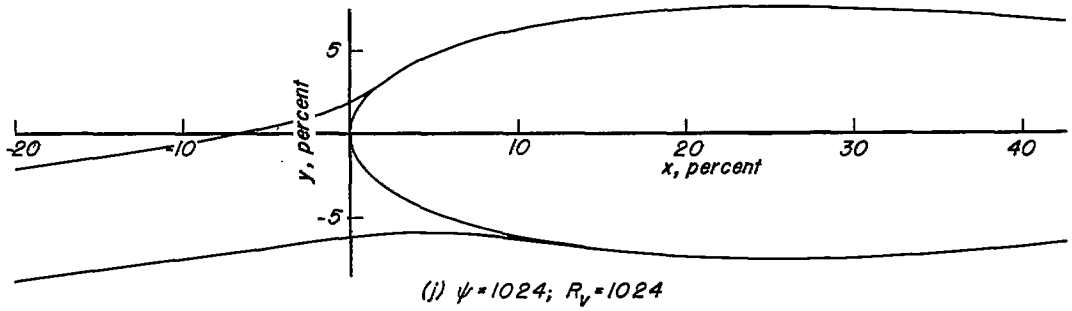


(j) $\psi = 1024$; $R_V = 1024$

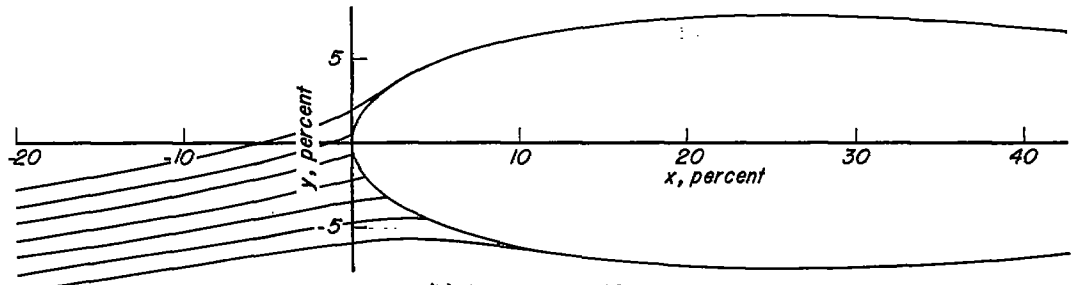


(k) $\psi = 128$; $R_V = 16$

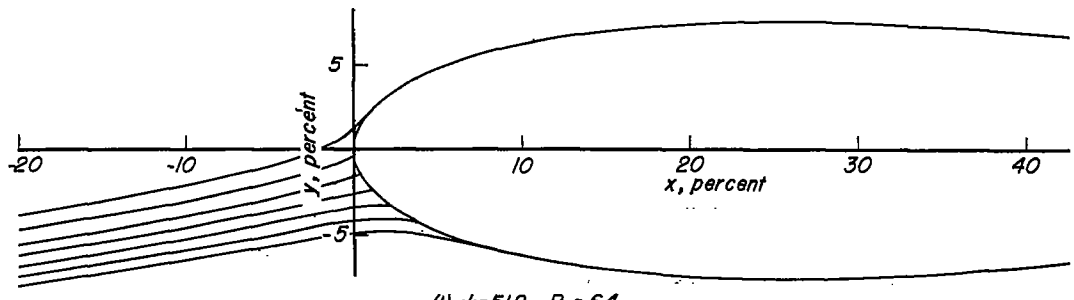


(l) $\psi = 512$; $R_V = 64$

Figure 4.- Continued.

81

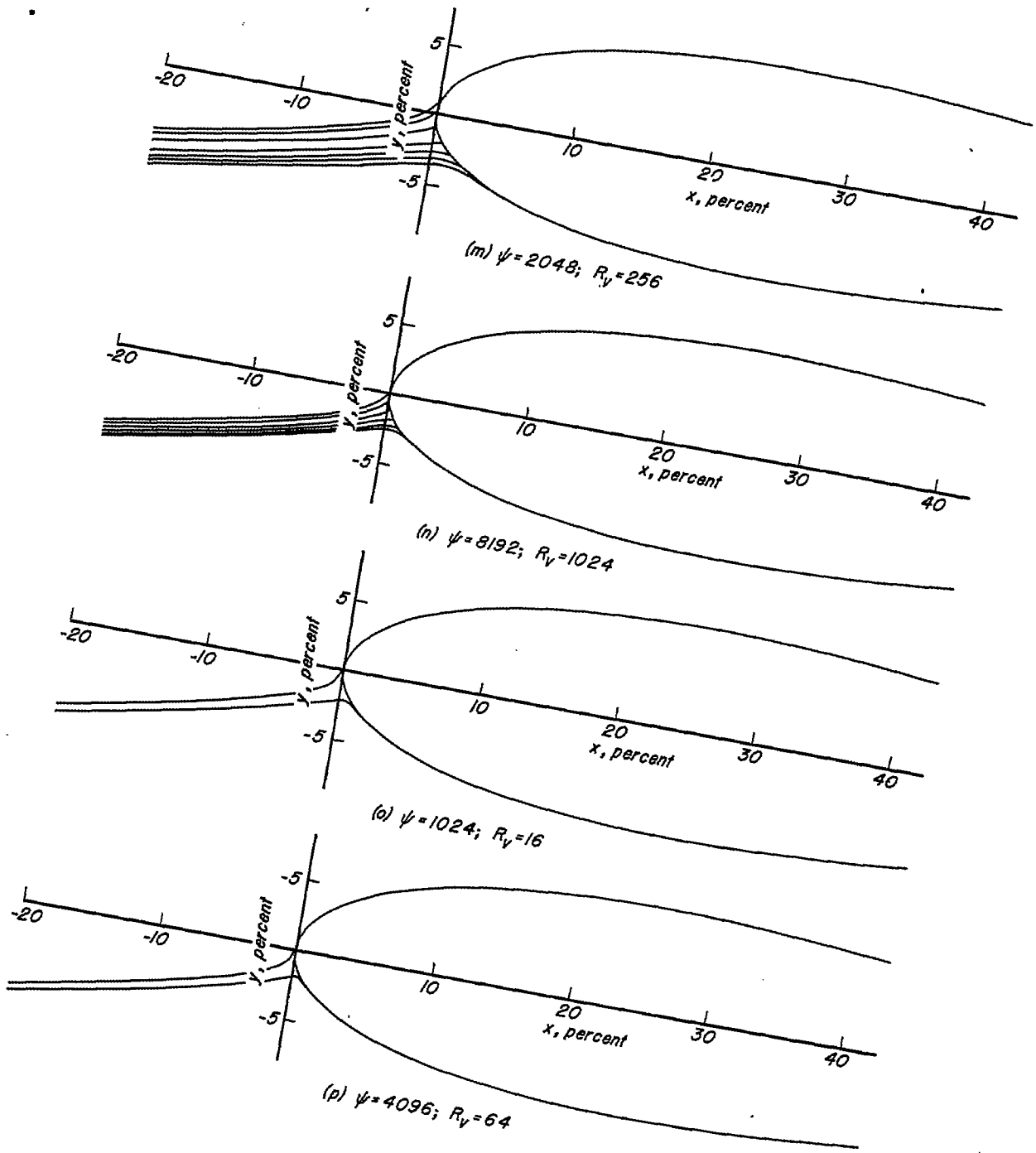


Figure 4.-Continued.

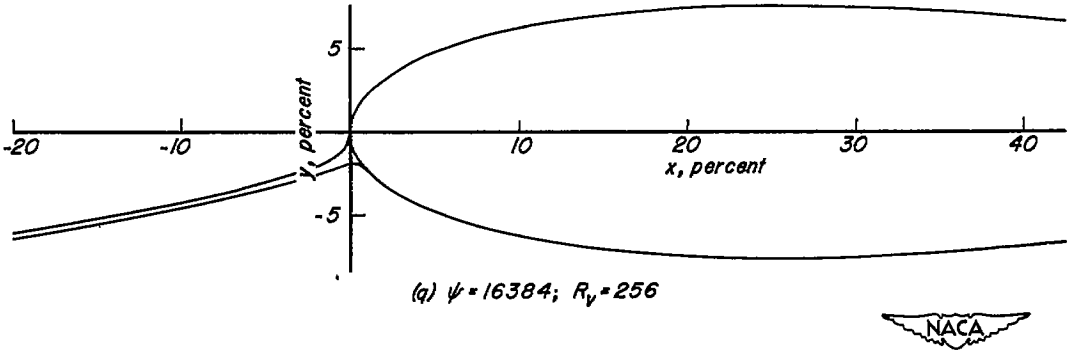


*Figure 4.- Concluded.*

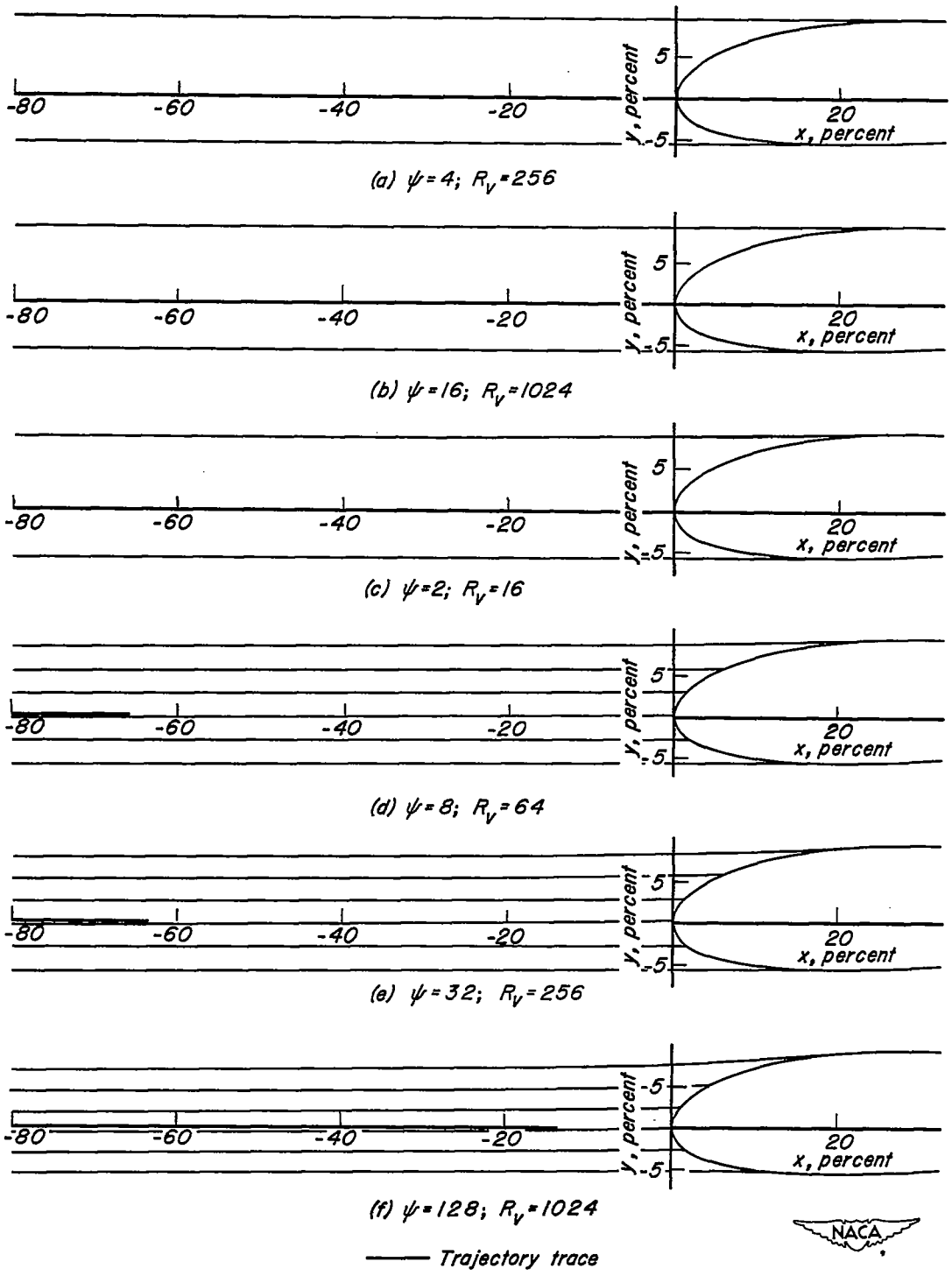


*Figure 5.- Water-drop trajectory traces from a differential analyzer for a 15-percent-thick cambered Joukowski airfoil; $a = 1.0$ mean line; $c_l = 0.44$; $\alpha = 0°$.*

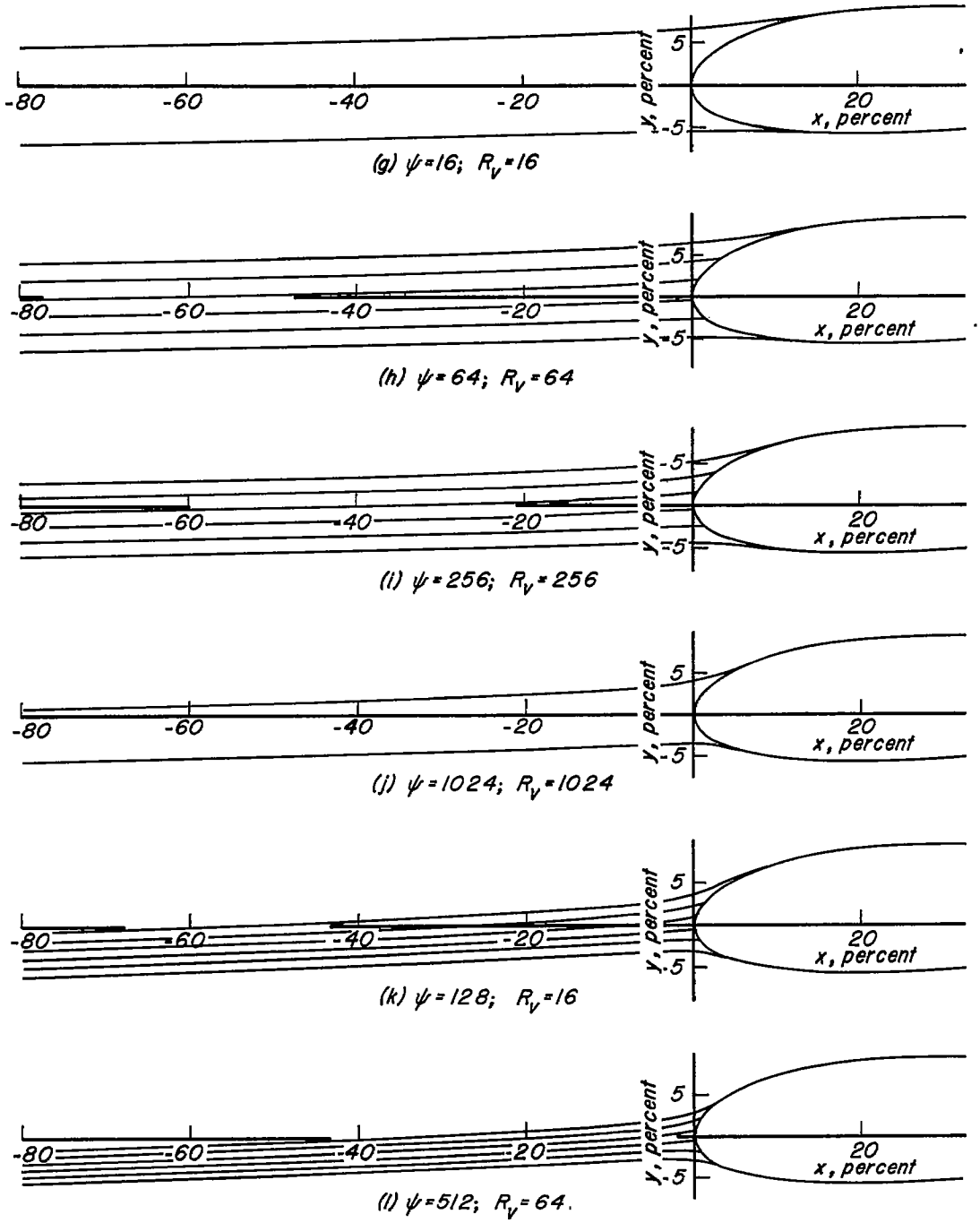


*Figure 5.- Continued.*

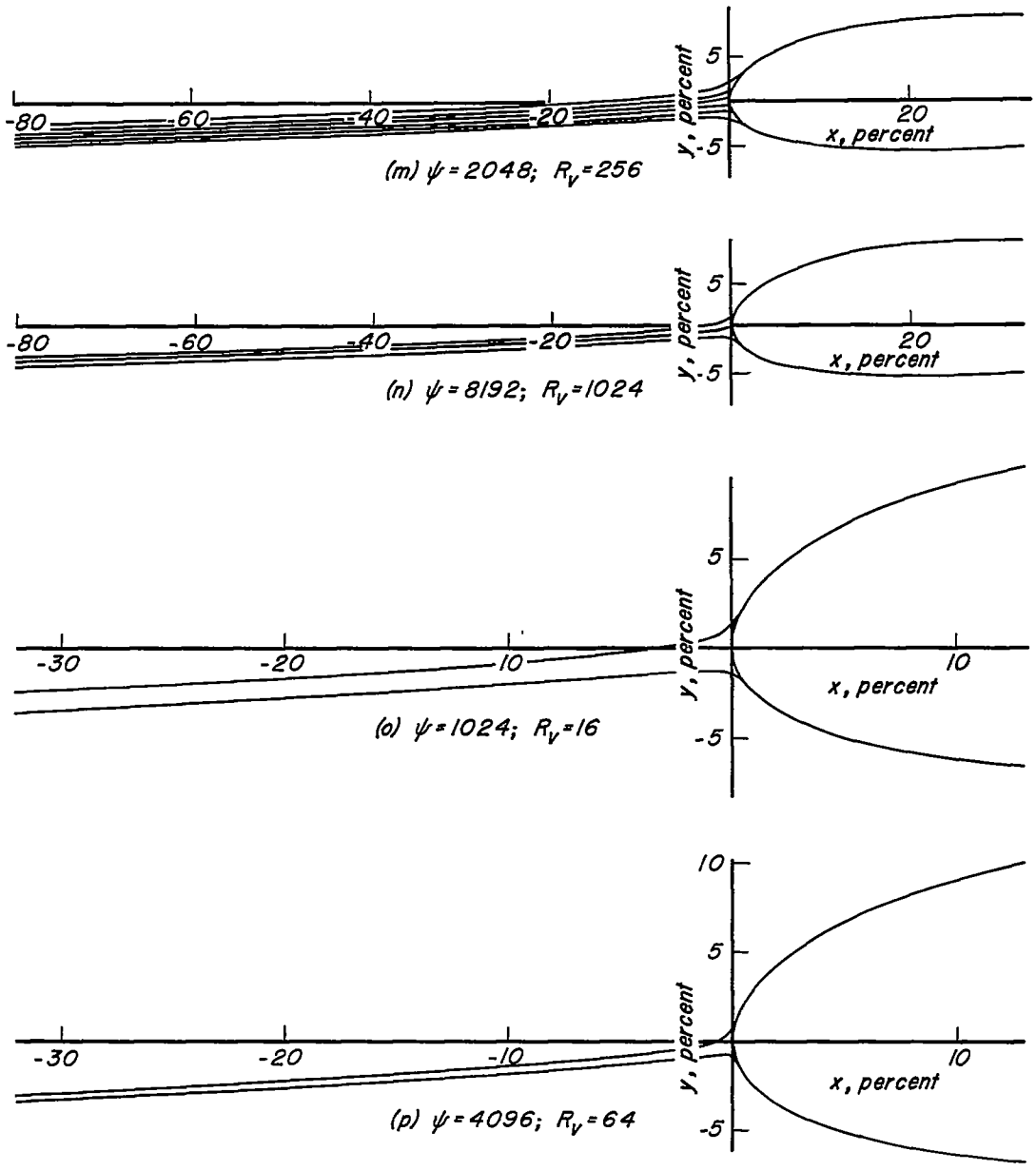


*Figure 5.- Continued.*

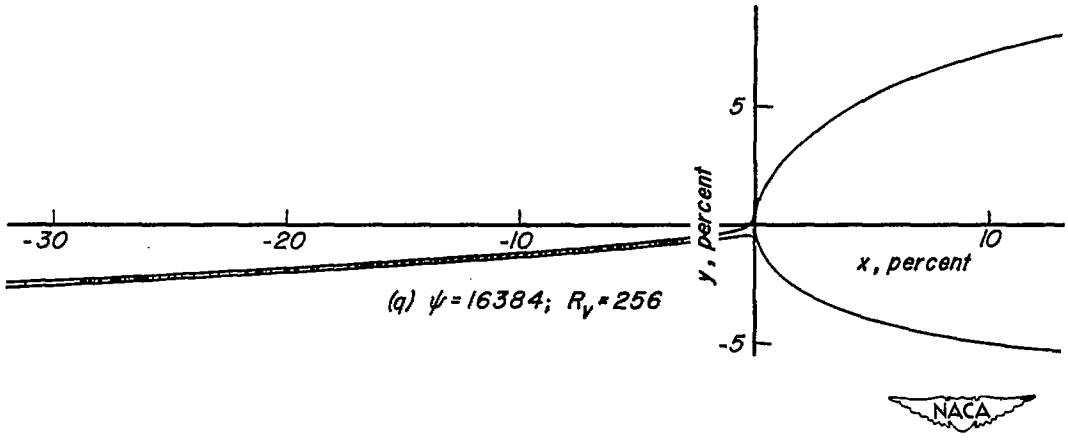


*Figure 5.-Concluded.*

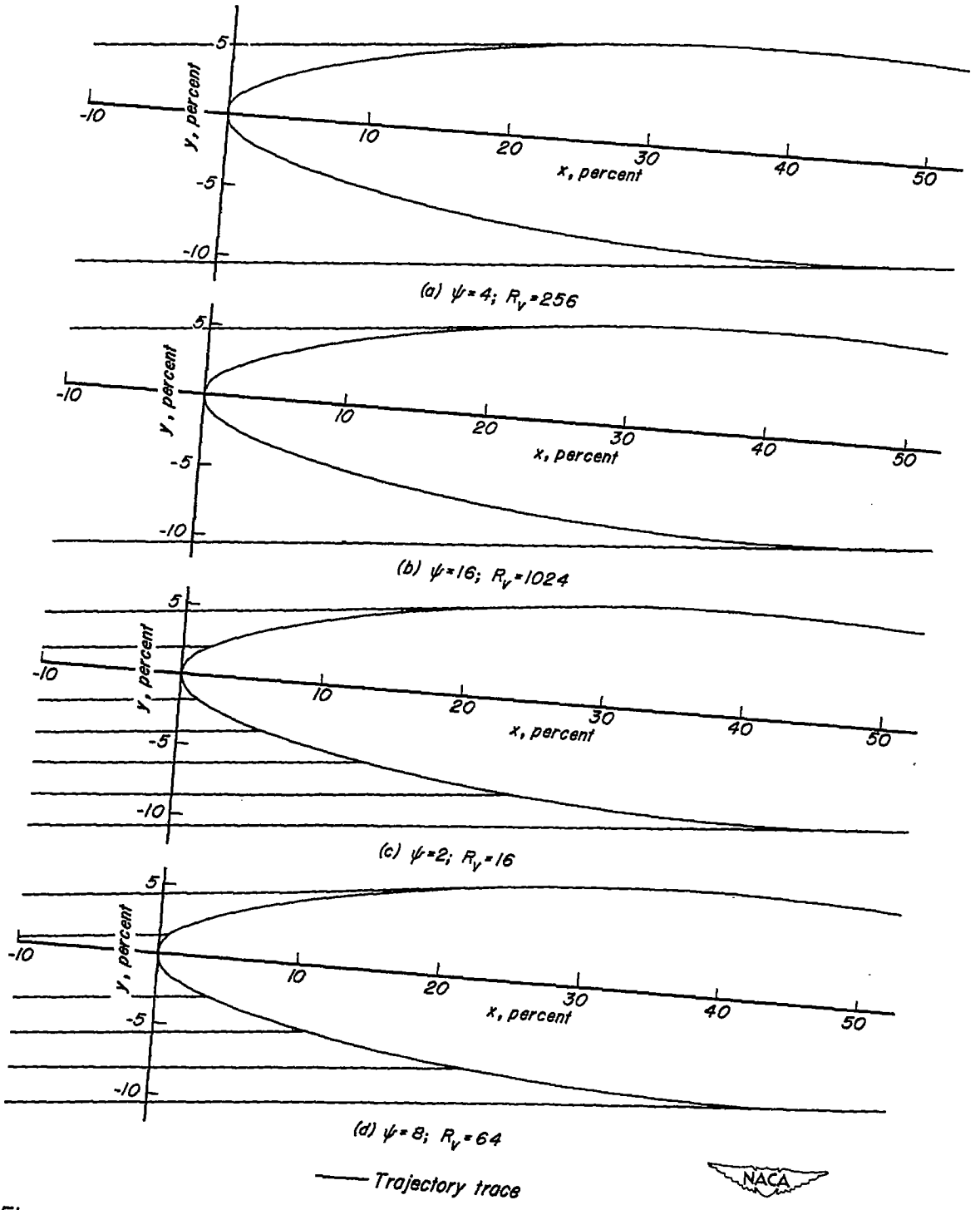


Figure 6.-Water-drop trajectory traces from a differential analyzer for an NACA $65_4$-015 airfoil; $c_l = 0.44$; $\alpha = 4°$.

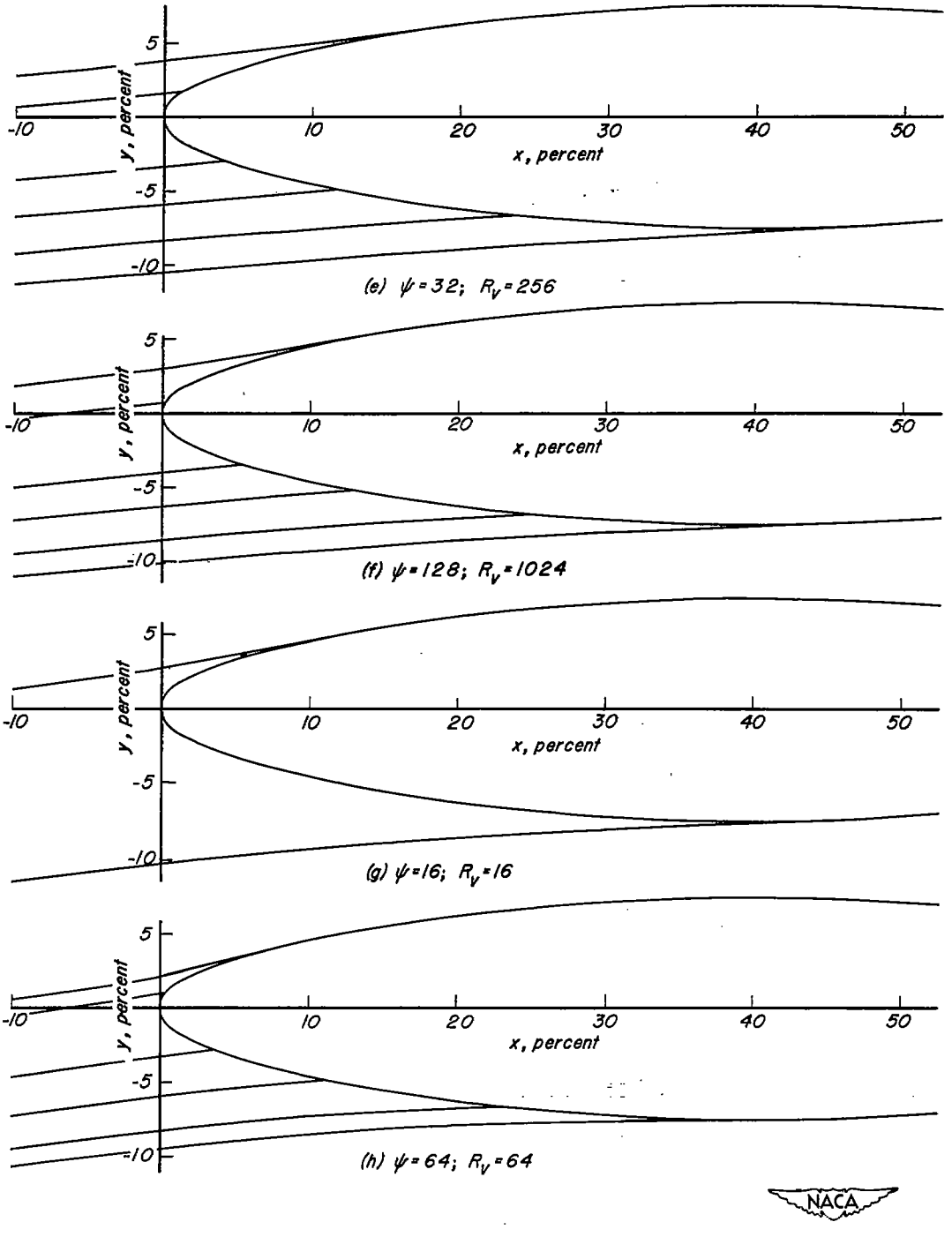


*Figure 6.-Continued.*

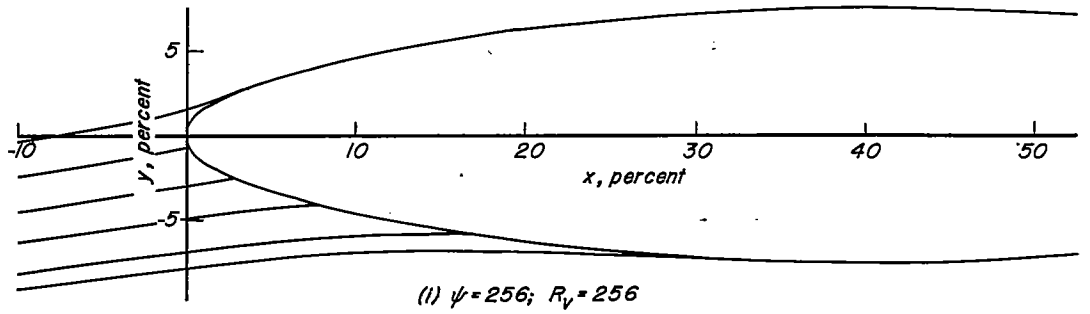


(i) $\psi = 256$; $R_V = 256$

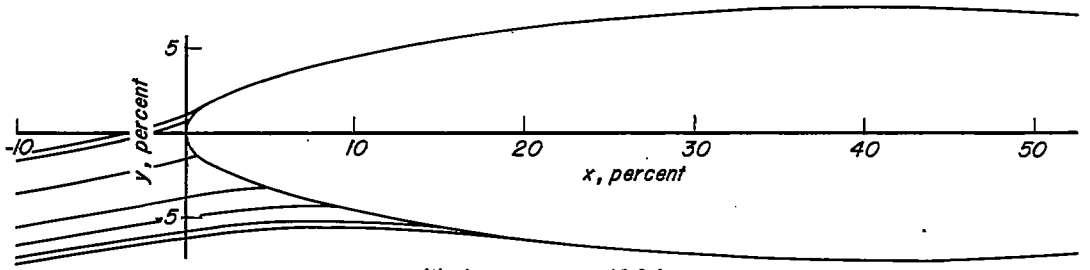


(j) $\psi = 1024$; $R_V = 1024$

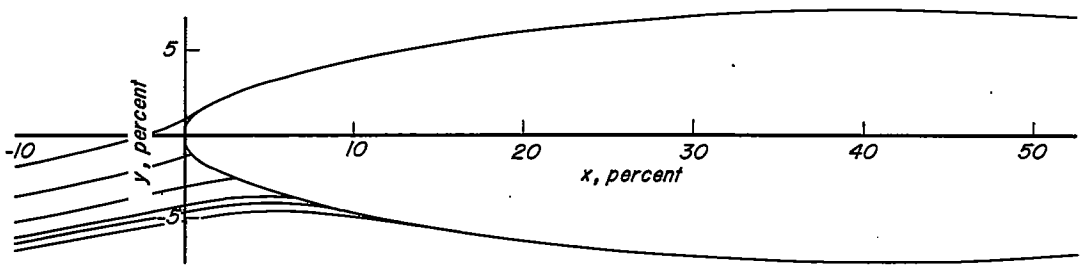


(k) $\psi = 128$; $R_V = 16$

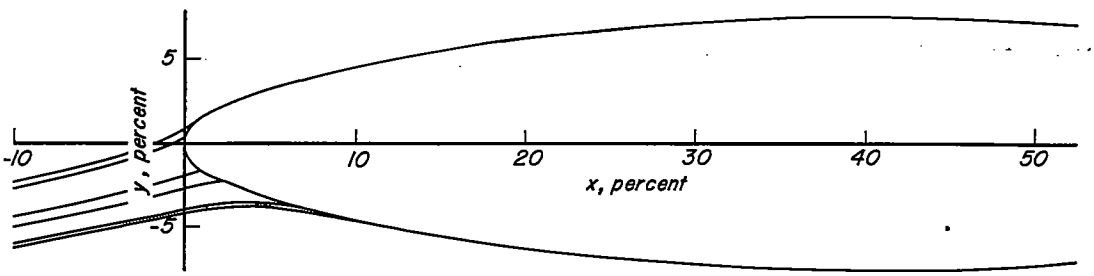


(l) $\psi = 512$; $R_V = 64$

Figure 6.- Continued.

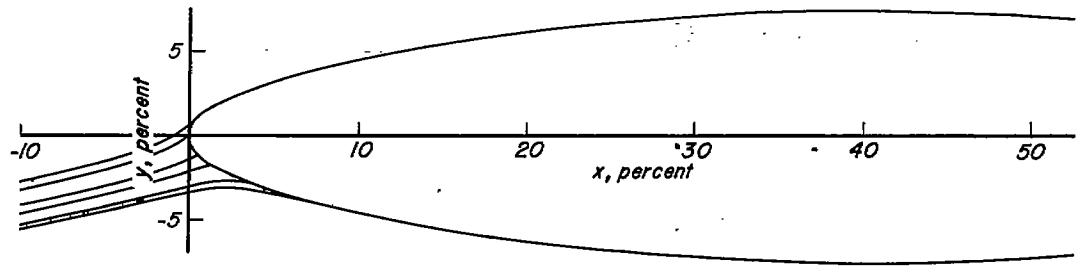


(m) $\psi = 2048$; $R_V = 256$

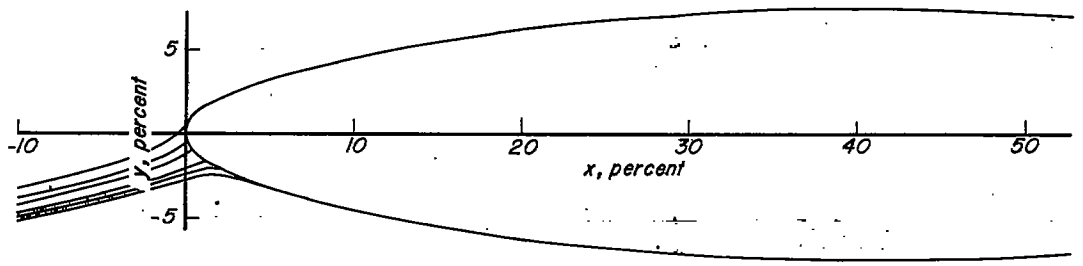


(n) $\psi = 8192$; $R_V = 1024$

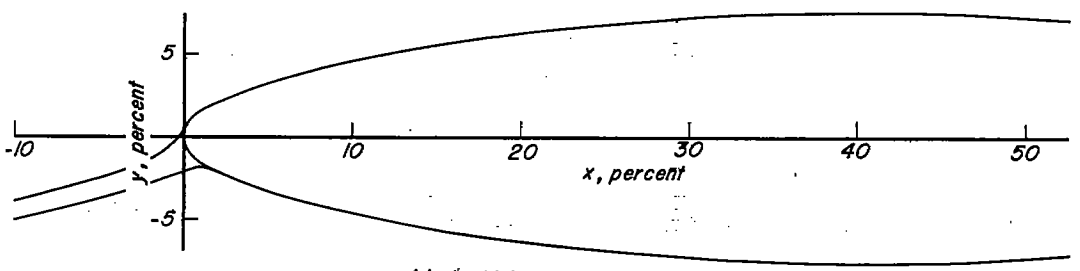


(o) $\psi = 1024$; $R_V = 16$

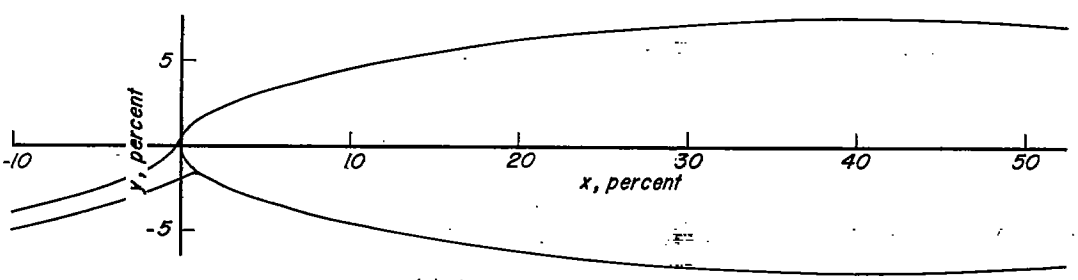


(p) $\psi = 4096$; $R_V = 64$

*Figure 6.- Continued.*

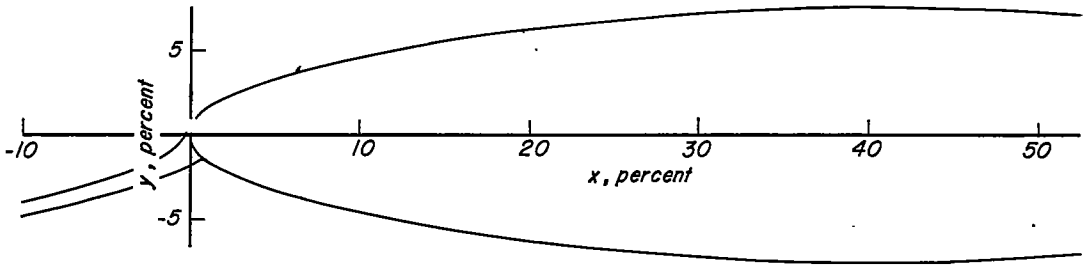


(g) $\psi = 16384$; $R_y = 256$

*Figure 6.- Concluded.*

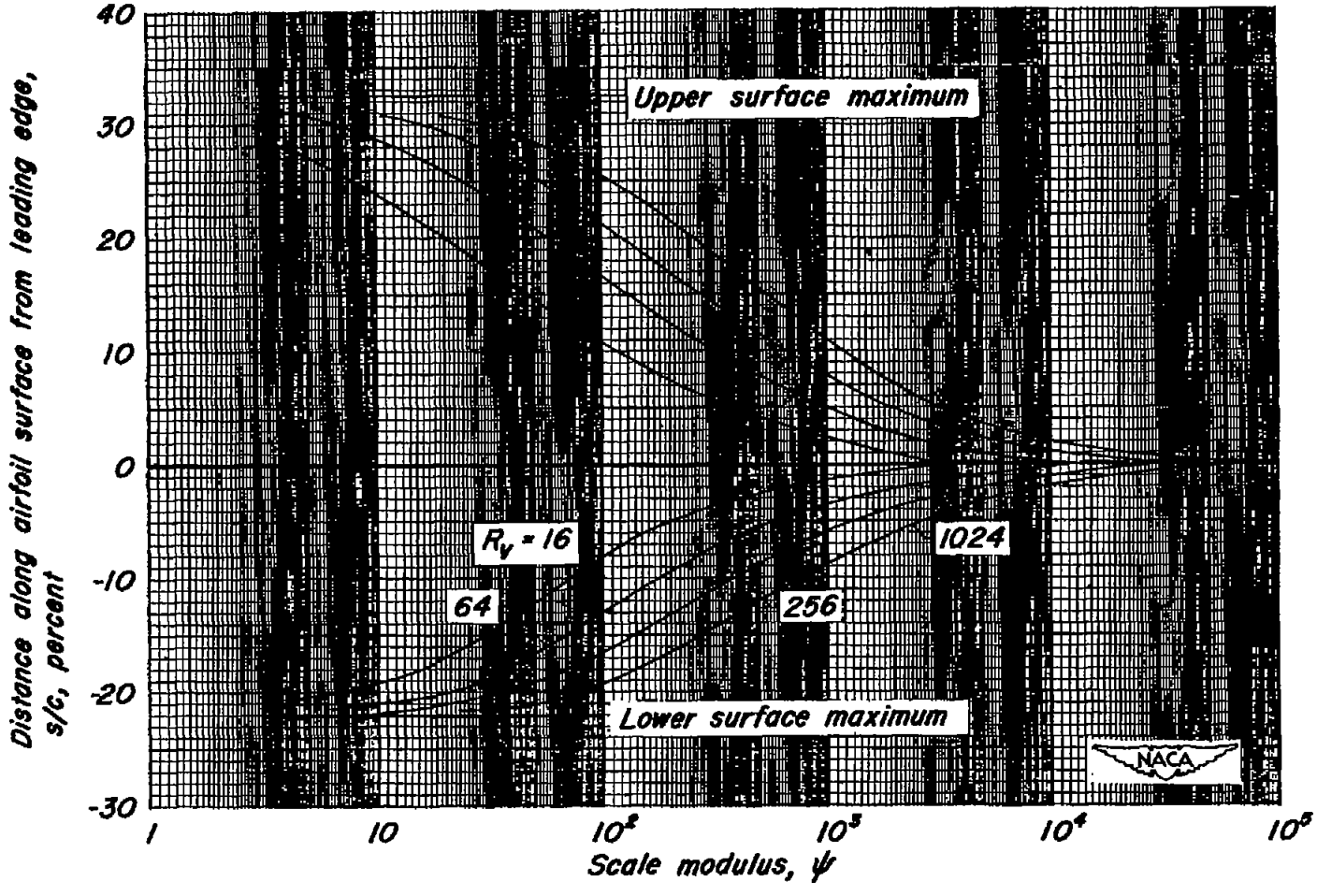


*Figure 7.– Typical relation between farthest position of drop impingement, scale modulus, and free-stream drop Reynolds number as exemplified by a 15-percent-thick cambered Joukowski airfoil; $c_2$=0.44; $\alpha$=0°; $a$=1.0 mean line.*

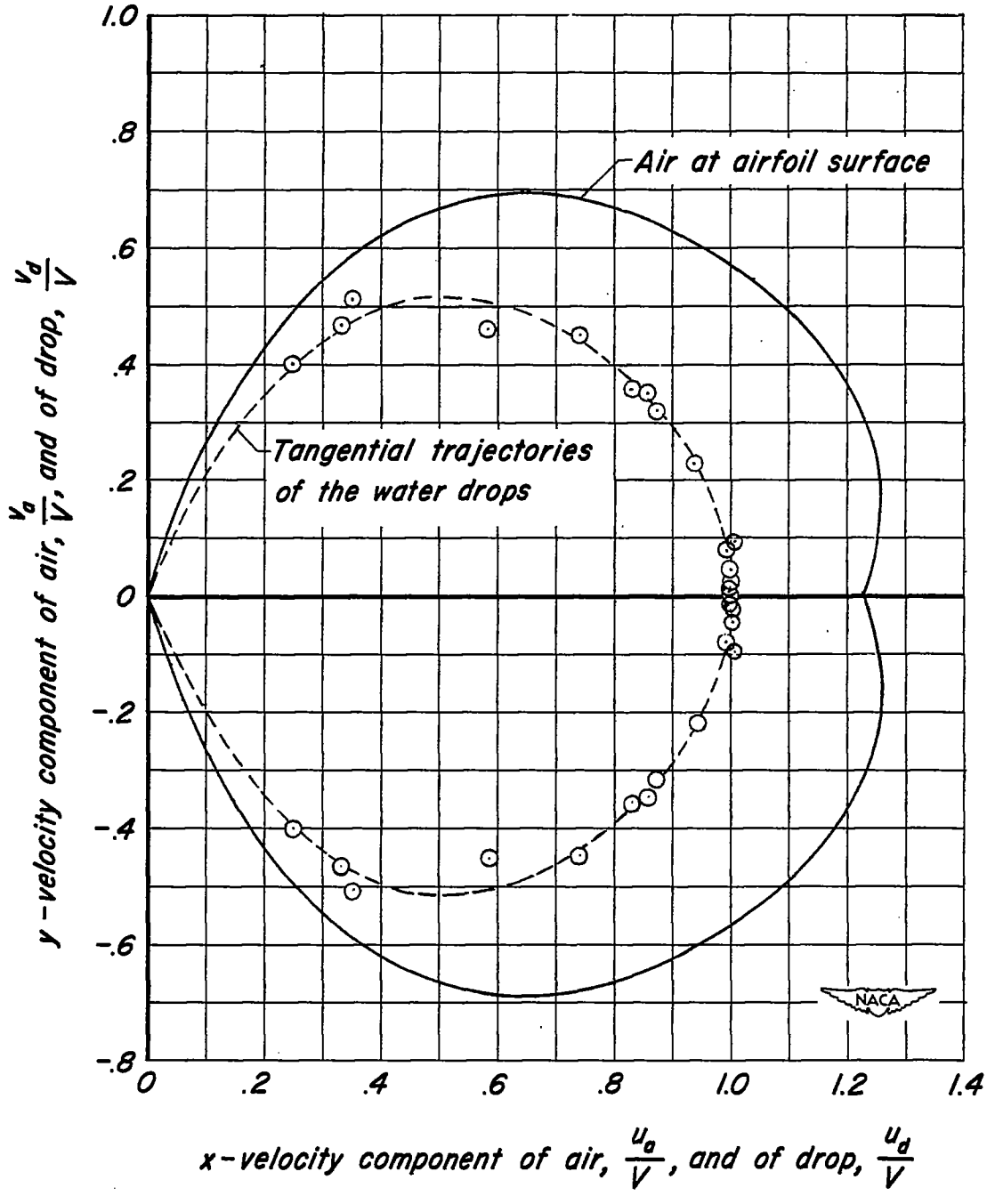


(a) 15-percent-thick symmetrical Joukowski airfoil, $\alpha = 0°$.

Figure 8.– Hodograph of tangential-trajectory velocities and hodograph of air velocities on the airfoil surface.

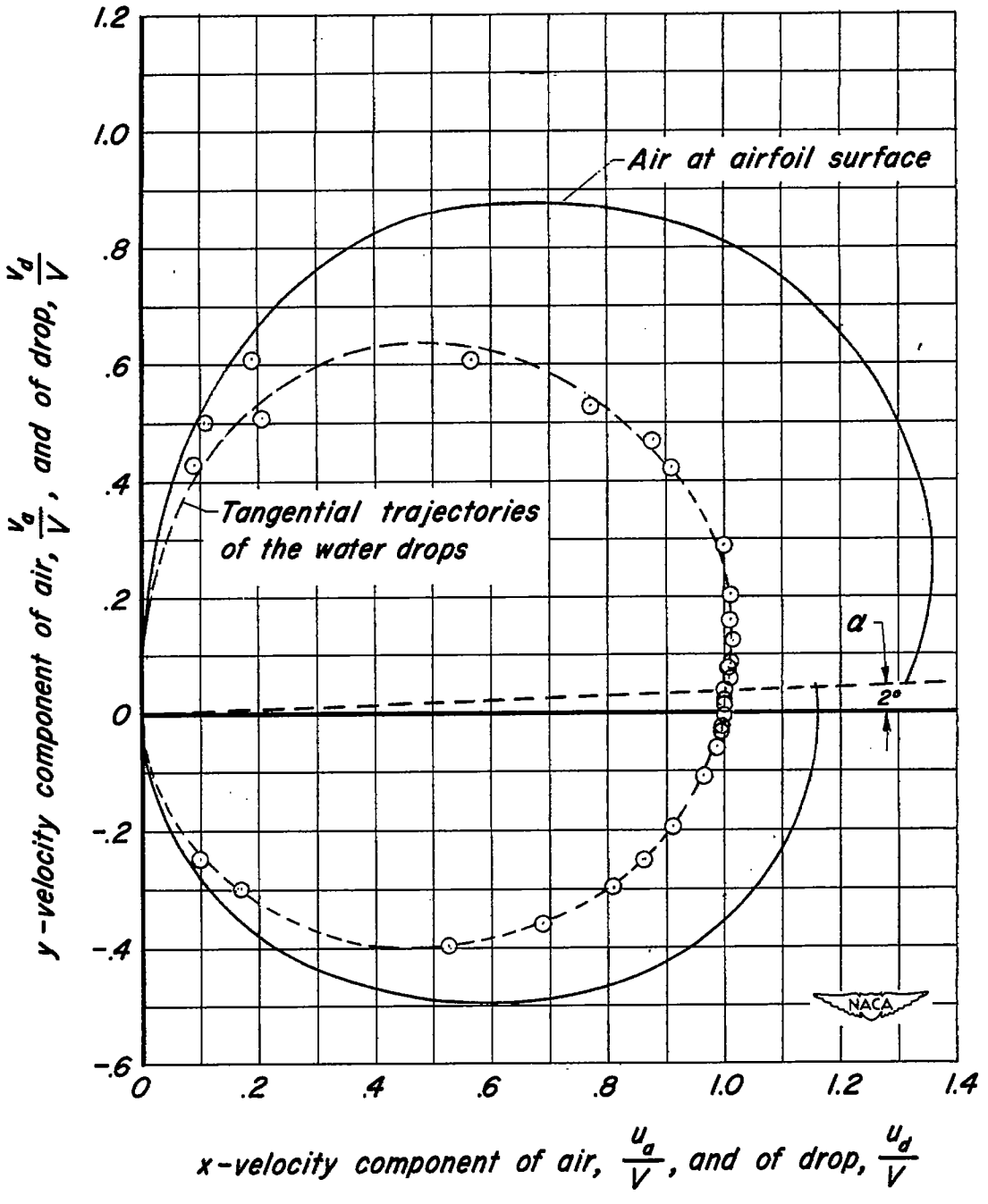


(b) 15-percent-thick symmetrical Joukowski airfoil, $\alpha = 2°$.

Figure 8. — Continued.

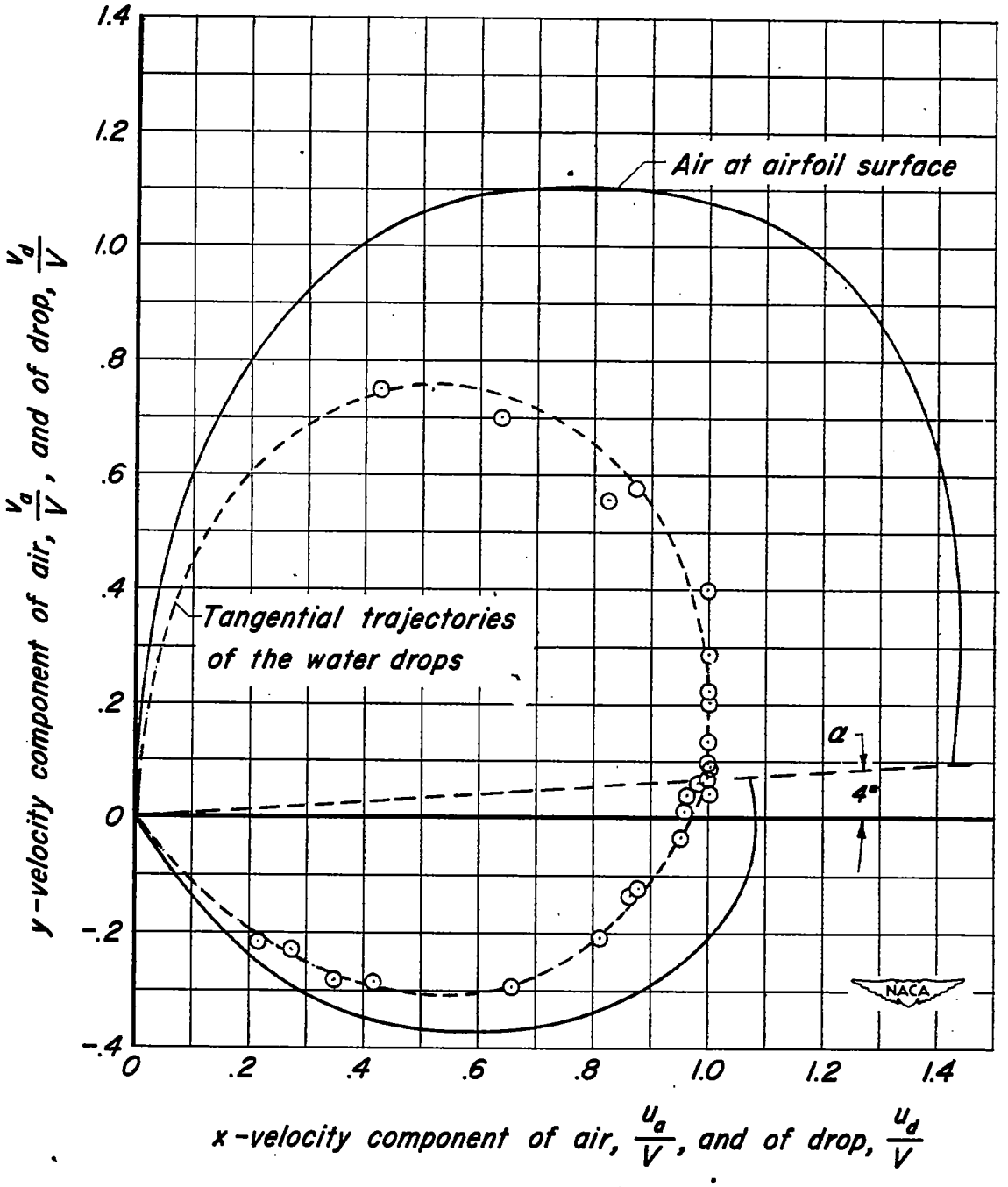


(c) 15-percent-thick symmetrical Joukowski airfoil, $\alpha = 4°$

Figure 8. — Continued.

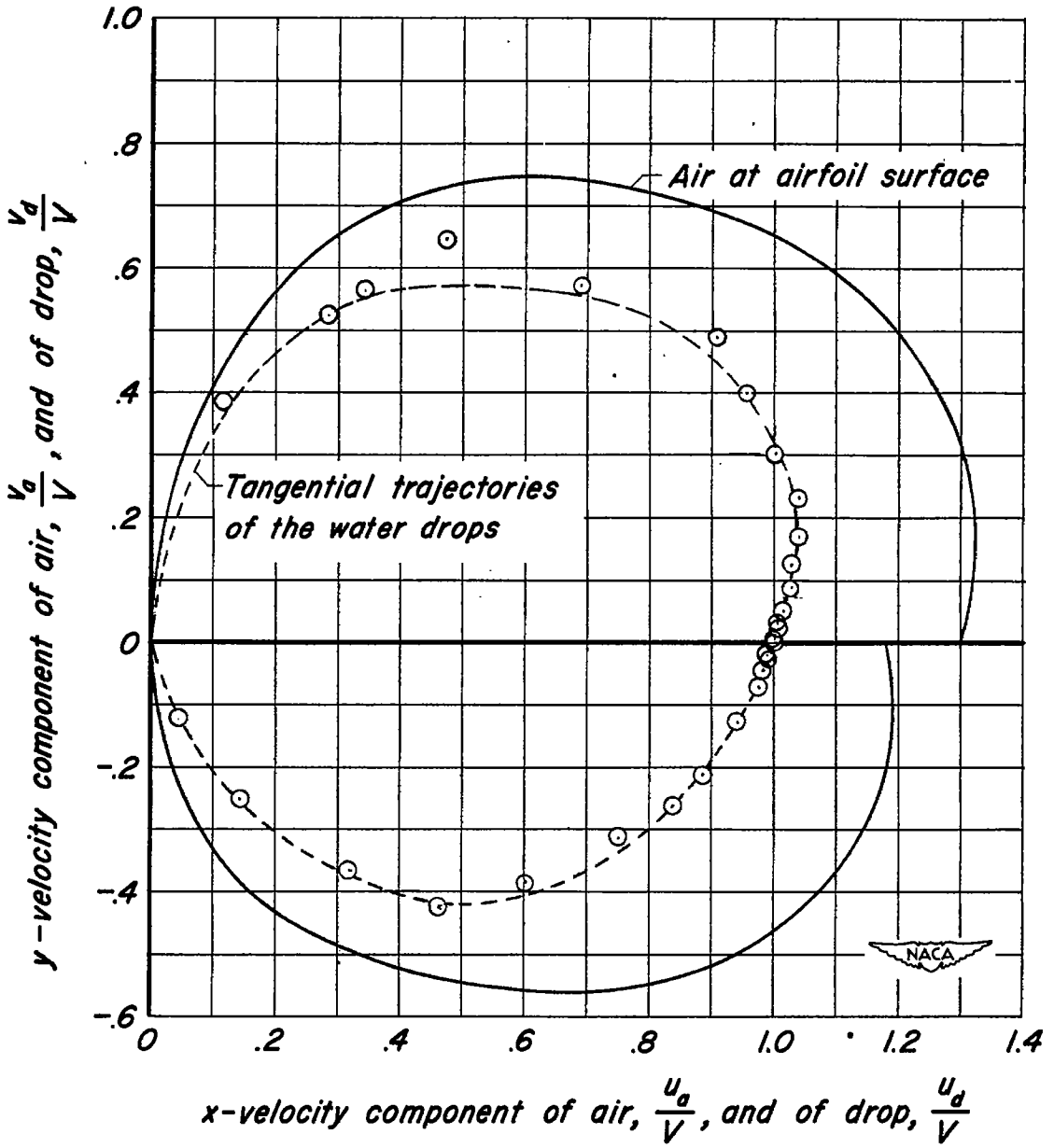


(d) 15-percent-thick cambered Joukowski airfoil; $a = 1.0$; $\alpha = 0°$.

Figure 8.- Continued.

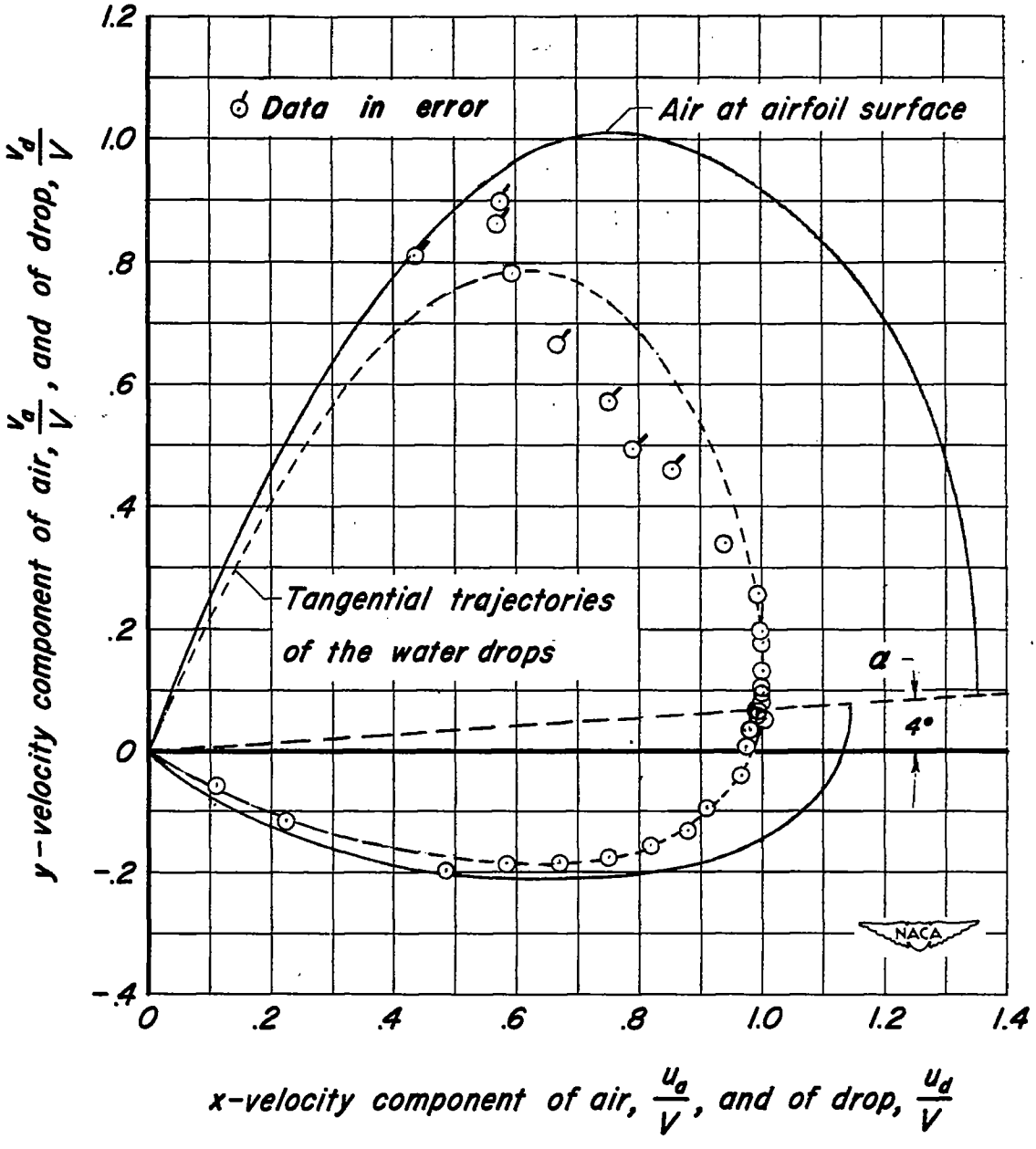


(e) NACA $65_2$-015 airfoil, $\alpha = 4°$.

Figure 8.- Concluded.

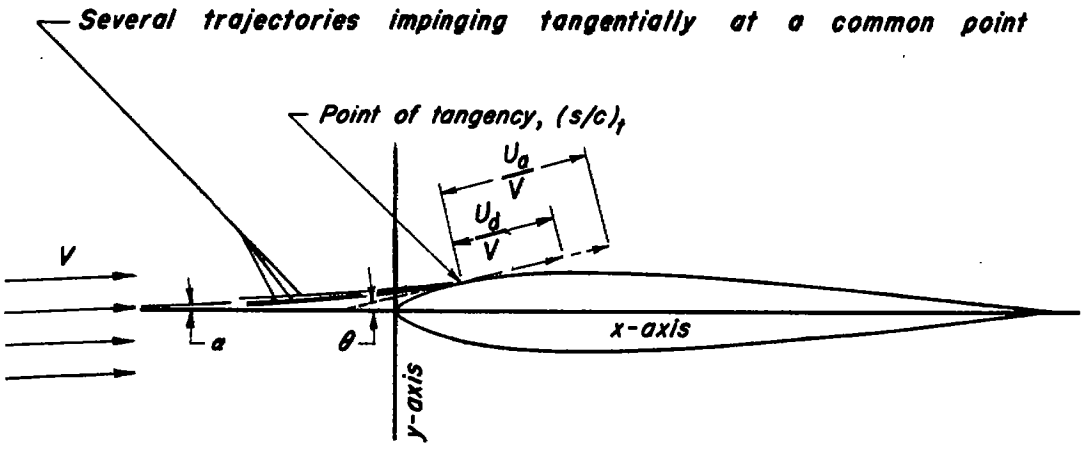


(a) Physical plane.

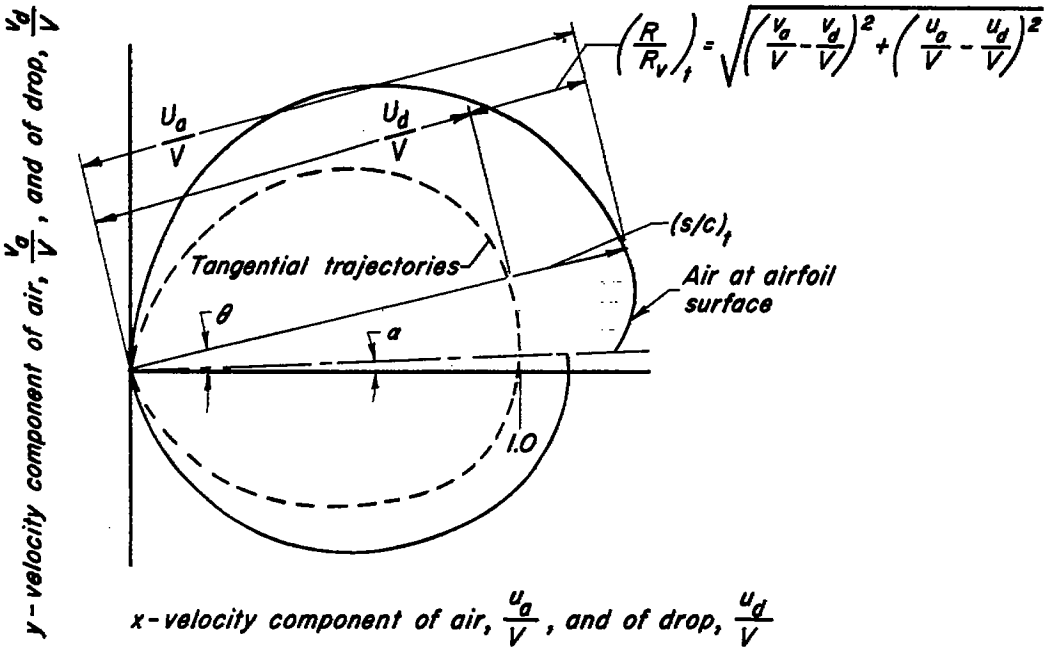


(b) Hodograph plane.

Figure 9.- Relationship between physical and hodograph planes for drop and air velocities at airfoil surface.

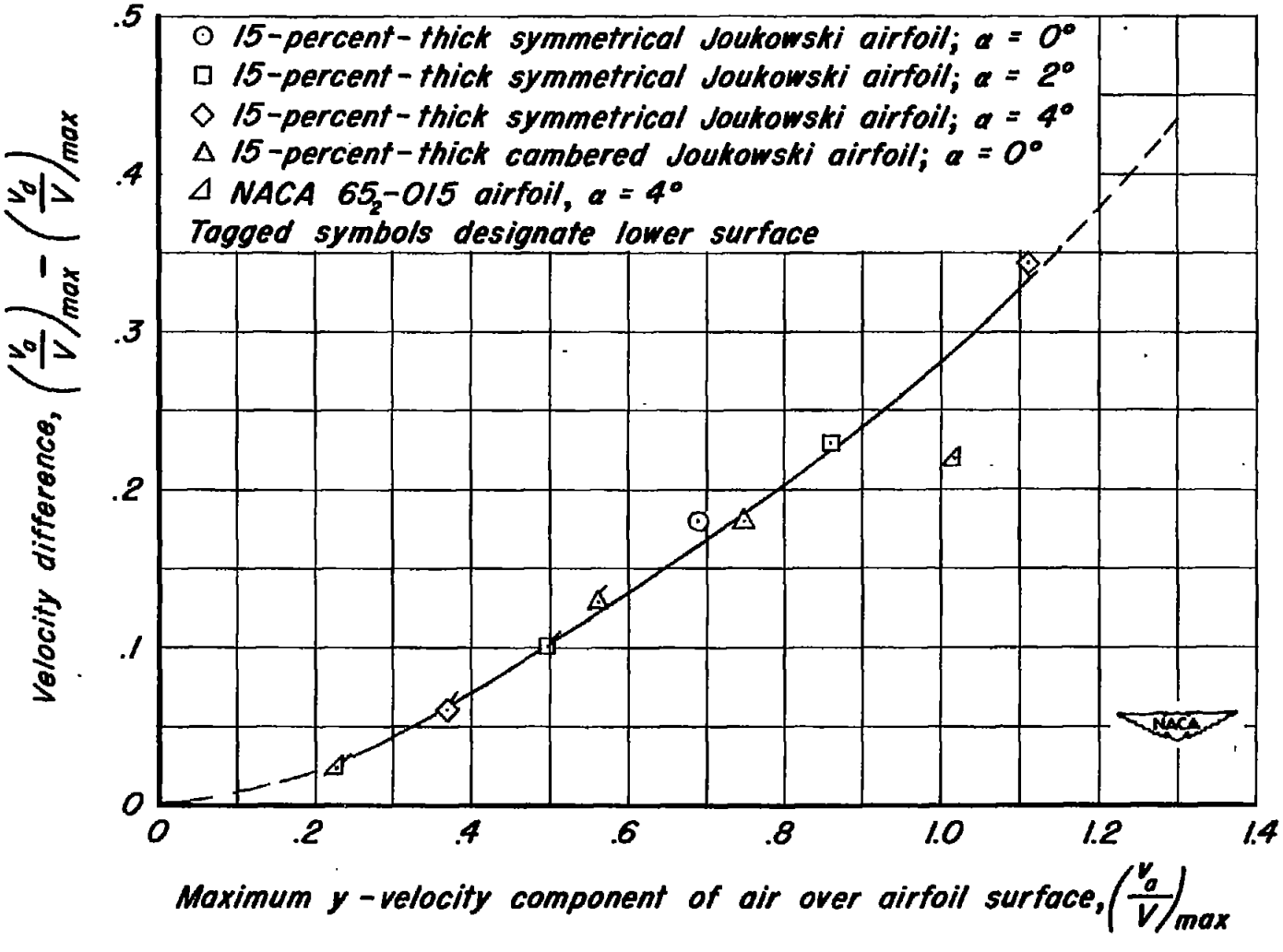


Figure 10.—Variation of velocity difference between drop and air with maximum y-velocity component of air for the five airfoil cases investigated.

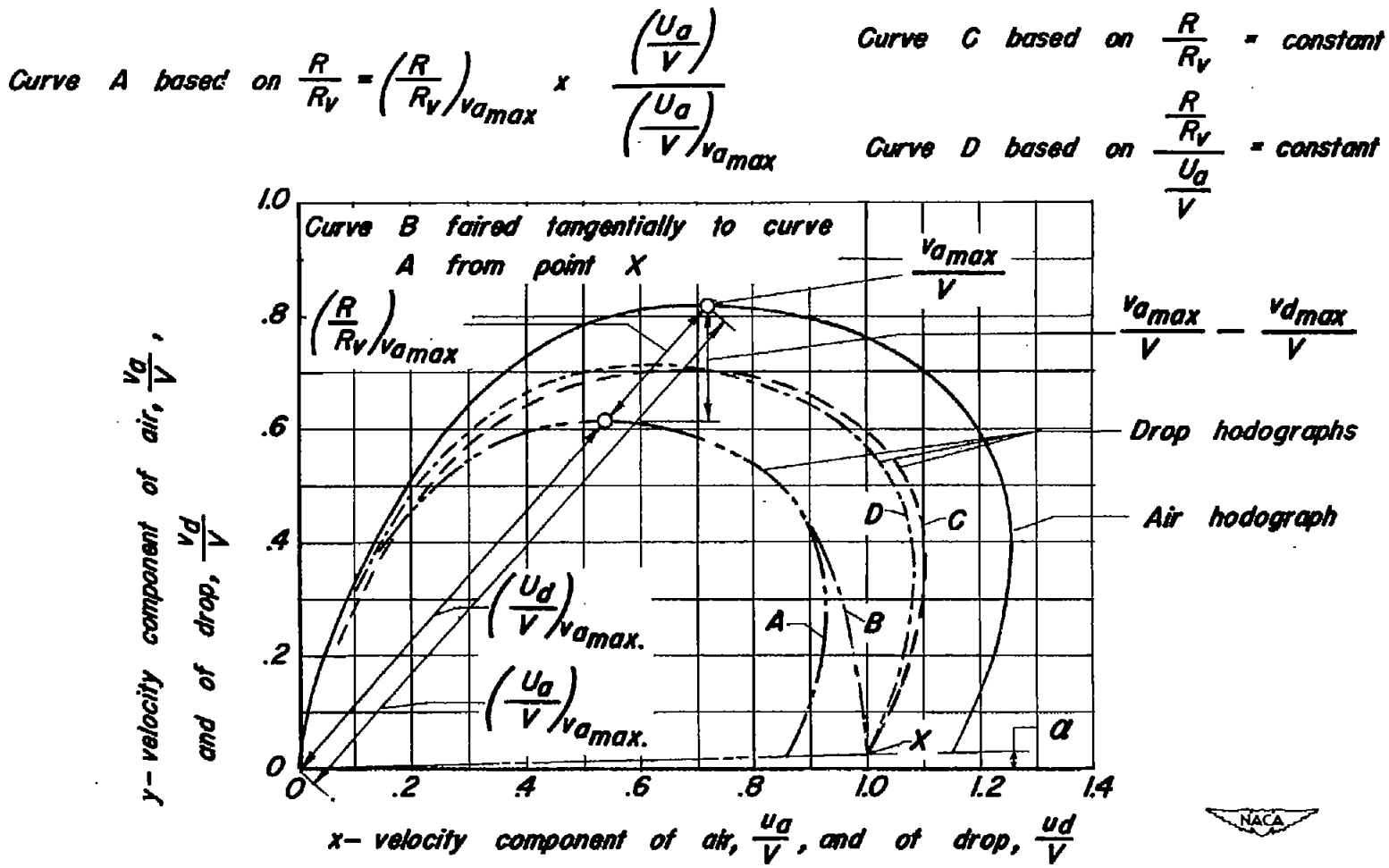


Figure 11.- Illustration of four possible techniques for the construction of a drop hodograph from a specified air hodograph.

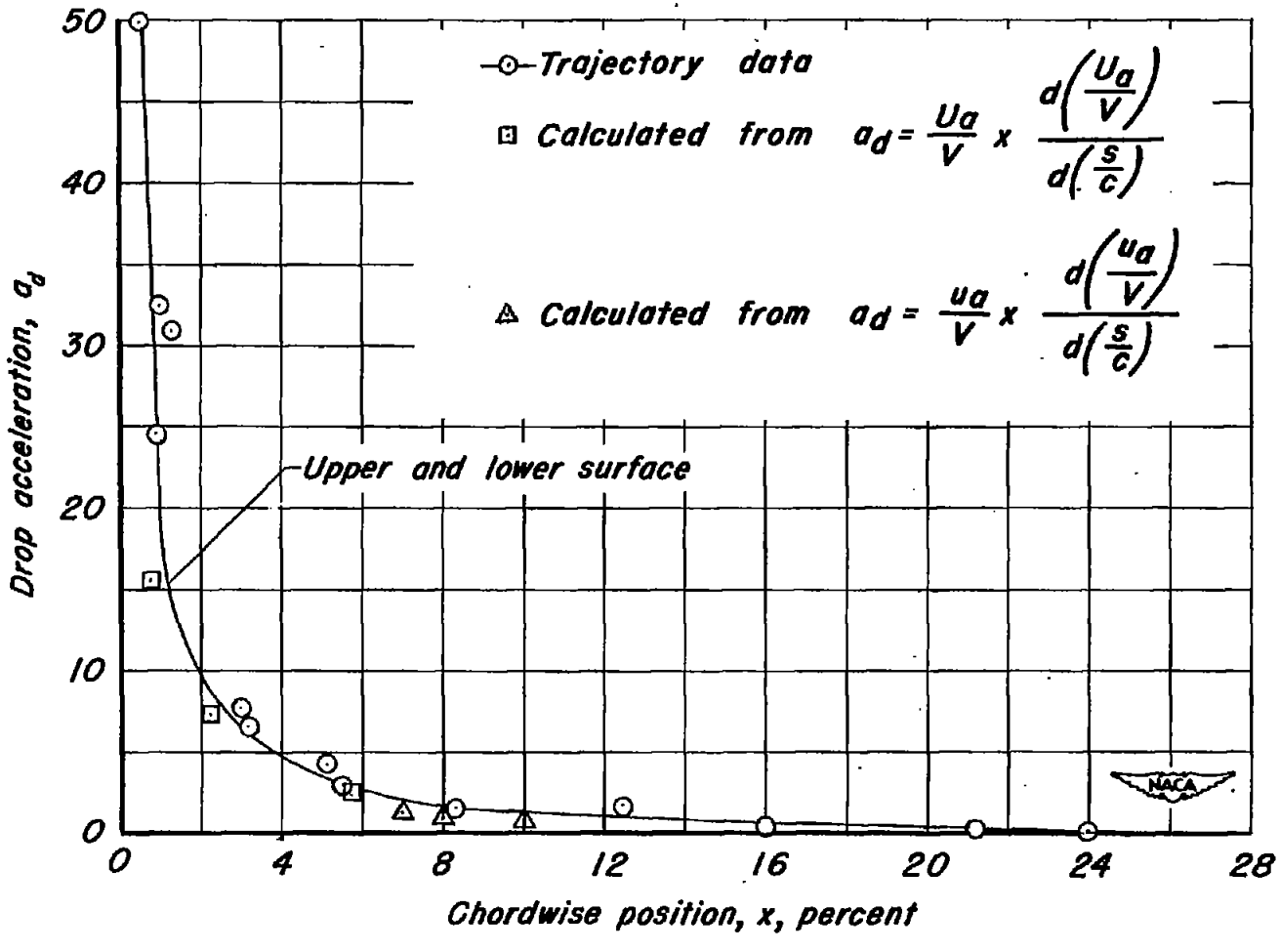


(a) 15-percent-thick symmetrical Joukowski airfoil; $\alpha = 0°$.

Figure 12.- Chordwise distribution of instantaneous drop-acceleration values for tangential trajectories at instant of drop impact.

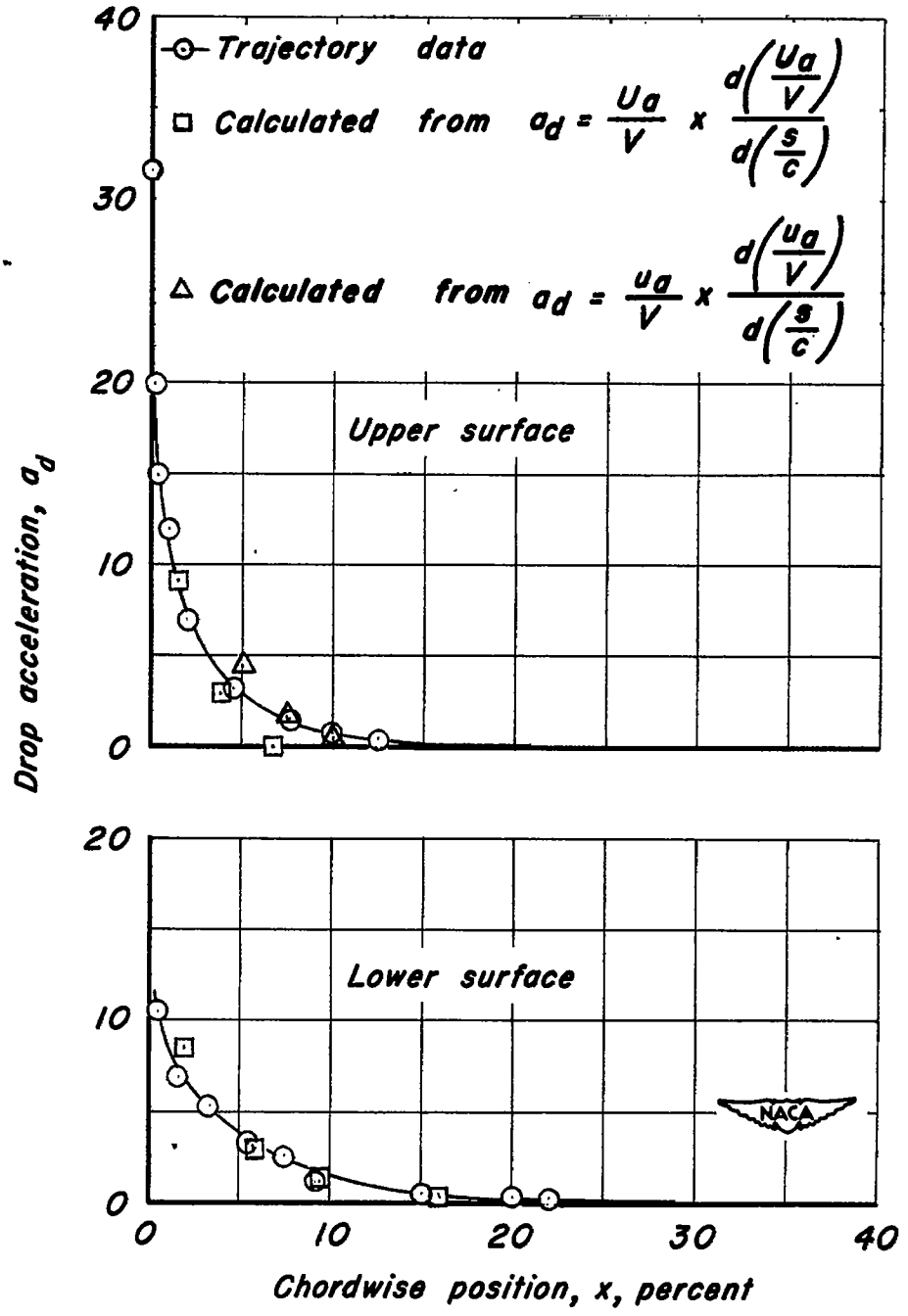


(b) 15-percent-thick symmetrical Joukowski airfoil; $\alpha = 2°$.

Figure 12.- Continued.

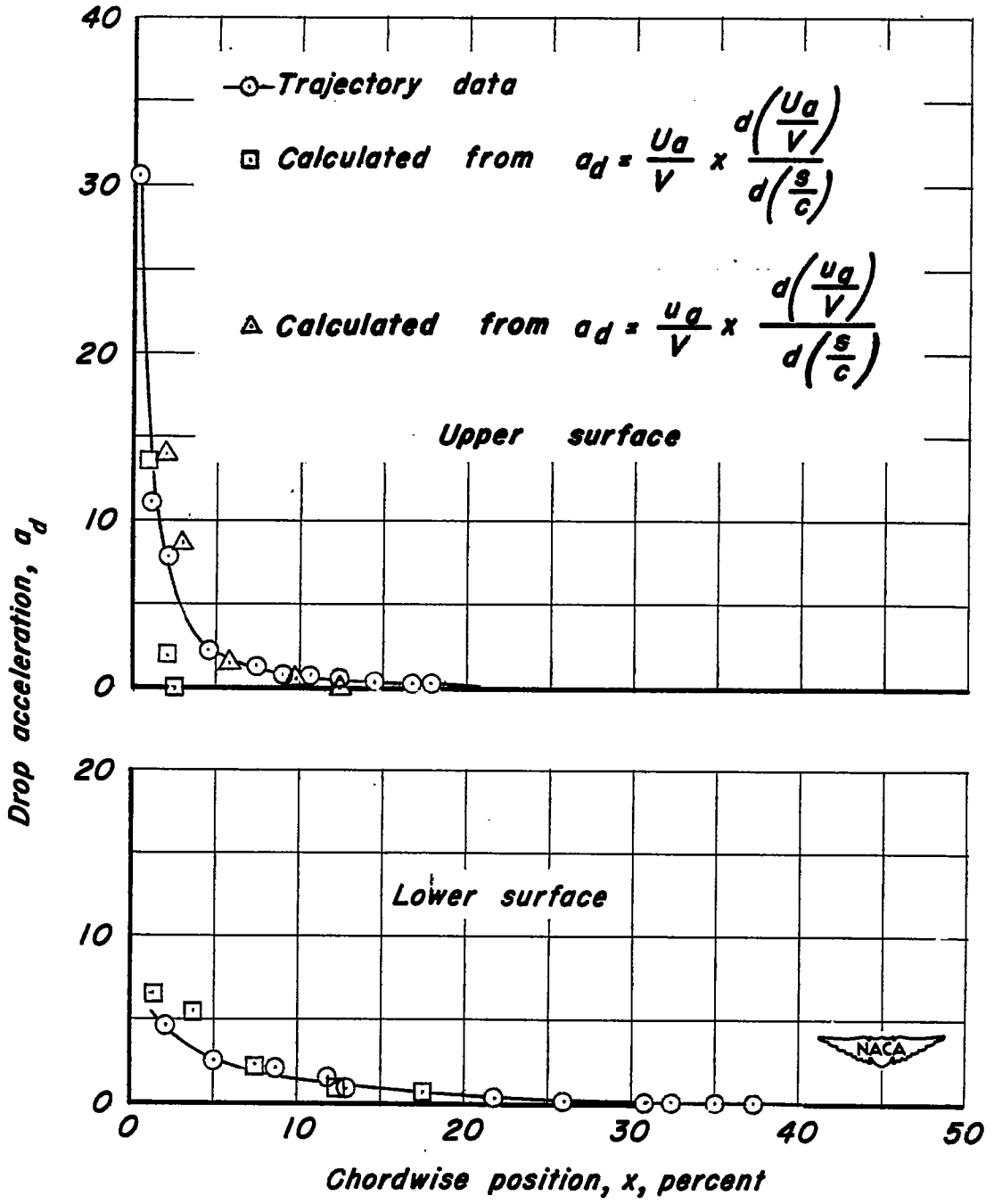


(c) 15-percent-thick symmetrical Joukowski airfoil; $\alpha = 4°$.

Figure 12.– Continued.

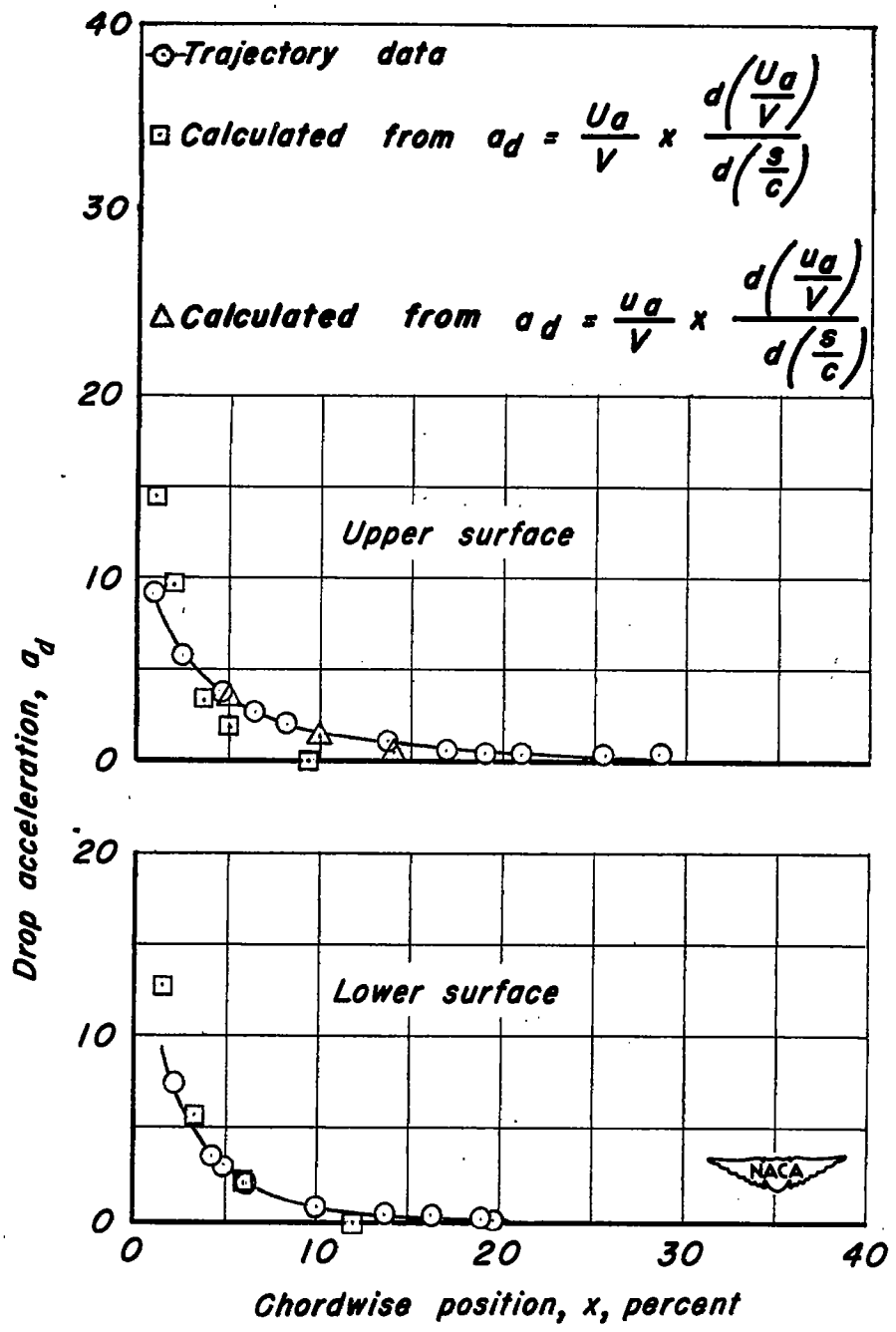


(d) 15-percent-thick cambered Joukowski airfoil; $\alpha = 0°$; $a = 1.0$ mean line.

Figure 12.- Continued.

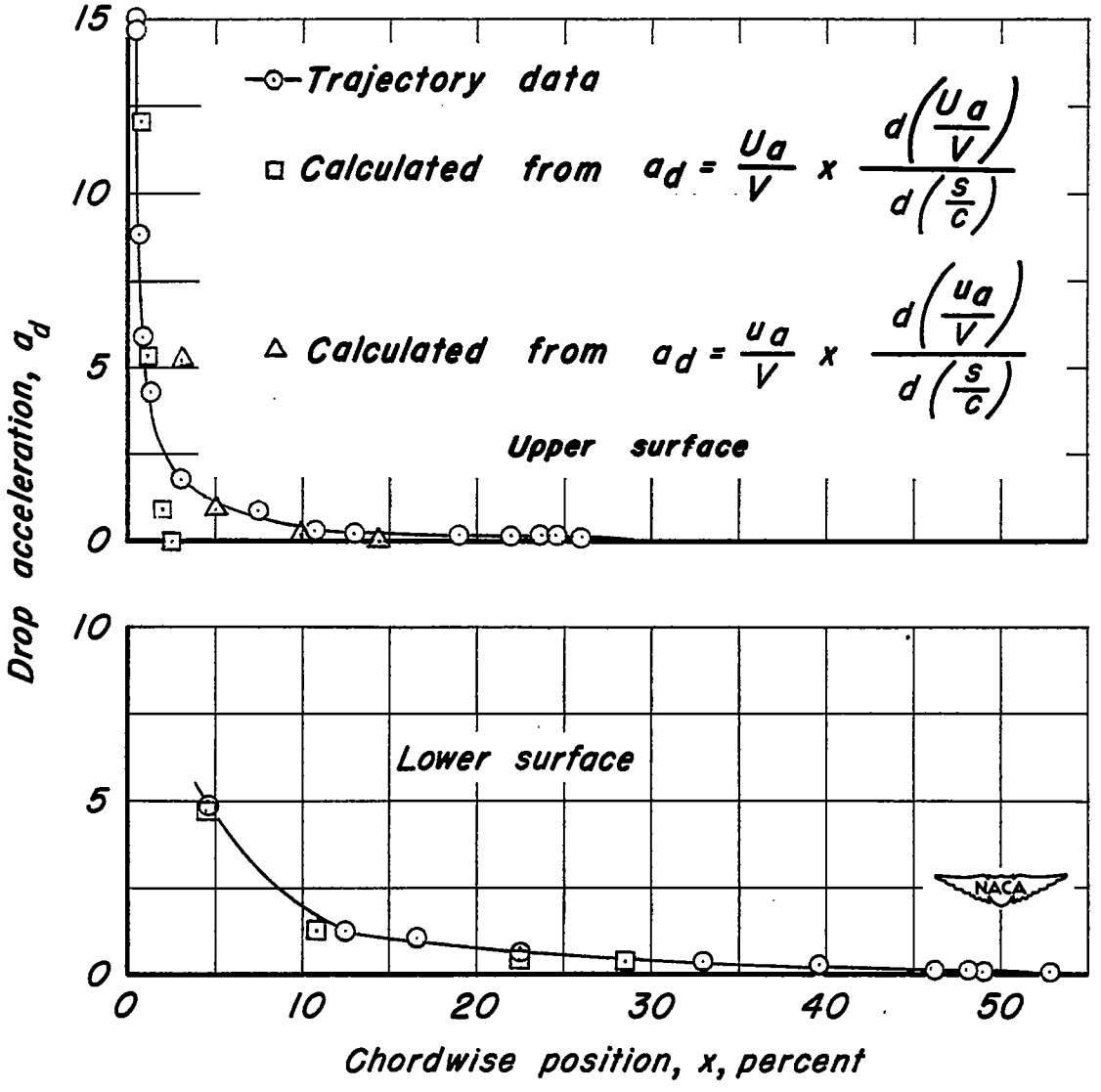


(e) NACA $65_2$-015 airfoil; $\alpha = 4°$.

Figure 12.- Concluded.

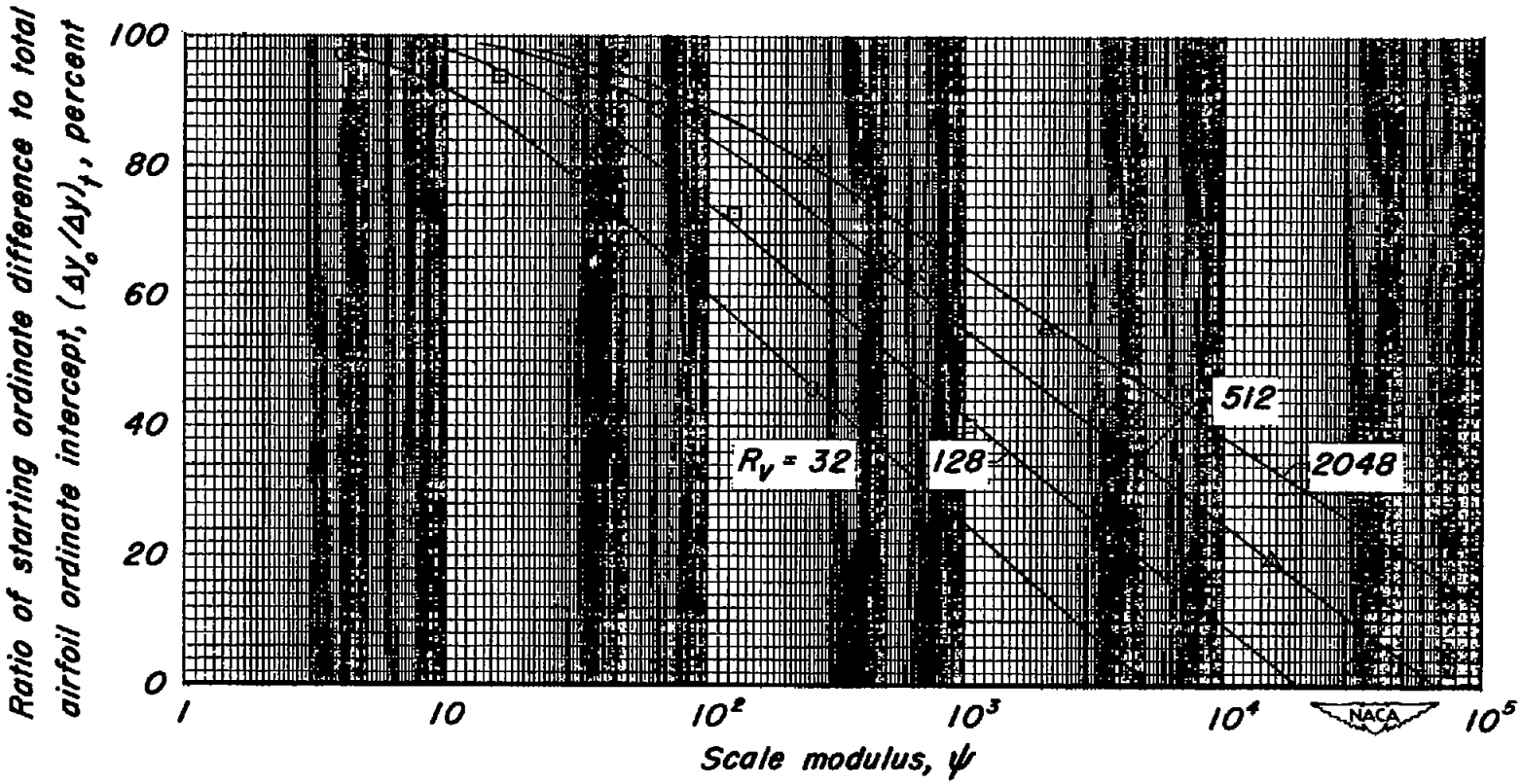


(a) 15-percent-thick symmetrical Joukowski airfoil; $\alpha = 0°$.

Figure 13.- Ratio of trajectory starting ordinate difference to total airfoil ordinate intercept as a function of scale modulus and free-stream Reynolds number.

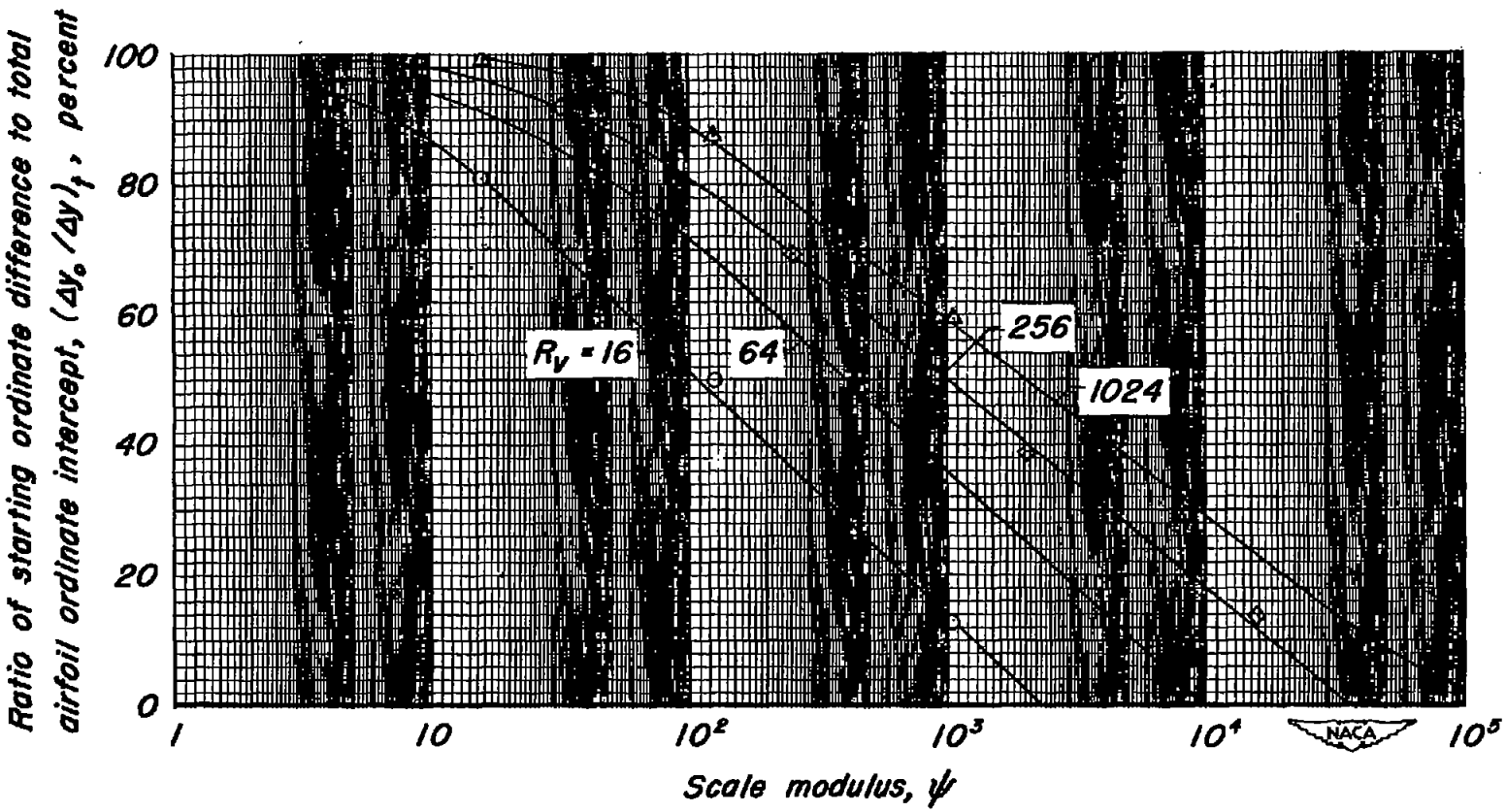


(b) 15-percent-thick symmetrical Joukowski airfoil; $\alpha = 2°$.

Figure 13.- Continued.

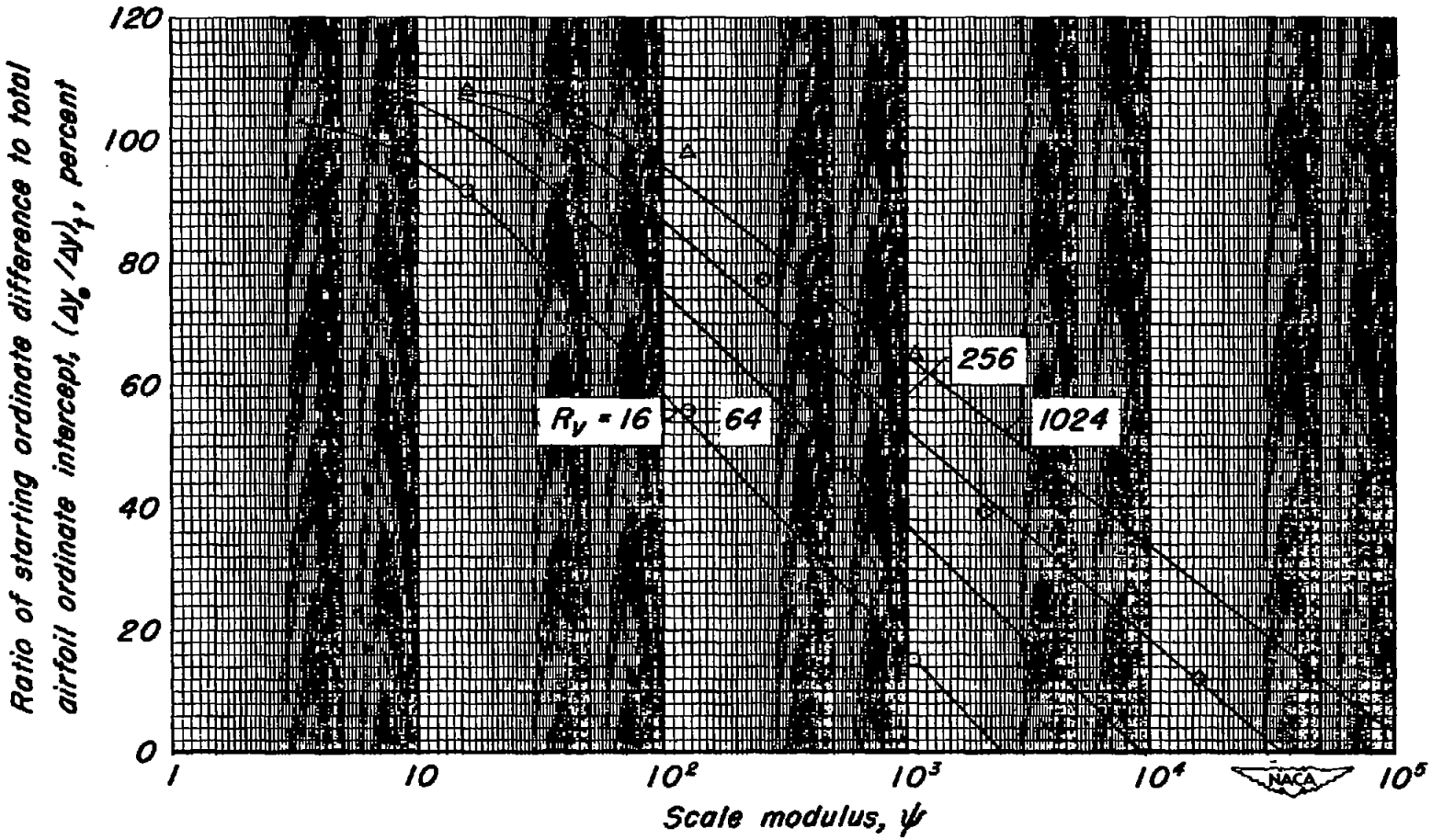


(c) 15-percent-thick symmetrical Joukowski airfoil; $\alpha = 4°$.

Figure 13.– Continued.

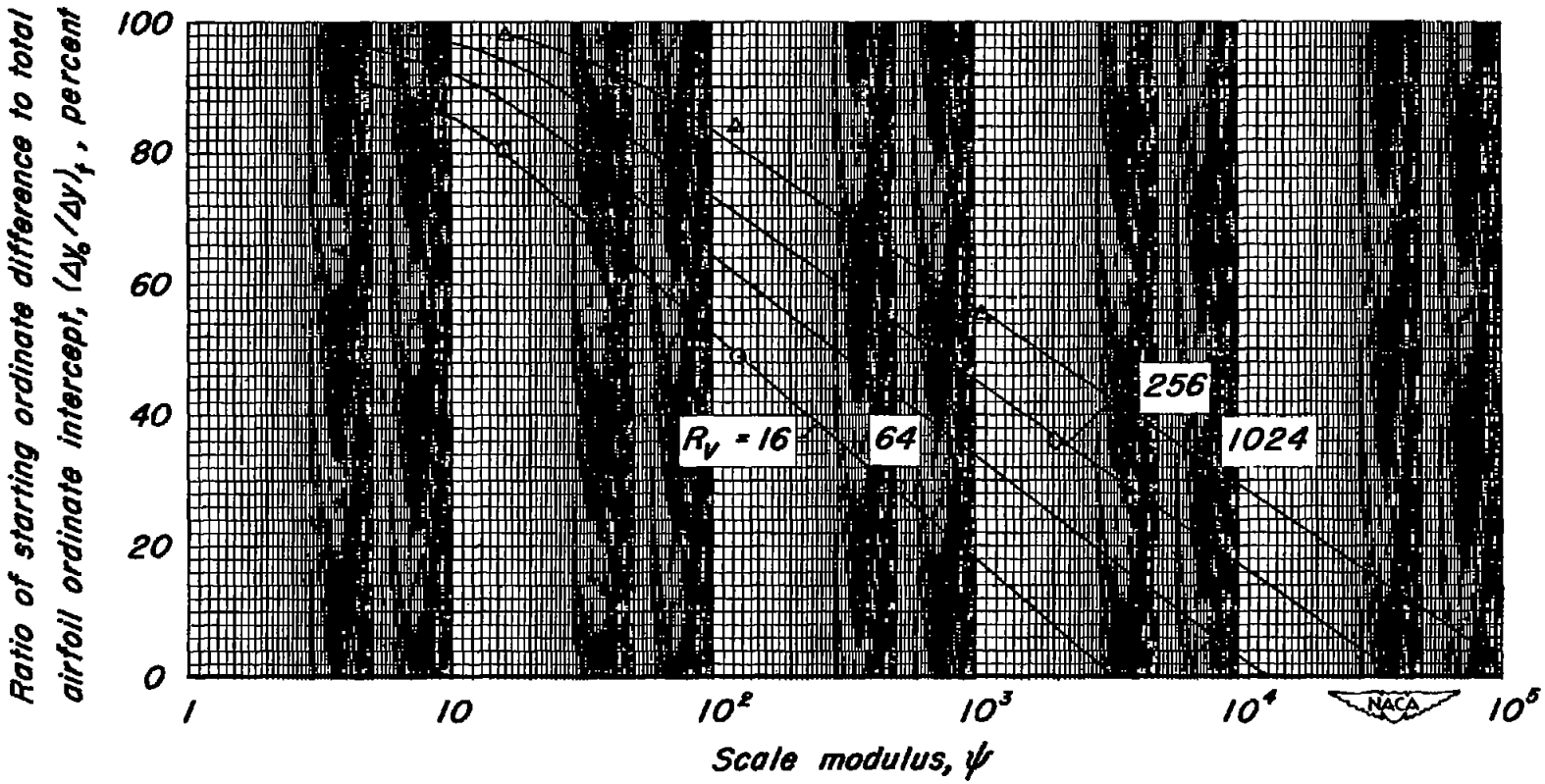


(d) 15-percent-thick cambered Joukowski airfoil; $a$ = 1.0 mean line; $\alpha$ = 0°.

Figure 13.- Continued.

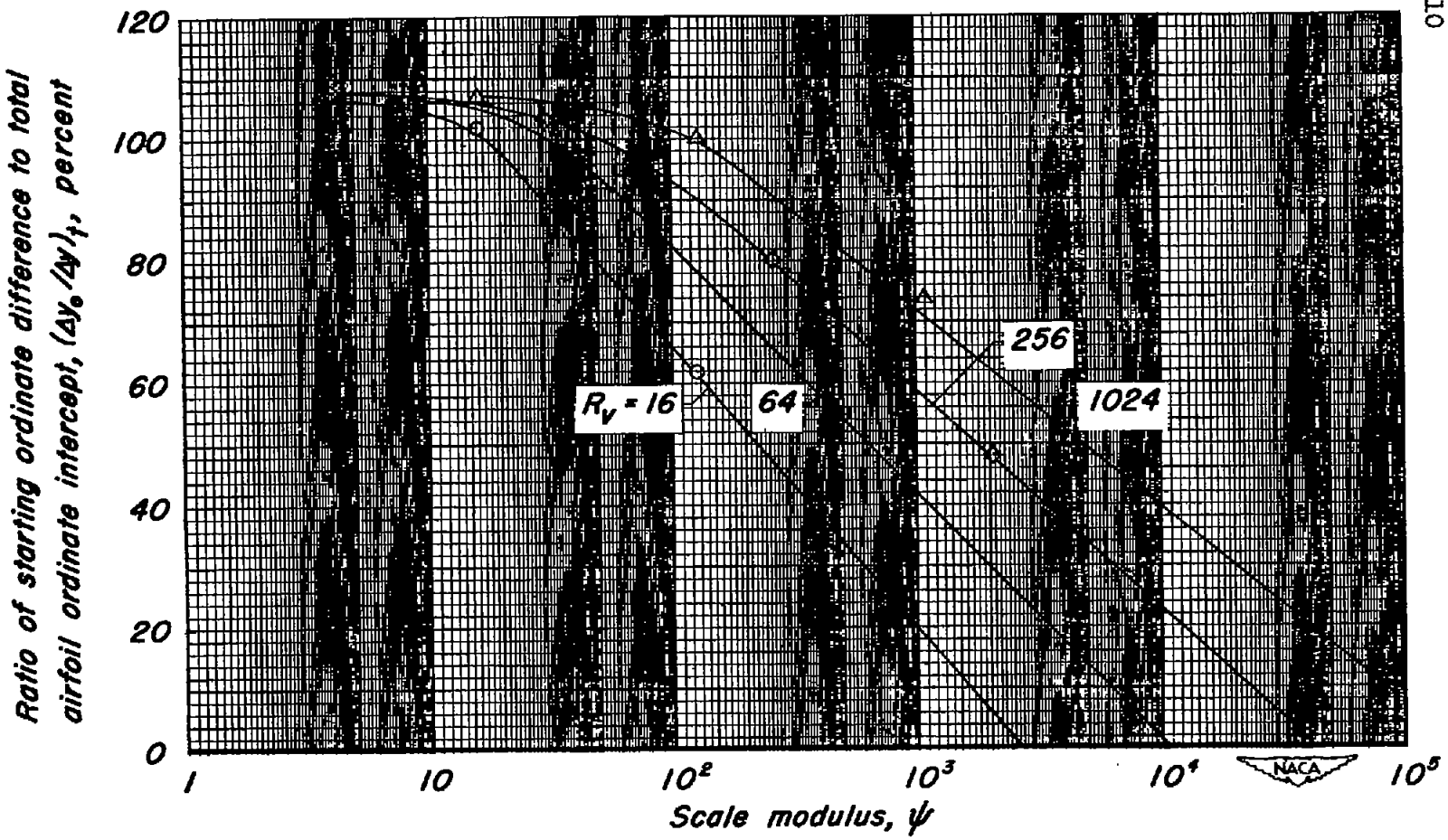


(e) NACA $65_2$-015 airfoil; $\alpha = 4°$.

Figure 13.- Concluded.

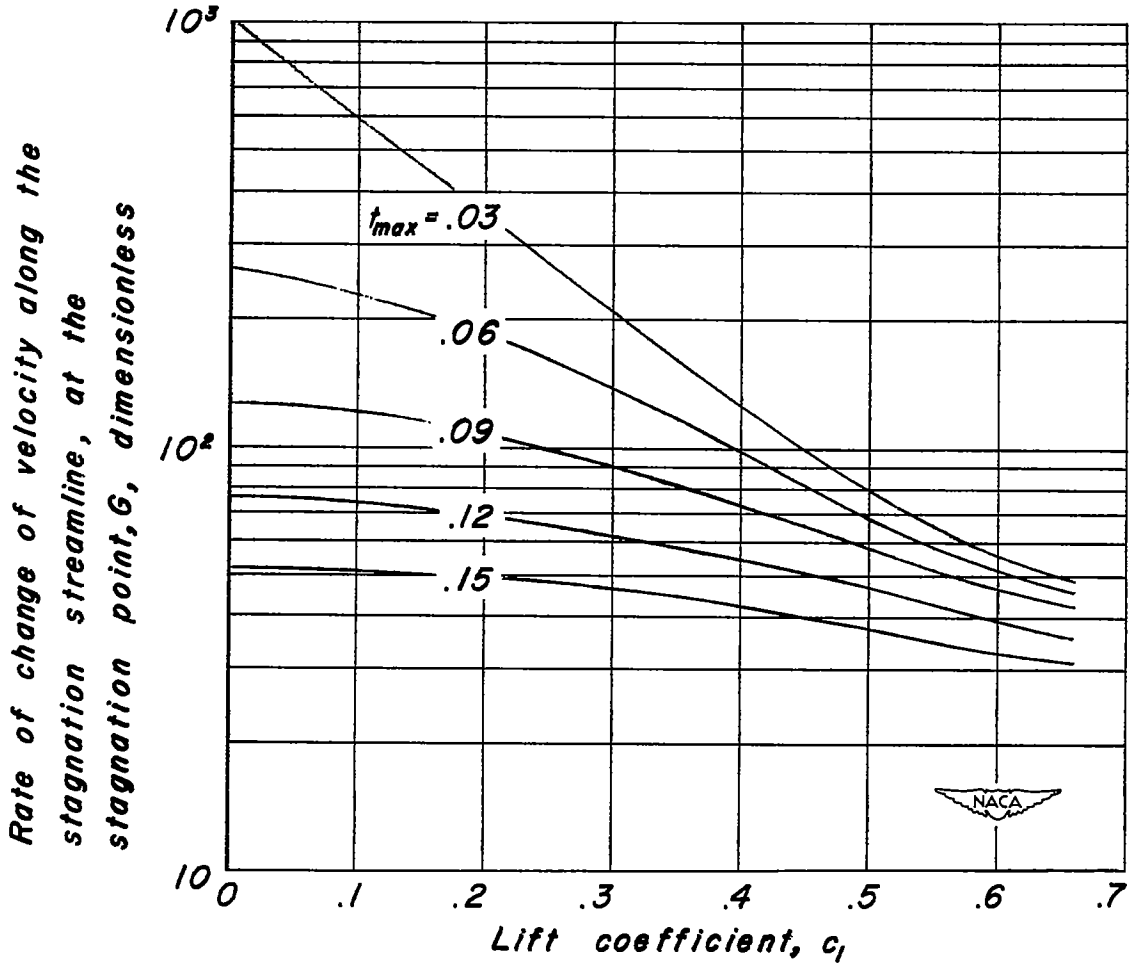


(a) Joukowski airfoil.

Figure 14. Velocity gradient along the stagnation streamline, at the stagnation point, as a function of lift coefficient and thickness ratio for two profiles.

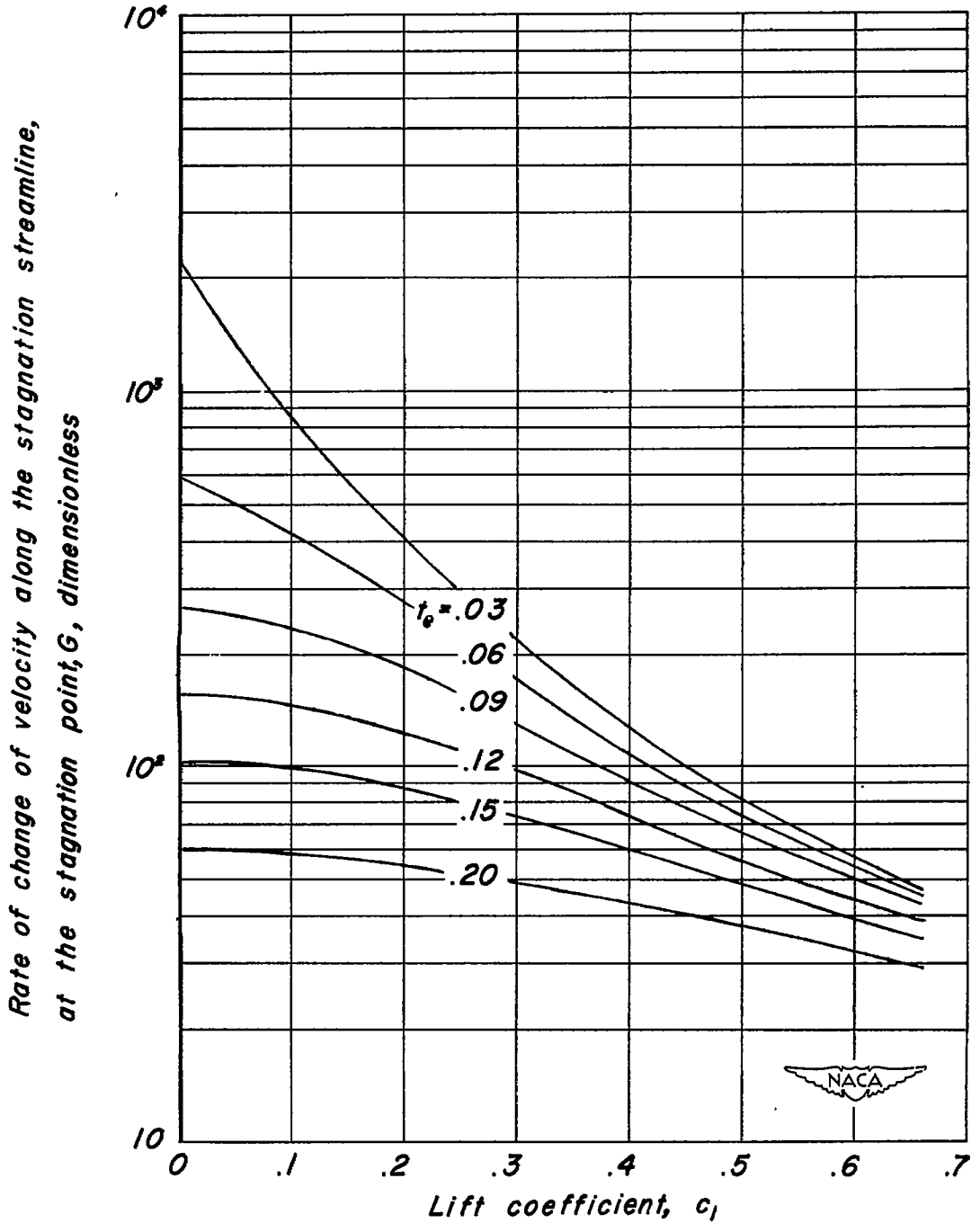


(b) Ellipse.

Figure 14. Concluded.

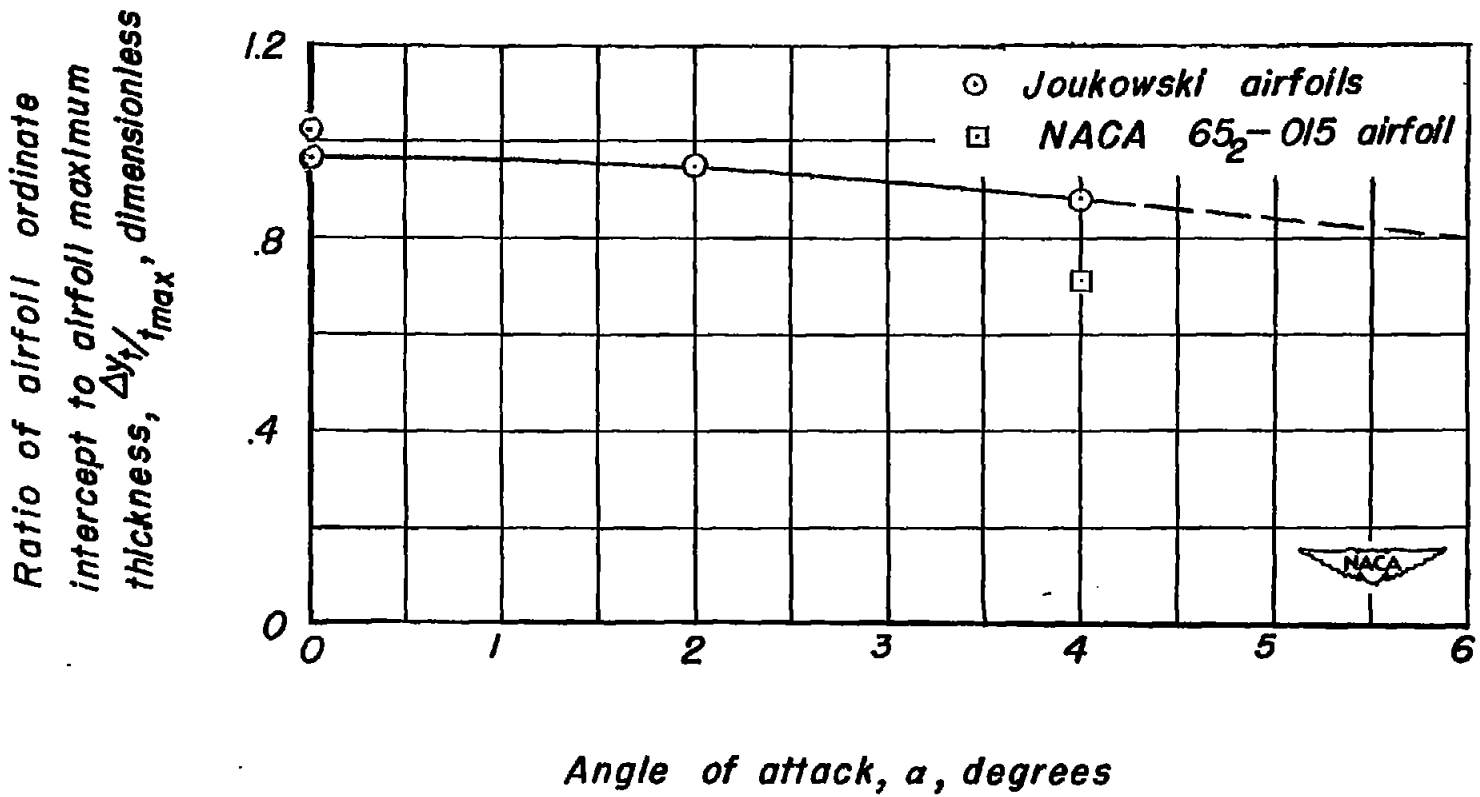


Figure 15.– Ratio of $\Delta y_t/t_{max}$ as a function of angle of attack for $(\Delta y_o/\Delta y)_t = 0.8$

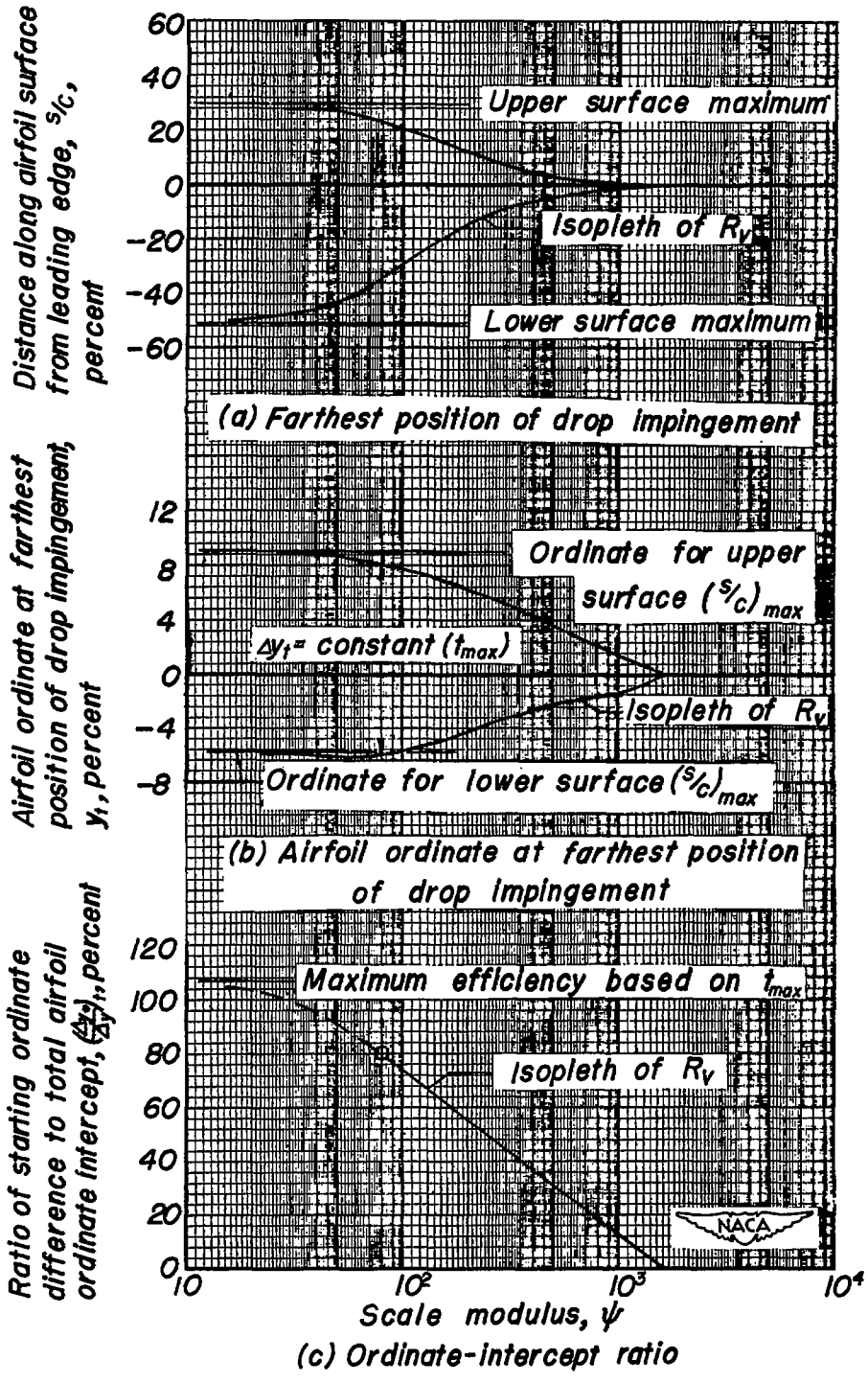


*Figure 16.— Graphical representation of the procedure used to obtain a value of $\psi$ corresponding to $(\Delta y_s/\Delta y)_t = 0.8$*

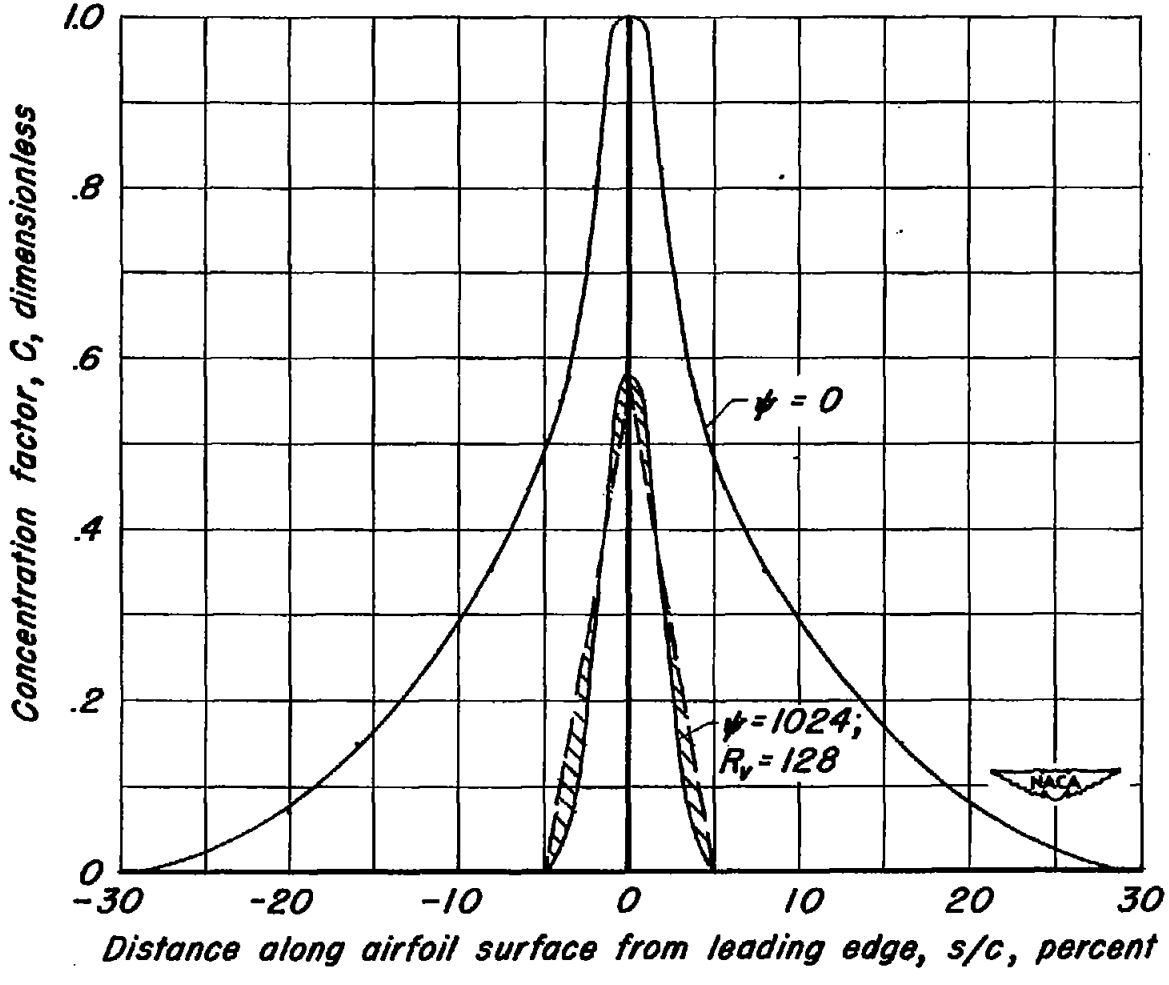


(a) 15-percent-thick symmetrical Joukowski airfoil; $\alpha = 0°$.

Figure 17.- Surface distribution of water-drop impingement for five airfoils.

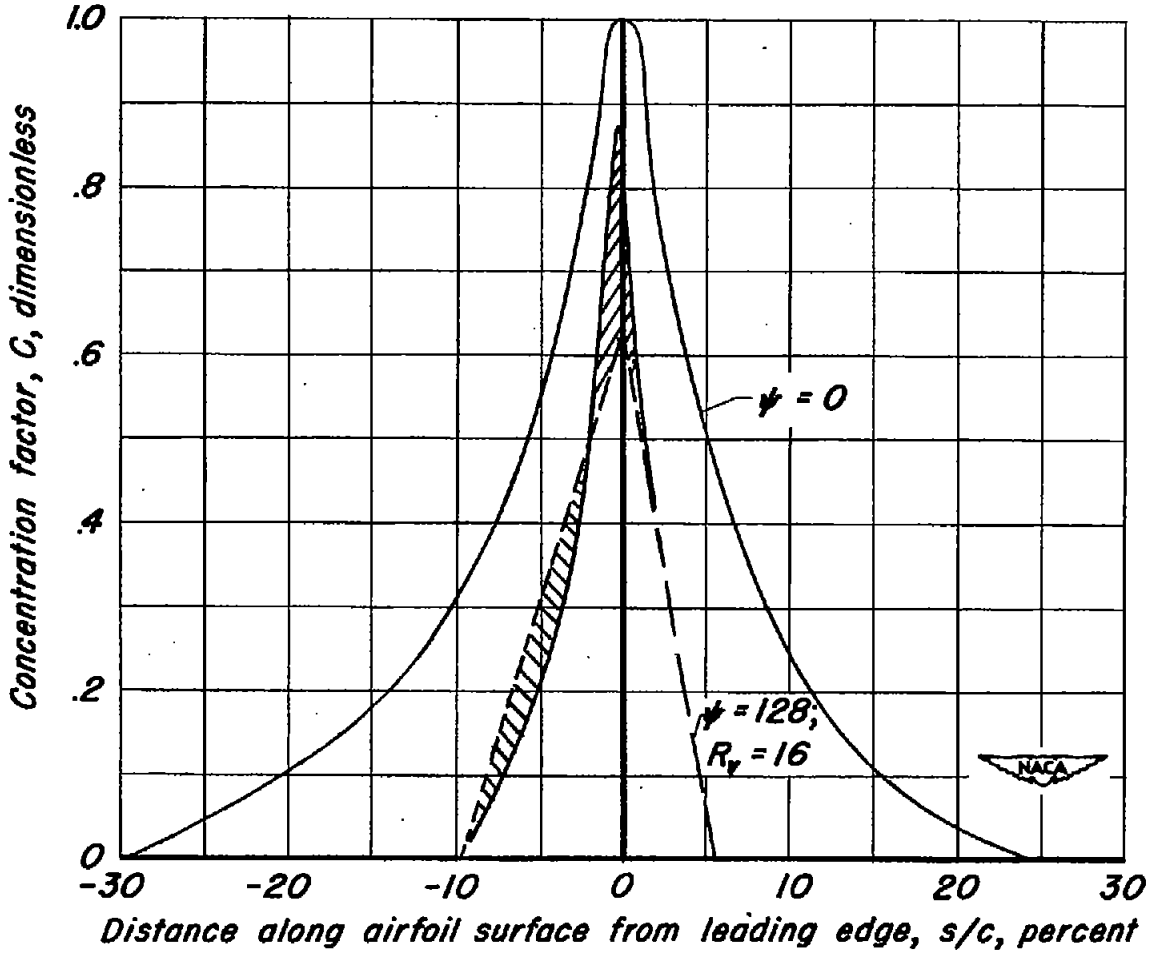


(b) 15-percent-thick symmetrical Joukowski airfoil; $\alpha = 2°$.

Figure 17.—Continued.

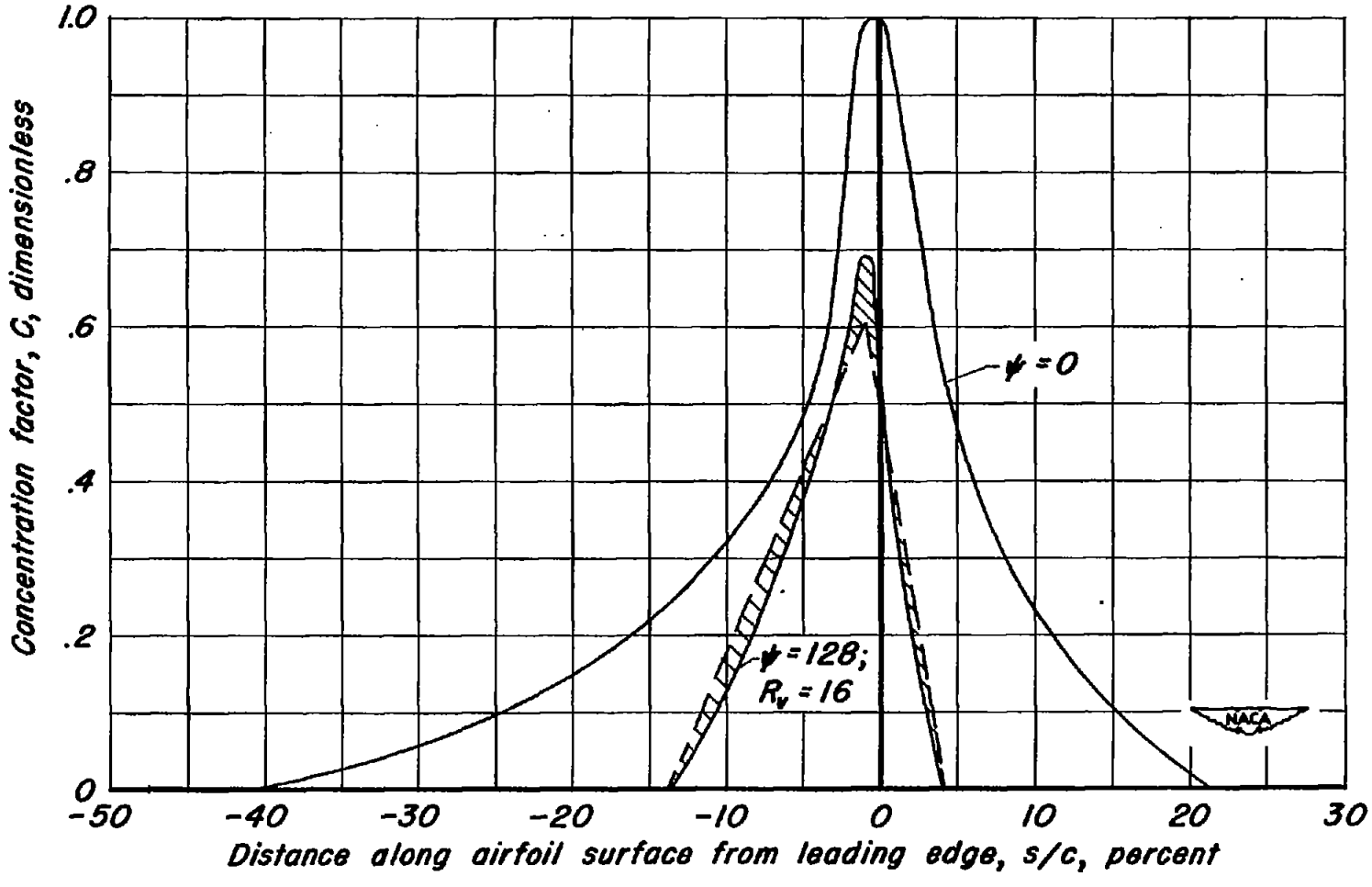


(c) 15-percent-thick symmetrical Joukowski airfoil; $\alpha = 4°$.

Figure 17.– Continued.

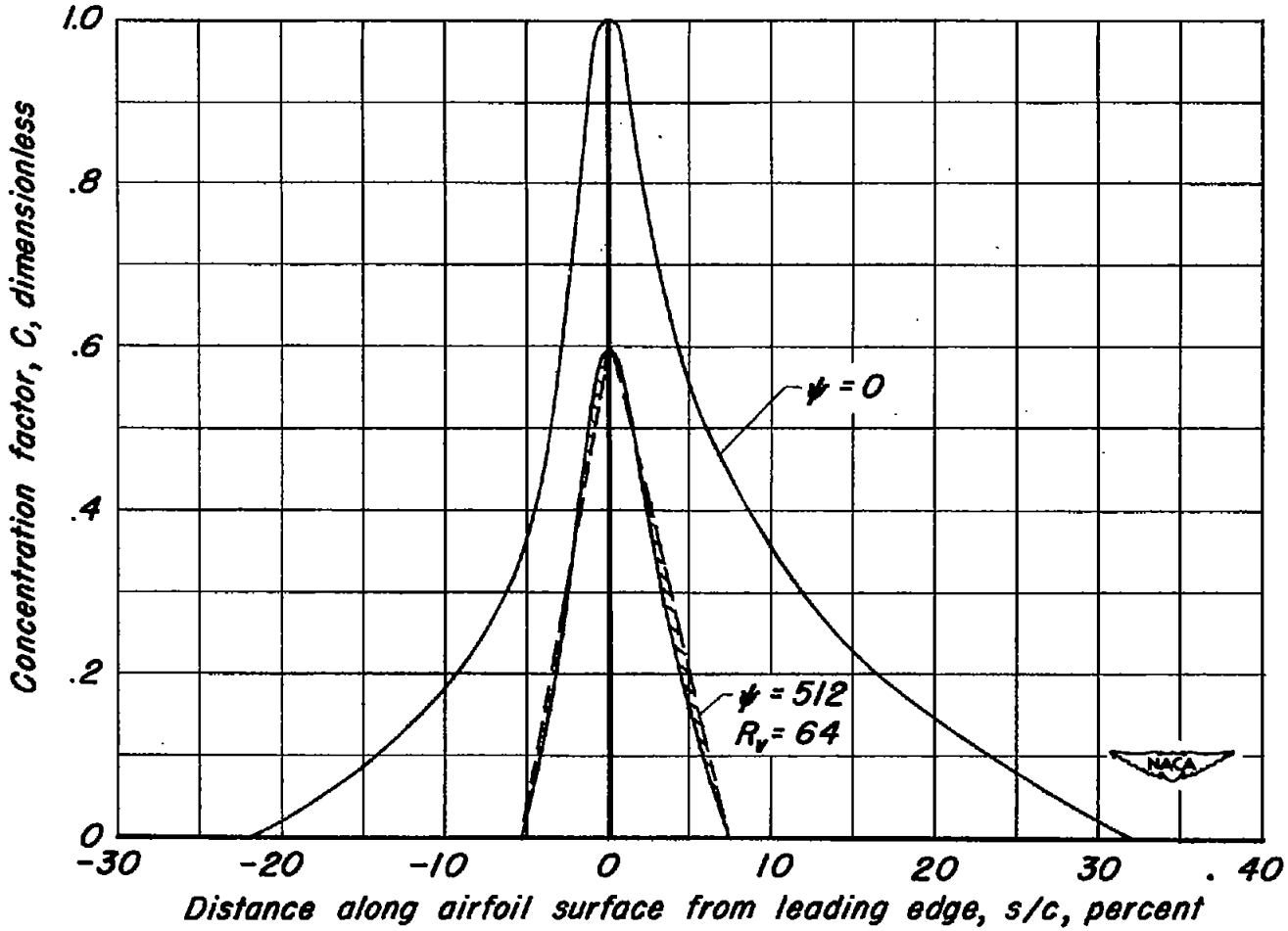


(d) 15-percent-thick cambered Joukowski airfoil; a = 1.0 mean line; α = 0°.

Figure 17.—Continued.

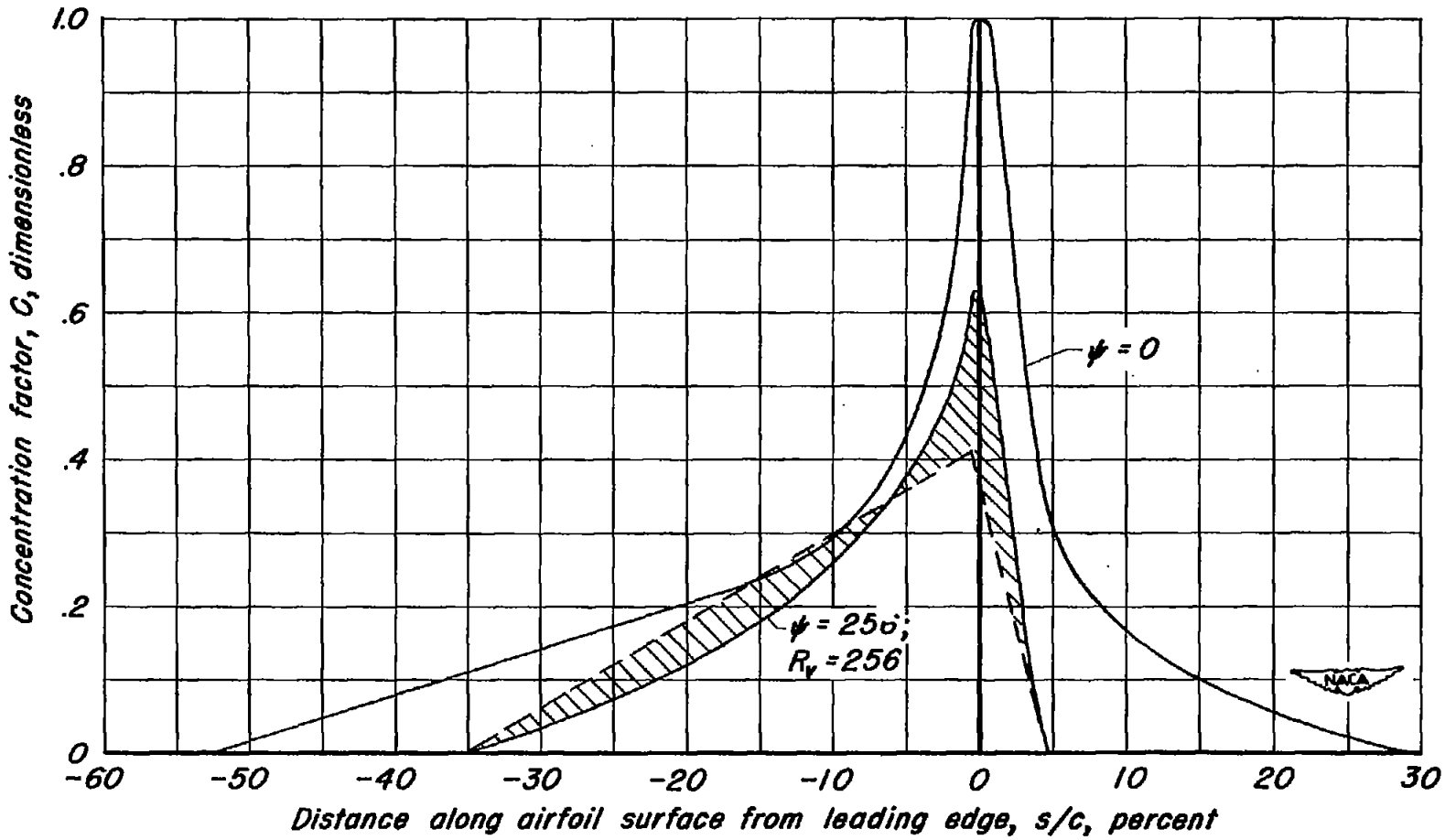


(e) NACA $65_2$-015 airfoil; $\alpha = 4°$.

*Figure 17. — Concluded.*

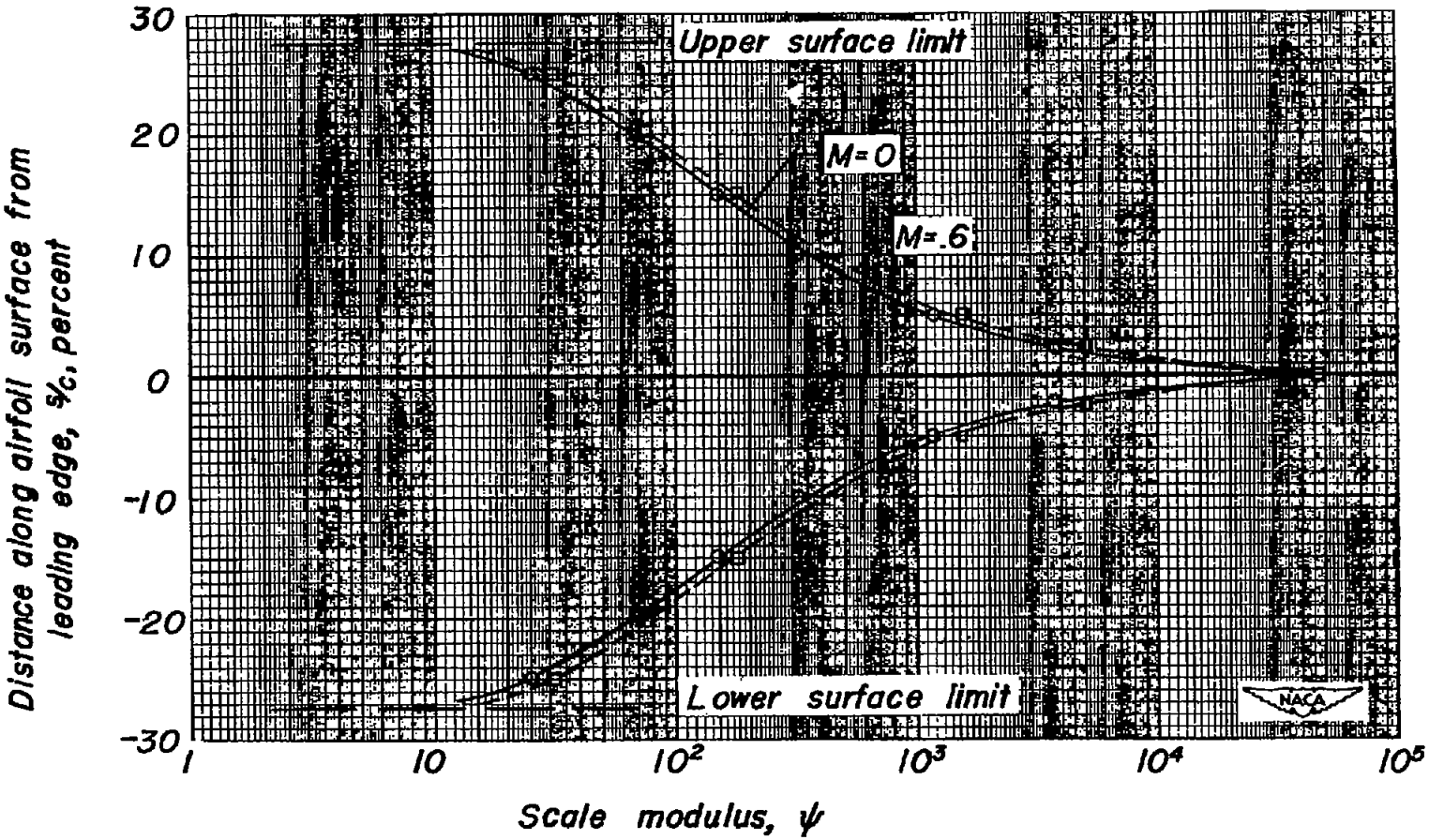


(a) Farthest position of impingement.

Figure 18.– Comparison between empirically calculated values of farthest position and efficiency of impingement for a 15-percent-thick symmetrical Joukowski airfoil, $c_l = 0$, at different Mach numbers; $R_v = 225$.

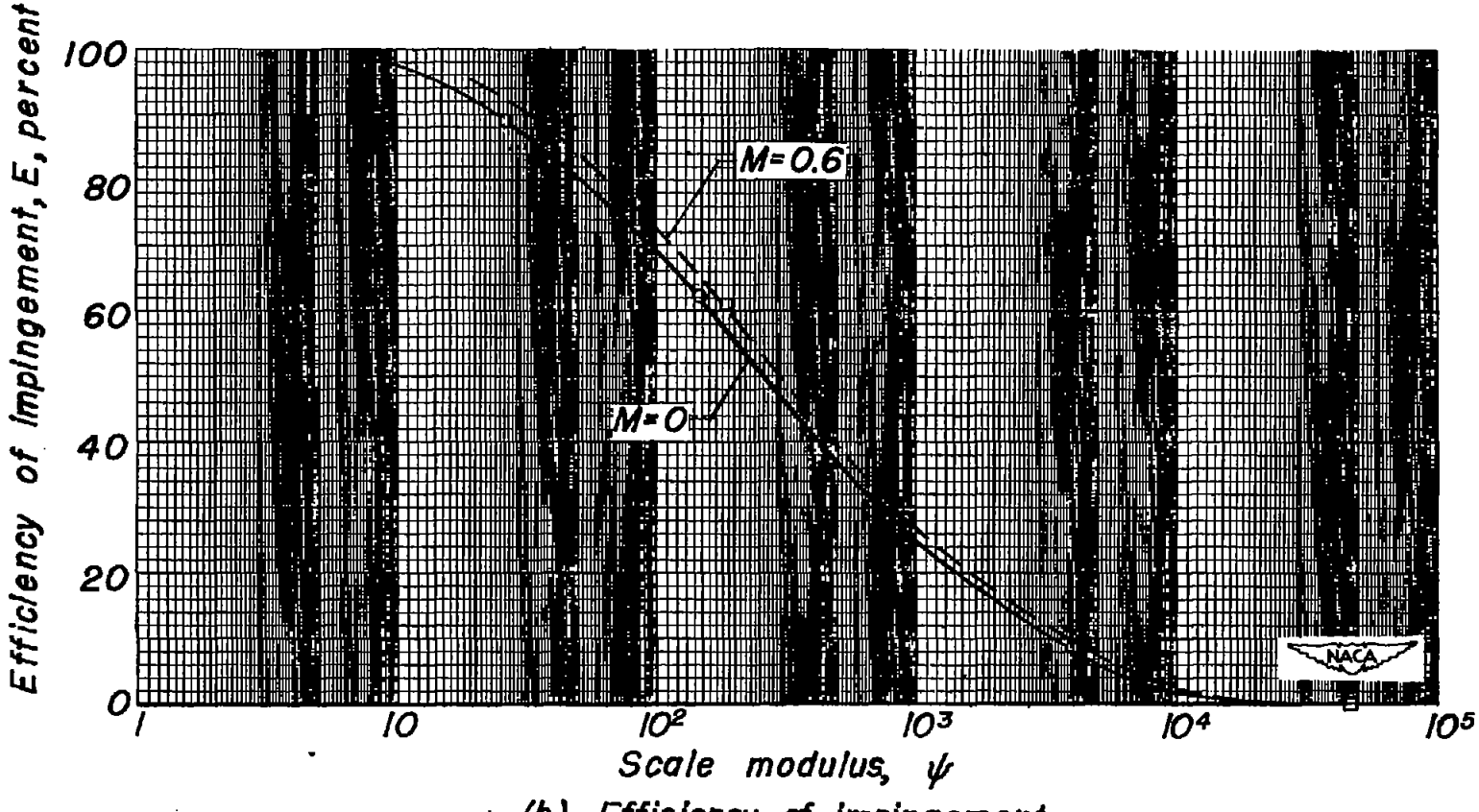


(b) Efficiency of impingement.

Figure 18.— Concluded.

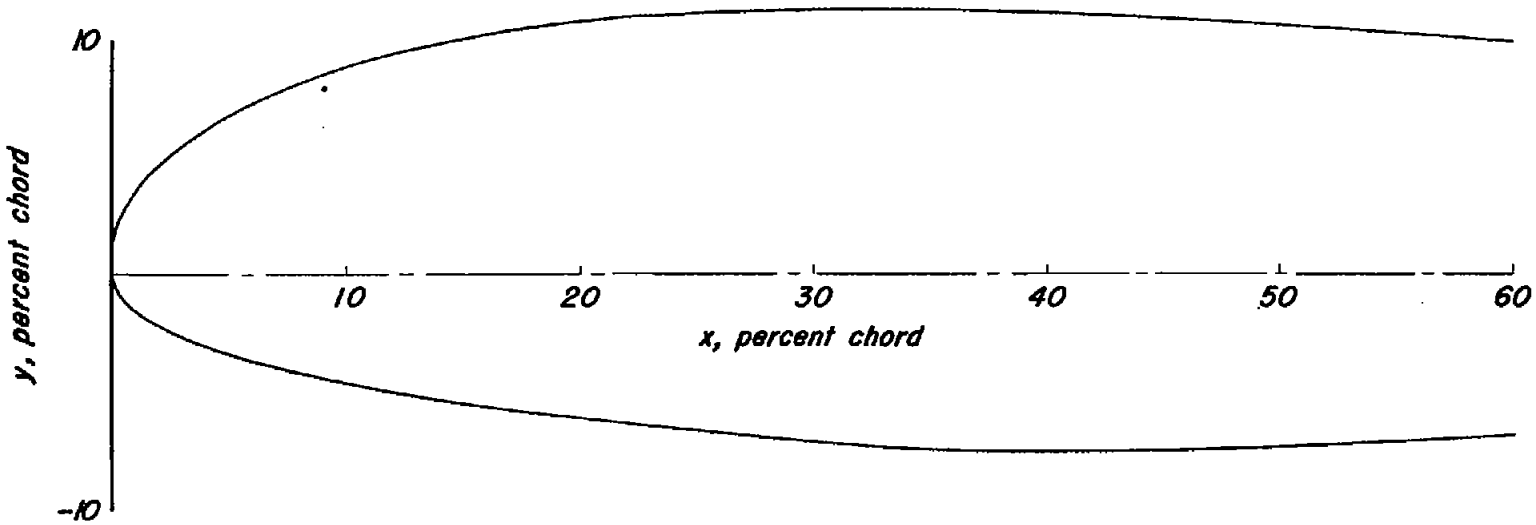


(a) Airfoil contour.

Figure 19.- Graphical relationships used in evaluating farthest position of impingement for an NACA 23015 airfoil; $\alpha = 3.6°$; $c_l = 0.5$.

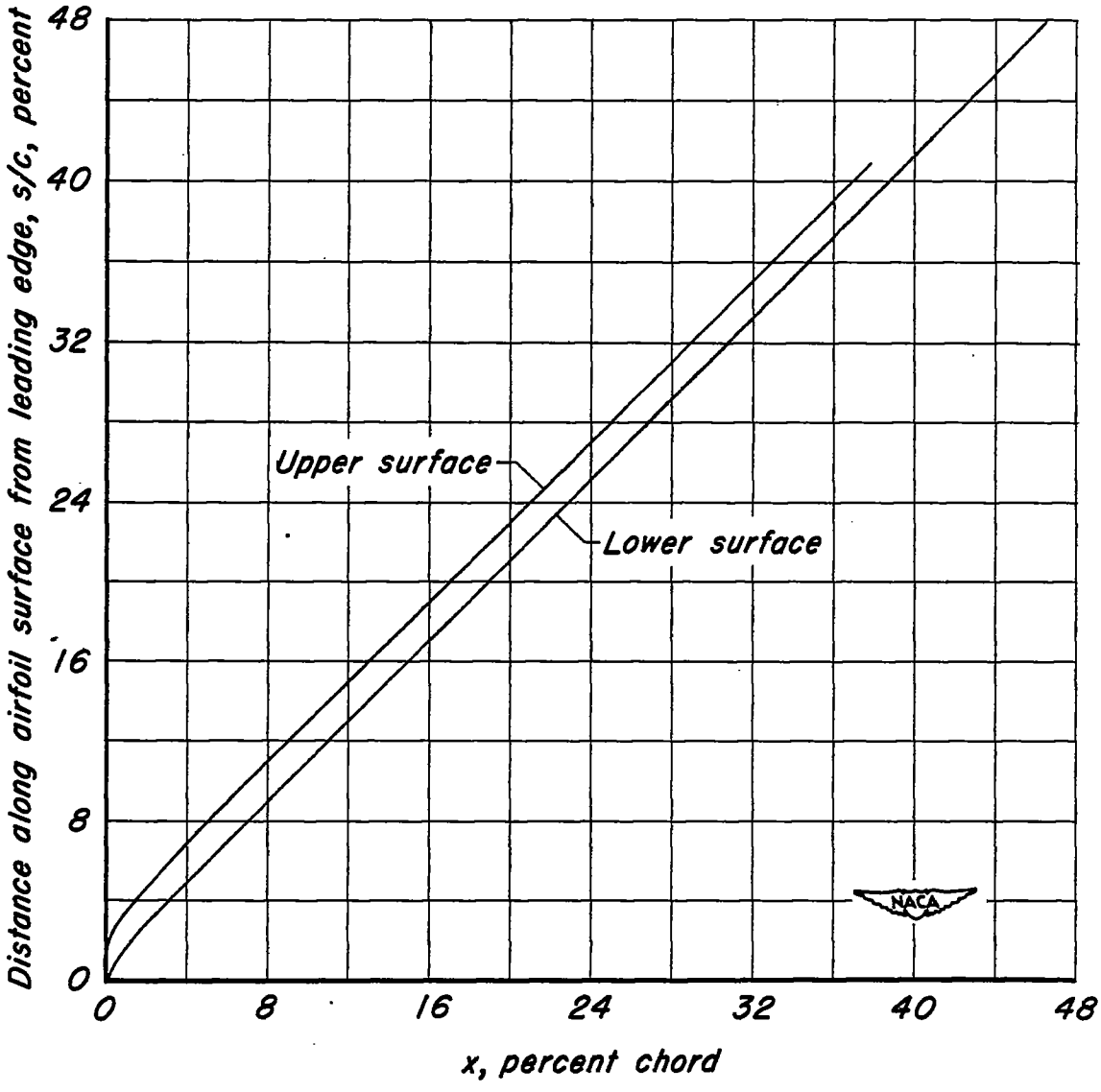


(b) Variation of s/c with chordwise position.

Figure 19. - Continued.

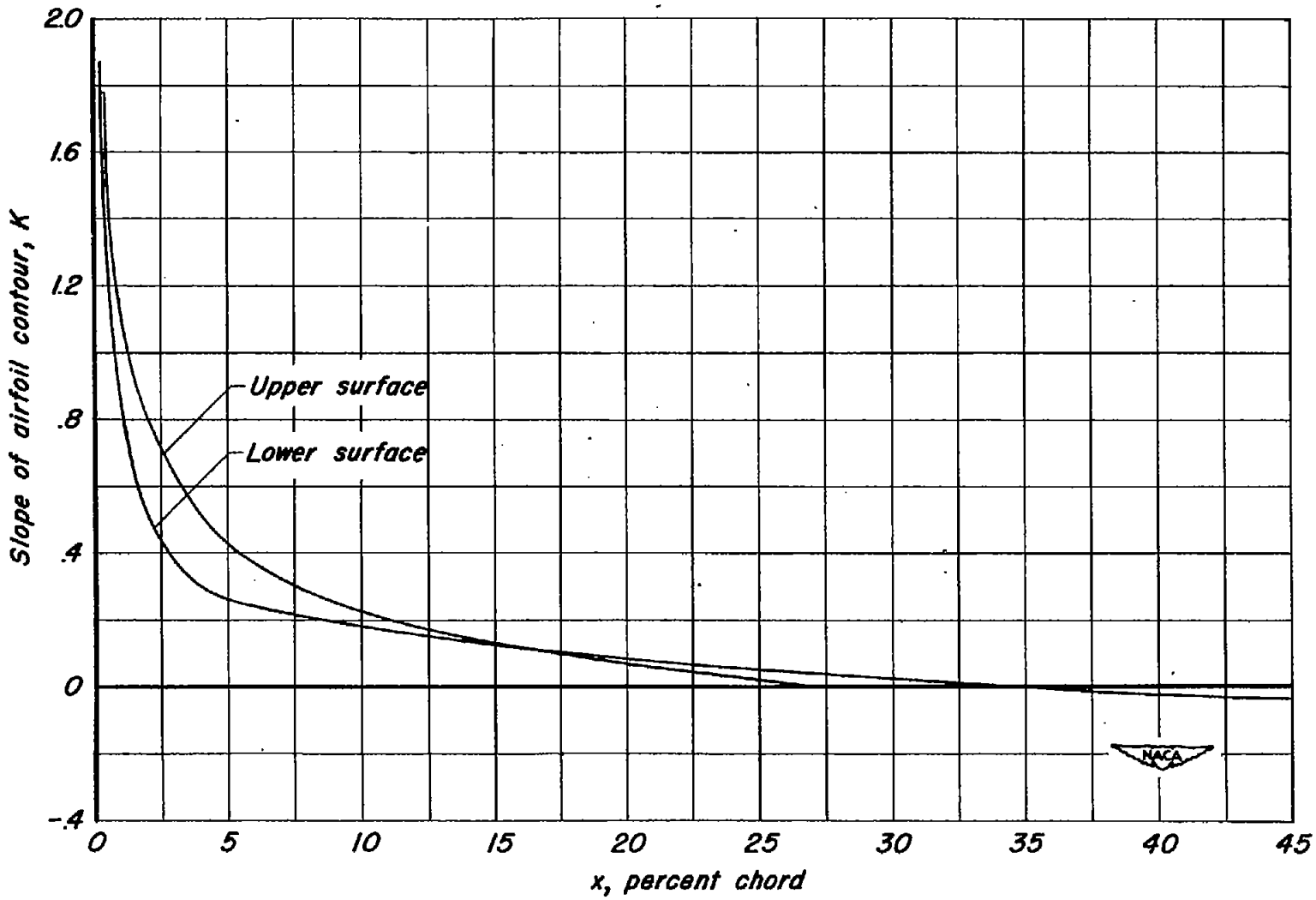


(c) Slope of airfoil contour as a function of chordwise position.

Figure 19. - Continued.

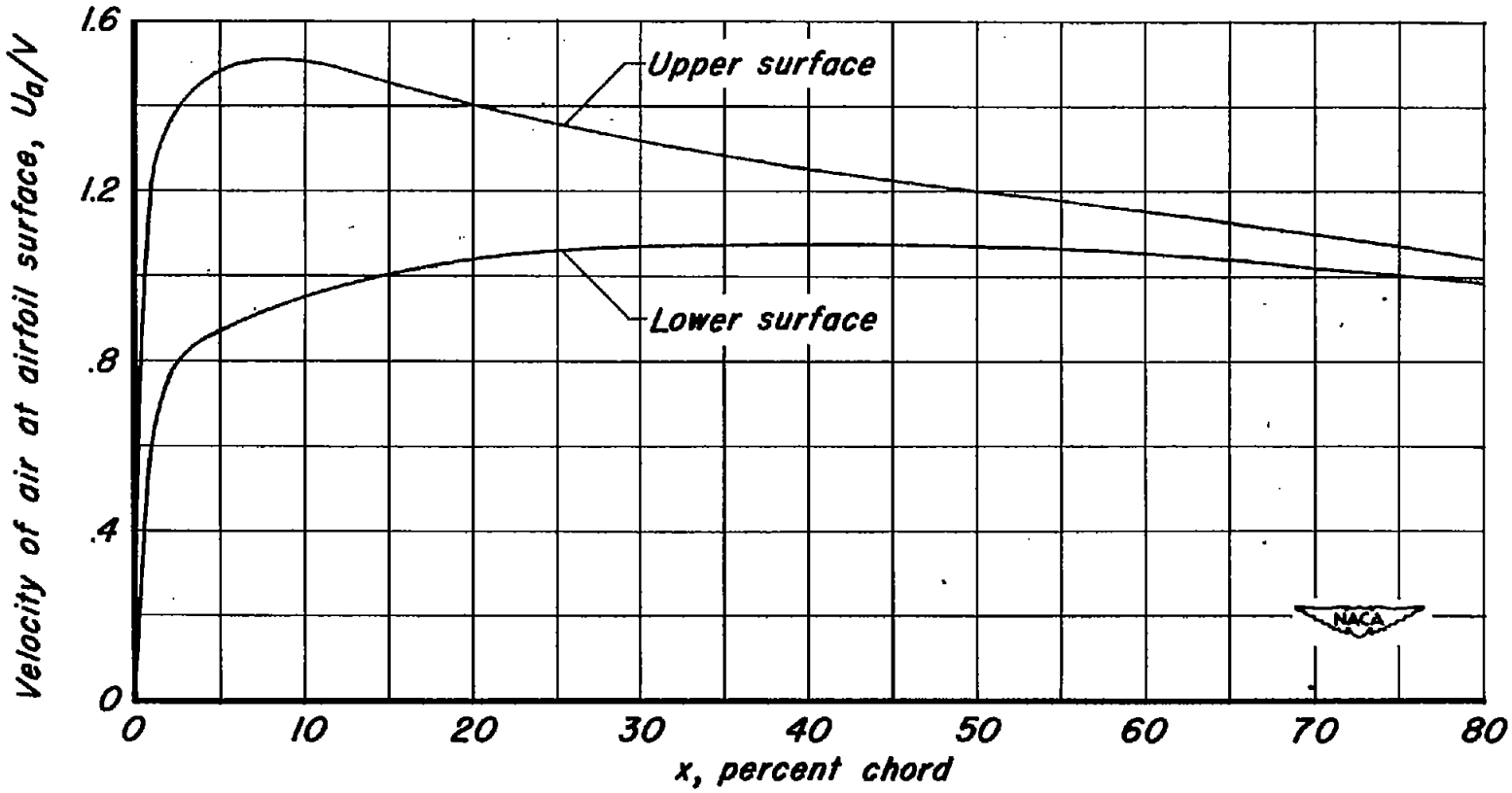


(d) Chordwise velocity distribution.

Figure 19. - Continued.

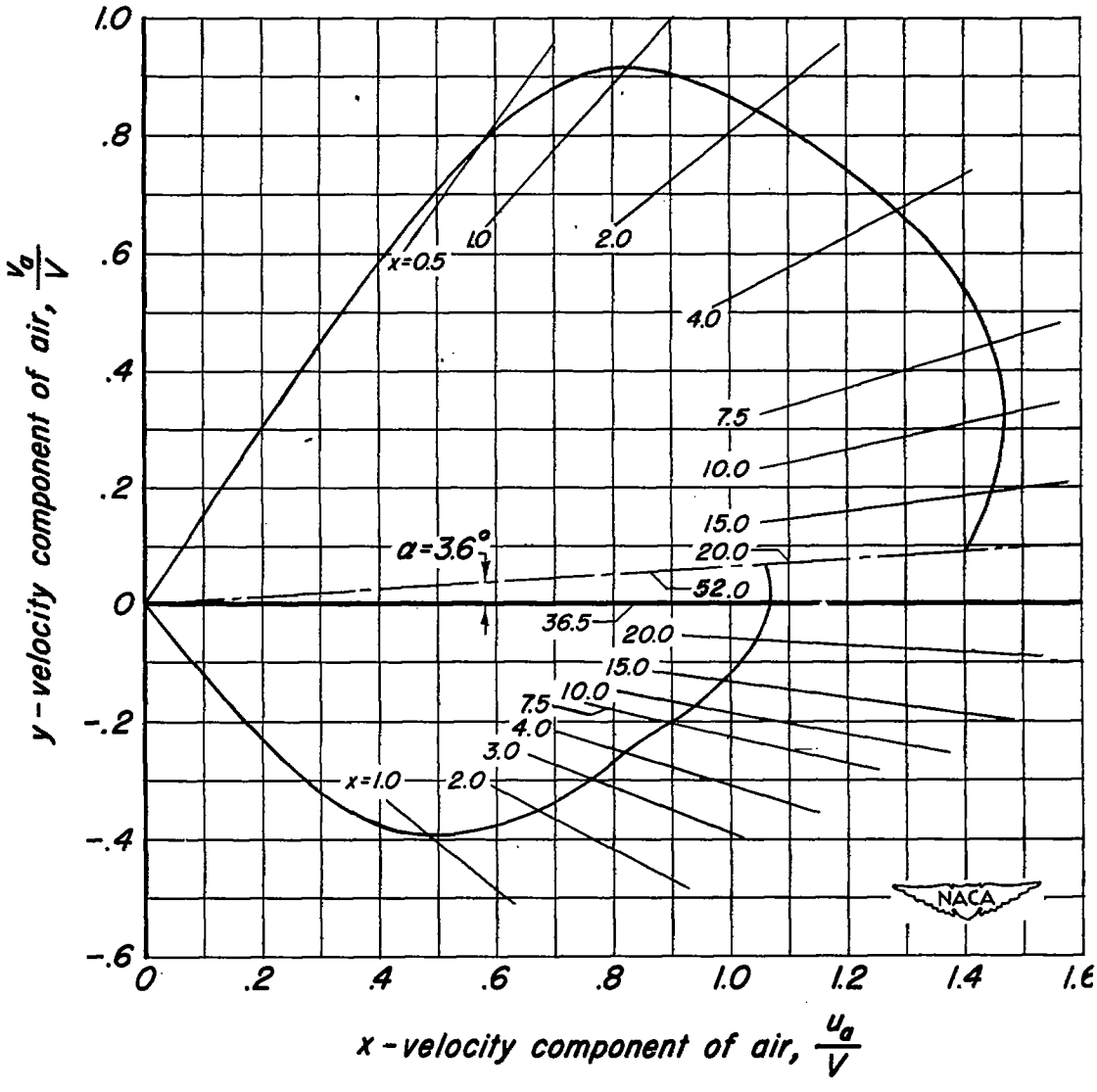


(e) Hodograph for air.

Figure 19. - Continued.

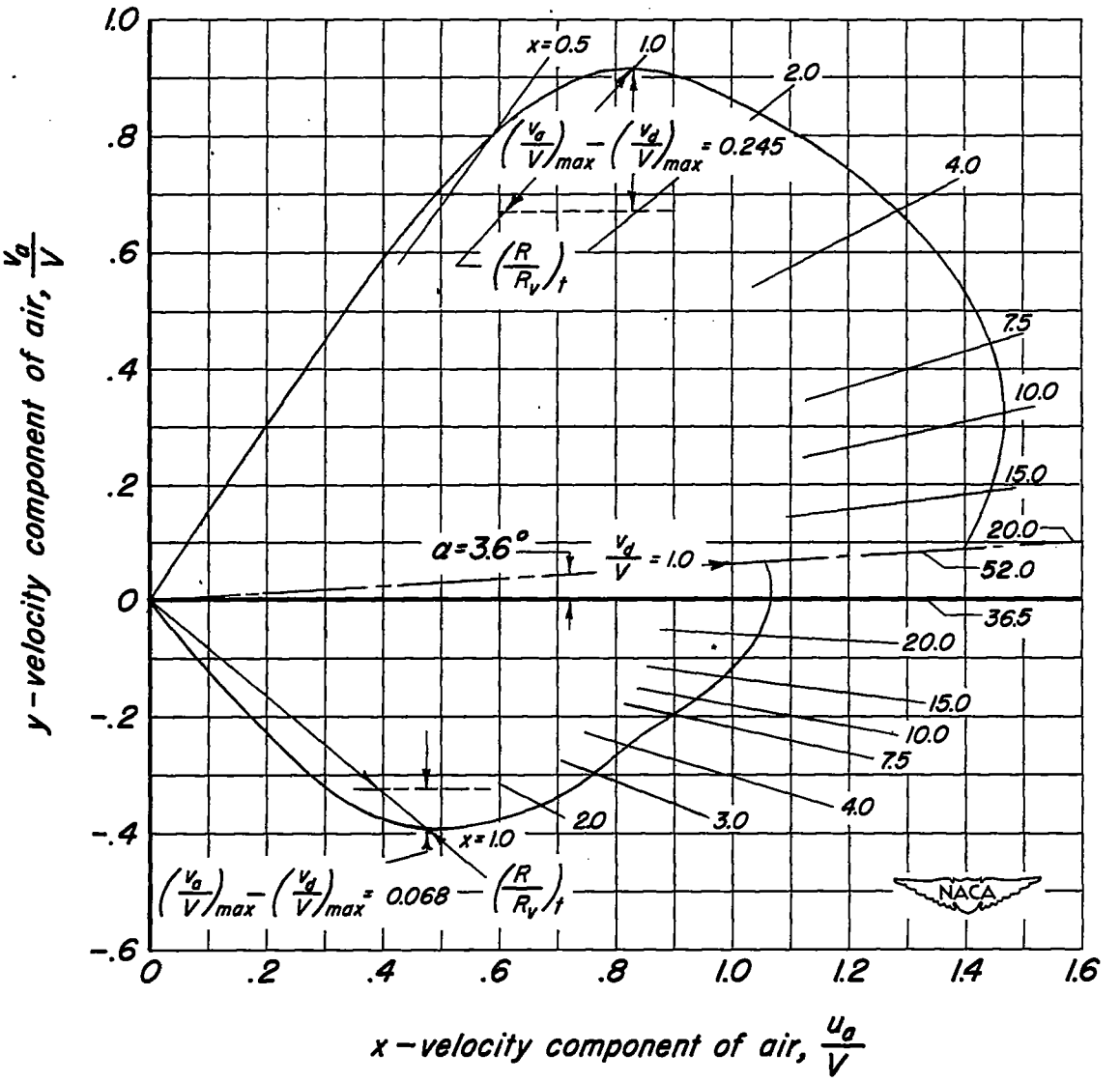


(f) Initial phase of drop hodograph.

Figure 19. - Continued.

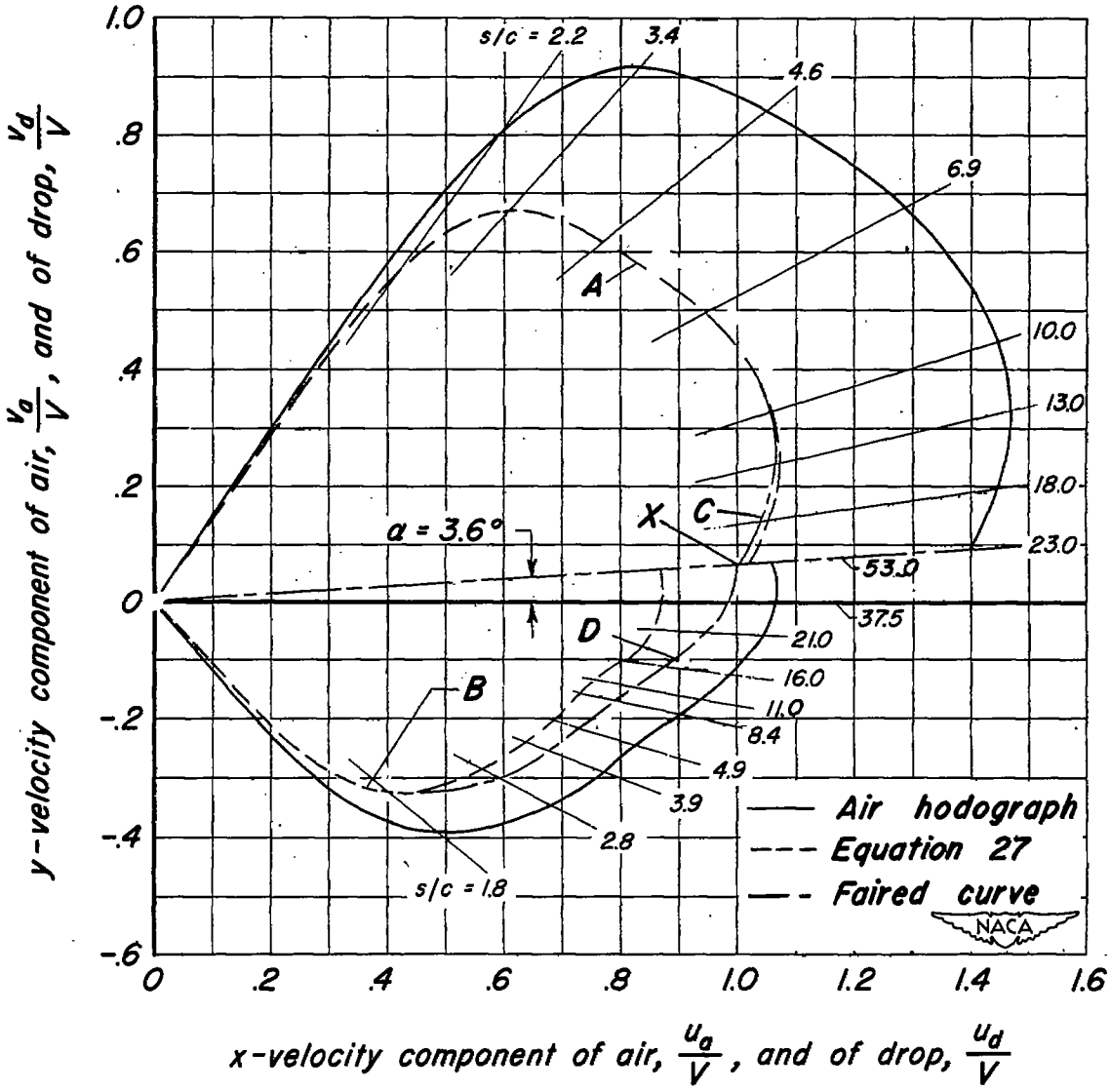


(g) Completed drop and air hodographs.

Figure 19. - Continued.

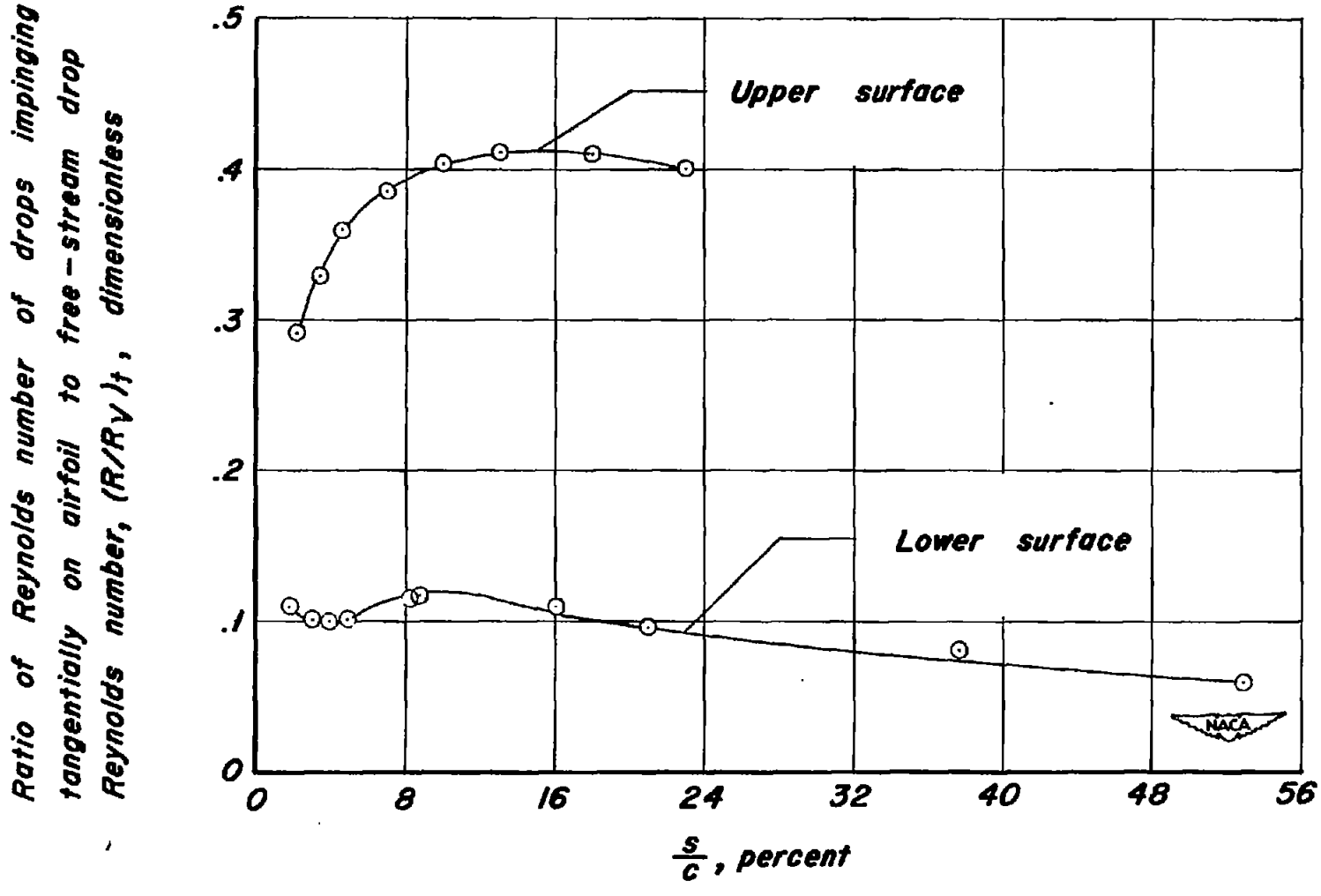


(h) $\left(\frac{R}{R_V}\right)_t$ as a function of $\frac{s}{c}$

Figure 19. – Continued.

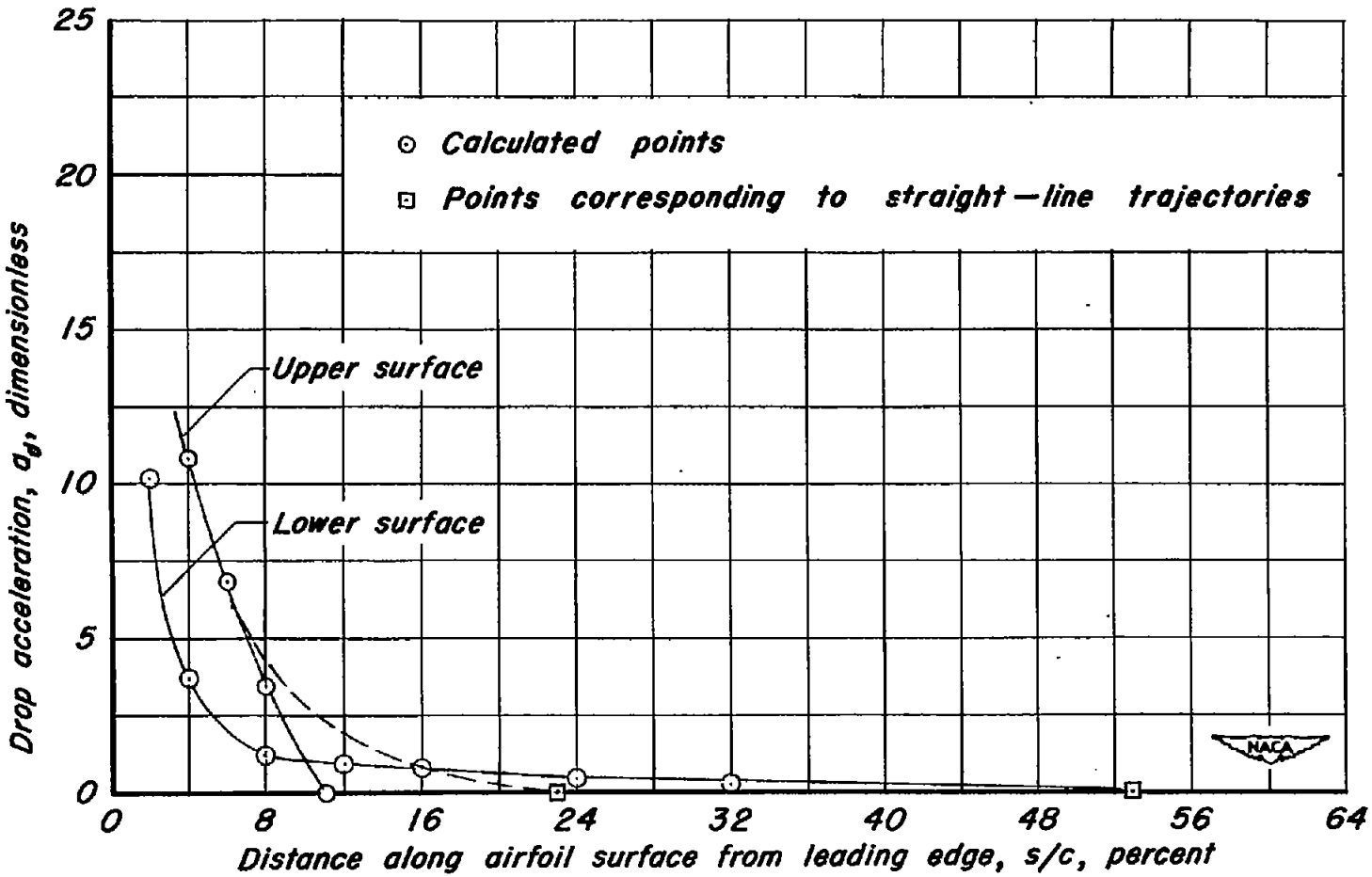


(i) Distribution of drop acceleration values over airfoil surface.

Figure 19.—Continued.

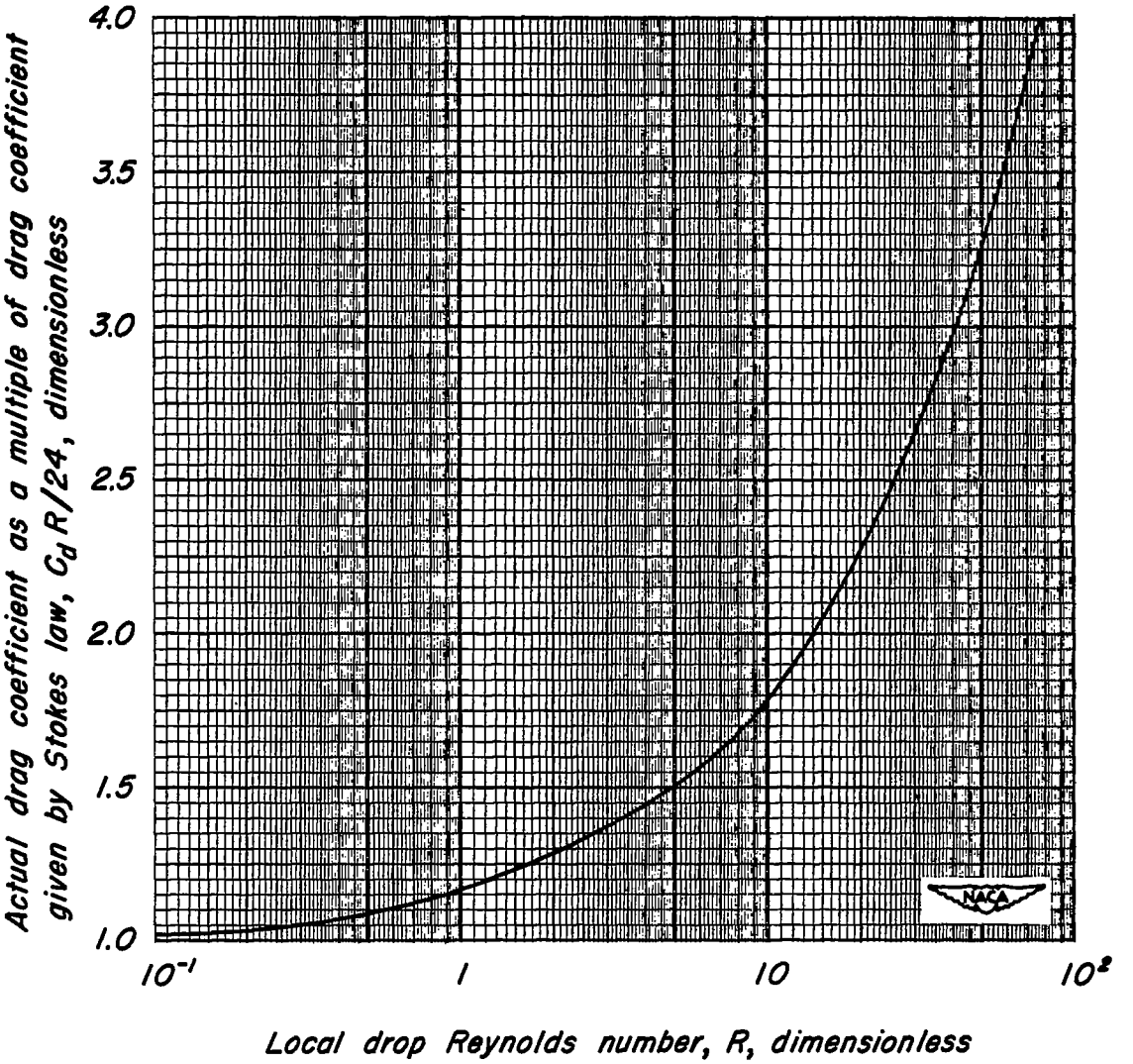


(j) $\frac{C_d R}{24}$ as a function of R.

Figure 19.-Continued.

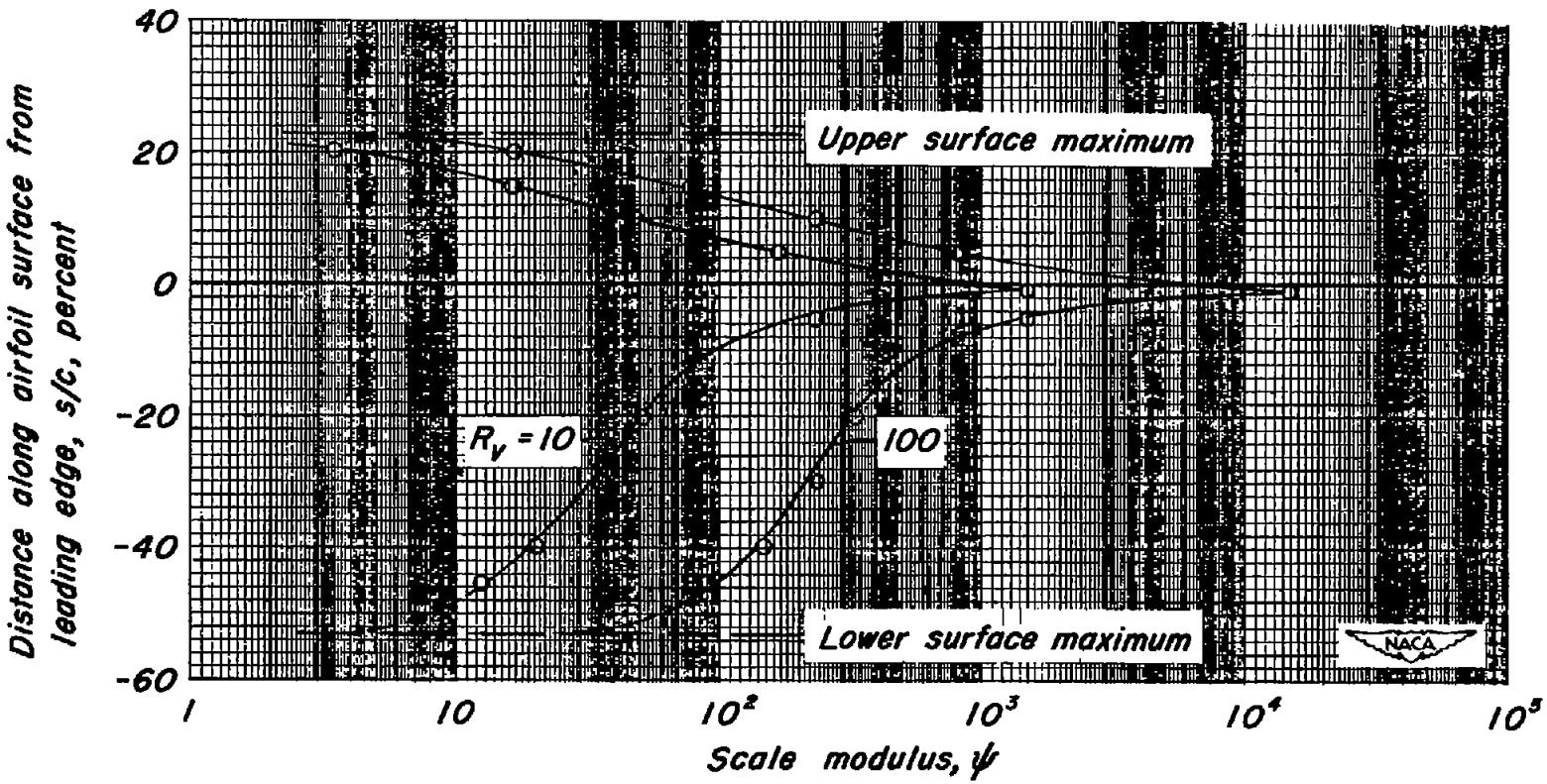


(k) Farthest position of impingement.

Figure 19.– Concluded.

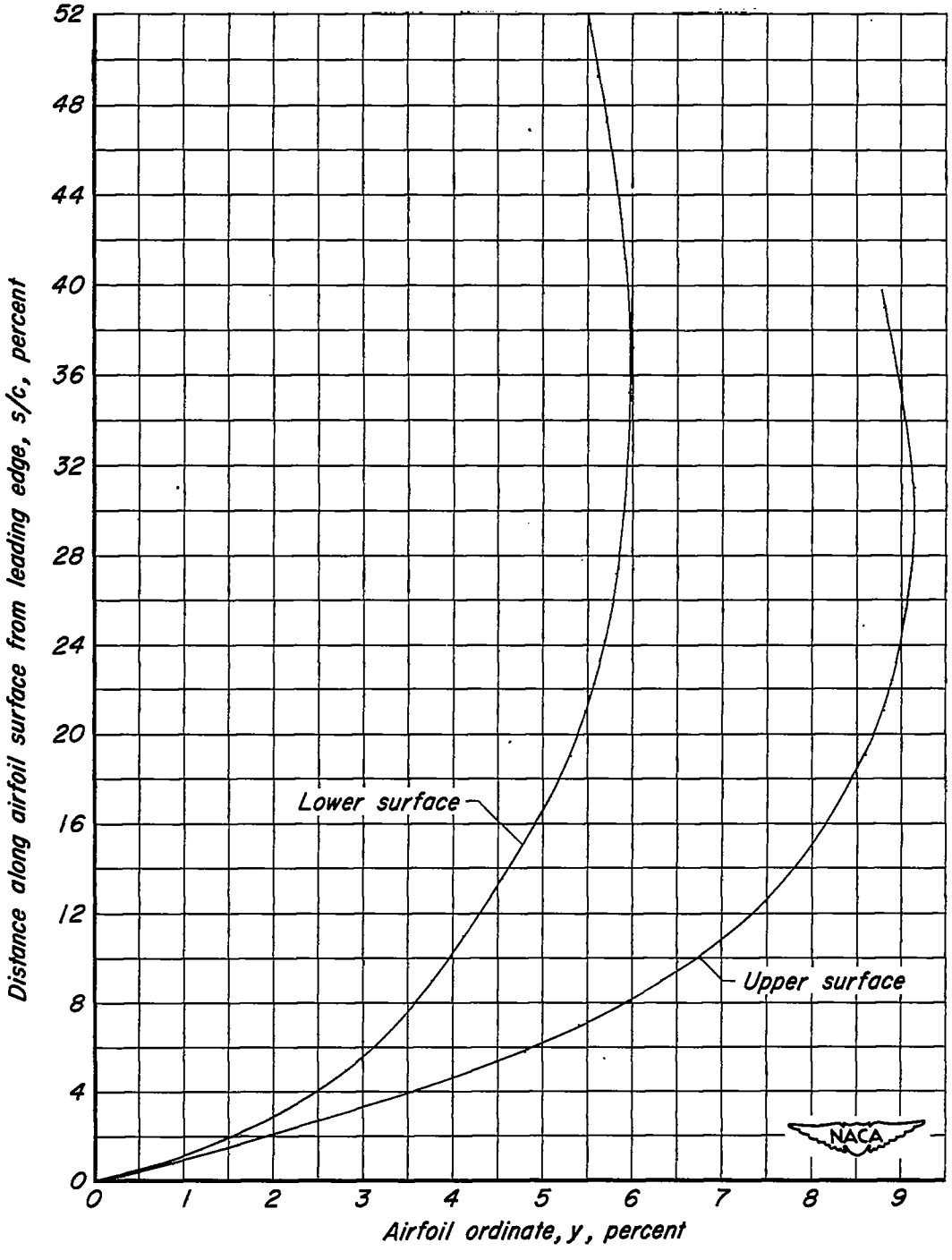


(a) Variation of s/c with airfoil ordinates.

Figure 20. – Graphical relationships used in evaluating impingement efficiency for an NACA 23015 airfoil; $\alpha = 3.6°$; $c_l = 0.5$ .

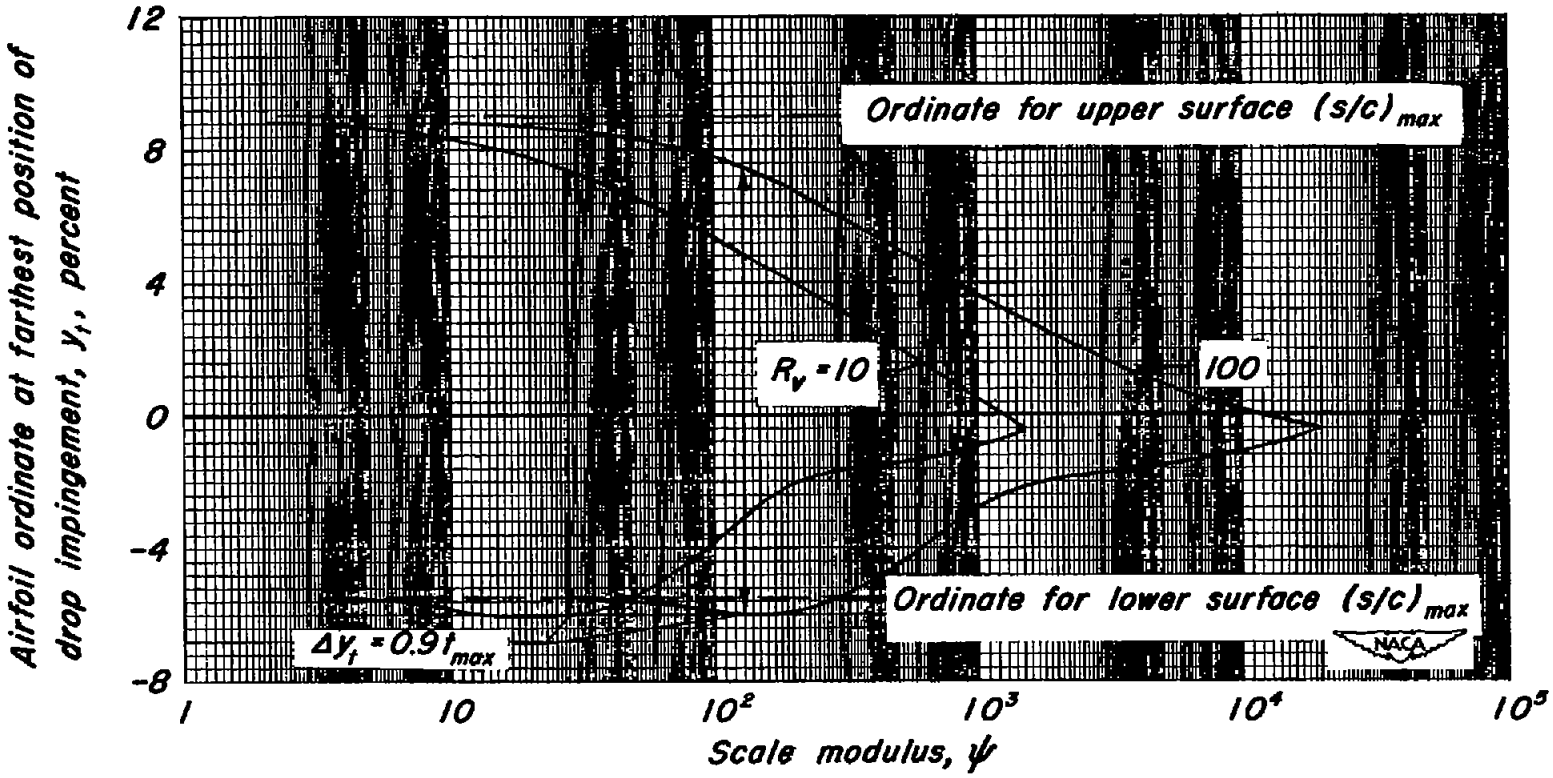


(b) Airfoil ordinate at farthest position of impingement.

Figure 20.- Continued.

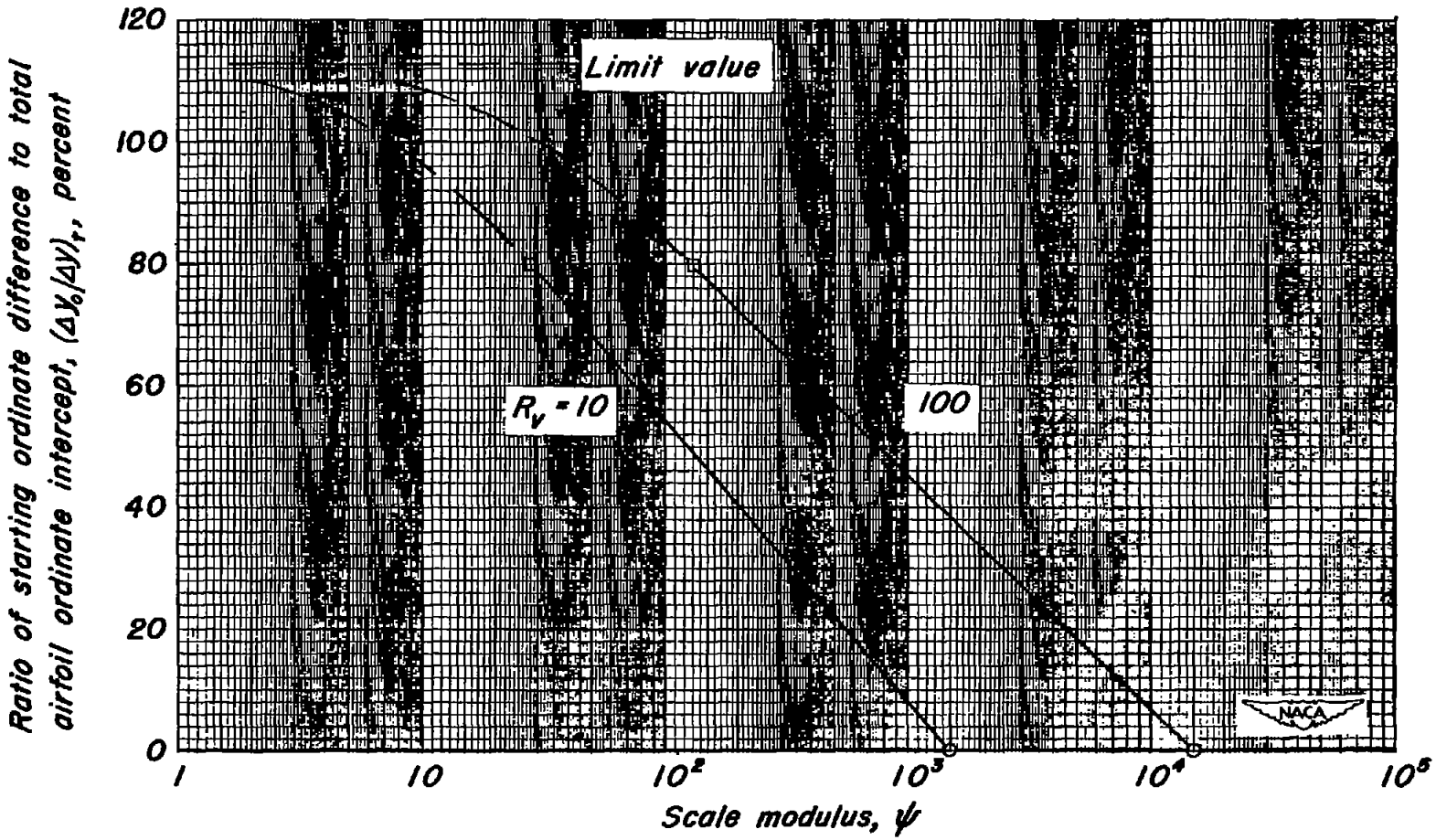


(c) Ordinate-ratio isopleths.

Figure 20.- Continued.

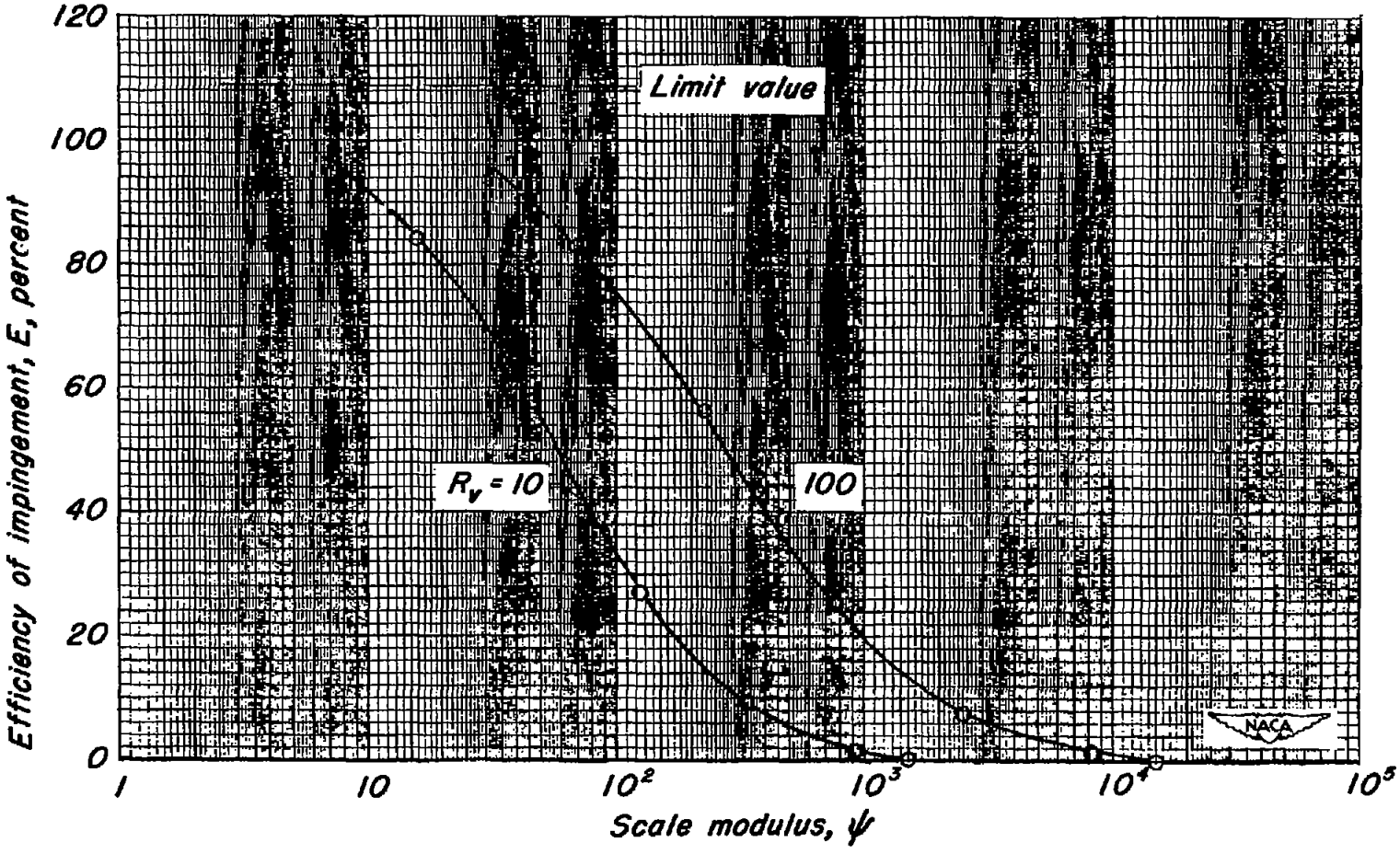


(d) Efficiency of impingement.

Figure 20.- Concluded.

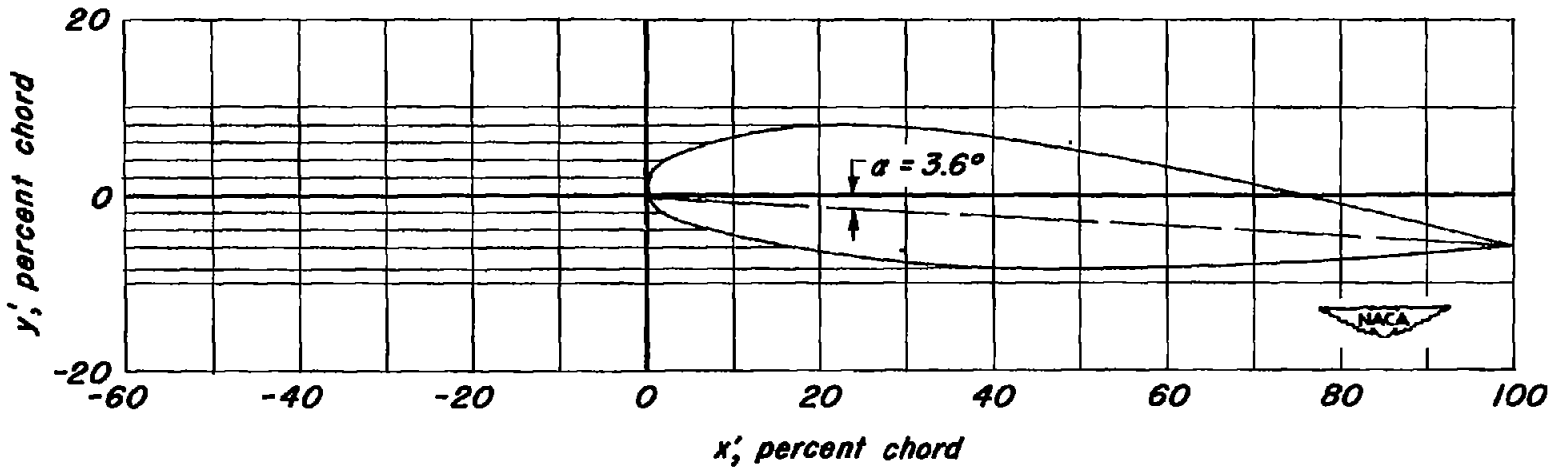


(a) Straight-line trajectories impinging on airfoil.

Figure 21. – Graphical relationships used in evaluating distribution of impingement for an NACA 23015 airfoil; $\alpha = 3.6°$; $c_l = 0.5$.

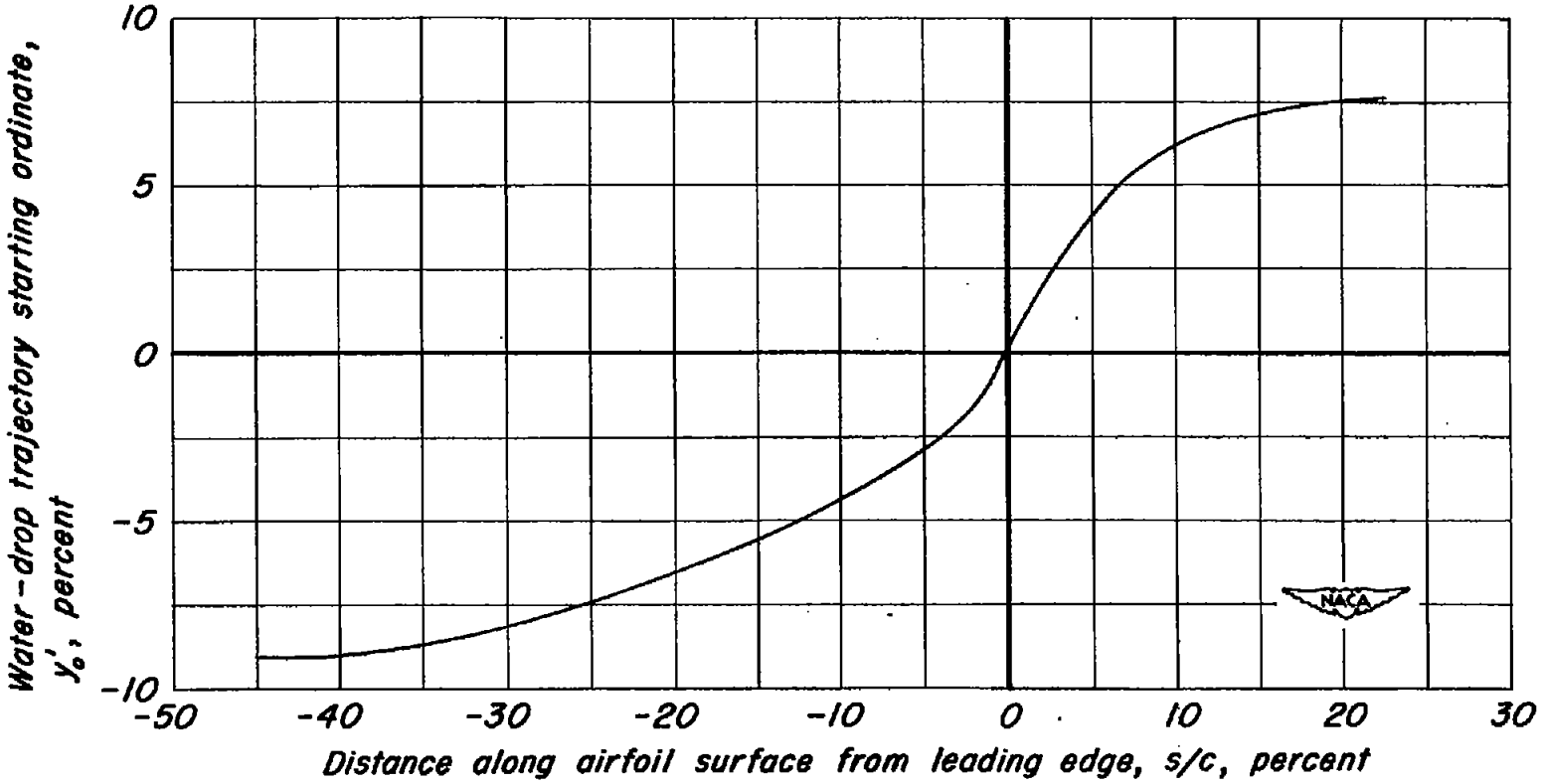


(b) Straight-line trajectory starting ordinates as a function of s/c.

Figure 21.- Continued.

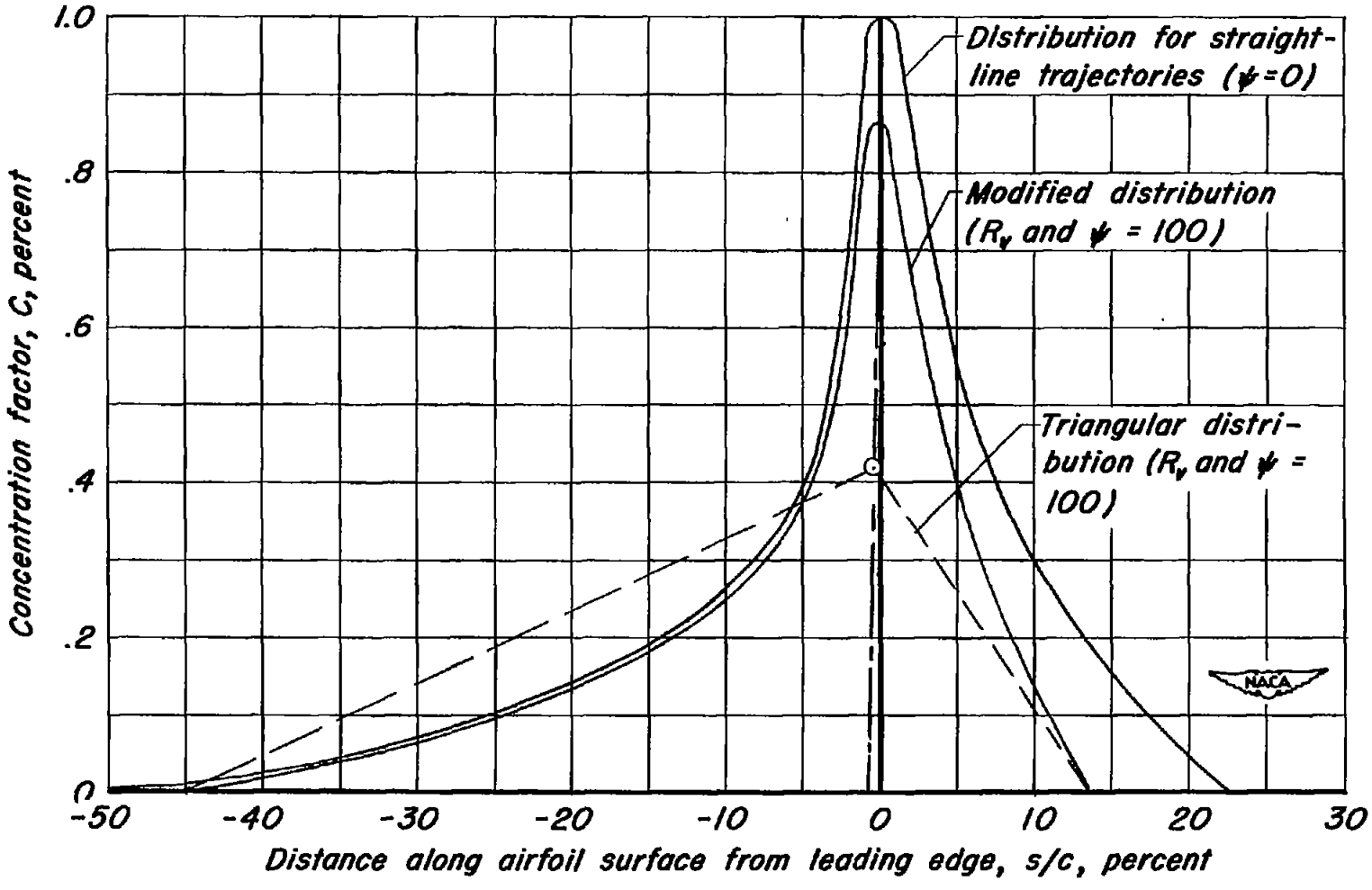


(c) Distribution of impingement.

Figure 21. - Concluded.

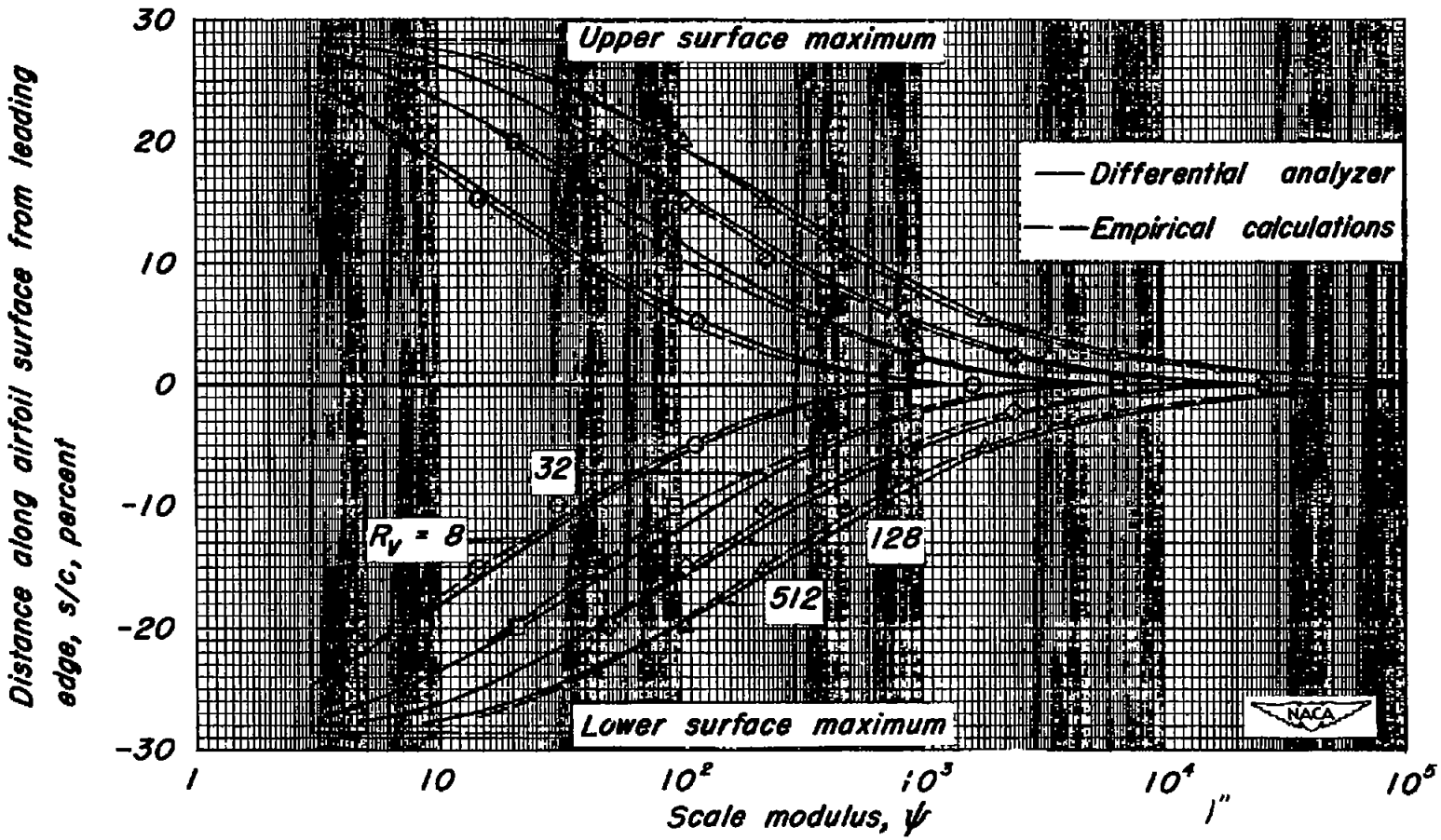


(a) 15-percent-thick symmetrical Joukowski airfoil; $\alpha = 0°$.

Figure 22.– Empirically calculated point values of farthest position of impingement for five airfoils in comparison with curves obtained from a differential analyzer.

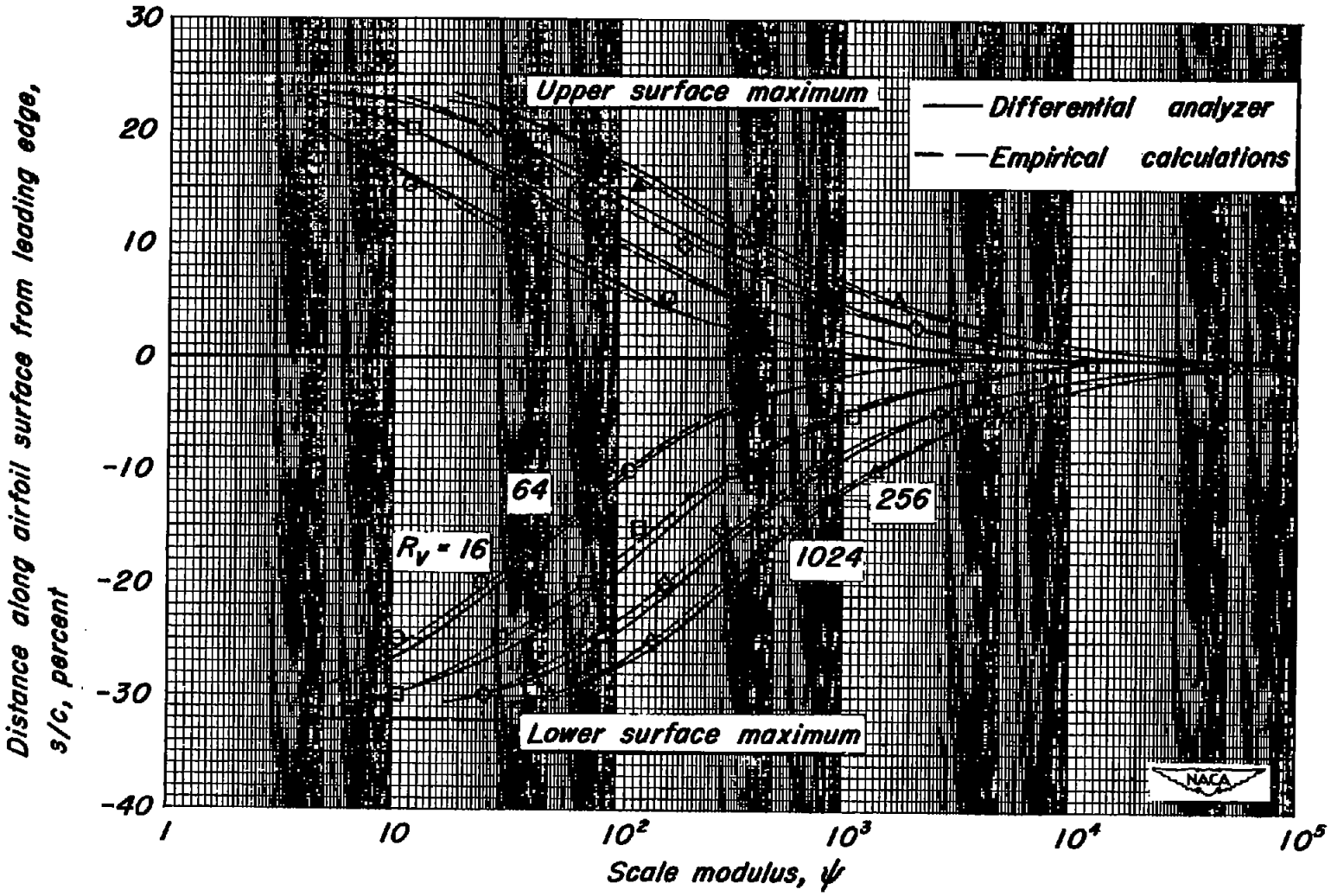


(b) 15-percent-thick symmetrical Joukowski airfoil; $\alpha = 2°$.

Figure 22.- Continued.

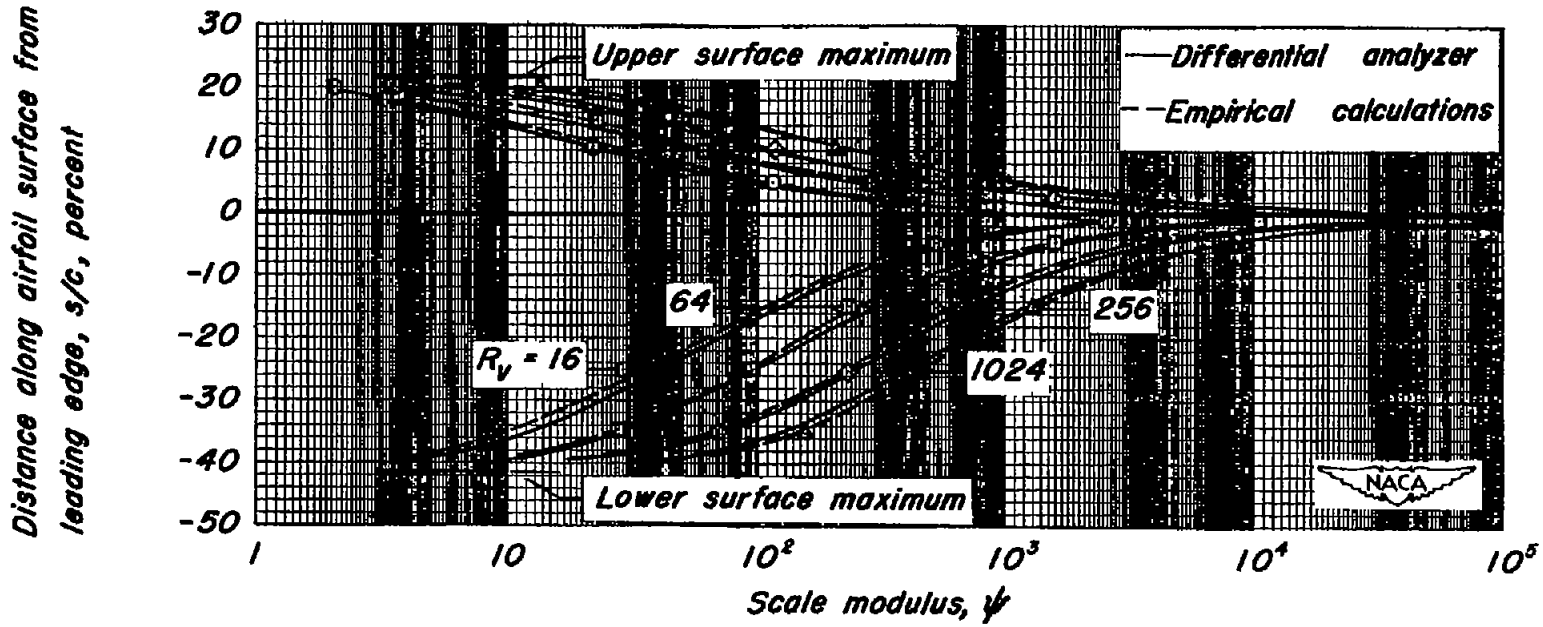


(c) 15-percent-thick symmetrical Joukowski airfoil; $\alpha = 4°$.

Figure 22.- Continued.

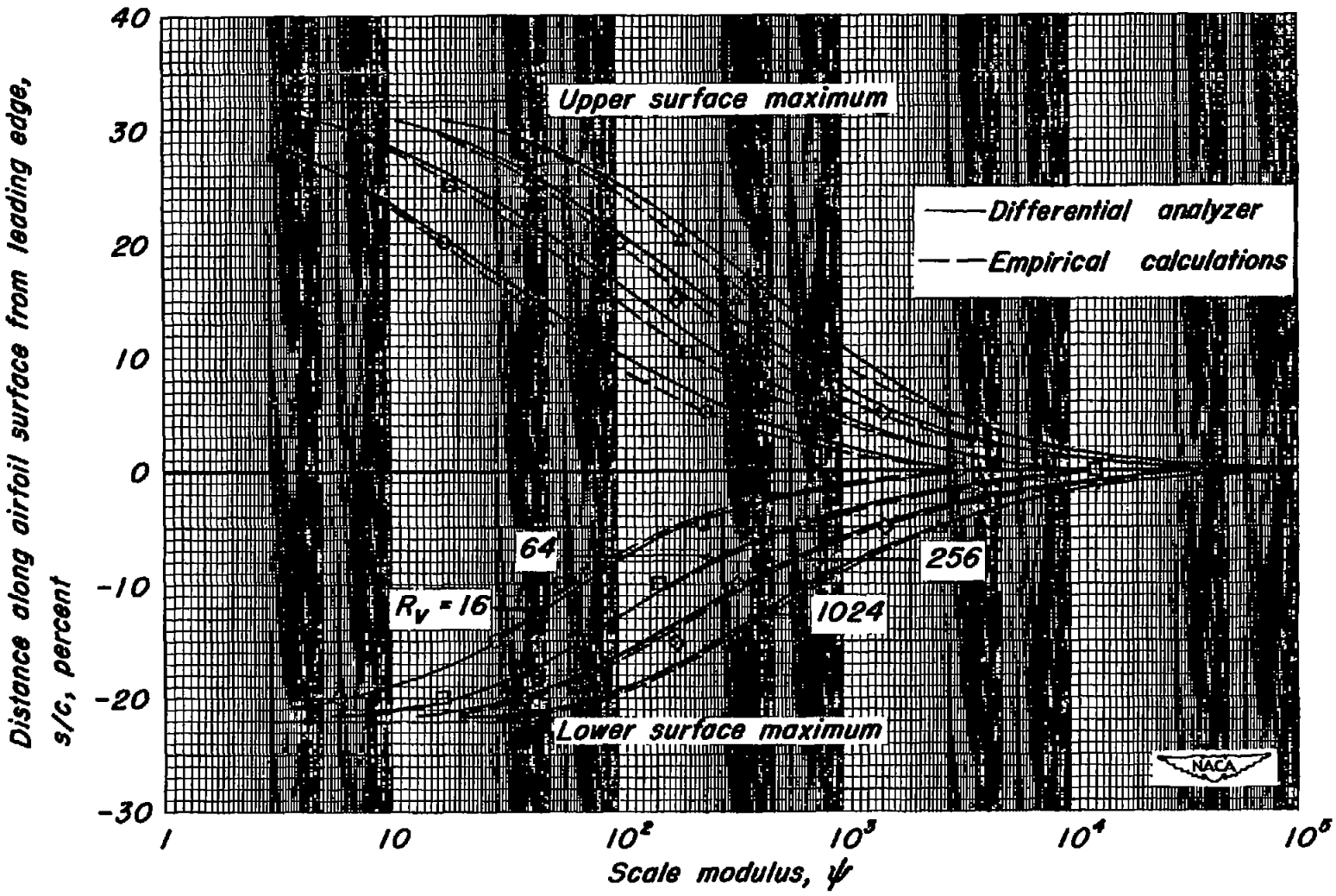


(d) 15-percent-thick cambered Joukowski airfoil; $a = 1.0$ mean line; $\alpha = 0°$.

Figure 22.- Continued.

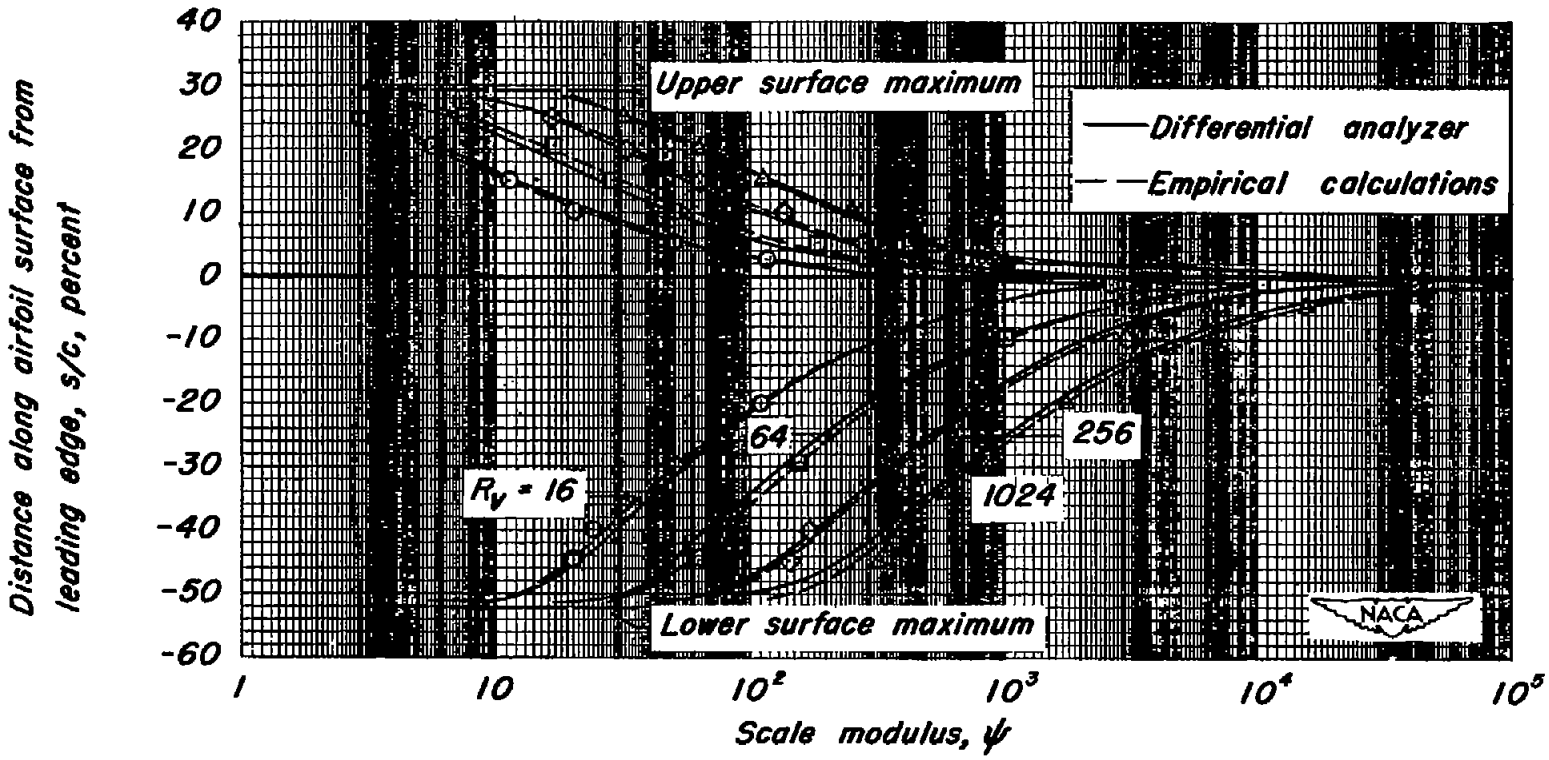


(e) NACA $65_2$-015 airfoil; $\alpha = 4°$.

Figure 22.- Concluded.

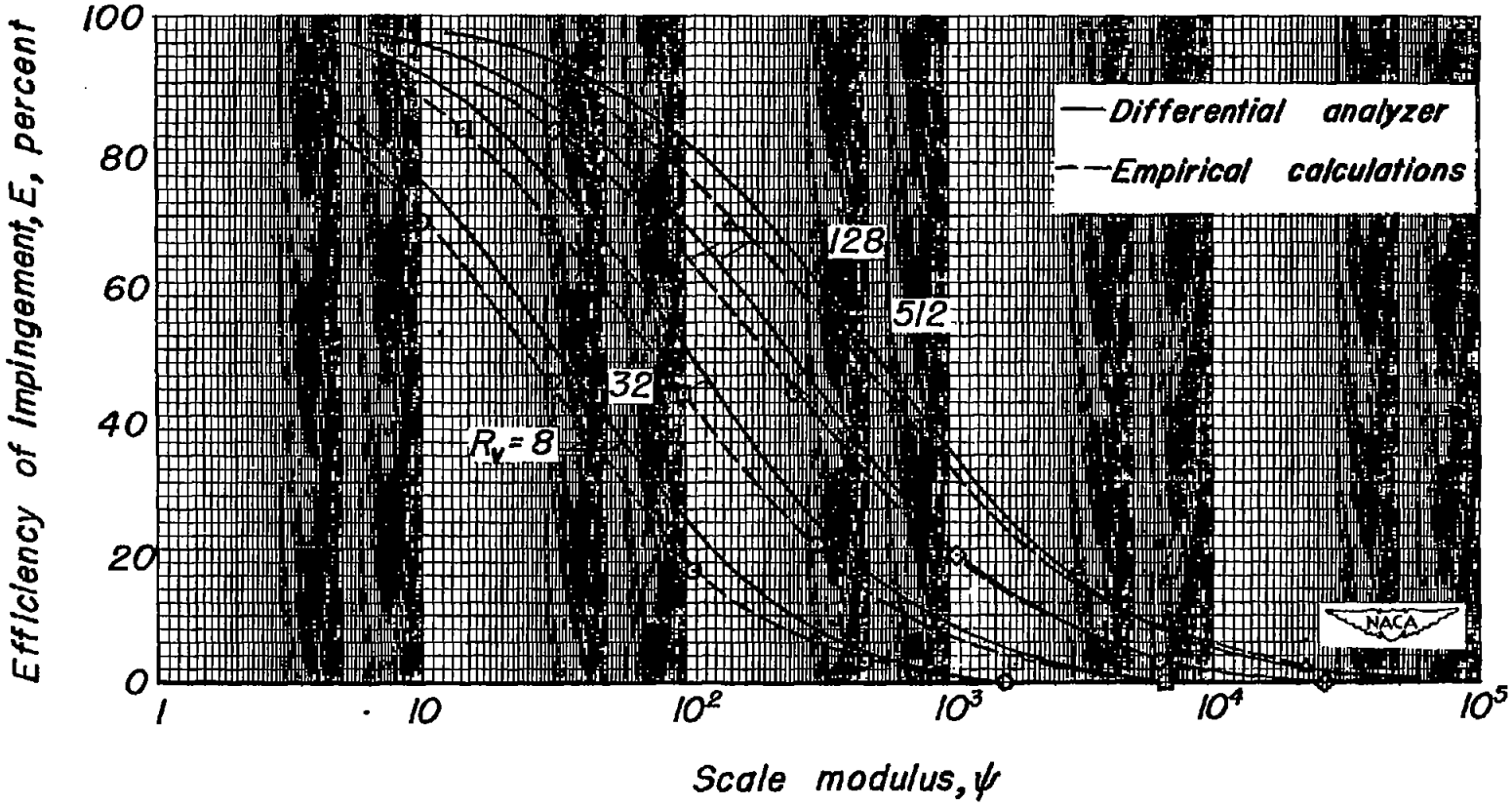


(a) 15-percent-thick symmetrical Joukowski airfoil; $\alpha = 0°$.

Figure 23.– Empirically calculated point values of efficiency of impingement in comparison with curves obtained from a differential analyzer.

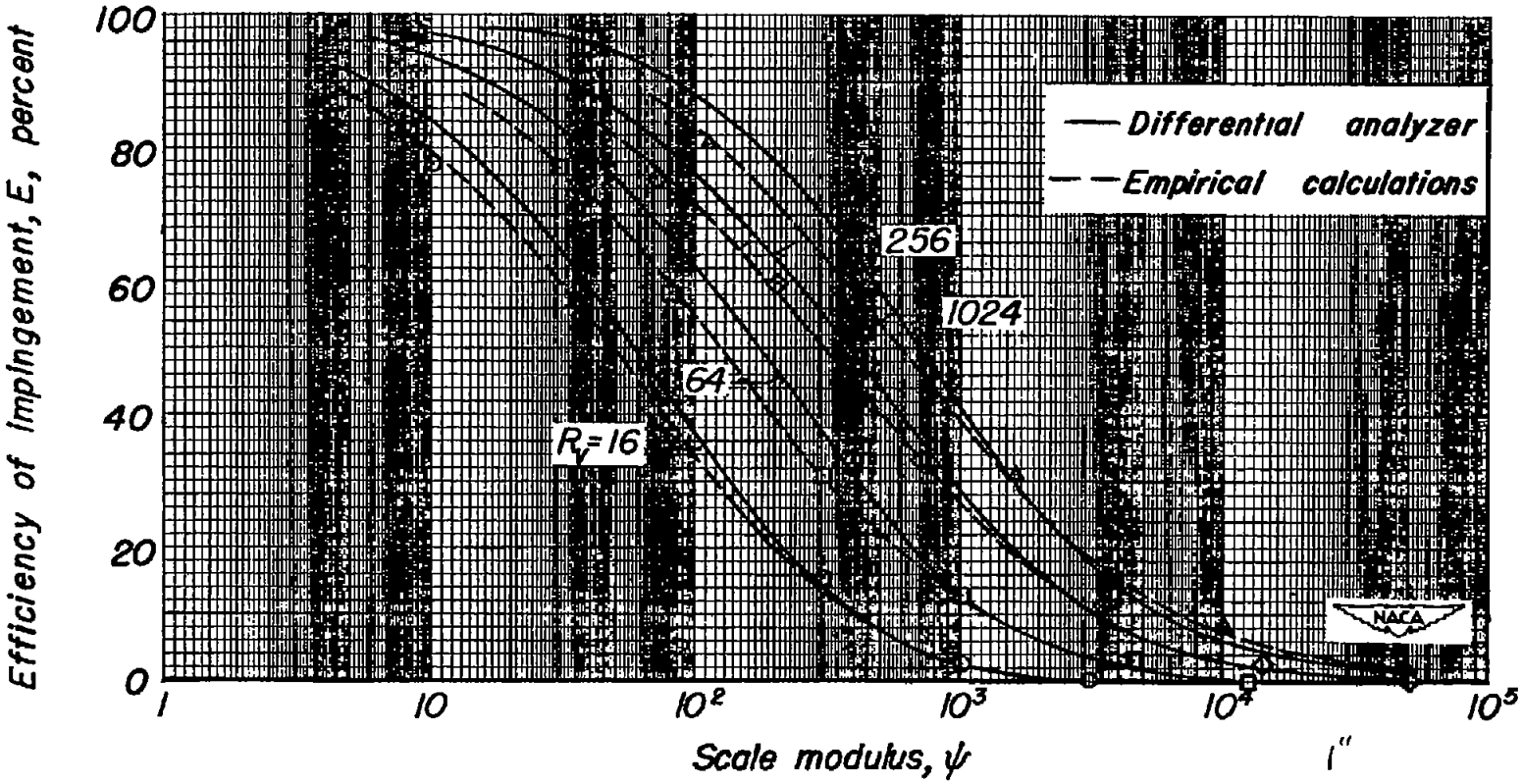


(b) 15-percent-thick symmetrical Joukowski airfoil; $\alpha$=2°.

Figure 23.— Continued.

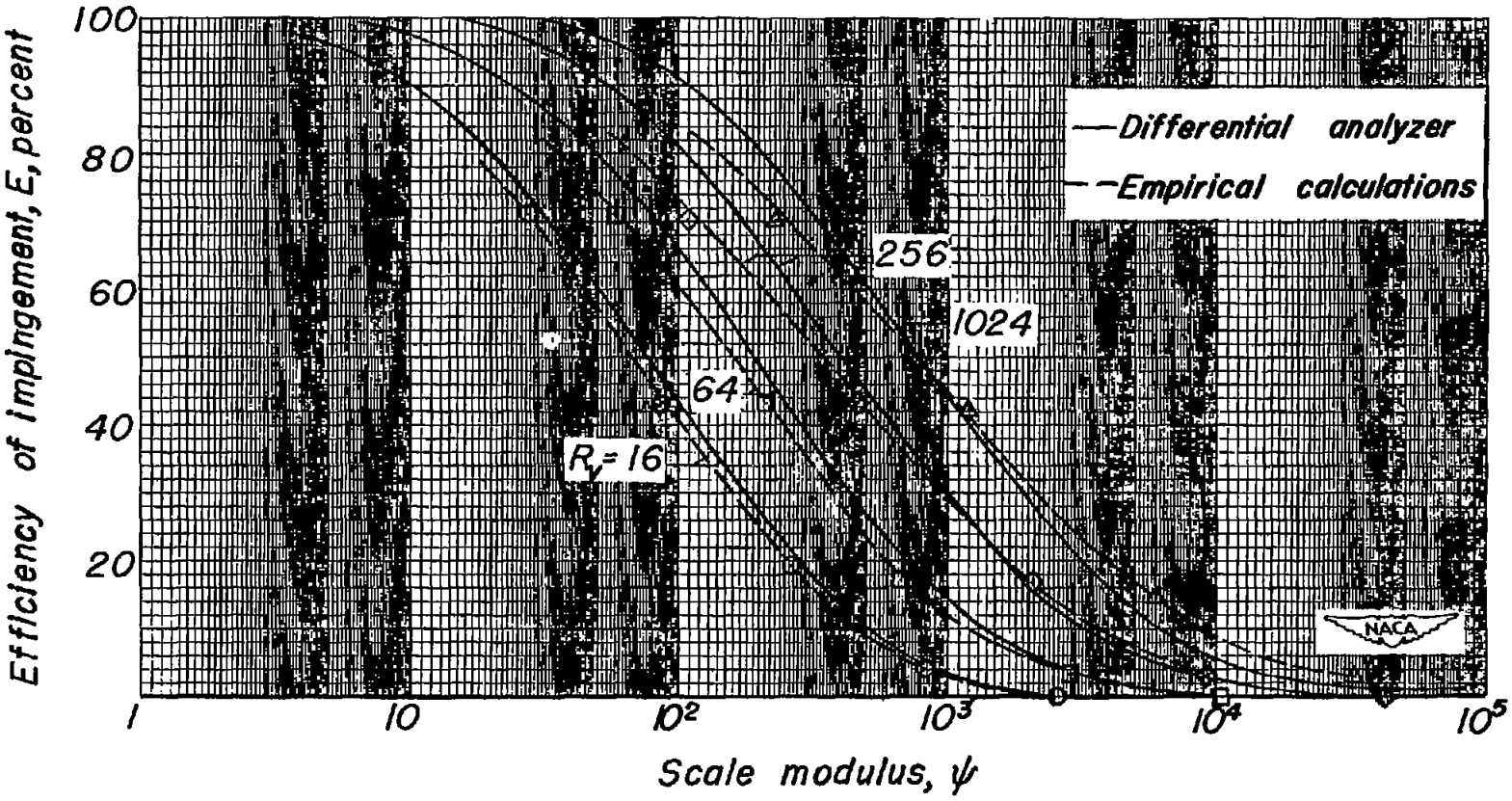


(c) 15-percent-thick symmetrical Joukowski airfoil; $\alpha$=4°.

Figure 23.— Continued.

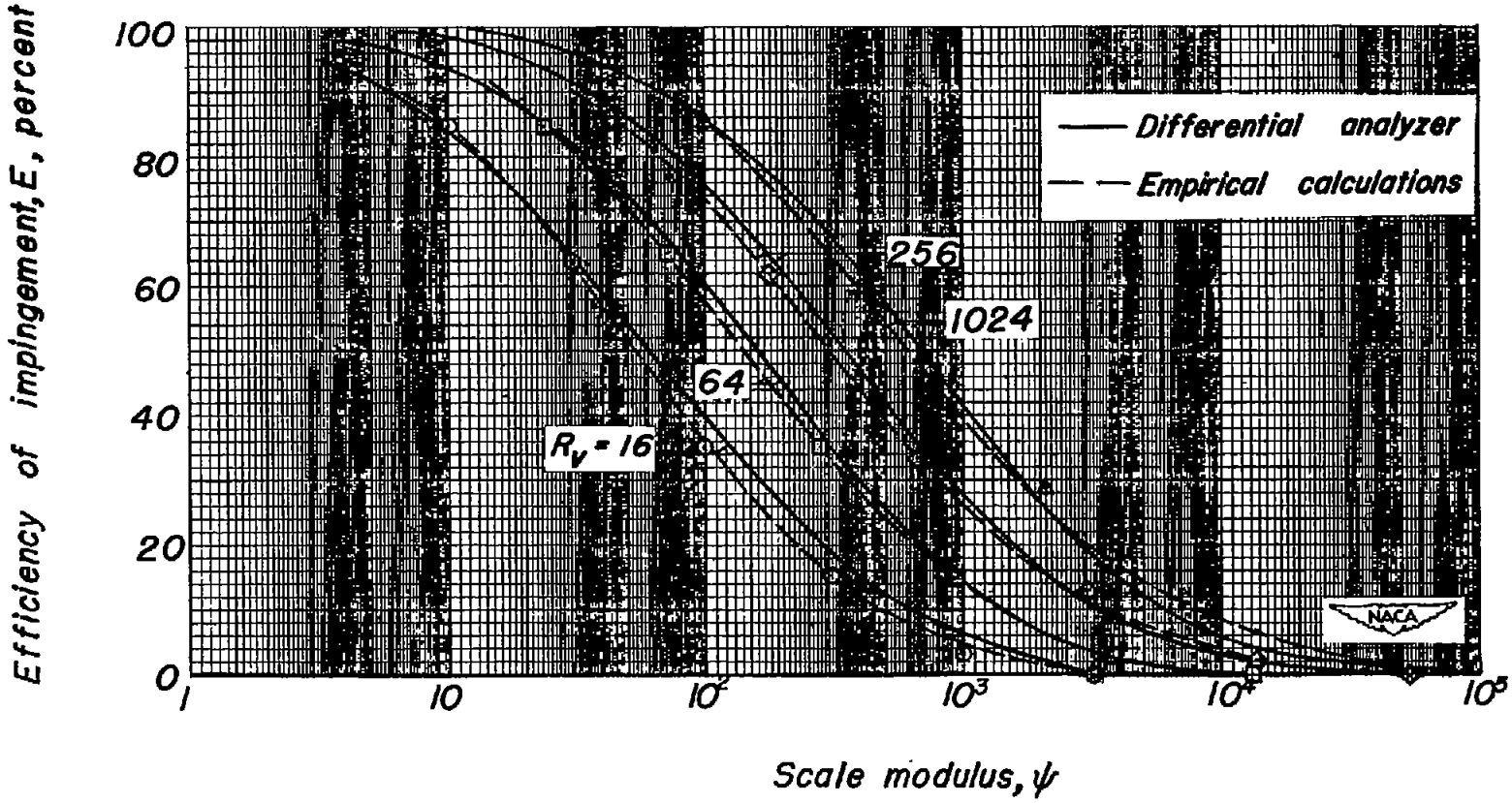


(d) 15-percent-thick cambered Joukowski airfoil; $a = 1.0$ mean line; $\alpha = 0°$.

Figure 23.– Continued.

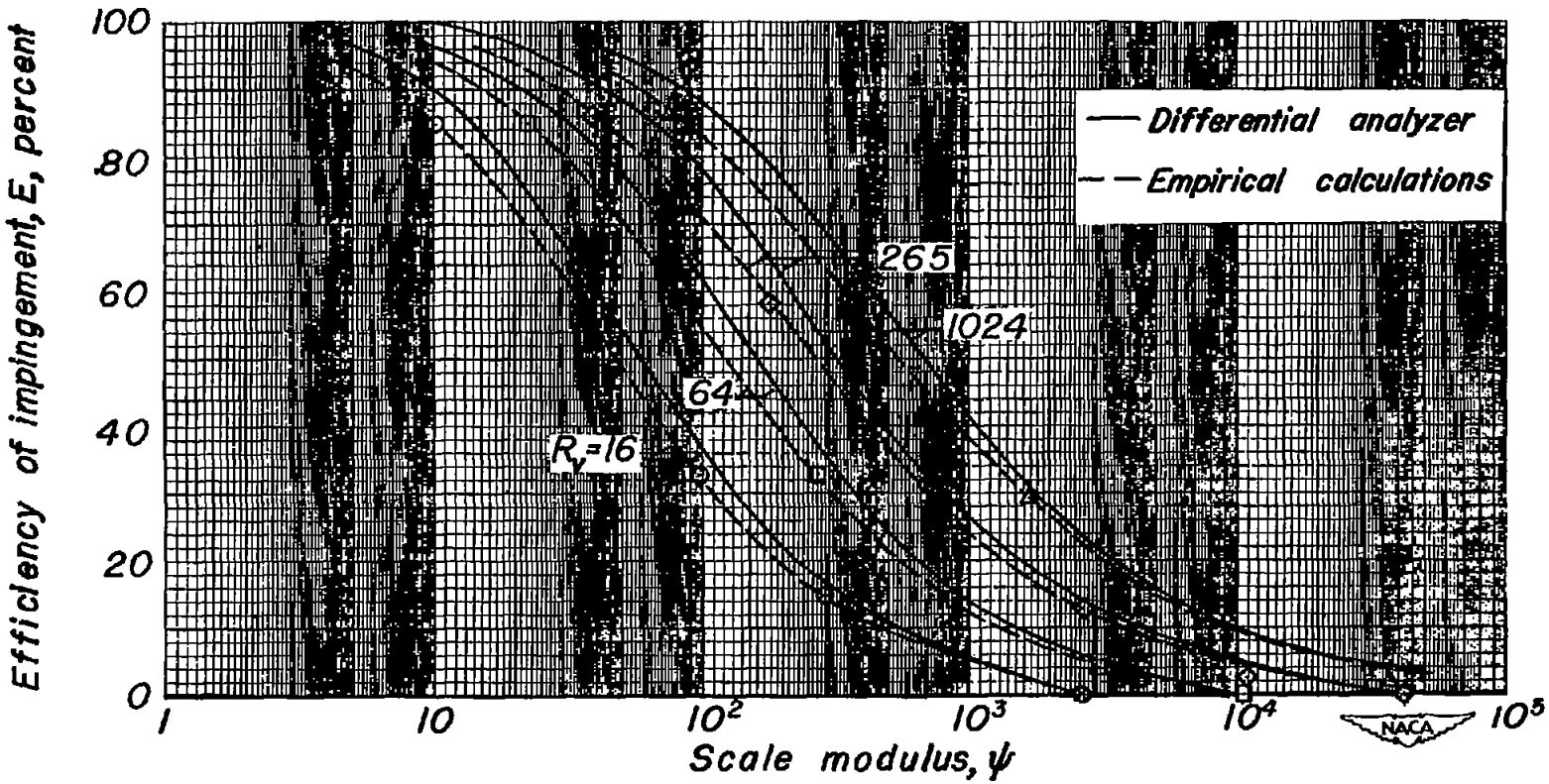


(e) NACA $65_2$-015 airfoil; $\alpha = 4°$.

Figure 23.— Concluded.

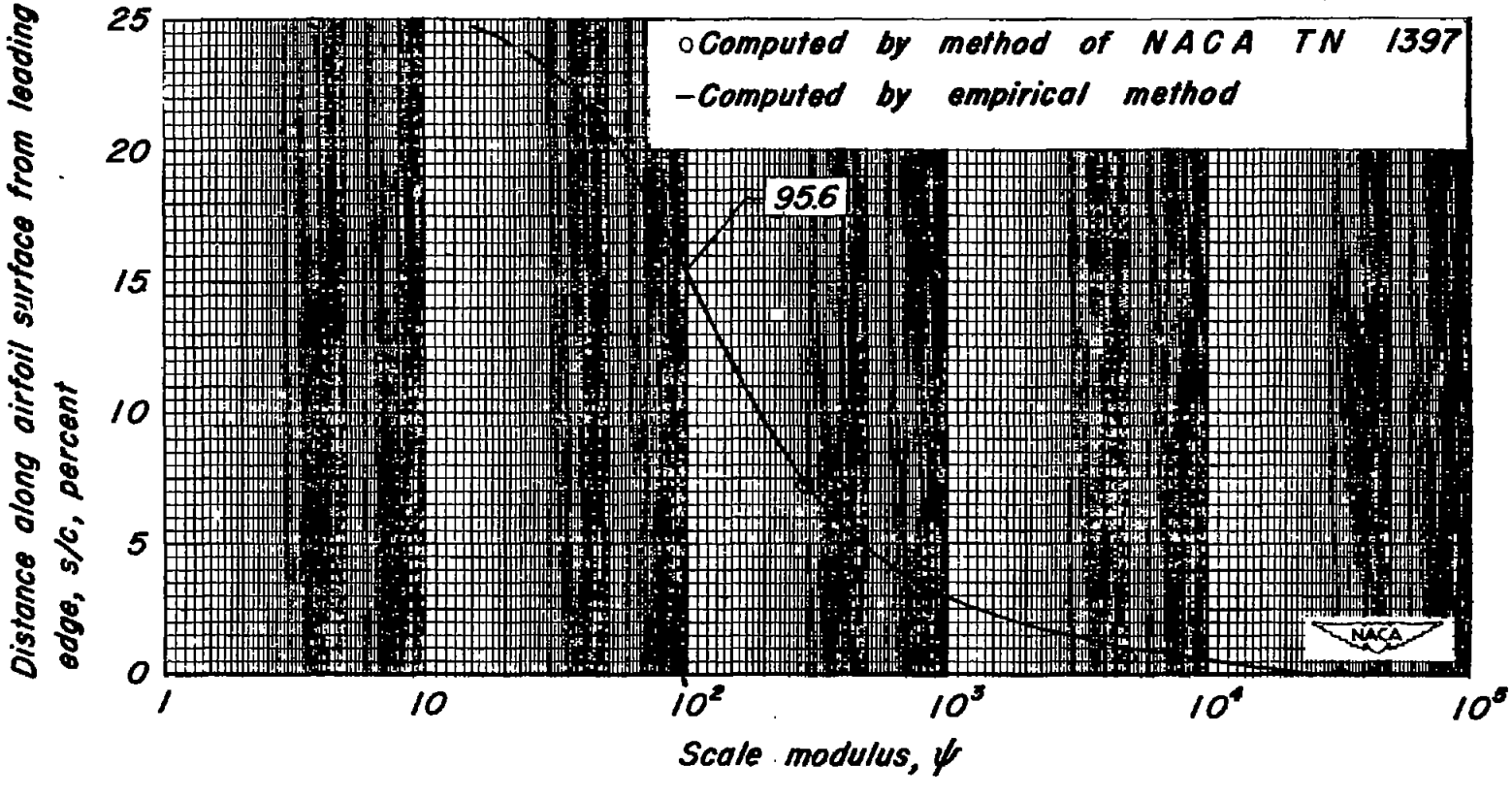


*Figure 24.- Empirically calculated curve of farthest position of impingement in comparison with point values obtained by stepwise computations for a 12-percent-thick symmetrical Joukowski airfoil, $\alpha = 0°$.*

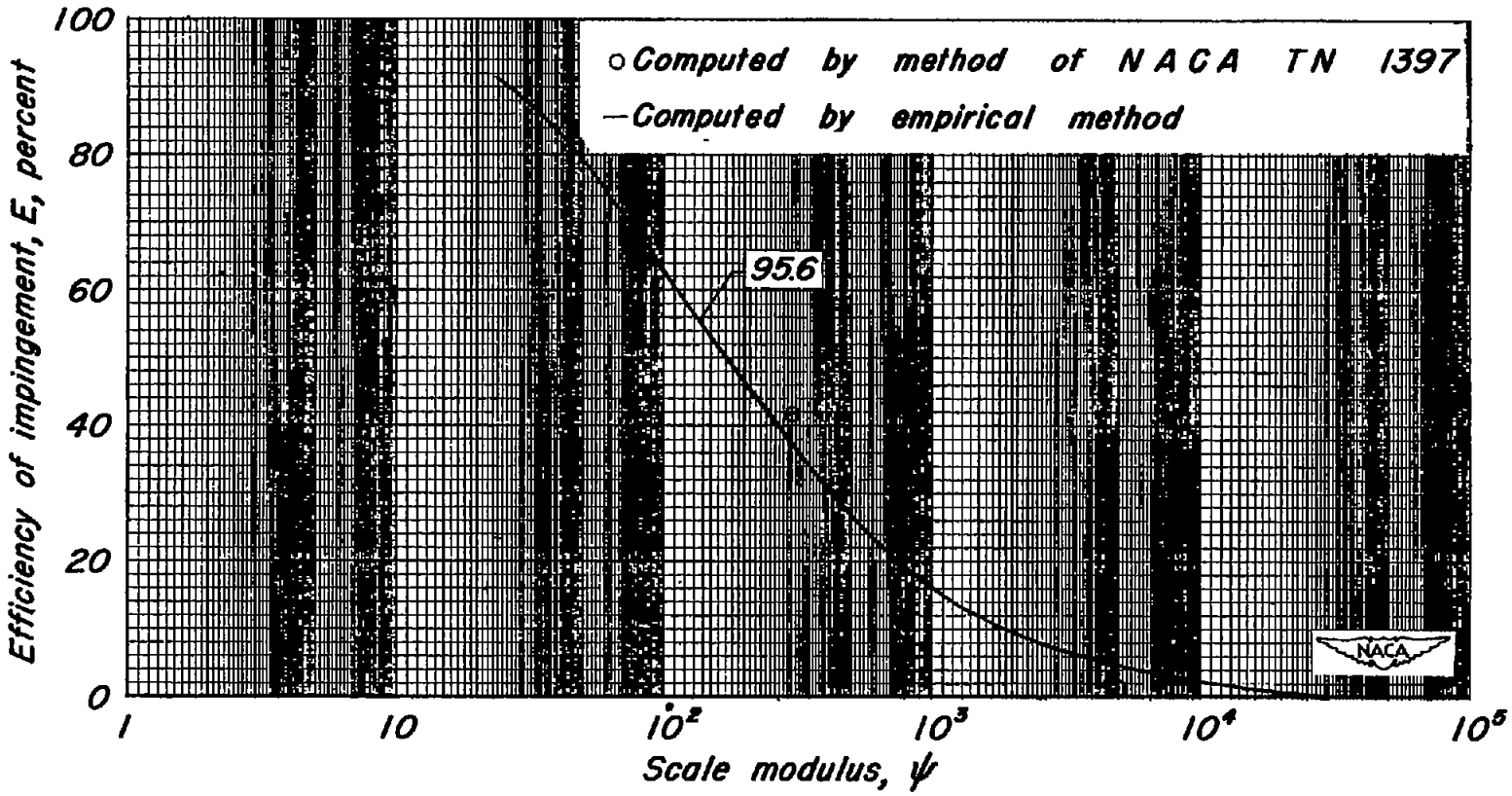


*Figure 25.- Empirically calculated curve of percent impingement in comparison with point values obtained by stepwise computations for a 12-percent-thick symmetrical Joukowski airfoil, $\alpha = 0°$.*



NACA-Langley - 8-14-51 - 1000